Gauge Field Amplification during Axion Inflation

A THESIS
SUBMITTED TO THE FACULTY OF THE GRADUATE SCHOOL
OF THE UNIVERSITY OF MINNESOTA
BY

Caner Ünal

IN PARTIAL FULFILLMENT OF THE REQUIREMENTS
FOR THE DEGREE OF
DOCTOR OF PHILOSOPHY

Prof. Marco Peloso, Adviser

August, 2018

Acknowledgements

During this five-year-long-PhD I have experienced multiple academic and personal phase transitions. It was one of the most radical periods of my life, which has dramatically changed my perception and consciousness. Although I may never express my feelings and thoughts accurately, I would like to make an honest try.

Foremost, I want to thank sincerely my adviser Marco Peloso. His dynamism, passion, and vision have shaped me into who I am today. I have learned a lot from Marco about the universe, the research process, and the life.

Second, I would like to thank Lorenzo Sorbo and Juan Garcia-Bellido for their insights on distinct areas of physics, and the collaboration on multiple papers, and supporting me for my academic journey. In addition, I am grateful to Nicola Bartolo and Angelo Ricciardone for our collaboration during early stage of my studies. It is also a pleasure for me to thank Ryo Namba, Maresuke Shiraishi and Alex Papageorgiou for our fruitful collaboration.

Since I started grad school at the University of Minnesota, I have benefited a lot from the courses given by the academic staff. I especially want to thank Joseph Kapusta, Keith Olive and Yong-Zhong Qian. The professors from my alma mater, including Seçkin Kürkçüoğlu, Bayram Tekin, Bilge Demirköz and Atalay Karasu, also deserve a special appreciation for their guidance and support since my undergrad years.

I also would like to thank my graduate student comrades that turned a department into my family : David Bosch, Yusuf Büyükdağ, Taher Ghasimakbari, Michael Kreshchuk, Ming Li, Alex Papageorgiou, Yahor Savich and Jiaming Zheng.

I am also grateful to Murat Altun, Sinan Erensü, Doğa Güçtenkorkmaz, Leah Humphries, Barış İne, Geoffrey Lawrence, Rick Leitzman, Laurel Lindahl, Angela Mertz, Allison Mikkalo, Zelha Nil, Natalie Pierson, Marnie See, Hasan Serçe and Cihan Yılmaz

for countless memories in my journey.

I would like to express my frank gratitude to Sonay Aydın, Barış Gökçe, Asutay Yıldırım, Alireza Behtash, Yasemin and Serhat Varolgüneş, Yunus Emre Yılmaz, Kağan and Hakan Erünsal, Mürsel Karadaş, Pınar Şen, Tuğcan Aktaş, Selim Özgen, Dilege Gülmez, Gökhan Alkaç and Candost Karani for their companionship all these years.

Finally I would like to thank my entire family, specifically my parents Hamiyet and Ömer Ünal for their love and support. They are a true source of wisdom and inspiration for me. Hakkınızı ödeyemem, bunun farkındayım. Umarım emeklerinize layık olabilirim.

Dedication

Anne ve Babama,

Ve

Evreni ve yaşamı derinden anlamak isteyen insanlara.

Abstract

This thesis studies the interaction of different fields during inflation and resultant phenomenology at different scales. It particularly focuses on one of the most well motivated inflationary models, called Axion inflation. Axions are pseudo-scalars that possess the shift symmetry at least at the approximate level, which protects their potential from quantum corrections and elevates them as a strong inflaton candidate. However, in the particle inventory of UV complete theories, axion particles are abundant, which motivates studying axions as inflaton or spectator field during inflation. In this work, we study a chiral shift symmetric dimension-five operator arising naturally in any axion theory. Due to this coupling, the gauge field's dispersion relation is modified and one helicity of the gauge field is produced abundantly as a function of a dimensionless parameter proportional to speed of the axion. This breaks the parity conservation. Furthermore, this amplified gauge quanta inversely decays (ie. sources back) to scalar and tensor degrees of freedom via two-to-one way; hence, the sourced perturbations obey non-Gaussian statistics. These sourced modes leave unique imprints on cosmological observables such as : Chiral gravitational wave (GW) background, large tensor non-Gaussianity, non-zero TB and EB correlators, detectable GW background at interferometer scales and the production of primordial black holes.

Contents

Acknowledgements **i**

Dedication **iii**

Abstract **iv**

List of Tables **ix**

List of Figures **x**

1 Introduction **1**

2 Inflationary Cosmology **5**

2.1 Big Bang summary and problems 6

2.1.1 Homogenous and Isotropic Universe and Big Bang Framework . 6

2.1.2 The Shortcomings of standard Big Bang Framework 9

2.2 Inflationary Physics at the Classical Level 11

2.3 Inflationary Physics at the Quantum Level 16

2.3.1 Scalar Perturbations 18

2.3.2 Tensor Perturbations 20

3 The Interaction of Axion and Abelian Gauge Field **22**

3.1 Gauge field amplification in Axion Inflation 23

3.1.1 Nearly constant gauge field from $\frac{\alpha}{f}\,\phi\,F\,\tilde{F}$ 25

3.1.2 Bump in gauge field production from $\frac{\alpha}{f}\,\sigma\,F\,\tilde{F}$ 28

4 CMB Phenomenology of Axion-Gauge Interaction **31**
4.1 The model, Background Evolution and Gauge Field Production 36
4.2 Sourced primordial perturbations 38
4.2.1 Generation of scalar perturbations 39
4.2.2 Generation of tensor perturbations 42
4.3 Results and phenomenology 43
4.3.1 Scalar and tensor correlators 43
4.3.2 Phenomenology 46
4.4 Summary 59

5 Small Scale Phenomenology of Axion-Gauge Interaction **61**
5.1 Limits on scalar perturbations, and prospects for the detection of a stochastic GW background 67
5.2 Production from a rolling inflaton ϕ 70
5.2.1 Production of scalar and tensor modes 70
5.2.2 Phenomenology at sub-CMB scales 74
5.3 Production from a rolling field σ different from the inflaton 79
5.3.1 Production of scalar and tensor modes 81
5.3.2 Direct Detection of Inflationary Signatures at Interferometer Scales 83
5.3.3 GWs from merging PBHs 85
5.4 Summary 88

6 Constraints on the Axion-Gauge Coupling **91**
6.1 Phenomenological signatures of the gauge field amplification 93
6.1.1 Signatures for $X = \phi$ 94
6.1.2 Signatures for $X = \sigma$ 94
6.2 Backreaction 96
6.2.1 Backreaction for $X = \phi$ 97
6.2.2 Backreaction for $X = \sigma$ 97
6.3 Perturbativity 99
6.3.1 Perturbativity for $X = \phi$ 102
6.3.2 Perturbativity for $X = \sigma$ 105
6.4 Discussion of the constraints 107

6.4.1 Discussion for $X = \phi$ . . . 107
6.4.2 Discussion for $X = \sigma$ . . . 108
6.5 Summary . . . 109

7 Conclusion and Discussions **112**

References **115**

Appendix A. Axion Inflation and its Coupling to Gauge Fields **128**

Appendix B. Details of the Abelian Gauge Field Amplification for Non-Adiabatic Evolution **133**
B.1 Details of the derivation of $A_+(\tau, k)$ . . . 133
B.2 Energy Density in the Abelian Gauge Field . . . 136

Appendix C. CMB Phenomenology For Rolling Axion Bump **138**
C.1 Sourced scalar modes at constant ξ . . . 138
C.2 Scalar Modes . . . 139
C.2.1 Scalar Power Spectrum . . . 141
C.2.2 Scalar Bispectrum . . . 143
C.3 Tensor Modes . . . 145
C.3.1 Tensor Power Spectrum . . . 147
C.3.2 Tensor Bispectrum . . . 149
C.4 Shape and properties of the bispectrum . . . 151
C.5 Deviation from gaussianity . . . 154

Appendix D. Small Scale Phenomenology **157**
D.1 Non-Gaussian scalar modes, and PBH formation . . . 157
D.1.1 $M - N$ relation . . . 157
D.1.2 $P_\zeta - \beta$ relation . . . 159
D.2 Suppression factor $\mathcal{F}$ . . . 161

Appendix E. Details of Perturbativity Constraint Calculations **164**
E.1 Computation of the perturbativity limits for $X = \phi$ . . . 164
E.2 Computation of the perturbativity limits for $X = \sigma$ . . . 167

E.2.1 $\delta\sigma$ vacuum solutions 167
E.2.2 Vector field renormalization 168
E.2.3 Pseudo-scalar field renormalization 170

List of Tables

4.1 ξ_* dependence of the functions entering in (4.41), for $\delta = 0.2$. Among the entries in the first column, only $f^c_{3,+}$ is negative, while the other $f^c_{i,j}$ are positive. 47

4.2 ξ_* dependence of the functions entering in (4.41), for $\delta = 0.5$. Among the entries in the first column, only $f^c_{3,+}$ is negative, while the other $f^c_{i,j}$ are positive. 47

5.1 First column: list of observational windows on inflation. Second column: order of magnitude of the wavenumber of the primordial modes in the corresponding window. Third column: estimated number of efolds before the end of inflation at which corresponding modes exit the horizon. The 3rd, 4th and 5th rows refer to GWs produced by the mergers of BH binaries originated by PBHs due to enhanced primordial scalar perturbations. The last three rows denote primordial stochastic GW from inflation. . . 63

List of Figures

3.1 Time evolution of the gauge field energy density for a given comoving momentum k for three approximated solutions (3.8), (3.9) and (3.10). . 26

3.2 Time evolution of the contribution to the gauge field physical energy density from modes with different comoving momenta. $x_* \equiv -k\tau_* = \frac{k/a_*}{H}$ is the ratio between the physical momentum of the mode and the Hubble horizon at $\tau = \tau_*$. 30

4.1 Comparison of the exact function $f_{2,\zeta}$ (green dots) and of the approximate form (red dashed line) given in eq. (4.41), for the two values of δ, 0.2 and 0.5. 46

4.2 ξ_* dependence of the fitting $f_{2,\zeta}$, $x^c_{2,\zeta}$ and $\sigma_{2,\zeta}$ entering in (4.41), for $\delta = 0.2$ (an analogous agreement is obtained for $\delta = 0.5$, and for other $\{i, j\}$ functions). The red dots denote the values at different ξ_* and the solid lines are polynomial fits. 46

4.3 Black-solid lines: tensor-to-scalar ratio. Orange dashed (Blue dotted) lines show the ratio between the sourced and the vacuum tensor (scalar) power spectrum. All ratios are evaluated at the peak of the sourced GW power spectrum. 48

4.4 Solid lines: Largest value of ξ_* allowed by the WMAP TT data as a function of ϵ_ϕ, and for different values of k_* (controlling the bump scale of the sourced modes). Dashed lines: ratio of $\mathcal{P}^{(1)}_\zeta/\mathcal{P}^{(0)}_\zeta$ at the peak of the GW bump. 50

4.5 Temperature-temperature correlation of WMAP data [65, 66] is compared against the three theoretical curves for three different values of k_* and with limiting value $\xi_* = \xi_{*,\mathrm{limit}}$, evaluated for $\epsilon_\phi = 10^{-5}$ and for $\delta = 0.2$ (left) and $\delta = 0.5$ (right). 51

4.6 First row: Forecasted signal-to-noise ratio for B-mode auto-correlations in a CMB experiment with *Planck*-like sensitivity (Colored solid lines), and in a cosmic variance limited (ideal noise-free) CMB experiment (Black dotted line). Second row: C_l^{BB} coefficients are shown for chosen parameters with solid color lines. The C_l^{BB} coefficients for scale invariant tensor-to-scalar-ratio (r) for 10^{-1}, 10^{-2} and 10^{-3} are shown with dots from top to bottom respectively. 52

4.7 First row: Forecasted signal-to-noise ratio for the detection of the TB correlation in a realistic CMB experiment with *Planck*-like sensitivity (Colored solid lines), and in a cosmic variance limited, CMB experiment (Colored dotted lines), as a function of the maximum multipole ℓ included in the analysis. Second row: TB spectra. 54

4.8 First row: Forecasted signal-to-noise ratio for the detection of the sourced TTT bispectrum in a cosmic variance-limited, CMB experiment, as a function of the maximum multipole ℓ included in the analysis. Second row: TTT reduced bispectrum for equilateral triangles of multipole ℓ. The colored lines are for the same parameters as in the previous figures. Solid (dotted) lines refer to the contribution to TTT from the sourced scalar (tensor) modes. The forecasted S/N ratio for scale-invariant equilateral non-gaussianity of magnitude $f_{\mathrm{NL}}^{\mathrm{equil}} = 150$ is added for comparison. 56

4.9 Left panel: Forecasted signal-to-noise ratio for the detection of the sourced BBB bispectrum in a realistic CMB experiment with *Planck*-like sensitivity (Colored solid lines), and in a cosmic variance limited, CMB experiment (Colored dotted lines), as a function of the maximum multipole ℓ included in the analysis. Right panel: BBB reduced bispectrum for equilateral triangles of multipole ℓ. The examples shown are for $\delta = 0.5$; the other parameters are chosen as in the previous figures. 58

5.1 Left panel: Limits on the rescaled black hole fraction $\tilde{\beta}$ as a function of the black hole mass. Right panel: Same limits, written as a bound on the primordial curvature(density) perturbations as a function of number of e-folds before the end of inflation, assuming a constant Hubble rate $H = 10^{13}\,\mathrm{GeV}$ during inflation, and a χ^2 statistics of the density perturbations (see Appendix D.1). 67

5.2 On left: Scalar power spectrum in axion inflation for a linear inflaton potential, in the approximation (5.8). The coupling to gauge field is chosen as large as allowed by the PHB bounds shown in the figure; this gives $\xi_{\mathrm{CMB}} \lesssim 1.66$ at 60 e-folds before the end of inflation. On right: Corresponding GW signal for the same model and parameters chosen in the left panel. The modes that left the horizon $30, 20$, and 10 e-folds before the end of inflation are shown with red dots. 74

5.3 The solid line shows the inflaton potential (5.9) spanned by the inflation from $N = 60$ to $N = 5$, with parameters leading to the spectra of Figure 5.4. The two arrows indicate the position of the two transition regions (the potential is linear both at $\phi < \phi_1$ and $\phi > \phi_2$, but with a different slope). The dotted lines shows an unmodified linear inflaton potential. 77

5.4 As in Figure 5.2, but with a larger coupling of the inflaton to the gauge field, and with the modified inflaton potential (5.9). The solid lines are the spectra obtained in this case (the corresponding potential is shown in the solid line of Figure 5.3). The dashed lines show how the spectra would continue at small scales if the instead the inflaton potential remained linear at all values (corresponding to the dashed line in Figure 5.3). . . 77

5.5 Scalar and tensor signals for a linear inflation potential. The solid lines show the signal if $\mathcal{N} = 6$ gauge fields are amplified. For comparison, the dashed lines show the signal when 1 gauge field is amplified. 79

5.6 Scalar power spectrum and GW power spectrum produced during inflation in the two field mode (5.11), assuming a bump at PTA scales. We see that, it is possible to produce a visible GW signal without violating the PBH bounds. 84

5.7 Scalar power spectrum and GW power spectrum produced during inflation in the two field mode (5.11), assuming a bump at LISA scales. We see that, similarly to the example shown in Figure 5.4, it is possible to produce a visible GW signal without violating the PBH bounds. 85
5.8 Scalar power spectrum and GW power spectrum produced during inflation in the two field model (5.11), assuming a bump at AdvLIGO scales. 85
6.1 Diagrammatic representation of the one loop terms (6.22) and (6.25). Dashed lines denote δX modes, while wiggly lines denote vector field A_+ modes. The small bullets denote the interaction (6.21). 102
6.2 Ratio $\mathcal{R}_A$ for the $X = \phi$ case, as a function of ξ. The ratio is evaluated for a fixed mode of the size of the Planck pivot scale (due to approximate scale invariance, nearly the same bound is obtained at smaller scales). The different curves shown correspond to different values of the rescaled time $x \equiv -k\tau$ at which $\mathcal{R}_A$ is evaluated. For instance $x_{0.1}$ indicates that $\mathcal{R}_A$ is evaluated when the energy density in that mode is 10% of the peaked value that it had previously assumed (as shown in Figure 3.1, the energy density in one given mode reaches a peak value, and it then decreases). 104
6.3 Ratio R_A (left panel) and R_A (right panel) for $\delta = 0.2$ and for varying ξ_*. The different lines correspond to different times at which the ratios are evaluated. 106
6.4 Ratio R_A (left panel) and R_A (right panel) for $\delta = 0.5$ and for varying ξ_*. The different lines correspond to different times at which the ratios are evaluated. 106
B.1 Total Energy density in the gauge field, rescaled by $\epsilon_\phi \, \rho_\phi$, as a function of time, for fixed values of ξ_* 137

C.1 Exact (black solid lines) vs. approximate (purple dashed lines; eq. (C.66)) expression for the scalar (left panel) and tensor (right panel) bispectrum, for isosceles triangles, $k_2 = k_3$, and for $\xi_* = 5$ and $\delta = 0.5$. The black (purple) dot indicates the triangle for which the exact (approximate) bispectrum is maximum. The contour lines indicate the triangles for which the bispectrum evaluates to (from inner to outer, respectively) a fraction of $0.9, 0.7, 0.5, 0.3, 0.2$ than the maximum value of the exact bispectrum. The red line at $x_2/x_1 = 1$, indicates the equilateral triangles, while the lower slope $x_2 = x_1/2$ line indicates folded triangles (smaller ratios are not possible for isosceles triangles). 153

C.2 Left (right) panel: parameter $r_\zeta(k)$ ($r_+(k)$) for the greatest value of ξ_* used in the previous figures, for $\delta = 0.2$, 0.5 and for $\epsilon_\phi = 10^{-5}$. 156

D.1 Fraction of the universe that collapses to a PBH for any given mode, as a function of the ratio between the root-mean-square of scalar curvature and critical curvature value. The same power spectrum results in a much greater PBH fraction in the case of χ^2 statistics with respect to a Gaussian statistics. 160

D.2 Correction factor on the power spectrum, $\mathcal{F}$, as a function of the number of e-folds of inflation, for a linear potential, and for an inflaton-gauge coupling that saturates the Planck bounds. The solid line is obtained from generic eq. (D.16) which is for both negligible and strong backreaction regimes. The dashed line uses the negligible backreaction approximation in (D.17) which results in an incorrect expression due to overestimation of suppression. 163

E.1 Power spectrum of the pseudo-scalar $\delta\sigma$ sourced by the gauge field, for two specific values of δ and ξ_*. The time τ/τ_* is chosen to be the moment at which the total energy density in the gauge field has decreased to 10% than the value it had at its peak. The red dots are the values obtained from a numerical evolution of eq. (E.29). The blue solid line is the fitting function (E.30). 172

Chapter 1

Introduction

" The effort to understand the universe is one of the very few things which lifts human life a little above the level of farce and gives it some of the grace of tragedy." Steven Weinberg

Historically, the modern cosmology era can be traced back to the discovery of the Cosmic Microwave Background (CMB) radiation in the mid 1960s [1]. The CMB radiation was emitted about 380,000 years after the Big Bang, when protons and electrons in the universe combined to form hydrogen atoms and the universe became transparent to radiation. Hence CMB carries valuable information about our universe at that early time. A number of satellite, balloon and ground missions have studied its properties with high accuracy, allowing us to test different cosmological theories. Following the discovery of the CMB, there has been tremendous amount of effort to scan our universe in different length and energy scales via various experiments such as Lyman-α forest, supernovae, γ-ray observations and galaxy surveys. The precise measurements had astonishing results: It has been revealed that most of the current energy content of our universe is in the form of mysterious "dark energy", which is responsible for the present accelerated expansion of the universe. Moreover, inter- and intra-galactic observations have also shown that, besides dark energy, the universe is filled with dark matter (a particle that does not interact with light, and which therefore cannot be directly seen, but only inferred from its gravitational effects), in an amount which is about 5 times

greater than that of regular matter that we are made of.

The idea that the energy content of the universe determines its expansion, and ultimately its fate, has been known since the application of GR to distinct spacetimes, starting around 1920s. This is why the questions in cosmology and particle physics have overlapped. In result of this fascinating conclusion, that observations conducted at largest scales can provide information on the elementary particles, and vice versa, the universe emerged as the largest and richest particle physics laboratory. Since the energies in the early universe are much greater than those that we can produce on terrestrial laboratories, this gives us a unique opportunity to study the laws of nature in a regime which cannot be accessed in any other way.

CMB observations have also shown that the conventional Big Bang picture (namely, the generation of a thermal bath starting from an initial "explosion") is not complete. The CMB is extremely uniform, with fluctuations of only about 10^{-5} from the average. This homogeneity cannot be obtained in a universe filled with only matter and radiation, but it can be explained by a period of accelerated expansion [2]. The field responsible for the acceleration, denoted as "inflaton", produces primordial density perturbations with properties in excellent agreement with observations. When inflation ended, the inflaton decayed by forming an extremely dense, energetic and expanding plasma, which characterizes the Big Bang phase. Nowadays, inflation is widely accepted as the first stage of standard cosmology. Several details of inflation remain to be understood and proven experimentally.

Having a prolonged accelerated expansion requires that the inflaton potential is extremely flat. In generic models, the flatness of the potential can be spoiled by quantum loop corrections, that originate from the inflaton couplings to other fields. In the class of models of axion inflation, the inflaton is assumed to have only derivative couplings to other fields. As a consequence, quantum loops involving these interactions do not modify the inflaton potential. Namely, since the couplings are invariant under the shift $\phi \to \phi + \text{constant}$, they cannot generate an inflaton potential at the perturtbative level. A shift symmetric coupling of an axion to an anomalous gauge field can however generate a potential at the nonperturbative level [5]. This potential has periodicity $\phi \to \phi + 2\pi f$, where f is a quantity of mass dimension one denoted as axion decay constant.[1] The

[1] The reason for the name is that the operator that couples the axion to gauge fields has the form

original model of axion inflation, denoted as natural inflation [3], requires an axion scale greater than the Planck scale [4], which might be problematic in quantum gravity [7]. We discuss in Appendix A how a super-Planckian scale can be generated starting from two or more axions with sub-Planckian scale.

As indicated above, due to symmetry restrictions, there are two mass-dimension-5-operators that might have role in axion physics. One couples axion to gauge fields, $\mathcal{L}_{\text{int, gauge}} = \frac{\alpha}{4f}\phi F\tilde{F}$, and the other to fermions, $\mathcal{L}_{\text{int, fermion}} = \frac{1}{f}\,\bar{\psi}\,\gamma^{\mu}\,\gamma_5\,\psi\,\partial_{\mu}\phi$. This thesis studies the operator that couples an axion to gauge fields during inflation. We have studied various aspects of this operator and its distinct phenomenological signatures at different length and energy scales of our universe. During the inflationary expansion, this chiral coupling introduces a modification to the dispersion relation of the gauge field that has opposite sign for the two helicities. This results in an amplification of the helicity for which this contribution is negative, starting from a few efolds before horizon crossing. On the other hand, the other helicity remains in an unexcited state. In result of this unequal amplification of the different helicites, the model breaks parity and generate correlators that vanish when parity is conserved (specifically TB and EB correlators where the T is the temperature anisotropy, E and B are the gradient and curl of the CMB polarization). In addition, because the amplified helicity mode generates scalar and tensor particles in a two-to-one fashion (schematically $\delta A + \delta A \to \delta\phi$ and $\delta A + \delta A \to \delta g^{\text{TT}}$), the sourced scalar and tensor modes strongly deviate from gaussian statistics. This results in Non-Gaussian signals in various cosmological observables, one remarkable correlation being BBB. The signatures can be detected for a wide spectrum of scales depending on the parameters of the model. They consist of the parity violation in tensor sector via primordial chiral GWs, breaking the direct link between tensor-to-scalar-ratio and the energy scale of inflation, efficient PBH production with amplified non-Gaussian density fluctuations, CMB distortion and GW background detectable at spatial and terrestrial interferometers. It is remarkable that this rich phenomenology can arise from a single operator.

The outline of the thesis is as follows : In Chapter 2, we summarized the inflationary cosmology and provide relevant concepts, observables and parameters that would be

$\frac{\phi}{f}F\tilde{F}$, where F is the gauge field strength, and $\tilde{F}$ its dual. We then see that $\frac{1}{f}$ also controls the decay rate of the axion to gauge fields.

used in the following chapters extensively. We review classical and quantum aspects of the simplest models of inflation, namely in the case of a single slowly rolling scalar field inflaton. Chapter 3 is devoted to the study of the modification of the mode function of Abelian gauge fields due to their chiral coupling to an axion. We study this coupling both for the case in which axion is the inflaton, and for the case in which axion is a field different from the inflaton and it evolves for only a limited portion of inflation (In the second case, the axion has negligible energy as compared to that of the inflaton; such a field is denoted in the literature as "spectator" field.). In Chapter 4, we study the phenomenology of this axion-gauge coupling at the largest observable scales. We show that in the spectator axion case, it is possible to produce sourced [2] GWs at CMB scales that dominate over the GWs from vacuum fluctuations of the metric without producing too much sourced Non-Gaussian density fluctuations. The sourced perturbations in this model have distinctive properties that allow to distinguish them from the standard vacuum modes. Chapter 5 is devoted to the small scale phenomenology, specifically GWs detectable at gravitational interferometers such as Pulsar Timing Arrays (PTA), LISA and LIGO scanning different frequencies of GW spectrum from nHz to tens of Hz. We show that this mechanism can leave detectable imprints on these interferometers, without producing too many primordial black holes (PBHs). We devote Chapter 6 to the verification of our findings under various constraints including backreaction and quantum corrections. We determine the regions of validity in perturbative particle production mechanism and show our results are in these regions. Chapter 7 is for summary, conclusions and potential directions. We have detailed appendices for Axion inflation and every corresponding chapter in the main text except Chapters 1 and 2).

In this thesis, the following conventions are followed for physical quantities and notation: $\hbar = c = 1$, $M_p = \frac{1}{\sqrt{8\pi G_N}} \simeq 2.44 \cdot 10^{18}$ GeV, where M_p is the reduced Planck Mass and G_N is the Newton's constant. Greek indices $(\mu, \nu, \alpha, ..)$ denote spacetime labels and Latin indices (i, j, k,...) denote spatial coordinates. For repeated indices, summation is assumed. We use "density" fluctuations/perturbations and "scalar" fluctuations/perturbations, also Abelian gauge field and vector field, and also axion and psuedo-scalar interchangeably. The metric convention is (- + + +).

[2] By sourced perutrbations, we mean those produced by the gauge field through inverse decay process. By vacuum perturbations, those produced by the inflationary expansion irrespectively of interactions.

Chapter 2

Inflationary Cosmology

"Despite its name, the big bang theory is not really a theory of a bang at all. It is really only a theory of the aftermath of a bang." Alan Guth

Although the standard Big Bang model gives reasonably satisfactory description for the evolution of the universe after Big-Bang Nucleosynthesis (BBN), it has conceptual problems in explaining the origins of the hot and dense plasma stage and the CMB results. Today, inflation is the most compelling early universe scenario to explain the primordial universe. The generic inflationary predictions are in excellent agreement with various experiments.

According to the inflationary scenario, the universe experienced a rapid and accelerated spatial expansion for a period before BBN. As a result, for a long enough inflationary era, the regions in the different parts of the sky, which are assumed to be causally disconnected in standard Big Bang scenario, were actually in causal contact in the very early universe. Furthermore, inflation erases any previous inhomogeneities (if there were) and relics. During inflation, tiny scalar and tensor perturbations are generated by the inflaton and metric fluctuations with nearly identical amplitude at all scales. These perturbations are stretched to out of the causal horizon and become frozen, until they re-enter the horizon after inflation, to construct the seeds of the inhomogeneities.

Although it is possible to realize inflation with extremely low energy scale, it can

be as high as $10^{16}\,\mathrm{GeV}$, which shows that inflation is an important and probably the only probe for such high energy levels that are not accessible on terrestrial experiments. Inflation has passed successfully all the tests up to now and many of its features are still waiting to be understood theoretically and proven experimentally.

We devote this Chapter to briefly review the modern cosmology starting from Big Bang picture. We summarize the fundamentals of inflationary cosmology at the classical and quantum level using the simplest inflationary models with a single slowly rolling scalar field. This Chapter is mostly based on [60, 61, 62]

2.1 Big Bang summary and problems

2.1.1 Homogenous and Isotropic Universe and Big Bang Framework

The current universe is homogenous and isotropic at the largest observable scales. Moreover, there are numerous evidences that the universe was more homogenous at early times at all scales. It is thought that the inhomogeneities that exist at smaller scales in the present universe, such as stars ($\delta\rho/\rho \sim 10^{30}$), galaxies ($\delta\rho/\rho \sim 10^{5}$), clusters of galaxies ($\delta\rho/\rho \sim 10 - 10^{3}$), have been seeded by tiny fluctuations ($\sim 10^{-5}$) that have grown rapidly due to gravitational interaction.

The maximally symmetric spacetime satisfying this cosmic principle (homogeneity and isotropy) is the Friedmann-Lemaitre-Robertson-Walker (FLRW) metric

$$ds^2 = -dt^2 + a(t)^2 \left[\frac{dr^2}{1 - K\,r^2} + r^2 d\theta^2 + r^2\,\sin\theta^2 d\phi^2\right] \tag{2.1}$$

where ds denotes the differential line element, a(t) the scale factor, t is physical time and $\{r,\,\theta,\,\text{and}\,\phi\}$ are comoving coordinates of the spherical coordinate system. The constant K is the curvature signature which is -1 for open, 0 for flat and $+1$ for closed geometry.

We also introduce "conformal time" which is another time variable that is frequently used in expanding spacetimes.

$$d\tau \equiv \frac{dt}{a(t)} = \frac{d\ln a}{a\,H} \tag{2.2}$$

The evolution of the universe can be determined from the Einstein equations

$$G_{\mu\nu} = R_{\mu\nu} - \frac{1}{2} R\, g_{\mu\nu} = \frac{1}{M_p^2}\, T_{\mu\nu} \quad , \tag{2.3}$$

where $G_{\mu\nu}$ is Einstein tensor, $R_{\mu\nu}$ is the Ricci tensor ($R_{\mu\nu} = R^{\lambda}_{\mu\lambda\nu}$) [1], $g_{\mu\nu}$ is the metric, R is the Ricci scalar ($R \equiv g_{\mu\nu}\, R^{\mu\nu}$) and $T_{\mu\nu}$ is the energy momentum tensor. Using eq (2.3) with perfect fluid assumption for the contents filling the universe, ie. $T^{\mu}_{\nu} = (-\rho, P, P, P)$, we have

$$\begin{aligned} H^2 &\equiv \left(\frac{\dot{a}}{a}\right)^2 = \frac{\rho}{3M_p^2} - \frac{K}{a^2} \\ \frac{\ddot{a}}{a} &= -\frac{\rho + 3P}{6M_p^2} \end{aligned} \tag{2.4}$$

where H is the Hubble rate.

These equations combined to give energy conservation/continuity equation as [2]

$$\dot{\rho} + 3H(\rho + P) = \dot{\rho} + 3H\rho\,(1 + w) = 0 \tag{2.6}$$

where above w is the equation of state defined as $w \equiv \frac{P}{\rho}$. This conservation equation is valid for every independently evolving matter content. For constant w, the above equation is solved analytically as

$$\rho(t) = \rho_i \left(\frac{a_i}{a}\right)^{3(1+w)} \tag{2.7}$$

We summarize the equation of state and the scaling of energy density as a function of scale factor for some types of energy content as follows

- Ultra-relativistic gas (Radiation) : $w = 1/3 \;\; \rightarrow \;\; \rho \propto a^{-4}$
- Non-relativistic Dust (Matter) : $w = 0 \;\; \rightarrow \;\; \rho \propto a^{-3}$
- Cosmological Constant : $w = -1 \;\; \rightarrow \;\; \rho = \text{const.}$

The physical interpretation of the scalings above can be expressed as follows: For radiation, in addition to the dilution of the particle density with the expansion of the volume

[1] $R^{\lambda}_{\sigma\,\mu\,\nu} = \partial_\mu \Gamma^{\lambda}_{\sigma\nu} - \partial_\nu \Gamma^{\lambda}_{\sigma\mu} + \Gamma^{\lambda}_{\mu\rho}\Gamma^{\rho}_{\nu\sigma} - \Gamma^{\lambda}_{\nu\rho}\Gamma^{\rho}_{\mu\sigma}$, where $\Gamma^{\mu}_{\nu\lambda} = \frac{1}{2} g^{\mu\rho}\left(\frac{\partial g_{\rho\nu}}{\partial x^{\lambda}} + \frac{\partial g_{\rho\lambda}}{\partial x^{\nu}} - \frac{\partial g_{\nu\lambda}}{\partial x^{\rho}}\right)$ are the so-called Christoffel symbols.

[2] This equation can be obtained from thermodynamics in the case entropy conservation as follows:

$$\begin{aligned} dU &= -P\,dV \\ d(\rho V) = \dot{\rho}\cdot V dt + \rho dV &= -P\,dV \quad \Rightarrow \quad \dot{\rho} = -\frac{(\rho + P)\,dV}{V\,dt} = -3H(\rho + P) \end{aligned} \tag{2.5}$$

$\propto a^{-3}$, the energy of individual photons decrease with $\propto a^{-1}$ as their wavelengths are stretched by the expansion. For non-relativistic dust, the density gets diluted with the volume, so it has a^{-3} dependence. For cosmological constant, it is by definition inert to cosmological expansion.

If the energy density is dominated by one of the energy contents indicated above, the time dependence of the scale factor and of the Hubble parameter can be written as

- Radiation Domination : $a \propto t^{1/2}$, $H = \frac{1}{2t}$ and $a \propto \tau$
- Matter Domination : $a \propto t^{2/3}$, $H = \frac{2}{3t}$ and $a \propto \tau^2$
- Cosmological Constant : $a \propto \mathrm{e}^{\mathrm{Ht}}$, $H = \text{const.}$ and $a \propto -1/H\tau$

From the expressions given above, when the evolution of the universe is traced back to the earliest times, assuming that the cosmological constant does not dominate from the beginning, the scale factor becomes zero for some initial time independent of the value of K term. Even though this trace back cannot be trusted very close to the singularity, which requires infinite energy density, historically this moment of singularity is dubbed as Big Bang.

Our universe was radiation dominated at very early stages (starting at least from the BBN era), then became matter dominated and recently it has been dominated by a source leading to accelerated expansion, with an equation of state equal or very close to that of a cosmological constant. The Cosmic Microwave Background radiation reveals that the universe was hot and dense in the early stages, with full of ultra-relativistic particles. Due to adiabatic expansion, the entropy is conserved, and the temperature is related with the scale factor as

$$g_f\, T_f^3\, a(t_f)^3 = g_i\, T_i^3\, a(t_i)^3 \;\; \Rightarrow \;\; T \propto g^{-1/3}\, a^{-1} \tag{2.8}$$

where "g" denotes the number of degrees of freedom in the relativistic plasma.

With the expansion, the universe cooled down and underwent multiple phase transitions (PTs), such as (if there is) the breaking of some higher symmetry of Grand Unified Theories (GUTs) at $t \sim 10^{-36}s (T \sim 10^{15}\text{GeV})$, electroweak PT at $t \sim 10^{-10}s (T \sim$ 100GeV) and Quantum Chromodynamics (QCD) PT at $t \sim 10^{-5}s (T \sim 300$ MeV). Around $t \sim 1s$ ($T \sim$ MeV), the neutrinos decouple from photon gas, and later Big

Bang Nucleosynthesis happen around $10 - 0.1$ MeV. Afterwards, ions combine with the electrons and make the plasma in the universe neutral. As a result, light decouples from matter, and it propagates almost freely carrying valuable information about that early moment [3]. This process is called as last scattering and occurs around $t \sim 380,000$ years ($T \sim 0.3$eV). This summarized some cornerstones in the evolution of the universe.

2.1.2 The Shortcomings of standard Big Bang Framework

(i) Horizon Problem

In FLRW geometry, the physical distance covered by a particle traveling with the speed of light, from some initial time 0 to t, is defined as "particle horizon" or simply "horizon" and it is given as

$$R_H(t) = a(t) \int_0^t \frac{dt'}{a(t')} = \int_0^a \frac{da'}{a'} \frac{1}{a'H(a')} \tag{2.9}$$

This value gives the distance between causally connected regions. For radiation and non-relativistic matter, $R_H(t) = \frac{\mathcal{O}(1)}{H}$. For all energy content for which time is related with the scale factor by a power law, the particle horizon is determined by some $\mathcal{O}(1)$ numerical factor times inverse Hubble parameter. Therefore, "Hubble radius", defined as $\frac{1}{H}$, is the natural scale for causality.

The physical scales grow with the scale factor ($\propto a$), but the causal horizon, which determines the max available distance for the interactions that obey Lorentz symmetry, grows as $\mathcal{O}(1)/H$. In result, the ratio of the horizon to physical scales evaluates to $\mathcal{O}(1)/aH$, which increases with time in both radiation and matter dominated universe, which means that the horizon grows faster with respect to a physical mode. Therefore, the modes that are in our causal contact today were not in causal contact in the past. They were much larger than the past horizon scale.

When the CMB is measured today, the signal for these large modes is coming from numerous causally disconnected horizons of the last scattering surface! Neglecting the recent cosmological constant domination and using eq (2.1.1), one can roughly calculate the number of causally disconnected regions inside a physical mode at the last scattering

[3] The energy density of radiation and matter become comparable around $t \sim 5 \cdot 10^4$ years ($T \sim eV$)

surface that corresponds to largest scales today as

$$\mathcal{N}_{\text{independent}} \gtrsim \left(\frac{a_{\text{CMB}}\, H_{\text{CMB}}}{a_0\, H_0}\right)^3 \gtrsim \left(\frac{T_{\text{CMB}}}{T_0}\right)^{3/2} \gtrsim 10^5 \tag{2.10}$$

This result puts a huge question mark about standard Big Bang framework. Because if there are $\mathcal{O}(10^5)$ causally independent regions when CMB was decoupled, how could such a perfect homogeneity can be satisfied from these independent regions within the Big Bang framework?

(ii) Flatness Problem

For observing the flatness problem, one can start expressing eq (2.5) as follows

$$\frac{d\ln\rho}{d\ln a} = -3(1+w) \tag{2.11}$$

The Friedmann equation (2.4) can be written as

$$1-\Omega = -\frac{K}{a^2} \tag{2.12}$$

where $\Omega \equiv \frac{\rho}{\rho_{\text{crit}}}$ and $\rho_{\text{crit}} = 3H^2M_p^2$. By differentiating the equation above and using eq (2.11), we obtain

$$\frac{d\Omega}{d\ln a} = (1+3w)\Omega(\Omega-1) \tag{2.13}$$

From this expression, we see that $\Omega = 1$ is an unstable equilibrium point. Therefore, one expects that during the course of the evolution of the universe, even if Ω starts near this value, it should deviate significantly from this value. However, Ω is strictly constrained to be around 1 [68].

$$\Omega_K \equiv 1-\Omega = -0.005^{+0.016}_{-0.017} \qquad (95\%, \mathit{Planck\ TT + lowP + lensing}) \tag{2.14}$$

In order to have such a small value today, we observe that the spatial curvature has to be much smaller in the far past. In order to quantify, we start solving the eq (2.13) by assuming that w is constant, and we express the result as a function of "N" (defined as $dN \equiv d\ln a$) for notational simplicity. We obtain

$$\Omega(N) = \frac{\Omega_i}{\Omega_i + (1-\Omega_i)\mathrm{e}^{(1+3w)(N-N_i)}} \tag{2.15}$$

Then we set $N_i = 0$ and revert the eq above for Ω_i, and employ the definition given in (2.14) to get

$$\begin{aligned} \Omega_i &= \frac{\Omega(N_0)\,\mathrm{e}^{(1+3w)N_0}}{(1-\Omega(N_0))+\Omega(N_0)\,\mathrm{e}^{(1+3w)N_0}} \simeq 1-\Omega_{K,0}\,\mathrm{e}^{-(1+3w)N_0} \\ \Omega_{K,i} &\simeq \Omega_{K,0}\,\mathrm{e}^{-(1+3w)N_0} = \Omega_{K,0}\left(\frac{a_i}{a_0}\right)^{1+3w} \end{aligned} \tag{2.16}$$

The current value of the spatial curvature parameter, $\Omega_{K,0}$, is constrained to the level of $\mathcal{O}(10^{-2})$. The last approximate equality arises from this fact. Armed with this, we set $\Omega_{K,0} = 10^{-2}$ and list sample values using the above formula:

- $\Omega_K(N_{\mathrm{CMB}}) \simeq 10^{-5}$ $\quad (w = 0,\ N_0 = \ln(1100))$
- $\Omega_K(N_{\mathrm{BBN}}) \simeq 10^{-22}$ $\quad (w = 1/3,\ N_0 = \ln(\mathrm{MeV}/10^{-4}\mathrm{eV}))$
- $\Omega_K(N_{10^{13}\mathrm{GeV}}) \simeq 10^{-54}$ $\quad (w = 1/3,\ N_0 = \ln(10^{13}\mathrm{GeV}/10^{-4}\mathrm{eV}))$
- $\Omega_K(N_{\mathrm{GUT}}) \simeq 10^{-60}$ $\quad (w = 1/3,\ N_0 = \ln(10^{16}\mathrm{GeV}/10^{-4}\mathrm{eV}))$

In result, Ω_K has to be tuned for more than 50 digits at early times (For Planck scale, it is more than 60 digits) in order to respect the experimental limits today. The flatness problem is this unnatural tuning.

(iii) The Seeds of Inhomogeneities

The above two problems cannot be explained by a causal mechanism in standard Big Bang, but can only be resolved via extremely fine-tuned initial conditions (ie. standard Big Bang can assume the scales outside causal horizon are very homogenous and the spatial flatness is arranged near 50 digits in the early universe). In addition to almost perfect homogeneity, early universe includes small fluctuations that are nearly scale invariant and obey Gaussian distribution. However, again since in Big Bang framework large scales are completely causally independent, it cannot explain this structure via a causal mechanism, but again can only assume it as an initial condition.

2.2 Inflationary Physics at the Classical Level

In order to solve the shortcomings discussed above, inflationary cosmology assumes that there exists an era in which the universe experienced a rapid acceleration before

the conventional Big Bang stage such that the regions that are thought to be causally independent in the standard Big Bang model are in fact in causal contact and the universe becomes locally flat.

In order to have an accelerated universe, one needs $\rho+3P<0$ (see eq (2.4)); in other words, the dominating energy content needs to satisfy an equation of state $w<-1/3$. What species can have an equation of state $w<-1/3$ other than cosmological constant?

Remarkably, a scalar field can realize this. A homogenous scalar field dominating the energy momentum content of the universe has the action

$$S=\int d^4x\left[\frac{M_p^2}{2}R-\frac{1}{2}g^{\mu\nu}\partial_\mu\varphi\,\partial_\nu\varphi-V(\varphi)\right]\ , \tag{2.17}$$

where R is the Ricci scalar, φ is the homogenous scalar field and V is the potential energy of the field. This field driving the inflation, and dominating the energy density is called as "inflaton". The energy density and pressure of the inflaton are given by

$$\begin{aligned}\rho &= \frac{\dot\varphi^2}{2}+V\\ P &= \frac{\dot\varphi^2}{2}-V\ ,\end{aligned} \tag{2.18}$$

and the equation of state gets the form

$$w=\frac{P}{\rho}=\frac{\frac{\dot\varphi^2}{2}-V}{\frac{\dot\varphi^2}{2}+V} \tag{2.19}$$

Accelerated expansion, $w<-1/3$, is possible for $\dot\phi^2<V$. Consistency with CMB results actually requires $\dot\phi^2\ll V$. In this case, $H\equiv H_{\rm inf}\simeq$ constant and $a\simeq a_i\,\mathrm{e}^{\int H(t')dt'}\simeq a_i\,\mathrm{e}^{H(t-t_i)}$.

After inflation starts, the spatial curvature decreases exponentially and eq (2.4) for homogenous scalar field becomes

$$H^2=\frac{1}{3M_p^2}\left[\frac{\dot\varphi^2}{2}+V(\varphi)\right]\ , \tag{2.20}$$

and the energy conservation eq (2.5) gets the form

$$\dot\rho+3H\rho\,\dot\varphi^2=0\quad\Rightarrow\quad\left[\ddot\varphi+3H\dot\varphi+V'(\varphi)\right]\dot\varphi=0 \tag{2.21}$$

where dot denotes derivative wrt cosmic time and prime denotes derivative wrt the field φ. The Friedman eq and the energy conservation together give the evolution equation of the scalar field. This equation can also be obtained by varying the action wrt φ as

$$\ddot{\varphi} + 3H\dot{\varphi} + V'(\varphi) = 0 \tag{2.22}$$

Here we note that for a wide choice of initial conditions, (for a "flat" enough potential) inflaton catches its *attractor* and continues its evolution on a common trajectory. This means that inflation also erases initial conditions via its attractor behaviour and allows consistent predictions for a given model. In this attractor, the potential energy dominates over kinetic energy and the inflaton rolls slowly through its potential. Therefore in Slow-Roll (SR) approximation the equations governing the evolution get the following form

$$\begin{aligned} H^2 &\simeq \frac{V(\varphi)}{3M_p^2} \\ 3H\dot{\varphi} &\simeq -V'(\varphi) \ . \end{aligned} \tag{2.23}$$

One can define the Slow-Roll (SR) parameters via the Hubble parameter

$$\epsilon_H \equiv -\frac{\dot{H}}{H^2} = \frac{\dot{\varphi}^2}{2H^2M_p^2} \quad , \quad \delta_H \equiv \frac{\ddot{H}}{2H\dot{H}} = \frac{\ddot{\varphi}}{H\dot{\varphi}} \tag{2.24}$$

where dots denote derivative wrt time. The SR parameters can also be defined via the inflaton potential

$$\epsilon_V \equiv \frac{M_p^2}{2}\left(\frac{V'(\varphi)}{V(\varphi)}\right)^2 \simeq \epsilon_H \quad , \quad \eta_V \equiv M_p^2\,\frac{V''(\varphi)}{V(\varphi)} \simeq \epsilon_H - \delta_H \tag{2.25}$$

where prime here denotes derivative with respect to inflaton, denoted as φ. We will use the latter definitions more frequently, so we will drop the subscript "V", and we will write simply ϵ and η from this point on for notational simplicity.

Observe that ϵ is proportional to slope of the potential and it controls the kinetic energy of the inflaton, while η is related to the curvature (mass) of the potential and controls the acceleration of the field. The slow roll conditions are satisfied when both parameters are small during inflation (ie. $\epsilon \ll 1$ and $|\eta| \ll 1$) which requires the potential to be very flat, which results in long enough inflation to cure the problems discussed in the Subsection 2.1.2.

As long as the SR parameters are small, inflation proceeds as we see from eq (2.4), with

$$\frac{\ddot{a}}{a} = \dot{H} + H^2 \simeq (1-\epsilon)H^2 > 0 \; . \tag{2.26}$$

When the field reaches near the bottom of its potential, the SR parameters are no longer small, and inflation ends when $\rho = -3P$, namely when $\dot{\varphi}^2_{\rm end} = V(\varphi_{\rm end})$ corresponding to $\epsilon \simeq \mathcal{O}(1)$.

During the inflationary expansion, the amount of spatial growth is expressed conventionally by the number of efolds, "N" , defined as

$$dN \equiv d\ln a = H dt \quad \Rightarrow \quad N_f - N_i = \Delta N = \ln \frac{a_f}{a_i} \tag{2.27}$$

Therefore, 5-efolds mean that the universe has expanded e^5 times in one spatial dimension. It is also conventional that final moment (a_f) is defined as the end of inflation and "N" denotes the number of efolds left until the end of inflation. In terms of field dynamics, one can express the expansion as follows

$$N = \int_t^{t_{\rm end}} H \, d\tilde{t} = \int_\varphi^{\varphi_{\rm end}} \frac{H d\tilde{\varphi}}{\dot{\tilde{\varphi}}} \simeq \frac{1}{M_p^2} \int_{\varphi_{\rm end}}^{\varphi} \frac{V(\tilde{\varphi})}{V'(\tilde{\varphi})} d\tilde{\varphi} \tag{2.28}$$

where prime denotes derivative wrt inflaton and SR expressions given in eq (2.23) are employed in the last equality. Depending on the details of the subsequent stages especially "reheating" [4], the inflationary era is required to be at least 50-60 efolds in order to solve the problems of standard Big Bang era and satisfy a causal contact for the large modes of the observable universe.

During inflation, the expansion almost exponentially grows with time as $a \simeq a_i e^{H(t-t_i)}$, and H being nearly constant. In this era, conformal/comoving quantities are used frequently to factorize the expansion in an overall factor that multiplies the Minkowski

[4] This is the phase connecting the inflationary phase with the radiation dominated era, namely the energy from the inflaton is transferred to ultra-relativistic particles. After inflation ends, the inflaton oscillates at the bottom of the potential and it eventually decays on a timescale given by the inverse of its decay rate. The details of reheating are very model-dependent, and they can vastly change depending on the nature of the inflaton and on its couplings. In all cases, the produced particles ultimately reach thermal equilibrium and set the stage for the conventional standard Big Bang expansion. This details of reheating are extremely important, but they are not the focus of this thesis.

geometry. We already introduced comoving coordinates and conformal time (see eq (2.2)) in the first part of this Chapter. Here we give a short math interlude for some comoving variables that will be used extensively in the rest of the thesis.

The quantity corresponding to the Hubble radius in comoving coordinates is called simply comoving Hubble radius and it is

$$\frac{1}{aH} = \frac{1}{\mathcal{H}} = \frac{1}{a'/a}, \tag{2.29}$$

where prime denotes derivative wrt conformal time. In addition, the comoving particle horizon is defined as

$$\tau_H \equiv \frac{1}{a} R_H(t) \tag{2.30}$$

Finally, we define comoving wavenumber, k, for a given physical length scale, λ as

$$k \equiv \frac{2\pi\, a}{\lambda} \Rightarrow p_{\rm physical} = \frac{k}{a} \tag{2.31}$$

Therefore, $k \gg aH$ means that a physical length scale is deep inside the horizon and $k \ll aH$ deep outside the horizon (superhorizon). During inflation, the conformal time has the following relation $\tau = -\frac{1}{aH}$. Therefore this observation can be expressed with conformal time as follows:

$-k\tau \ll 1 \Rightarrow$ scale is superhorizon

$-k\tau \gg 1 \Rightarrow$ scale is inside the horizon.

Armed with these observations, let us return on how inflation solves the shortcomings of standard Big Bang model:
(i)Horizon problem : In order for inflation to solve the horizon problem, the largest scales that we observe today should be in causal contact in the far past (during inflation). Since $H_{\rm inf} \simeq$ const., the mode with a wavelength comparable to the Hubble radius today, $1/H_0$ (subscript "0" indicates current value), should be in inflationary horizon, which translates as

$$\begin{aligned} \frac{1}{H_0}\left(\frac{a_{\rm i}}{a_0}\right) &= \frac{1}{H_0}\left(\frac{a_i}{a_{\rm end}}\right)\left(\frac{a_{\rm end}}{a_0}\right) \lesssim \frac{1}{H_i} \\ \frac{1}{H_0}\,{\rm e}^{-N_{\rm tot}}\left(\frac{a_{\rm end}}{a_0}\right) &\simeq \frac{1}{H_0}\,{\rm e}^{-N_{\rm tot}}\left(\frac{T_0}{T_{\rm end}}\right) \lesssim \frac{1}{H_i} \end{aligned} \tag{2.32}$$

where above a_i and $a_{\rm end}$ denotes the beginning and the end of inflation respectively. $H_0 \simeq 10^{-42}$ GeV and assuming $H_i \sim 10^{13}$GeV and $T_{\rm end} \sim 10^{16}$GeV, we find $N_{\rm tot} \gtrsim 60$.

(ii) Flatness problem: As shown in the Subsection 2.1.2, in order for inflation to solve the flatness problem, the spatial curvature parameter $\Omega_K = -K/(a^2H^2)$ has to decrease very roughly $\mathcal{O}(10^{-50})$ times at the end of inflation in order to solve the flatness problem. This is indeed the case in the inflationary scenario because during inflation we have $\frac{\Omega_{K,\rm end}}{\Omega_{K_i}} = \left(\frac{a_{\rm end}H{\rm end}}{a_i\,H_i}\right)^{-2} \simeq {\rm e}^{-2N_{\rm tot}}$. We see that 50 digits of fine-tuning can be removed by $N_{\rm tot} \gtrsim 60$ efolds of inflation depending on the details of the subsequent evolution of the universe.

2.3 Inflationary Physics at the Quantum Level

Although inflation has been first proposed to solve the horizon and flatness problems of standard Big Bang model, it became a theory with strong predictive power after it was understood that the small quantum fluctuations could be the seeds of the inhomogeneities of our universe. During the inflationary phase, these perturbations are stretched, and leave the horizon. Outside the causal horizon, their amplitude is frozen. However, these perturbations re-enter the horizon during radiation and matter domination eras because in those regimes, the horizon grows faster than physical scales. As a result, these perturbations lead to tiny inhomogeneities in the matter content. The amount of inhomogeneity is conventionally expressed in terms of a dimensionless parameter called density contrast, $\delta \equiv \frac{\rho(x)-\bar{\rho}}{\bar{\rho}}$. The density contrast grows relatively slow in the radiation dominated era (with logarithmic dependence on the scale factor), but really fast in the matter dominated era (proportional to the scale factor). When δ becomes $\mathcal{O}(1)$, it grows even faster due to nonlinear evolution. These clumps of matter decouple from the expansion and the rest of the universe when the internal gravitational attraction is stronger than the stretching due to the Hubble expansion. In this subsection, we give a brief overview of the generation of scalar and tensor type primordial perturbations during inflation. For this subsection, we will mostly follow Refs. [60, 62].

In the previous section, we focus on the effects of the inflation at the classical level and neglect the quantum nature of the fields in our formulations, and the effects of

these fluctuations on the background evolution. The quantum fluctuations really do not modify the background evolution as long as

- The energy scale of inflation is low enough so that "quantum jumps" of the inflaton, $\frac{\Delta\phi}{\Delta N} \sim \mathcal{O}(H)$, are subdominant wrt the classical evolution $\left(\frac{\Delta\phi}{\Delta N} \simeq \frac{dV/d\phi}{3H^2}\right)$ (See [63] for details.)

- The inflaton does not enter a Ultra-Slow-Roll phase [5] (See [64] for details.)

Assuming that the inflaton slowly rolls through its potential (ie. the second bullet above is satisfied automatically), let us show that the stochastic quantum diffusion jumps have subdominant effect with respect to the classical force term $(V'(\varphi)/H^2)$.

$$\left|\frac{F_{\rm quantum}}{F_{\rm classical}}\right| \simeq \left|\frac{H}{V'/3H^2}\right| \simeq \left|\frac{H^2}{3\dot{\phi}}\right| \simeq \frac{2\pi}{3}\sqrt{P_{\rm pert}} \lll 1 \ , \tag{2.33}$$

where we employ eq (2.23) as we assume SR conditions are satisfied. We have also used $P_{\rm pert} = \left(\frac{H}{2\pi}\right)^2 \frac{H^2}{\dot{\phi}^2}$ for the power spectrum of the curvature perturbations generated during slow roll inflation. Observationally, $P_{\rm pert} = \mathcal{O}(10^{-9})$ [6].

Although they play a subdominant role for the background evolution of the universe during inflation (see eq (2.4)), these quantum fluctuations become the seeds of the structure (inhomogeneities) when they re-enter the horizon after the inflationary expansion. In addition, quantum fluctuations can reveal extremely valuable information about the fundamental properties of the inflationary era and of high energy physics. The generic treatment of perturbations require various technical details which will be discussed in the various chapters of this thesis. Therefore, this section focuses on the basics of the inflationary observables.

The General Relativity is concisely expressed as "Spacetime tells matter how to move; matter tells spacetime how to curve." by Wheeler's words. (In GR, "matter"

[5] When the inflaton potential is extremely flat, the inflaton enters Ultra-Slow-Phase (USR). In this phase, although one of the SR parameters, ϵ, is tiny, the other one η is not. This phase is qualitatively very different than SR phase because during USR, quantum diffusion becomes important and statistical features of the perturbations change. [64]

[6] It is possible that potential might be flatter or steeper for the modes produced after CMB scales and this changes the $P_{\rm pert}$, but as long as $P_{\rm pert} \ll 1$, quantum fluctuations will only negligibly change the background evolution.

is used for anything but the gravitational field.) This is not any different during inflationary expansion and both matter and metric (geometry) perturbations should be considered together. For an inflationary model with a single scalar field inflaton, there are 11 perturbations in total. One of them belongs to the inflaton, $\varphi = \phi(t) + \delta\phi(t, \vec{x})$, $\phi(t)$ denoting the homogenous inflaton background. 10 of these belong to the metric perturbations. As it is symmetric, it has $\frac{n\,(n+1)}{2}$ perturbations. Among these 10 perturbations, 4 of them are scalar, 4 (2×2) of them are transverse vector and 2 of them are transverse traceless tensor. At first order in perturbation theory, scalar, vector and tensor type perturbations decouple from each other and can be analyzed separately [62].

$$g_{\mu\nu} = a^2(t) \begin{pmatrix} -(1+2\Phi) & \partial_i B + B_i \\ \partial_i B + B_i & (1-2\Psi)\delta_{ij} + D_{ij}E + \partial_{(i}E_{j)} + h_{ij}^{\mathrm{TT}} \end{pmatrix} , \tag{2.34}$$

where $D_{ij} = \left(\partial_i\partial_j - \frac{\delta_{ij}}{3}\nabla^2\right)$, and Φ, B, Ψ, E are scalar, B_i and E_j are transverse vectors and h_{ij}^{TT} is transverse and traceless tensor. Not all these perturbations correspond to physically independent propagating modes. Two combinations of the scalar perturbations and one combination of vector perturbations are not dynamical, so they can be determined by other fields. From the remaining 7 perturbations, 4 modes (2 scalar and 2 vector modes) can be eliminated through a change of coordinates and this leaves 3 independent physical modes: a (gauge invariant) scalar curvature and the two polarizations of a tensor gravitational wave.

2.3.1 Scalar Perturbations

The gauge invariant curvature perturbation is conventionally defined as [7]

$$\zeta \equiv \Psi + H\frac{\delta\rho}{\dot{\rho}} \ , \tag{2.35}$$

where $\delta\rho$ is the perturbation in energy density and Ψ is one of the spatial scalar perturbation given in (2.34). Although the details of the reheating and the evolution from the end of inflation until today are not known precisely, we can still have unambiguous predictions about the primordial perturbations because "independent from the equation

[7] Another conventional definition, for comoving hypersurfaces, is $\mathcal{R} \equiv \Psi + H\frac{\delta\phi}{\dot{\phi}}$. For superhorizon scales, both these variables become equivalent $\zeta \simeq \mathcal{R}$

of state inside the horizon", the curvature modes are conserved outside the horizon (see Ref. [60, 62]).

The only dynamical scalar degree of freedom reveals valuable information about the inflationary era through its distinct correlators. The dimensionless power spectrum of ζ, P_ζ, is defined from the two-point function as

$$\left\langle \zeta_{\vec{k}}\, \zeta_{\vec{k}'} \right\rangle \equiv \frac{2\pi^2}{k^3}\, P_\zeta(\vec{k})\, \delta^{(3)}(\vec{k}+\vec{k}')\ , \tag{2.36}$$

where $\zeta_{\vec{k}}$ is the Fourier transform of $\zeta(\vec{x})$ and $k \equiv |\vec{k}|$, and $\delta^{(3)}$ is the 3-dimensional Dirac-Delta function, which implies momentum conservation. If fluctuations are isotropic, namely they are rotationally invariant, then power spectrum only depends on the magnitude of the wavenumber $\vec{k}$, ie. $P_\zeta(\vec{k}) = P_\zeta(k)$.

The power spectrum is conventionally parametrized as

$$P_\zeta(k) = \mathcal{A}_s \left(\frac{k}{k_*}\right)^{n_s - 1 + \frac{1}{2}\alpha_s \ln(k/k_*)}\ , \tag{2.37}$$

where $\mathcal{A}_s$ is the amplitude at pivot scale, n_s is the scalar spectral index, α_s is the running of the scalar spectral index, and k_* is the pivot wavenumber which is usually taken as $k_* = 0.05\,\mathrm{Mpc}^{-1}$ or $0.002\,\mathrm{Mpc}^{-1}$.

The parameters in Planck '18 (for the pivot scale $k_* = 0.05\mathrm{Mpc}^{-1}$) are given as follows [149]:

- $\mathcal{A}_s = (2.1 \pm 0.03)\cdot 10^{-9}$ $\quad (Planck\ TT,\ TE,\ EE + lowE + lensing)$, 68% CL
- $n_s = 0.9649 \pm 0.0042$ $\quad (Planck\ TT,\ TE,\ EE + lowE + lensing)$, 68% CL
- $\alpha_s = -0.0045 \pm 0.0067$ $\quad (Planck\ TT,\ TE,\ EE + lowE + lensing)$, 68% CL

In slowly rolling single scalar field case, the curvature perturbation is obtained as[8]

$$P_\zeta \simeq \frac{H^4}{4\pi^2\dot{\phi}^2}\left(\frac{k}{k_*}\right)^{2\eta-6\epsilon} \simeq \frac{H^2}{8\pi^2\,\epsilon\,M_p^2}\left(\frac{k}{k_*}\right)^{2\eta-6\epsilon} \tag{2.38}$$

[8] In spatially flat gauge, one can read how it is found as: $\zeta \simeq H\frac{V'\delta\phi}{\dot{\rho}}$, so $P_\zeta \simeq \frac{H^2 V'^2 \langle\delta\phi^2\rangle}{(\dot{\phi}\,\ddot{\phi}+V'\dot{\phi})^2} \simeq \frac{H^4}{4\pi^2\dot{\phi}^2}$, where in the last step we employ that $\delta\phi$ is nearly massless, so its power spectrum is $\left(\frac{H}{2\pi}\right)^2$.

Hence in single scalar field slow roll, $\mathcal{A}_s = \frac{H^2}{8\pi^2 M_p^2}$ and $n_s - 1 = 2\eta - 6\epsilon \ll 1$ [9].

The observed fluctuations in CMB experiments show that they are consistent with a Gaussian distribution. If the primordial signal were completely Gaussian, then one expects all the odd correlators (ie. $\langle\zeta^3\rangle$, $\langle\zeta^5\rangle$, ...) to vanish perfectly. However, although it is suppressed by the strength of the gravity, there exist nonlinear interactions between curvature perturbations. As a result, even single slowly rolling scalar field has nonzero but tiny primordial non-Gaussianity [10]. The detection of non-negligible amount of non-Gaussianity might be a sign of a multifield inflation or the different interactions during inflation. Hence, the bispectrum is an important indicator for primordial non-Gaussianity and also an indicator for the inflationary physics, defined as

$$\langle\zeta_{\vec{k}_1}\,\zeta_{\vec{k}_2}\,\zeta_{\vec{k}_3}\rangle \equiv B_\zeta(k_1,k_2,k_3)\delta^{(3)}(\vec{k}_1+\vec{k}_2+\vec{k}_3) \tag{2.40}$$

where k_i indicate the magnitude of the corresponding vector as $|\vec{k}_i|$, and 3 dimensional Dirac Delta is due to momentum conservation. The 3 momentum vectors satisfy $\vec{k}_1 + \vec{k}_2 + \vec{k}_3 = 0$, and they form a triangle. Therefore, in addition to the amplitude, the bispectrum depends on the "shape" of this triangle and overall scale of the momenta. For example, the slowly rolling single scalar field bispectrum peaks at the squeezed configuration ($k_1 \ll k_2 \simeq k_3$), while as shown in Chapter 4, the bispectrum resulting from the pseudo-scalar vector interaction peaks in the equilateral shape ($k_1 \sim k_2 \sim k_3$). As a result, together with the overall amplitude, the shape and the scale-dependence, the bispectrum conveys valuable information about the inflationary physics.

2.3.2 Tensor Perturbations

Primordial gravitational waves (GWs) is another important physical observable related with the inflationary era. They are the transverse and traceless fluctuations of the metric. Since they are massless, they propagate with the speed of light and have two

[9] The scale dependence can be read off as $\frac{d\ln P}{dlnk} \simeq 4\frac{d\ln H}{d\ln k} - 2\frac{d\ln\dot{\phi}}{d\ln k} = -4\epsilon + 2\eta - 2\epsilon = 2\eta - 6\epsilon$

[10] The non-Gaussianity is usually parametrized by the "nonlinearity parameter" called $f_{\rm NL}$, which can be expanded as

$$\zeta(\vec{x}) = \zeta_G(\vec{x}) + \frac{3}{5}f_{\rm NL}\left(\zeta_G^2 - \langle\zeta_G\rangle\right) + \mathcal{O}(\zeta_G^3) \tag{2.39}$$

where ζ_G is a Gaussian field. The $f_{\rm NL}$ is predicted to be $\mathcal{O}(1)(n_s-1) \simeq (10^{-2})$ for single field SR models.

polarizations $(+, \mathrm{x})$ or in a different basis (L, R). The gravitational wave power spectrum from the two-point function is defined as

$$\left\langle h_\lambda(\vec{k})\, h_{\lambda'}(\vec{k}')\right\rangle = \frac{2\pi^2}{k^3}\, P_\lambda(k)\delta_{\lambda\,\lambda'}\,\delta^{(3)}(\vec{k}+\vec{k}') \tag{2.41}$$

where $\lambda = \{L, R\}$ or $\{+, x\}$, again Dirac Delta implies momentum conservation (or translation invariance) and we assume rotational invarinace (isotropy) so that P_λ depends only on the magnitude of the vector $\vec{k}$. The total power spectrum is obtained by summing over both polarizations.

$$P_{\mathrm{gw}} = P_L + P_R. \tag{2.42}$$

In single scalar field models each polarization has the same strength, namely $P_L = P_R$.

$$P_{\mathrm{gw}} = \frac{2H^2}{\pi^2 M_p^2}\left(\frac{k}{k_*}\right)^{n_T} \tag{2.43}$$

Here n_T is defined as tensor spectral tilt and for single field models it is 2ϵ.

A cosmological observable giving the ratio of the scalar power to tensor power is called as tensor-to-scalar-ratio and defined as

$$r \equiv \frac{P_{\mathrm{gw}}}{P_\zeta} \tag{2.44}$$

Using eqns (2.38 and 2.43), tensor-to-scalar-ratio becomes

$$r \simeq 16\epsilon \tag{2.45}$$

for single field models. Note that with $r\ (\propto \epsilon)$ and $\mathcal{A}_s\ (\propto \frac{V}{\epsilon})$, the energy scale of inflation can be determined as long as GW background is produced by the vacuum fluctuations of the metric. The A_s has been known since COBE experiment, and there is a strong effort to detect the other one. If measured, r also needs to be compared with tensor tilt n_T because in single field models, they satisfy the "consistency relation", $r = 8n_T$. According to the very recent results from the joint analysis of BICEP2/Keck Array and *Planck*, $r < 0.064$ with 95% CL, at the scale $0.002\,\mathrm{Mpc}^{-1}$ [149].

Chapter 3

The Interaction of Axion and Abelian Gauge Field

"Everything which is not forbidden is compulsory."

Axion inflation is a compelling class of inflationary models which was first proposed to protect the flatness of the inflaton potential from large quantum corrections by employing a Pseudo-Nambu-Goldstone-Boson(PNGB), axion, with an approximate shift symmetry (see Appendix A). This symmetry constrains the possible interactions of the axion to other fields. We study the mass-dimension-five-operator, $\frac{1}{f}\phi F_{\mu\nu}\tilde{F}^{\mu\nu}$, that couples axion to gauge fields[1].

This chapter is devoted to the chiral coupling between an axion rolling through its potential and Abelian gauge field during inflation, and becomes a basis for most of the following chapters in this thesis. In result of this rolling, via the chrial coupling, one helicity of the gauge field experiences a tachyonic instability (the square of its frequency becomes negative) around the horizon crossing and gets amplified. In return,

[1] It is immediate to see that this operator is shift symmetric. Since $\Delta S = \int d^4x\sqrt{-g}\ c\cdot F\tilde{F}$ is a complete boundary term (c is an arbitrary constant), as ϕ is shifted by a constant amount, the equations of motion and any perturbative process are not affected by this transformation.

the produced vector particles source scalar and tensor(GW) perturbations in a non-Gaussian two-to-one fashion, schematically $\delta A + \delta A \to \delta\phi$ and $\delta A + \delta A \to \delta g$, and lead to interesting phenomenology for distinct cosmological observations.

The study in this chapter is for a generic pseudo-scalar field, namely axion can either be the inflaton field driving inflationary expansion or a spectator field which constitutes a subdominant portion of the energy density and rolls down thorugh its potential for a limited period of inflation. For the case that the axion is the inflaton, the particle production parameter that controls the vector field amplification evolves adiabatically, but in the spectator case, this parameter can be strongly time-dependent (depending on the choice of the axion potential). For both cases, we explicitly compute the modified mode function (for the amplified helicity) and show the time evolution of the contribution to the energy density from a particular vector field mode. The validity of various approximations to capture this particle production process in the adiabatic evolution case has also been worked out in detail. This chapter is mostly based on the work conducted in Refs. [171, 172]

3.1 Gauge field amplification in Axion Inflation

The portion of the Lagrangian containing Abelian gauge field is

$$\mathcal{L}_A = -\frac{1}{4} F_{\mu\nu} F^{\mu\nu} - \frac{\alpha}{4\,f}\, X\, F_{\mu\nu}\, \tilde{F}^{\mu\nu} \,, \tag{3.1}$$

where X is the pseudo-scalar coupled to the vector field, f is the axion decay constant (or axion scale) and α is a dimensionless coupling constant, $F_{\mu\nu}$ is field strength tensor of the Abelian field and $\tilde{F}_{\mu\nu}$ is the dual tensor of the field strength.

The field strength is defined as

$$F_{\mu\nu} = \partial_\mu A_\nu - \partial_\nu A_\mu \,, \tag{3.2}$$

and dual tensor is defined as

$$\tilde{F}^{\mu\nu} \equiv \frac{\epsilon^{\mu\nu\alpha\beta}}{2\sqrt{-g}} F_{\alpha\beta} \quad , \tag{3.3}$$

where the quantity $\epsilon^{\mu\nu\alpha\beta}$ is totally anti-symmetric, and normalized to $\epsilon^{0123} = 1$.

As indicated, we analyze two cases:

- $X = \phi$ is the inflaton field, and $\dot{\phi}$ evolves adiabatically;
- $X = \sigma$ is a field with an energy density much smaller than that of the inflaton, which experiences a momentary speed-up for a few e-folds during inflation.

We work in the Coulomb gauge, namely $A_0 = \vec{\nabla} \cdot \vec{A} = 0$, and express the vector field with two helicites as

$$\begin{aligned}
\hat{A}_i(\tau, \vec{x}) &= \int \frac{d^3k}{(2\pi)^{3/2}} \, \mathrm{e}^{i\vec{k}\cdot\vec{x}} \hat{A}_i(\tau, \vec{k}) \\
&= \sum_{\lambda=\pm} \int \frac{d^3k}{(2\pi)^{3/2}} \left[\epsilon_i^{(\lambda)}(\vec{k}) \, A_\lambda(\tau, \vec{k}) \, \hat{a}_\lambda\left(\vec{k}\right) \, \mathrm{e}^{i\vec{k}\cdot\vec{x}} + \epsilon_i^{*(\lambda)}(\vec{k}) \, A_\lambda^*(\tau, \vec{k}) \, \hat{a}_\lambda^\dagger\left(\vec{k}\right) \, \mathrm{e}^{-i\vec{k}\cdot\vec{x}} \right] \\
&= \sum_{\lambda=\pm} \int \frac{d^3k}{(2\pi)^{3/2}} \, \mathrm{e}^{i\vec{k}\cdot\vec{x}} \, \epsilon_i^{(\lambda)}(\vec{k}) \, \left[A_\lambda(\tau, \vec{k}) \, \hat{a}_\lambda\left(\vec{k}\right) + A_\lambda^*(\tau, -\vec{k}) \, \hat{a}_\lambda^\dagger\left(-\vec{k}\right) \right] \qquad (3.4)
\end{aligned}$$

where the helicity vectors $\vec{\epsilon}^{(\pm)}$ satisfy $\vec{k} \cdot \vec{\epsilon}^{(\pm)} = 0$, $i\,\vec{k} \times \vec{\epsilon}^{(\pm)} = \pm k\,\vec{\epsilon}^{(\pm)}$, $\vec{\epsilon}^{(\pm)} \cdot \vec{\epsilon}^{(\mp)} = 1$ and $\vec{\epsilon}^{(\pm)} \cdot \vec{\epsilon}^{(\pm)} = 0$. [2] To obtain third line from the second line, we send $\vec{k} \to -\vec{k}$ for the second term in the square bracket and employ $\epsilon^{*\pm}(\vec{k}) = \epsilon^{\pm}(-\vec{k}) = \epsilon^{\mp}(\vec{k})$.

The creation and annihilation operators satisfy the usual commutation relations: $\left[\hat{a}_\lambda\left(\vec{k}\right), \hat{a}_{\lambda'}\left(\vec{p}\right)\right] = 0$, $\left[\hat{a}_\lambda^\dagger\left(\vec{k}\right), \hat{a}_{\lambda'}^\dagger\left(\vec{p}\right)\right] = 0$ and $\left[\hat{a}_\lambda\left(\vec{k}\right), \hat{a}_{\lambda'}^\dagger\left(\vec{p}\right)\right] = \delta(\vec{k} - \vec{p})\delta_{\lambda\,\lambda'}$

The equation of motion for the mode function of the gauge field becomes

$$\left(\partial_\tau^2 + k^2 \pm \frac{2\,k\,\xi}{\tau}\right) A_\pm = 0 \quad , \qquad (3.6)$$

where

$$\xi \equiv \frac{\alpha\,\dot{X}}{2\,f\,H} \qquad (3.7)$$

is the dimensionless particle production parameter, τ is the conformal time, which during inflation is related to the scale factor a by $a = -\frac{1}{H\,\tau}$ at zeroth order in slow roll.

As seen from the last term of the eq (3.6), depending on the sign of ξ, one of the two helicity modes is unstable starting from couple e-folds before horizon crossing. We assume $\xi > 0$, so that the unstable polarization is the + one (recall that $\tau < 0$ during

[2] For an arbitrary vector $\hat{u} = (\sin\theta\cos\phi,\, \sin\theta\sin\phi,\, \cos\theta)$, polarization vectors get the form

$$\vec{\epsilon}^{\,(\pm)}(\hat{u}) = \frac{1}{\sqrt{2}} \left(\cos\theta\,\cos\phi \mp i\,\sin\phi,\, \cos\theta\,\sin\phi \pm i\,\cos\phi,\, -\sin\theta\right) . \qquad (3.5)$$

inflation). This polarization can receive a substantial amplification (this is not the case for the negative helicity mode). The amplification is controlled by ξ, which has a different evolution in the two different cases mentioned above.

3.1.1 Nearly constant gauge field from $\frac{\alpha}{f}\,\phi\,F\,\tilde{F}$

If X is the inflaton field ϕ, which is slowly rolling during inflation, we have $\xi \simeq \frac{\alpha\sqrt{2\,\epsilon_\phi}\,M_p}{2f}$, where ϵ_ϕ is the standard slow roll inflaton parameter. This quantity is changing only at second order in slow roll. Therefore ξ can be approximated as a constant while any single mode (a mode with a given value of k) has a size comparable to the horizon. As we shall see, this is the time range during which a mode is produced, and can lead to potentially observable effects (before its energy is diluted away by the expansion of the universe). However, two different modes $k_1 \neq k_2$ leave the horizon at different moments, so they probe possibly different value of ξ, depending on the value of $\sqrt{\epsilon_\phi}$ at two different times at which the two modes left the horizon. In this case we treat ξ as an adiabatically evolving parameter, denoting by ξ_k the value of ξ assumed when a given mode k left the horizon (this is the constant value of ξ that we take in computing the evolution of that specific mode). [3]

Under the assumption of constant ξ (for a given mode k), eq. (3.6) can be solved analytically. The normalized solution satisfying adiabatic vacuum initial conditions is given in terms of the irregular Coulomb function

$$A_\pm \simeq \frac{1}{\sqrt{2k}}\,H_0^\pm\left(\pm\xi,\,-k\tau\right)\,. \tag{3.8}$$

The approximated equality above is due to the fact that ξ is not exactly constant. In the limit $\xi \gg -k\tau$, this solution is very-well approximated by

$$A_+ \simeq \sqrt{\frac{-\tau}{2}}\left[2\,\mathrm{e}^{\pi\xi}\,\pi^{-1/2}\,K_1\left(\sqrt{-8\,\xi\,k\,\tau}\right) + i\,\mathrm{e}^{-\pi\xi}\,\pi^{1/2}\,I_1\left(\sqrt{-8\,\xi\,k\,\tau}\right)\right]\,, \tag{3.9}$$

where, K_1 and I_1 are modified Bessel functions of second and first types, respectively. Since, $\xi \gtrsim O(1)$ in all phenomenologically interesting cases and the field amplification occurs around horizon crossing, one can further simplify this result by taking the large

[3] Improving over this will provide corrections proportional to the slow roll parameters.

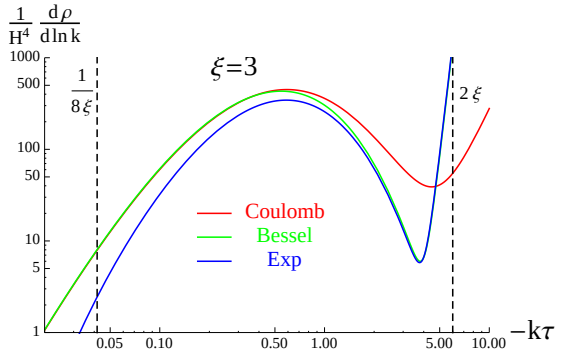

Figure 3.1: Time evolution of the gauge field energy density for a given comoving momentum k for three approximated solutions (3.8), (3.9) and (3.10).

argument limit of Bessel functions

$$A_+ \simeq \frac{1}{\sqrt{2k}}\left(\frac{-k\tau}{2\xi}\right)^{1/4} e^{\pi\xi-2\sqrt{-2\xi k\tau}} + \frac{i}{\sqrt{2k}}\left(\frac{-k\tau}{2^5\xi}\right)^{1/4} e^{-\pi\xi+2\sqrt{-2\xi k\tau}} \quad , \quad \frac{1}{8\xi} \ll -k\,\tau \ll 2\,\xi \ , \tag{3.10}$$

and

$$A'_+ \simeq \sqrt{\frac{k}{2}}\left(\frac{2\xi}{-k\tau}\right)^{1/4} e^{\pi\xi-2\sqrt{-2\xi k\tau}} - i\sqrt{\frac{k}{2}}\left(\frac{\xi}{-8k\tau}\right)^{1/4} e^{-\pi\xi+2\sqrt{-2\xi k\tau}} \quad , \quad \frac{1}{8\xi} \ll -k\,\tau \ll 2\,\xi \ . \tag{3.11}$$

The real part of the approximations (3.10) and (3.11) encodes the amplification of the positive helicity gauge mode. The imaginary part guarantees that the Wronskian condition $A_+ A'^*_+ - c.c. = i$ is satisfied for canonical commutation relations. We note that these expressions are related by

$$\frac{dA'_+(k,\,\tau)}{d\tau} \simeq \sqrt{\frac{2\,k\,\xi}{-\tau}}\,A^*_+(k,\,\tau) \ . \tag{3.12}$$

To appreciate the difference among the three approximations (3.8), (3.9) and (3.10), and to understand the timescale of the gauge field amplification and subsequent dilution, we show in Figure 3.1 the time evolution of the physical energy density of the gauge field modes for a given comoving momentum k. Details of the computation are given in Appendix B.2.

Time flows from right to left in the figure, with $-k\tau = \frac{p}{H} = 1$ denoting horizon crossing (p is the physical momentum of the mode, while H is the Hubble rate). At

the earliest times shown, the mode is deep inside the horizon, and the figure shows the energy density associated to the vacuum mode solution. Namely, at very large $\frac{k}{a}$, the term proportional to ξ can be disregarded in eq. (3.6), and the mode has the standard (comoving) dispersion relation $\omega^2 = k^2$. The energy density of the vacuum mode is UV-divergent, and it needs to be renormalized away (we stress that this has nothing to do with the gauge field amplification studied in this chapter). As done in the literature, we simply cut-off this UV regime when we compute the observable effects of the gauge modes. Following the time evolution of the curves in the figure, we observe a decrease of this vacuum energy contribution, and then a growth of the energy density. For $\xi = \mathrm{O}(1)$, this growth takes place near horizon crossing (for definiteness, $\xi = 3$ was assumed in the evolutions shown in the figure). This growth is then followed by a decrease at the latest times shown in the figure, leading to a peak of the physical energy density close to horizon crossing. We stress that we are showing only the energy density of modes with a given comoving momentum k. At any time during inflation, there is a nearly constant energy density in gauge fields, due to the modes that have size comparable to the horizon at that given moment.

The growth visible in the figure shows the gauge field amplification due to its coupling to $X(t)$. The dilution is due to the expansion of the universe. The resulting peak is well separated from the UV-diverging part (we note that the vertical axis of the figure is in log scale), leading to a clear distinction between the physical field amplification, and the standard divergence associated with the empty vacuum state.

The produced gauge field, before being diluted away, sources scalar perturbations and gravitational waves. The phenomenological implications have been studied in a number of works in the literature that have used the approximate solution (3.10) [4].

The condition $\frac{1}{8\xi} \ll -k\tau \ll 2\xi$ are mathematical conditions for (3.9) to reproduce (3.8), and for (3.10) to reproduce (3.9). However, we can see from the figure that the specific values $-k\tau = \frac{1}{8\xi}, 2\,\xi$ do not have an immediate physical meaning. In setting a UV cut-off, we rather use $-k\tau|_{\max} = \xi$, which, as visible in the figure, well approximates the position of the minimum between the unphysical vacuum energy density, and the physical bump in the energy density due to the gauge field amplification (this is true in the $\xi \sim 3 - 5$ range we are interested in).

[4] We verified that the results change only slightly if one instead uses the Coulomb functions (3.8).

3.1.2 Bump in gauge field production from $\frac{\alpha}{f}\,\sigma\,F\,\tilde{F}$

We now discuss the gauge amplification for the case in which ξ is significant for only a few e-folds during inflation, namely strongly time dependent. For that, we assume that the field X has a momentary faster roll in that period. The pseudo-scalar X is denoted as σ and it is not the inflaton, but a spectator field.

We assume the simplest and most natural potential for a pseudo-scalar field σ

$$V(\sigma) = \frac{\Lambda^4}{2}\left[\cos\left(\frac{\sigma}{f}\right) + 1\right] \,. \tag{3.13}$$

This term is added to the inflaton potential and we assume no direct coupling between the inflaton and σ (ie. $V = V_\phi(\phi)) + V_\sigma(\sigma))$. We define the parameter

$$\delta \equiv \frac{\Lambda^4}{6H^2 f^2} \,, \tag{3.14}$$

that controls the period that axion speed is considerable. The slow roll equation of motion of σ is found as

$$\sigma = 2\,f\,\mathrm{Arctan}\left[\mathrm{e}^{\delta\,H(t-t_*)}\right] \quad \Rightarrow \quad \dot{\sigma} = \frac{f\,H\,\delta}{\cosh\left[\delta\,H\,(t-t_*)\right]} \,, \tag{3.15}$$

under the assumption that H is constant and that (3.13) is much smaller than the inflaton potential (ie. $V_\sigma \ll V_\phi$). In this solution, t_* denotes the time at which σ becomes $\frac{\pi f}{2}$ and reaches its maximum speed $\dot{\sigma}_* \equiv \dot{\sigma}\,(t_*)$. We also see that $\dot{\sigma}$ is significant only for a number of e-folds around $t = t_*$ as $\Delta N \simeq \frac{1}{\delta}$.

By using $\tau = -\frac{1}{a\,H}$ (zeroth order in slow-roll), we can express particle production parameter explicitly as

$$\xi\,(\tau) = \frac{\alpha\,\dot{\sigma}}{2Hf} = \frac{\alpha\,\delta}{2\,\cosh\left[\delta\,H\,(t-t_*)\right]} = \frac{2\,\xi_*}{\left(\frac{-\tau}{-\tau_*}\right)^\delta + \left(\frac{-\tau_*}{-\tau}\right)^\delta} \,, \tag{3.16}$$

ξ_* and by τ_* are, respectively, the value of ξ and τ at $t = t_*$. We note that the particle production parameter gets its maximum value at t_*, and it is $\xi_* = \alpha\,\delta/2$.

Then the generic mode eqn (3.6) for gauge field becomes

$$A_\pm'' + \left(k^2 \pm \frac{4\,k\,\xi_*}{\tau\left[(\tau/\tau_*)^\delta + (\tau_*/\tau)^\delta\right]}\right) A_\pm = 0 \,, \tag{3.17}$$

As we set $\xi_* > 0$,without loss of generality, only positive helicity modes are amplified, and we can neglect the A_- mode. Since ξ varies rapidly, the mode function solutions for the gauge field obtained in the previous subsection are no longer valid.

The solution of eq. (3.17) cannot be written in closed form. However we can obtain a good analytical approximation of the time dependence of $A_+(\tau, k)$ using the WKB approximation, finding (see Appendix B.1)

$$A_+(\tau,k) \simeq \left[\frac{-\tau}{8\,k\,\xi(\tau)}\right]^{1/4} \tilde{A}(\tau,k)\ , \quad A'_+(\tau,k) \simeq \left[\frac{k\,\xi(\tau)}{-2\,\tau}\right]^{1/4} \tilde{A}(\tau,k)\ , \tag{3.18}$$

where we have defined

$$\tilde{A}(\tau,k) \equiv N[\xi_*,\, x_*,\, \delta] \exp\left[-\frac{4\,\xi_*^{1/2}}{1+\delta}\left(\frac{\tau}{\tau_*}\right)^{\delta/2}(-k\tau)^{1/2}\right]\ , \tag{3.19}$$

with $x_* \equiv -k\tau_* = k/(a_*H)$. We determine the time-independent normalization factor $N[\xi_*,\, x_*,\, \delta]$ by matching A_+ at late time $-k\tau \ll 1$ with numerical solution of (3.17).

Similar to nearly constant rolling case, in this scenario we see that the amplitude of the real part of the mode function is much larger than the imaginary part in the amplification regime. To obtain the imaginary part of the mode function one can employ canonical commutation relations (see Appendix B.1 for details)

$$\begin{aligned} A_+(\tau>\tau_*) \;\simeq\; & N[\xi_*,\, x_*,\, \delta]\left(\frac{-\tau}{8\,k\,\xi(\tau)}\right)^{1/4} \exp\left[-\frac{4\xi_*^{1/2}}{1+\delta}\left(\frac{-\tau}{-\tau_*}\right)^{\delta/2}(-k\tau)^{1/2}\right] \\ & + \frac{i}{N[\xi_*,\, x_*,\, \delta]}\left(\frac{-\tau}{2^7\,\xi(\tau)\,k}\right)^{1/4} \exp\left[\frac{4\xi_*^{1/2}}{1+\delta}\left(\frac{-\tau}{-\tau_*}\right)^{\delta/2}(-k\tau)^{1/2}\right]\ , \end{aligned} \tag{3.20}$$

Note that the mode is not amplified considerably (and negligibly small) for $\tau < \tau_*$. Recall that τ_* is the conformal time corresponding to the physical time t_*, while x_* and ξ_* denote the values of x and ξ when axion is fastest, namely $x_* = -k\,\tau_*$ and $\xi_* = \frac{\alpha\,\delta}{2}$.

The time-independent normalization can be well fitted by a Gaussian shape [171]

$$N[\xi_*,\, x_*,\, \delta] \approx N^c[\xi_*,\, \delta] \exp\left(-\frac{1}{2\,\sigma^2[\xi_*,\, \delta]}\ln^2\left(\frac{x_*}{q^c[\xi_*,\, \delta]}\right)\right)\ . \tag{3.21}$$

The coefficients N^c, σ, and q^c control, respectively, the amplitude, the width, and the position of the bump. They can be evaluated numerically, and in Appendix B.1 we

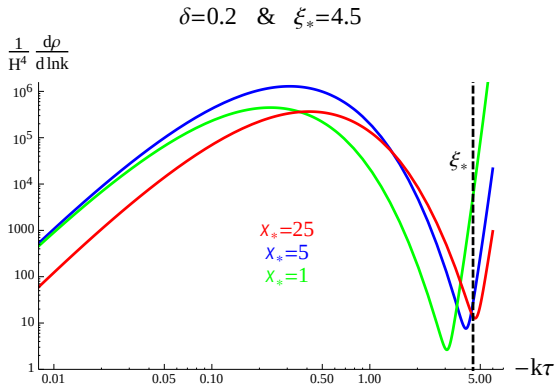

Figure 3.2: Time evolution of the contribution to the gauge field physical energy density from modes with different comoving momenta. $x_* \equiv -k\tau_* = \frac{k/a_*}{H}$ is the ratio between the physical momentum of the mode and the Hubble horizon at $\tau = \tau_*$.

provide their functional dependence on ξ_* for the two choices $\delta = 0.2,\, 0.5$. We see in eq (3.21) that the position of the peak is at $k_{\rm peak} = \frac{q^c}{-\tau_*} = k_* \cdot q^c$, where k_* is the mode that leaves the horizon at the moment of τ_*. (It can be also expressed as the mode with $x_* = 1$). We expect that modes with $x_* = \mathcal{O}\,(1)$ are the maximally amplified ones, and indeed we find $q^c \gtrsim 1$ in the range of parameters we have studied (see Appendix B.1).

In Figure 3.2 we show the contribution to the energy density from three different modes of the gauge field (the result has been obtained by inserting (3.20) in eq. (B.20)). As in the previous figure, we note the unphysical UV-divergent vacuum energy density decreases with time and it is followed by the physical amplification, followed by the dilution due to the expansion of the universe.

We note that, among the modes shown, the one with $x_* = 5$ is the one with greatest amplification. We verified that this is the case also among the modes that we do not show here. The amplification becomes progressively smaller at values of x_* greater and smaller than those shown here, in agreement with the Gaussian profile (3.21). We see from the figure that, for the maximally amplified $x_* = 5$ mode, the value $-k\,\tau = \xi_*$ provides a good position to separate between the unphysical vacuum energy density and the physical amplification.

Chapter 4

CMB Phenomenology of Axion-Gauge Interaction

"The Big Bang is the poor man's particle accelerator." Yakov B. Zel'dovich

In Chapter 3, we have studied the amplification of the Abelian gauge field via its chiral coupling to a rolling axion field. In this chapter, we direct our attention to how the amplified gauge particles source scalar and tensor particles, and to the resulting phenomenology at the largest observable scales, namely CMB scales. Because in this interaction only one helicity of the gauge field is amplified, parity symmetry is broken, and the model produces non-zero primordial TB and EB correlators (that are expected to vanish in models that preserve parity). Moreover, since the scalar and tensor fluctuations are sourced via $2 \to 1$ processes, the sourced fluctuations deviate from Gaussian statistics (specificaly, they have a χ^2 distribution). As a result, this mechanism results in distinguishable signatures at CMB scales. In this chapter, we assume that the axion is a spectator field, not the inflaton.

There is currently strong experimental effort to detect the gravitational waves (GWs) generated during inflation. This signal is conventionally parameterized by the tensor-to-scalar ratio r, which is the ratio between the GW power spectrum (summed over both polarizations) and the density fluctuation power spectrum at a given large scale.

A joint BICEP2/Keck Array and *Planck* analysis has recently reported the 95% CL bound $r < 0.064$ at the scale $0.002\,\mathrm{Mpc}^{-1}$ [149]. It is expected that this limit will be improved by several ongoing and forthcoming CMB polarization measurements. For example, a statistical uncertainty $\sigma(r) = 0.001$ or below is quoted in the proposed stage 4 of ground-based CMB experiments [9].

It is commonly stated that observing the GWs generated during inflation provides both *(i)* the energy scale of inflation, and *(ii)* a lower bound on the excursion of the inflaton field during inflation (the so-called Lyth bound [10], which holds in the case of single field inflation). In terms of r, these results read

$$V_{\mathrm{inf}}^{1/4} \simeq 10^{16}\,\mathrm{GeV}\left(\frac{r_{\mathrm{vac}}}{0.01}\right)^{1/4} \quad , \quad \frac{\Delta\phi}{M_p} \gtrsim \left(\frac{r_{\mathrm{vac}}}{0.01}\right)^{1/2} . \tag{4.1}$$

The observation of an inflationary GW signal does not guarantee that the expressions (4.1) are valid, as they rely on the assumption that the observed GWs are vacuum modes of the metric, amplified by the inflationary expansion, while it is possible that the observed GWs are sourced by some other field during inflation. Several recent studies have shown that it is rather nontrivial to realize such mechanisms. Whatever the GW source is, it couples at least gravitationally not only to the tensor metric perturbations, but also to the scalar ones, and so it unavoidably affects also the scalar perturbations to some degree. The source typically leads to a statistics that is significantly less gaussian than that of the vacuum modes. Therefore, respecting the stringent limits imposed by the gaussianity of the scalar perturbations often restricts the source term to a too low level to lead to observable GWs.

This problem manifest itself for example [1] in one of the most studied mechanisms of GW generation [31, 32, 33, 34]. In this mechanism, the mass of a scalar field χ depends

[1] Other mechanisms for the generation of GWs which are alternative to the standard vacuum production, but are still embedded in the inflationary scenario include the use of spectator fields with low sound speed [11, 12, 13], the modification of the dispersion relation of the tensor modes in the effective-field-theory approach [14, 15], varying sound speed of the tensor [16], the strong tachyonic growth of chiral tensor modes in the chromo-natural inflation [17, 18, 19] and in the gauge-flation model [20], and preheating [21, 22, 23, 24, 25, 26, 27, 28] (in this last case the produced GW signal is typically at scales much shorter than the CMB ones). It has also been investigated [29, 30] whether the presence of many light degrees of freedom could modify the standard relation (4.1) between the energy scale of inflation and r; as shown in [30], this does not appear to be the case.

on the value of the inflaton, and it is arranged in such a way that it vanishes when the inflaton reaches a given value ϕ_* during inflation. As the inflaton crosses ϕ_*, a burst of quanta of the field χ is generated non-perturbatively [35] and can source GWs. In all the implementations of this mechanism that have been worked out in some details the GW production is however negligible; as soon as the inflaton moves past ϕ_*, the quanta of χ rapidly become non-relativistic. This suppresses their quadrupole moment, so that the sourced GW signal is below the observational level [33]. On the contrary, the production of scalar perturbations from these quanta is not suppressed. The bounds on the non-gaussianity of scalar modes put strong bounds on this mechanism.

To have a successful mechanism for the production of a visible GWs during inflation it is therefore crucial to maximize the ratio between the sourced GWs and the sourced scalar modes [33]. [2] For example, one could imagine that the mass of χ is controlled by a field σ different from the inflaton. The absence of a direct coupling between the inflaton and χ decreases the amount of scalar perturbations produced by the latter. Even in this case, however, the gravitational coupling between χ and the inflaton leads to a much greater production of scalar than tensor perturbations, due to the non-relativistic nature of χ. Therefore Ref. [33] studied the case in which the source of GW is both *(i)* only gravitationally coupled to the inflaton, and *(ii)* a relativistic gauge field A_μ.

It was shown in [38] that the pseudo-scalar coupling $\frac{\phi}{f} F \tilde{F}$ amplifies one helicity of the vector field. This helicity mostly sources the GWs of one definite chirality [39], through the two-body interaction $\delta A + \delta A \to \delta g$. The chiral nature of the signal is particularly interesting, [3] since it leads to the parity violation in the CMB that can [42, 43, 44, 45] allow to discriminate the GWs produced by this mechanism from the vacuum ones [4]. However, the vector quanta also inverse decay to inflaton perturbations, [5] $\delta A + \delta A \to$

[2] We note that also in warm inflation [36] the tensor-to-scalar ratio is reduced compared to the standard case due to the dissipative effects and the much greater production of scalar with respect to tensor perturbations due to the coupled inflaton [37].

[3] Moreover, the $\phi F \tilde{F}$ interaction does not lead to a ghost instability as the mechanism of chiral GW production from a gravitational Chern-Simons term coupled to the inflaton [40, 41].

[4] The phenomenological constraints on the production of chiral magnetic fields and their subsequent sourcing of chiral gravitational waves have been studied in [46, 47].

[5] At the technical level, in the presence of a direct coupling the sourced scalar power is enhanced with respect to the sourced tensor power by a factor of $\frac{1}{\epsilon_\phi^2}$, cf. eqs. (8) and (10) of [48] and the discussion in section 4.1 of [39].

$\delta\phi$. This again would lead to an exceedingly large CMB non-gaussianity [48, 49], and, typically, to a growth of the power spectrum which is constrained by smaller scale CMB experiments [50] and the non-observation of primordial black holes [51]. Once the limits from the scalar production are respected, the produced GWs are undetectable at CMB scales. The scalar non-gaussianity can be reduced if the inflation sources a large number S of vector species, so that the inflaton perturbations sourced by these vectors are gaussian due to the central limit theorem (obtaining a visible GW signal however requires $S \sim$ few hundreds $-$ thousands [39]). An observable GW signal may be also achieved if the CMB anisotropies are due to a curvaton [39]. Instead Ref. [33] studied the case in which the rolling pseudo-scalar is a field σ decoupled as much as possible from the inflaton (thus realizing the conditions (i) and (ii) mentioned above [6]). It was shown there that, in this case, the $\delta A + \delta A \rightarrow \delta\phi$ gravitational interaction produces a negligible amount of inflaton perturbations, so that the mechanism can indeed lead to a visible GW signal. Various aspects of this model, including its embedding in a UV-complete theory, were explored in [54].

The mechanism in Ref. [33], predicting blue GW spectrum, was further studied in [55] to reconcile the BICEP2 measurements [56] and the upper bounds on r at larger scales. It was found that for the mechanism to be successful, one should also ensure that σ does not contribute to the observed CMB perturbations. One of the simplest ways to achieve this is to impose that σ becomes massive short after the CMB modes leave the horizon. This issue was further studied in [57] and in [58]. It was shown that the $\delta\phi$ production is dominated by their linear interaction with the $\delta\sigma$ quanta that are sourced by the gauge field and that the amplitude of the $\delta\phi$ fluctuations sourced this way is proportional to the number of e-folds during which σ is rolling (ie. σ has appreciable speed). Therefore, in this chapter, we focus on the case that $\delta\phi$ fluctuations are sourced only for a few e-folds of inflation during which the roll of axion is significant. We further note that the constraints from the scalar bispectrum are relatively weak for modes with $\ell \lesssim 100$. As a consequence, if $\dot{\sigma} \simeq 0$ when modes with $\ell \gtrsim \mathcal{O}(10^2)$ leave the horizon, then the constraints from non-gaussianity can be more easily evaded.

[6] A similar mechanism that also satisfies these conditions, and that also leads to observable GW, has been recently studied in [52]. In this study, the sourcing vector field is produced by a rolling dilation field σ (only gravitationally coupled to the inflaton) through the Ratra $f(\sigma)\, F^2$ mechanism [53].

Earlier studies have made computations with the assumption that $\dot{\sigma}$ is constant. Here we study the generation of primordial perturbations in a more realistic setup, namely in a model in which the field σ evolves in a given potential. The simplest potential for an axion field, which is a simple sine potential as given in eq.(4.3), allows for very small $\dot{\sigma}$ both at early and late times, when σ is, respectively, close to the maximum ($\sigma = 0$) and the minimum of the potential ($\sigma = f\pi$). The speed has a peak at an intermediate time. (See Section 3.1.2 for detailed study of gauge field amplification in this scenario). We assume that V_σ is subdominant with respect to the inflaton potential and that the inflaton potential is very flat, so that the Hubble rate H can be treated as constant. The peak lasts for a number of e-folds roughly of $\mathrm{O}\left(\frac{H^2}{m_\sigma^2}\right)$, where m_σ is the curvature of (4.3). So, remarkably, the simplest axion potential is a perfect candidate for generating a visible GW signal, while keeping the $\delta\phi$ production under control. In the following sections, we show that this is indeed the case through explicit computations.

We present some specific examples, namely some choice of parameters in the model, for which the sourced tensor mode strongly dominates over the vacuum one at large scales, leading to observable B modes of the CMB polarization. The GW signal also leads to a marginally observable TB correlation (as a consequence of the broken parity invariance of the mechanism) and to a well observable (high signal-to-noise ratio) BBB correlation. At the same time, in such examples we find no statistically significant signatures in the TT, and TTT temperature correlators.

The plan of the chapter is the following. In Section 4.1 we present the model, the background evolution, and the vector field production. In Section 4.2 we study the cosmological perturbations (scalar and tensor modes) sourced by the vector field. In Section 4.3 we summarize our results for the two- and three-point scalar and tensor perturbations, and we discuss their phenomenology. In Section 4.4 we present our conclusions. This chapter is complemented by multiple appendix sections. In Appendix C.1 we review the computation of scalar modes produced in the case of constant $\dot{\sigma}$. In Appendices C.2 and C.3 we give details of, respectively, the scalar and tensor mode computation. In Appendix C.4 we present some properties of the bispectra produced in the model. In Appendix C.5 we estimate the departure of sourced modes from gaussianity. This chapter is mostly based on the work conducted in Ref. [171].

4.1 The model, Background Evolution and Gauge Field Production

We will consider a system containing the inflaton ϕ and a second rolling field σ which interacts with the $U(1)$ gauge field A_μ via chiral coupling, so that the lagrangian reads

$$\mathcal{L} = -\frac{1}{2}(\partial\phi)^2 - \frac{1}{2}(\partial\sigma)^2 - V(\phi, \sigma) - \frac{1}{4}F^2 - \alpha\frac{\sigma}{4f}F\tilde{F}\,. \tag{4.2}$$

The rolling of σ provides a time dependent background for the gauge field and amplifies its vacuum fluctuations. This amplification has been studied in detail in Section 3.1.2. Such a phenomenon, on a de Sitter Universe with expansion rate H, is controlled by the dimensionless quantity ξ, which must be larger than unity or so to give observable effects [38].

In order to decouple as much as possible the fluctuations in the gauge field from the scalar perturbations that are strongly constrained by CMB measurements, we will assume as in [33] that there is no direct coupling between the inflaton and the field σ, and we will write $V(\phi, \sigma) = V_\phi(\phi) + V_\sigma(\sigma)$.

As we have discussed in the introduction of this chapter, if $\dot{\sigma}$ is approximately constant throughout inflation, then exceedingly large non-gaussian metric perturbations are generated. However, a large weight in the constraints on the primordial bispectrum from cosmic microwave background radiation measurements is carried by relatively high multipoles, $\ell = \mathcal{O}(100 - 1000)$, whereas a possible observation of primordial tensor modes relies on measurements at larger scales, corresponding to $\ell \sim \mathcal{O}(10 - 100)$. As a consequence, this chapter is devoted for the case where $\dot{\sigma}$ is large only during the epoch when the scales corresponding to the about the fraction or one tenth $(10^{-2} - 10^{-1})$ of the size of the current observable Universe have left the inflationary horizon. The most natural potential for an axion-like field such as σ, does this job remarkably:

$$V_\sigma(\sigma) = \frac{\Lambda^4}{2}\left[\cos\left(\frac{\sigma}{f}\right) + 1\right]\,. \tag{4.3}$$

Assuming $V_\sigma \ll V_\phi$, one finds the slow roll solution

$$\sigma = 2f\,\arctan\left[\mathrm{e}^{\delta H(t-t_*)}\right]\,, \tag{4.4}$$

where $\delta \equiv \Lambda^4/(6\,H^2\,f^2)$ and where we have denoted by t_* the time at which $\sigma = \frac{\pi}{2}\,f$. As a consequence,

$$\dot{\sigma} = \frac{f\,H\,\delta}{\cosh\left[\delta H\,(t-t_*)\right]}\,. \tag{4.5}$$

The slow roll condition gives

$$\frac{\ddot{\sigma}}{3H\dot{\sigma}} = -\frac{\delta}{3}\,\tanh\left[\delta H\,(t-t_*)\right]\,, \tag{4.6}$$

so, to ensure that the slow-roll solution is valid, we require that $\delta \ll 3$. The particle production parameter, ξ, is given by

$$\xi(\tau) \equiv \frac{\alpha\,\dot{\sigma}}{2Hf} \equiv \frac{\alpha\,\delta}{2\cosh\left[\delta H\,(t-t_*)\right]} = \frac{2\,\xi_*}{\left(\frac{a}{a_*}\right)^{\delta} + \left(\frac{a_*}{a}\right)^{\delta}}\,, \tag{4.7}$$

where ξ_* and by a_* are, respectively, the value of ξ and of a at $t = t_*$. $\xi_* = \alpha\,\delta/2$. The value of ξ is significantly different from zero and of the order of ξ_* only for $(2\,\xi_*)^{-1/\delta} \lesssim a/a_* \lesssim (2\,\xi_*)^{1/\delta}$.

Before we proceed we have to make sure that the dynamics of σ does not affect significantly the background dynamics of the inflaton and of the geometry. The two fields σ and ϕ are only gravitationally coupled, so we only need to require that σ provides a negligible contribution to H and $\dot{H}$. This is equivalent to requiring $V_\sigma \ll V_\phi$, and $\dot{\sigma}^2 \ll \dot{\phi}^2$ (given that the inflaton is slowly rolling, the last equation also ensures that $\dot{\sigma}^2 \ll V_\phi$). From eq. (4.3), and from the definition of δ, we have $V_\sigma \leq \Lambda^4 = 6H^2f^2\delta$, which is subdominant to $V_\phi \simeq 3H^2M_p^2$ provided that $\frac{f}{M_p} \ll \frac{1}{\sqrt{2\delta}}$. Let us now discuss the second condition: a sizable $\dot{\sigma}$ would modify $\dot{H}$, which, in turn, would affect the spectral tilt of the inflaton perturbations. We note from (4.5) that $\dot{\sigma}$ is exponentially small at $|t-t_*| > \frac{1}{\delta H}$. So, even if the peak value $\dot{\sigma}_*$ was significant, it would alter the spectral tilt only for a narrow set of modes that left the horizon while σ was rolling. Therefore, $\dot{\sigma}_*^2 > \dot{\phi}^2$ does not automatically implies a significant phenomenological impact (at the very least, one cannot naively apply limits on the spectral tilt that assume a very small running). Nonetheless, to be conservative, we impose that $\dot{\sigma}_*^2 = (fH\delta)^2 \ll \dot{\phi}^2 \simeq 2\epsilon_\phi H^2 M_p^2$. Therefore, we impose the two conditions

$$\frac{f}{M_p} \ll \frac{1}{\sqrt{2\delta}} \;\;\text{and}\;\; \frac{\sqrt{2\,\epsilon_\phi}}{\delta}\,. \tag{4.8}$$

which can be easily enforced.

The last term in the lagrangian (4.2) is responsible for the amplification of the vacuum fluctuations of the gauge field. This process has been studied in Section 3.1.2 and the details of the computation has been presented in Appendix B.1. Here we only mention the results here to set the stage for the scalar and tensor fluctuations sourced by the amplified vector field.

The decomposition of gauge field by distinct modes is given in eq (3.4) and the generic form of the mode function is given in eq (3.20). The time-independent normalization is fitted with a gaussian shape function of x_*, ξ_* and δ. The results for two sample δ values, $\delta = 0.2, 0.5$ are given in Appendix B.1. Since negative helicity is neglected, effectively we end up with the following expression for the gauge field

$$\hat{A}_0 = 0\,, \qquad \hat{A}_i\left(\tau,\vec{k}\right) \simeq \int \frac{d^3k}{(2\pi)^{3/2}}\, \mathrm{e}^{i\vec{k}\cdot\vec{x}}\, \epsilon_i^{(+)}\left(\hat{k}\right) A_+\left(\tau,\, k\right)\left[\hat{a}_+\left(\vec{k}\right) + \hat{a}_+^{\dagger}\left(-\vec{k}\right)\right]\,, \tag{4.9}$$

with the function $A_+(\tau,\, k)$ given by eq. (3.18) and $\tilde{A}$ by eq. (3.19).

For future reference we give here also the "electric" and "magnetic" field, [7] which are related to the vector potential by

$$\hat{E}_i = -\frac{1}{a^2}\,\hat{A}_i'\,, \qquad \hat{B}_i = \frac{1}{a^2}\,\epsilon_{ijk}\,\partial_j \hat{A}_k\,, \tag{4.10}$$

and therefore read

$$\begin{aligned}
\hat{E}_i\left(\tau,\vec{k}\right) &= -\int \frac{d^3k}{(2\pi)^{3/2}}\, \mathrm{e}^{i\vec{k}\cdot\vec{x}}\, \epsilon_i^{(+)}\left(\hat{k}\right) H^2\tau^2 \left[\frac{k\,\xi(\tau)}{-2\,\tau}\right]^{1/4} \tilde{A}\left(\tau,k\right)\left[\hat{a}_+\left(\vec{k}\right) + \hat{a}_+^{\dagger}\left(-\vec{k}\right)\right]\,, \\
\hat{B}_i\left(\tau,\vec{k}\right) &= \int \frac{d^3k}{(2\pi)^{3/2}}\, \mathrm{e}^{i\vec{k}\cdot\vec{x}}\, \epsilon_i^{(+)}\left(\hat{k}\right) H^2\tau^2 \left[\frac{-k^3\,\tau}{8\,\xi(\tau)}\right]^{1/4} \tilde{A}\left(\tau,k\right)\left[\hat{a}_+\left(\vec{k}\right) + \hat{a}_+^{\dagger}\left(-\vec{k}\right)\right]\,,
\end{aligned} \tag{4.11}$$

using the approximate solution (3.18).

4.2 Sourced primordial perturbations

This section is divided in two subsections. We study the scalar and tensor modes generated by the vector modes respectively in Subsection 4.2.1 and 4.2.2.

[7] We do not need to identify the gauge field considered here with the Standard Model photon. Nonetheless, we sometimes use electromagnetic notation for convenience.

4.2.1 Generation of scalar perturbations

The action (4.2) contains two scalar and two tensor degrees of freedom as dynamical modes. After taking the spatially flat gauge ($\delta g_{ij} = 0$), the scalar sector metric reads

$$ds^2 = a^2(\tau)\left[-(1+2\varphi)\,d\tau^2 + 2\partial_i B\,dx^i d\tau + \delta_{ij}dx^i dx^j\right] , \tag{4.12}$$

and, after solving for the non-dynamical variables φ and B, we decompose the remaining physical modes for inflaton, $\hat{\phi}(\tau,\vec{x})$, and axion, $\hat{\sigma}(\tau,\vec{x})$, as

$$\begin{aligned}\hat{\phi}(\tau,\vec{x}) &= \phi(\tau) + \int \frac{d^3k}{(2\pi)^{3/2}}\,\mathrm{e}^{i\vec{k}\cdot\vec{x}}\,\frac{\hat{Q}_\phi\left(\vec{k}\right)}{a(\tau)} ,\\ \hat{\sigma}(\tau,\vec{x}) &= \sigma(\tau) + \int \frac{d^3k}{(2\pi)^{3/2}}\,\mathrm{e}^{i\vec{k}\cdot\vec{x}}\,\frac{\hat{Q}_\sigma\left(\vec{k}\right)}{a(\tau)} ,\end{aligned} \tag{4.13}$$

and denote $(\phi_1,\phi_2)\equiv(\phi,\sigma)$ and $\left(\hat{Q}_1,\hat{Q}_2\right)\equiv\left(\hat{Q}_\phi,\hat{Q}_\sigma\right)$. The free part of the action for $\hat{Q}_i$ (at second ordder) reads

$$S^{(2)}_{\rm free}[\hat{Q}_i] = \frac{1}{2}\int d\tau d^3k\left[\hat{Q}_i'^{\dagger}\hat{Q}_i' - \hat{Q}_i^{\dagger}\left(k^2\delta_{ij} + \tilde{M}^2_{ij}\right)\hat{Q}_j\right] , \tag{4.14}$$

where prime denotes derivative with respect to the conformal time τ, and

$$\tilde{M}^2_{ij} = -\frac{a''}{a}\delta_{ij} + a^2V_{,ij} + \left(3 - \frac{\phi_k'\phi_k'}{2M_p^2}\,\frac{a^2}{a'^2}\right)\frac{\phi_i'\phi_j'}{M_p^2} + \frac{a^3}{M_p^2 a'}\left(\phi_i'V_{,j} + \phi_j'V_{,i}\right) , \tag{4.15}$$

with $V_{,i}\equiv\partial V/\partial\phi_i$. The interaction term in (4.2) gives

$$S_{\rm int} = -\int d^4x\sqrt{-g}\,\alpha\,\frac{\sigma}{4f}F_{\mu\nu}\tilde{F}^{\mu\nu} = \int d^4x\,a^4\,\alpha\,\frac{\sigma}{f}\,\vec{\hat{E}}\cdot\vec{\hat{B}} , \tag{4.16}$$

where the "electric" and "magnetic" fields are defined in (4.10).

The equations of motion for $\hat{Q}_\phi$ and $\hat{Q}_\sigma$, derived from (4.14) and (4.16), are [8]

$$\left(\frac{\partial^2}{\partial\tau^2} + k^2 + \tilde{M}^2_{\phi\phi}\right)\hat{Q}_\phi + \tilde{M}^2_{\phi\sigma}\hat{Q}_\sigma = 0 ,$$

[8] In principle the inflaton also couples to the gauge sector through gravity and receives contributions of the type $\delta A + \delta A \to \delta\phi$. This coupling term is a Planck suppressed operator, and parametrically one may expect its effects to be as large as the ones from $\delta A + \delta A \to \delta\sigma \to \delta\phi$, which is of our main interest. However, $\delta\sigma$ is produced near horizon exit and keeps sourcing $\delta\phi$ while being outside the horizon, whereas the direct production of $\delta\phi$ from the gauge field occurs only near horizon crossing and, as shown in [33], is negligible. Therefore the latter mechanism, mediated by $\delta\sigma$, provides the leading contribution from the gauge field to the curvature perturbations.

$$\left(\frac{\partial^2}{\partial\tau^2}+k^2+\tilde{M}^2_{\sigma\sigma}\right)\hat{Q}_\sigma+\tilde{M}^2_{\sigma\phi}\hat{Q}_\phi=\alpha\frac{a^3}{f}\int\frac{d^3x}{(2\pi)^{3/2}}\,\mathrm{e}^{-i\vec{k}\cdot\vec{x}}\,\vec{\hat{E}}\cdot\vec{\hat{B}}\,. \tag{4.17}$$

Expanding $\tilde{M}_{ij}$ to first order in the slow roll parameters, we have

$$\tilde{M}^2_{ij}\simeq-\frac{1}{\tau^2}\begin{pmatrix}2+9\,\epsilon_\phi+3\,\epsilon_\sigma-3\,\eta_\phi & 6\sqrt{\epsilon_\phi\epsilon_\sigma}\\ 6\sqrt{\epsilon_\phi\epsilon_\sigma} & 2+9\,\epsilon_\sigma+3\,\epsilon_\phi-3\,\eta_\sigma\end{pmatrix}\,, \tag{4.18}$$

where we have defined the slow-roll parameters as

$$\epsilon_{\phi_i}\equiv\frac{\dot{\phi}_i^2}{2M_p^2H^2}\,,\quad \eta_{\phi_i}\equiv M_p^2\frac{V_{,ii}}{V}\,, \tag{4.19}$$

with no summation for the repeated i indices. In the following computation, we focus on the production of $\delta\sigma$ from the gauge field δA and its subsequent sourcing of $\delta\phi$, namely the process $\delta A+\delta A\to\delta\sigma\to\delta\phi$. In this regard, we only take the dominant terms in (4.18) and approximate (4.17) as

$$\left(\frac{\partial^2}{\partial\tau^2}+k^2-\frac{2}{\tau^2}\right)\hat{Q}_\phi\simeq\frac{6}{\tau^2}\sqrt{\epsilon_\phi\epsilon_\sigma}\,\hat{Q}_\sigma\,, \tag{4.20}$$

$$\left(\frac{\partial^2}{\partial\tau^2}+k^2-\frac{2}{\tau^2}\right)\hat{Q}_\sigma\simeq\alpha\frac{a^3}{f}\int\frac{d^3x}{(2\pi)^{3/2}}\,\mathrm{e}^{-i\vec{k}\cdot\vec{x}}\,\vec{\hat{E}}\cdot\vec{\hat{B}}\equiv\hat{\mathcal{S}}_\sigma\left(\tau,\vec{k}\right)\,. \tag{4.21}$$

We note here that we are disregarding the backreaction of the $\hat{Q}_\phi$ quanta, sourced by $\hat{Q}_\sigma$, on the sourcing $\hat{Q}_\sigma$ modes; this effect is of higher order in slow-roll (the term that we disregard in (4.21) is $\epsilon_\phi\,\epsilon_\sigma$ suppressed with respect to the terms that we keep.) Let us also emphasize that since we are interested in the feature due to the change in $\dot{\sigma}$, we do "not" neglect the time dependence of ϵ_σ, while we treat ϵ_ϕ constant.

In the spatially flat gauge, the scalar curvature perturbations are related to the inflaton perturbations by [9]

[9] In a general two scalar field model, the curvature ζ is a linear combination $\zeta(t)=c_1(t)\,\delta\phi(t)+c_2(t)\,\delta\sigma(t)$, where the coefficients $c_{1,2}$ depend on the background (the orthogonal combination being an isocurvature mode). With the choice of potential (4.3), and with our assumptions on the parameters, the field σ becomes massive short after the CMB modes are produced. As σ becomes a massive field in an inflationary universe, its energy density and pressure very rapidly drop to zero, and so does c_2. The only potentially observable effect of $\delta\sigma$ is through its couplings to the inflaton and metric perturbations, which are effective only as long as $\dot{\sigma}\neq0$. The dominant among these interactions is the linear coupling to $\delta\phi$ that we are computing here (all the other couplings are nonlinear in $\delta\sigma$, and highly subdominant; they can be disregarded, once we impose that the effects of the linear coupling are below the observational level).

$$\hat{\zeta}\left(\tau,\vec{k}\right) \simeq -\frac{H}{\dot{\phi}}\,\delta\hat{\phi}\left(\tau,\vec{k}\right) \simeq \frac{H\tau}{\sqrt{2\,\epsilon_\phi}\,M_p}\,\hat{Q}_\phi\left(\tau,\vec{k}\right)\ , \tag{4.22}$$

assuming $\dot{\phi} > 0$. To find $\hat{Q}_\phi\left(\tau,\vec{k}\right)$, we solve eq. 4.20 by separating $\hat{Q}_\phi$ into two parts,

$$\hat{Q}_\phi = \hat{Q}_\phi^{(0)} + \hat{Q}_\phi^{(1)}\ , \tag{4.23}$$

where $\hat{Q}_\phi^{(0)}$ is the homogeneous solution of eq. (4.20) and $\hat{Q}_\phi^{(1)}$ is its particular solution. These two contributions are statistically uncorrelated. We decompose the operator $\hat{Q}_\phi^{(0)}$, corresponding to the vacuum fluctuations, as

$$\hat{Q}_\phi^{(0)}(\tau,\vec{k}) = Q_\phi^{(0)}(\tau,k)\,\hat{a}(\vec{k}) + Q_\phi^{(0)*}(\tau,k)\,\hat{a}^\dagger(-\vec{k})\ , \tag{4.24}$$

where $a^\dagger$ and a are the creation and annihilation operators for $\hat{Q}_\phi^{(0)}$, respectively, and the mode function $Q_\phi^{(0)}$ is solved to be, with the Bunch-Davies initial conditions [10],

$$Q_i^{(0)}(\tau,k) = \frac{\mathrm{e}^{-ik\tau}}{\sqrt{2k}}\left(1-\frac{i}{k\tau}\right)\ . \tag{4.25}$$

The particular solution $\hat{Q}_\phi^{(1)}$ is obtained by solving eq. (4.21) and plugging its solution into eq. (4.20):

$$\hat{Q}_\phi^{(1)} = 6\sqrt{\epsilon_\phi}\int d\tau'\,G_k(\tau,\tau')\,\frac{\sqrt{\epsilon_\sigma(\tau')}}{\tau'^2}\int d\tau''\,G_k(\tau',\tau'')\,\hat{\mathcal{S}}_\sigma(\tau'',\vec{k})\ , \tag{4.26}$$

where the retarded Green function $G_k(\tau,\tau')$ reads

$$G_k(\tau,\tau') = \Theta(\tau-\tau')\,\frac{\pi}{2}\sqrt{\tau\tau'}\left[J_{3/2}(-k\tau)\,Y_{3/2}(-k\tau') - Y_{3/2}(-k\tau)\,J_{3/2}(-k\tau')\right]\ , \tag{4.27}$$

where J and Y denote the Bessel function of real argument. Here we evaluate the sourced solution (4.26) in the case in which $\dot{\sigma}$ is time-dependent[11].

[10] We neglect the scale dependence of the homogeneous solutions of eq. (4.17) that can be induced by relatively large values of ϵ_σ and η_σ; we have checked that the mixing angle, see eq. (C.2), between $\hat{Q}_\phi$ and $\hat{Q}_\sigma$ can be made small enough that such a scale dependence will affect only the unobservable $\hat{Q}_\sigma$ mode and will not leak into the metric perturbations, that are associated to $\hat{Q}_\phi$.

[11] We deal with time-dependent $\dot{\sigma}$, but we briefly studied constant $\dot{\sigma}$ in Appendix C.1 for completeness.

4.2.2 Generation of tensor perturbations

Let us next focus on the tensor perturbations, considering a metric of the form

$$ds^2 = a^2(\tau)\left[-d\tau^2 + \left(\delta_{ij} + \hat{h}_{ij}(\tau, \vec{x})\right) dx^i dx^j\right], \tag{4.28}$$

where $\hat{h}_{ij}$ is transverse and traceless. The leading expression for $\hat{h}_{ij}$ is obtained by expanding the action to second order in $\hat{h}_{ij}$, including the first order interaction term with the gauge field: [12]

$$S_{\rm GW} = \int d^4x \left[\frac{M_p^2 a^2}{8}\left(\hat{h}'_{ij}\hat{h}'_{ij} - \hat{h}_{ij,k}\hat{h}_{ij,k}\right) - \frac{a^4}{2}\,\hat{h}_{ij}\left(\hat{E}_i\,\hat{E}_j + \hat{B}_i\,\hat{B}_j\right)\right]. \tag{4.29}$$

To obtain a canonically normalized field describing tensor modes in Fourier space we decompose

$$\hat{h}_{ij}\left(\tau, \vec{k}\right) = \frac{2}{M_p\,a(\tau)}\int \frac{d^3k}{(2\pi)^{3/2}}\,{\rm e}^{i\vec{k}\cdot\vec{x}} \sum_{\lambda=+,-} \Pi^*_{ij,\lambda}\left(\hat{k}\right)\,\hat{Q}_\lambda\left(\tau, \vec{k}\right), \tag{4.30}$$

where the polarization operators are

$$\Pi^*_{ij,\pm}\left(\hat{k}\right) \equiv \epsilon_i^{(\pm)}\left(\hat{k}\right)\epsilon_j^{(\pm)}\left(\hat{k}\right). \tag{4.31}$$

The equations of motion for $\hat{Q}_\lambda$

$$\left(\frac{\partial^2}{\partial\tau^2} + k^2 - \frac{2}{\tau^2}\right)\hat{Q}_\lambda\left(\vec{k}, \tau\right) = -\frac{a^3}{M_p}\,\Pi_{ij,\lambda}\left(\hat{k}\right)\int \frac{d^3x}{(2\pi)^{3/2}}\,{\rm e}^{-i\vec{k}\cdot\vec{x}}\left[\hat{E}_i\,\hat{E}_j + \hat{B}_i\,\hat{B}_j\right] \equiv \hat{\mathcal{S}}_\lambda(\tau, \vec{k}), \tag{4.32}$$

are solved, as in the scalar case considered in the previous subsection, by separating $\hat{Q}_\lambda$ into a vacuum mode $\hat{Q}^{(0)}_\lambda$, solution of the homogeneous equation, and a sourced mode $\hat{Q}^{(1)}_\lambda$[13]. The vacuum mode is given by

$$\begin{aligned}\hat{Q}^{(0)}_\lambda\left(\vec{k}\right) &= h_\lambda(\tau, k)\,\hat{a}_\lambda\left(\vec{k}\right) + h^*_\lambda(\tau, k)\,\hat{a}^\dagger_\lambda\left(-\vec{k}\right), \\ h_\lambda(\tau, k) &= \frac{{\rm e}^{-ik\tau}}{\sqrt{2k}}\left(1 - \frac{i}{k\,\tau}\right),\end{aligned} \tag{4.33}$$

[12] Interaction terms of the form $hhFF$ give contributions to the two-point function of the tensor perturbations that are of the same order in M_P^{-2} as those of the form hFF. However the terms of the form hFF give a contribution to the tensor power spectrum that is proportional to $e^{4\pi\xi}$, much larger than those of the form $hhFF$, whose contribution is proportional to $e^{2\pi\xi}$, which therefore will be neglected [59].

[13] These two solutions are "not" correlated as in the scalar case, so their power spectrum add up without interference term.

where $\hat{a}_\lambda^\dagger$ creates gravitons of helicity $2\,\lambda$.

For the sourced mode, we have the formal solution

$$\hat{Q}_\lambda^{(1)}\left(\tau,\,\vec{k}\right) = \int^\tau d\tau'\, G_k\left(\tau,\,\tau'\right)\,\hat{\mathcal{S}}_\lambda(\tau,\,\vec{k})\,, \tag{4.34}$$

where the retarded propagator is the same as that for the scalar perturbations, eq. (4.27).

4.3 Results and phenomenology

The gauge quanta, produced by the rolling pseudo-scalar σ, source quanta of σ through inverse decays $\delta A + \delta A \to \delta\sigma$. The gauge quanta also source inflaton perturbations and gravity waves through the $2 \to 1$ processes $\delta A + \delta A \to \delta\phi$ and $\delta A + \delta A \to h_\lambda$. Under the assumption of no direct coupling between the inflaton and σ in the potential, the $\delta A + \delta A \to \delta\phi$ interaction is of gravitational strength, and negligible with respect to the gravity wave production [33]. For this reason we disregard it in this study. On the other hand, the inverse decay into quanta of σ can produce a large signal, which has a much stronger departure from gaussianity than the vacuum mode [48]. In the model under consideration the field σ has a completely negligible energy density at the end of inflation / beginning of reheating (both at the background and at the perturbation level), so that the inflation perturbations can be identified with the observed curvature perturbations ζ, see eq. (4.22). However, $\delta\sigma$ is not completely irrelevant for observations: as long as σ is rolling, there is a linear gravitational coupling between perturbations of σ and of the inflaton with a strength proportional to the multiplication of their speed, ie. $\sqrt{\epsilon_\sigma \cdot \epsilon_\phi}$ (see the non-diagonal term in matrix (4.18)), leading to conversion of $\delta\sigma$ into $\delta\phi$ [57].

In the previous Section (see also appendices C.2 and C.3) we computed the curvature perturbations ζ and the gravity waves produced in the model. The results are summarized in Subsection 4.3.1 and we study the phenomenological implications of these results in Subsection 4.3.2.

4.3.1 Scalar and tensor correlators

We are interested in the power spectrum and bispectrum of the scalar curvature ζ and of the gravity wave polarizations $h_\pm$. They are defined as

$$\left\langle \hat{\zeta}\left(\vec{k}\right)\,\hat{\zeta}\left(\vec{k}'\right)\right\rangle \equiv \frac{2\pi^2}{k^3}\,\mathcal{P}_\zeta\,(k)\,\delta^{(3)}\left(\vec{k}+\vec{k}'\right)\,,$$

$$\left\langle \hat{\zeta}\left(\vec{k}_1\right)\,\hat{\zeta}\left(\vec{k}_2\right)\,\hat{\zeta}\left(\vec{k}_3\right)\right\rangle \equiv \mathcal{B}_\zeta\left(k_1,\,k_2,\,k_3\right)\delta^{(3)}\left(\vec{k}_1+\vec{k}_2+\vec{k}_3\right)\,, \tag{4.35}$$

and analogously for $h_\pm$. The scalar curvature ζ and gravity waves $h_\pm$ produced in the model (4.2) are the sum of a vacuum component and a component sourced by the gauge quanta. The two components, which we denote, respectively, as

$$\zeta = \zeta^{(0)} + \zeta^{(1)} \quad , \quad h_\pm = h_\pm^{(0)} + h_\pm^{(1)}\,, \tag{4.36}$$

are uncorrelated among each other, and therefore the power spectra and bispectra of these modes are the sum of the vacuum and of the sourced spectra:

$$\mathcal{P}_\zeta\left(k\right) = \mathcal{P}_\zeta^{(0)}\left(k\right) + \mathcal{P}_\zeta^{(1)}\left(k\right) \quad , \quad \mathcal{B}_\zeta\left(k\right) = \mathcal{B}_\zeta^{(0)}\left(k\right) + \mathcal{B}_\zeta^{(1)}\left(k\right)\,, \tag{4.37}$$

and analogously for $h_\pm$.

The vacuum power spectra are given by the standard relations [60]

$$\mathcal{P}_\zeta^{(0)}\left(k\right) = \frac{H^2}{8\pi^2\epsilon_\phi M_p^2} \quad , \quad \mathcal{P}_+^{(0)}\left(k\right) = \mathcal{P}_-^{(0)}\left(k\right) = \frac{H^2}{\pi^2 M_p^2}\,, \tag{4.38}$$

where we disregard subleading corrections in slow-roll. This gives the vacuum relation

$$r_{\rm vac} \equiv \frac{\mathcal{P}_+^{(0)} + \mathcal{P}_-^{(0)}}{\mathcal{P}_\zeta^{(0)}} \simeq 16\epsilon_\phi\,, \tag{4.39}$$

for the tensor-to-scalar ratio. The vacuum bispectra are known to be well below the current observational limits, and we disregard them [14].

The sourced terms $\zeta^{(1)}$ and $h_\pm^{(1)}$ present a localized bump in momentum space. This corresponds to modes that leave the horizon when $\dot{\sigma}$ is close to its maximum value. The gauge field production is exponentially sensitive to the parameter ξ, given in eq. (4.7). Therefore the height of the bump is exponentially proportional to the maximum value ξ_* acquired by ξ. The width of the peak decreases with increasing values of the parameter δ. This is because, as we have see in Section 4.1, the field σ has a significant evolution only for a number of e-folds $\Delta N \simeq \frac{1}{\delta}$. Therefore, the larger δ is, the fewer are the amplified modes.

[14] The local non-Gaussianity parameter for vacuum fluctuations, $f_{\rm NL,\,vac}$, has been shown to be order of scalar tilt, ie. $f_{\rm NL,\,vac} \propto \mathcal{O}(n_s - 1)$

As we show in Appendices C.2 and C.3, we can parametrize and express functional dependence of 2- and 3-point scalar and tensor correlators as follows

$$\begin{aligned}
\mathcal{P}_\zeta^{(1)}(k) &= \left[\epsilon_\phi\,\mathcal{P}_\zeta^{(0)}(k)\right]^2 f_{2,\zeta}\left(\frac{k}{k_*},\,\xi_*,\,\delta\right), \\
\mathcal{P}_\lambda^{(1)}(k) &= \left[\epsilon_\phi\,\mathcal{P}_\zeta^{(0)}(k)\right]^2 f_{2,\lambda}\left(\frac{k}{k_*},\,\xi_*,\,\delta\right) \quad , \quad \lambda = +,-\,, \\
\mathcal{B}_\zeta(k_1,\,k_2,\,k_3) &= \frac{\left[\epsilon_\phi\,\mathcal{P}_\zeta^{(0)}(k)\right]^3}{k_1^2\,k_2^2\,k_3^2}\, f_{3,\zeta}\left(\frac{k_1}{k_*},\,\frac{k_2}{k_*},\,\frac{k_3}{k_*},\,\xi_*,\,\delta\right), \\
\mathcal{B}_\lambda(k_1,\,k_2,\,k_3) &= \frac{\left[\epsilon_\phi\,\mathcal{P}_\zeta^{(0)}(k)\right]^3}{k_1^2\,k_2^2\,k_3^2}\, f_{3,\lambda}\left(\frac{k_1}{k_*},\,\frac{k_2}{k_*},\,\frac{k_3}{k_*},\,\xi_*,\,\delta\right) \quad , \quad \lambda = +,-\,. \qquad (4.40)
\end{aligned}$$

For brevity, we denote the functions at the right hand side as $f_{i,j}$, where $i \in \{2,\,3\}$ and $j \in \{\zeta,\,+,\,-\}$. These functions are dimensionless. The functions $f_{3,j}$ encode the full dependence of the bispectrum on the momenta k_i. In eq. (C.66) we provide an approximate relation for the shape dependence, written in terms only of the two point function and of the three point function in the exact equilateral case. The expression (C.66) is exact by construction on equilateral triangles, and it is very accurate where the signal is maximum (see Figure C.1). Therefore, in order to study the phenomenology of the scalar and tensor 2- and 3-point correlation functions, we simply need to provide the functions, $f_{2,j}$, as well as $f_{3,j}$ for equal momenta.

We first studied the momentum dependence of these functions for fixed values of ξ_* and δ. We found that they are well approximated by log-normal shape

$$f_{i,j}\left(\frac{k}{k_*},\,\xi_*,\,\delta\right) \simeq f_{i,j}^c\left[\xi_*,\,\delta\right] \exp\left[-\frac{1}{2\sigma_{i,j}^2\left[\xi_*,\,\delta\right]}\,\ln^2\left(\frac{k}{k_*\,x_{i,j}^c\left[\xi_*,\,\delta\right]}\right)\right]. \qquad (4.41)$$

Namely, the momentum dependence [15] is encoded by the three functions f^c, σ, x^c, which in turn depend on the evolution of $\dot\sigma$ through the model parameters ξ_* and δ. The function (4.41) has a bump at $k = k_*\,x^c$, where it evaluates to f^c. The parameter σ^2 controls the width of the bump. For each choice of ξ_* and δ, the values of $f_{i,j}^c$, $x_{i,j}^c$, and $\sigma_{i,j}$ are obtained by fitting the right hand side of (4.41) to reproduce the position, height, and curvature of the bump. In Figure 4.1 we verify the accuracy of the approximate

[15] For the three point functions ($i = 3$), the approximation (4.41) refers to the exact equilateral case, $k_1 = k_2 = k_3 = k$.

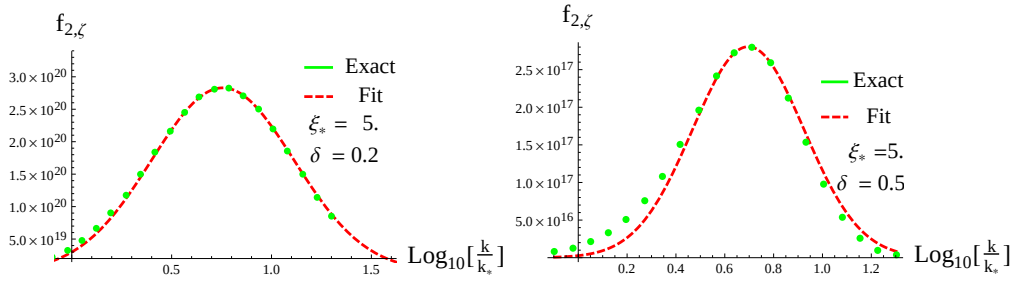

Figure 4.1: Comparison of the exact function $f_{2,\zeta}$ (green dots) and of the approximate form (red dashed line) given in eq. (4.41), for the two values of δ, 0.2 and 0.5.

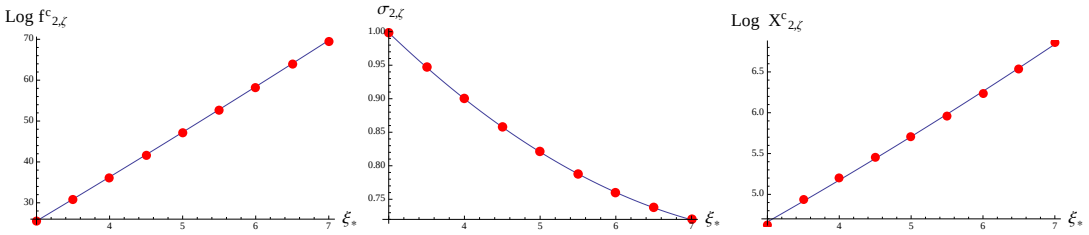

Figure 4.2: ξ_* dependence of the fitting $f_{2,\zeta}$, $x^c_{2,\zeta}$ and $\sigma_{2,\zeta}$ entering in (4.41), for $\delta = 0.2$ (an analogous agreement is obtained for $\delta = 0.5$, and for other $\{i, j\}$ functions). The red dots denote the values at different ξ_* and the solid lines are polynomial fits.

relation (4.41) by showing the comparison between the exact and approximate form of $f_{2,\zeta}$ for two choices of δ parameters. (These chosen values have no particular relevance, they are chosen for illustrative purpose only.) An analogous level of accuracy is obtained for the other $f_{i,j}$ functions and for the other choices of ξ_* that we have made.

Secondly, we need to specify the dependence of $f^c_{i,j}$, $x^c_{i,j}$, $\sigma^2_{i,j}$ on the model parameters ξ_* and δ. We evaluated these functions for $\delta = 0.2$ and $\delta = 0.5$, and for $\xi_* = \{2.5, 3, 3.5, 4, 4.5, 5, 5.5, 6, 7\}$. We found that the dependence on ξ_* is rather smooth, and can be well described by a second degree polynomial. We provide the fitting functions in Tables 4.1 and 4.2. As we see from the examples shown in Figure 4.2, the fitting functions are very accurate.

4.3.2 Phenomenology

In this subsection we study the phenomenology of the model (4.2). The total scalar and tensor modes produced during inflation are the sum of a nearly scale invariant

$\{i,\,j\}$	$\ln\lvert f^c_{i,j}\rvert \simeq$	$x^c_{i,j} \simeq$	$\sigma_{i,j} \simeq$
$\{2,\zeta\}$	$-5.60 + 10.1\,\xi_* + 0.0947\,\xi_*^2$	$3.26 + 0.435\,\xi_* + 0.0109\,\xi_*^2$	$1.41 - 0.166\,\xi_* + 0.00962\,\xi_*^2$
$\{2,+\}$	$-7.98 + 10.0\,\xi_* + 0.0979\,\xi_*^2$	$5.45 + 0.455\,\xi_* + 0.0316\,\xi_*^2$	$1.38 - 0.178\,\xi_* + 0.0103\,\xi_*^2$
$\{2,-\}$	$-13.8 + 9.96\,\xi_* + 0.104\,\xi_*^2$	$2.39 + 0.129\,\xi_* + 0.0214\,\xi_*^2$	$1.44 - 0.169\,\xi_* + 0.0102\,\xi_*^2$
$\{3,\zeta\}$	$-4.72 + 15.1\,\xi_* + 0.142\,\xi_*^2$	$3.37 + 0.353\,\xi_* + 0.0142\,\xi_*^2$	$1.13 - 0.143\,\xi_* + 0.00830\,\xi_*^2$
$\{3,+\}$	$-7.77 + 15.1\,\xi_* + 0.147\,\xi_*^2$	$5.24 + 0.361\,\xi_* + 0.0360\,\xi_*^2$	$1.11 - 0.150\,\xi_* + 0.00880\,\xi_*^2$

Table 4.1: ξ_* dependence of the functions entering in (4.41), for $\delta = 0.2$. Among the entries in the first column, only $f^c_{3,+}$ is negative, while the other $f^c_{i,j}$ are positive.

$\{i,\,j\}$	$\ln\lvert f^c_{i,j}\rvert \simeq$	$x^c_{i,j} \simeq$	$\sigma_{i,j} \simeq$
$\{2,\zeta\}$	$-6.47 + 9.04\,\xi_* + 0.0586\,\xi_*^2$	$1.64 + 0.630\,\xi_* + 0.00738\,\xi_*^2$	$0.823 - 0.0872\,\xi_* + 0.00558\,\xi_*^2$
$\{2,+\}$	$-6.85 + 9.05\,\xi_* + 0.0596\,\xi_*^2$	$2.70 + 0.896\,\xi_* + 0.0187\,\xi_*^2$	$0.768 - 0.0993\,\xi_* + 0.00608\,\xi_*^2$
$\{2,-\}$	$-12.5 + 8.97\,\xi_* + 0.0656\,\xi_*^2$	$1.22 + 0.396\,\xi_* + 0.00976\,\xi_*^2$	$0.858 - 0.0813\,\xi_* + 0.00530\,\xi_*^2$
$\{3,\zeta\}$	$-5.98 + 13.6\,\xi_* + 0.0861\,\xi_*^2$	$1.71 + 0.569\,\xi_* + 0.00972\,\xi_*^2$	$0.641 - 0.0792\,\xi_* + 0.00495\,\xi_*^2$
$\{3,+\}$	$-6.03 + 13.6\,\xi_* + 0.0870\,\xi_*^2$	$2.63 + 0.841\,\xi_* + 0.0193\,\xi_*^2$	$0.606 - 0.0844\,\xi_* + 0.00520\,\xi_*^2$

Table 4.2: ξ_* dependence of the functions entering in (4.41), for $\delta = 0.5$. Among the entries in the first column, only $f^c_{3,+}$ is negative, while the other $f^c_{i,j}$ are positive.

vacuum mode, plus a peaked sourced signal (see Figure 4.1 for the scale dependence of the latter). The sourced scalar and tensor modes modify the tensor-to-scalar ratio from its vacuum value (4.39), $r_{\rm vac} \simeq 16\,\epsilon_\phi$, to

$$r\,(k) \equiv \frac{P_{\rm GW,vacuum} + P_{\rm GW,sourced}}{P_{\zeta,\rm vacuum} + P_{\zeta,\rm sourced}} \simeq \frac{\mathcal{P}^{(0)}_+\,(k) + \mathcal{P}^{(0)}_-\,(k) + \mathcal{P}^{(1)}_+\,(k)}{\mathcal{P}^{(0)}_\zeta\,(k) + \mathcal{P}^{(1)}_\zeta\,(k)} = r_{\rm vac}\,\frac{1 + \frac{\epsilon_\phi}{16}\,\mathcal{P}^{(0)}_\zeta\,(k)\;f_{2,+}\,(k)}{1 + \epsilon^2_\phi\,\mathcal{P}^{(0)}_\zeta\,(k)\;f_{2,\zeta}\,(k)}\,, \tag{4.42}$$

where we have disregarded the sourced $h^{(1)}_-$ mode (given that $f_{2-} \ll f_{2+}$). Both the numerator and the denominator of the fraction appearing in eq. (6.6) have been written as $1 + \mathcal{P}_{\rm sourced}/\mathcal{P}_{\rm vacuum}$, so that we can immediately compare the impact of the sourced tensor modes vs. the sourced scalar modes on r. We see that, relative to the sourced scalars, the sourced tensors are more relevant at smaller values of ϵ_ϕ. This is the regime of greatest interest for our study, since it corresponds to a small $r_{\rm vac}$.

This is confirmed by the contour lines shown in Figure 4.3, where we show the

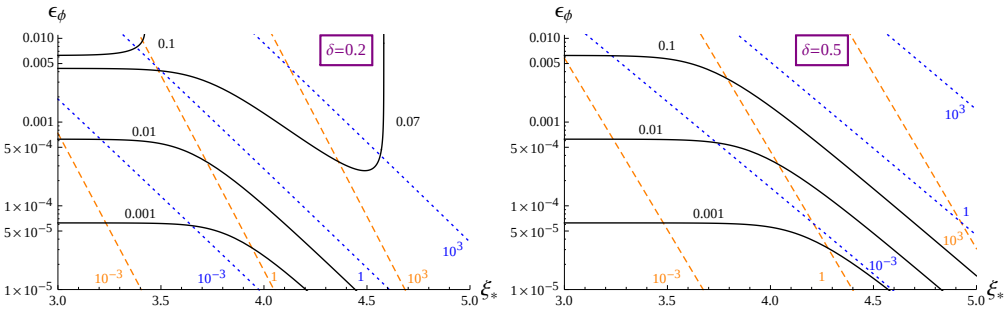

Figure 4.3: Black-solid lines: tensor-to-scalar ratio. Orange dashed (Blue dotted) lines show the ratio between the sourced and the vacuum tensor (scalar) power spectrum. All ratios are evaluated at the peak of the sourced GW power spectrum.

tensor-to-scalar ratio (black solid lines), the ratio between the sourced and the vacuum tensor power spectrum (orange dashed lines), and the ratio between the sourced and the vacuum scalar power spectrum (blue dotted lines), evaluated at the peak of the sourced GW signal. The ratios are shown as functions of ξ_* and ϵ_ϕ. The sourced modes are negligible at the smallest values of ξ_* shown in the figure, so that $r \simeq r_{\rm vac} \simeq 16\epsilon_\phi$. Hence the contour lines of same r are ξ_* independent and horizontal, in this region). At greater values of ξ_*, and, particularly, at the smallest ϵ_ϕ shown, we see that $r \gg r_{\rm vac}$.

Figure 4.3, and several of the following figures, are comprised of two panels. In the left (right) panel we show results for $\delta = 0.2$ ($\delta = 0.5$). The roll of σ is substantial for a number of e-folds $\Delta N \simeq \frac{1}{\delta}$, cf. eq. (4.5). Increasing δ therefore decreases the amount of time during which σ is rolling. This decreases the amplitude of the produced signal (encoded in the parameter $f^c_{i,j}$, cf. eq. (4.41)), as well as its width (encoded in $\sigma_{i,j}$). The latter effect is due to the fact that, the smaller ΔN is, the fewer are the modes that exited the horizon while $\dot\sigma$ was non-negligible. By comparing the results given in Tables 4.1 and 4.2, we can also see that increasing δ decreases the scalar production more than the tensor one. This is also visible by comparing the left and the right panel of Figure 4.3, as well as from the following figures. We can notice that greater values of δ corresponds to a greater production of tensor vs. scalar modes. This occurs because inflaton is sourced by $\delta\sigma$ via gravitational coupling with a strength proportional to the geometric mean of the speeds of σ and ϕ and the sourcing is effective only when $\dot\sigma$ is

significant [16]. In result, a decrease of ΔN affects the sourced scalar modes more than the tensor modes because it decreases both (i) the number of modes that are sourced (namely, the width of the peak)[17], and (ii) the interval of time during which the $\delta\sigma$ modes (produced by the gauge field) can be converted into inflaton perturbations.

In the following analysis, we show that the model admits choices of parameters that result in a sourced signal visible in correlators involving the B-mode of the CMB polarization, and that are consistent with the well-analyzed $\langle TT \rangle$ and $\langle TTT \rangle$ correlators. To have visible effects from the sourced GWs, we choose values of k_* leading to a peak of the sourced signal at large CMB scales. Specifically, we choose k_* ranging from $7 \times 10^{-5}\,\mathrm{Mpc}^{-1}$ (affecting only the first few multipoles) to $5 \times 10^{-3}\,\mathrm{Mpc}^{-1}$ (affecting multipoles up to the first acoustic peak).

4.3.2.1 CMB power spectra

The main goal of this chapter is to provide a concrete example of a particle physics process that can enhance the GW signal from inflation, while being "consistent with the TT and TTT data". With this, we mean that this additional signal should not significantly worsen the fit to the TT and the TTT data of the standard cosmological model which does not include this signal. The signal that we are studying manifests itself at the largest cosmological scales and we compare it against the latest WMAP data [65, 66], which are cosmic variance limited at such scales. We fix all the cosmological parameters consistently with the best fit values reported in [66] and denote this set of values as $\mathcal{C}_0$ [18]. We express by $\mathcal{L}_0$ the likelihood of the fit to the WMAP TT data of the standard cosmological model with these values of the parameters

$$\mathcal{L}_0 = \mathrm{e}^{-\chi^2_{\xi_*=0}/2} \quad . \tag{4.43}$$

[16] Assuming inflaton speed is nearly constant, the sourcing of inflaton is controlled with $\sqrt{\epsilon_\sigma}$

[17] This affects tensor modes as well.

[18] Specifically, we fix the physical baryon density $\Omega_b h^2 = 0.02264$, the physical cold dark matter density $\Omega_c\, h^2 = 0.1138$, the ionization optical depth $\tau = 0.089$, the Hubble constant $H_0 = 70.0$ km/sec/Mpc. The parameters relevant to the initial condition, i.e., the scalar amplitude $\Delta^2_\zeta = 2.41 \times 10^{-9}$, the scalar spectral index $n_s = 0.972$ and the WMAP pivot scale $k_0 = 0.002\ \mathrm{Mpc}^{-1}$, fix our vacuum power spectrum $\mathcal{P}^{(0)}_\zeta(k) = \Delta^2_\zeta (k/k_0)^{n_s - 1}$. We have also assumed a flat universe, with 3.046 relativistic species and no massive neutrino. Planck experiment also obtained consistent results, [67, 68].

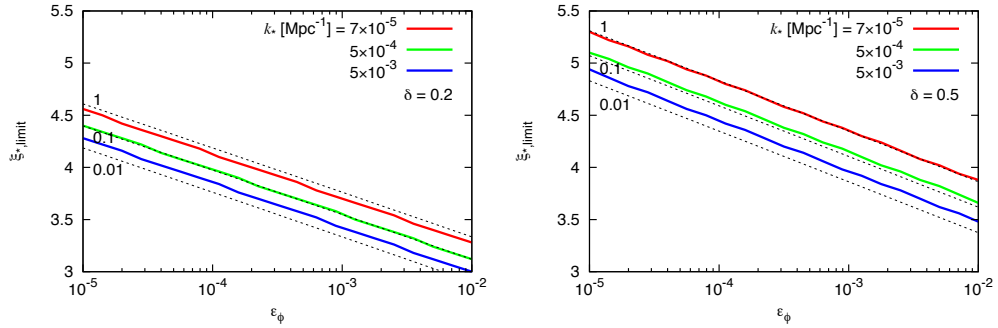

Figure 4.4: Solid lines: Largest value of ξ_* allowed by the WMAP TT data as a function of ϵ_ϕ, and for different values of k_* (controlling the bump scale of the sourced modes). Dashed lines: ratio of $\mathcal{P}_\zeta^{(1)}/\mathcal{P}_\zeta^{(0)}$ at the peak of the GW bump.

We then add the sourced scalar and tensor modes obtained from the mechanism presented in the previous sections. For illustrative purposes, we fix three values of k_* (controlling the peak scale of the sourced signals) and two values of δ (controlling the width of the sourced signal). For any of these six choices, we then increase ξ_* (the parameter that controls the amplitude of the sourced signal) until the likelihood of the fit decreases by a factor e^2 with respect to $\mathcal{L}_0$, namely, we find the value $\xi_* = \xi_{*,\mathrm{limit}}$ for which $\chi^2_{\xi_{*,\mathrm{limit}}} = \chi^2_{\xi_*=0} + 4$ [19]. An experimentalist fitting the WMAP data with the cosmological parameters $\mathcal{C}_0$, would obtain a fit that is two sigmas worse if he/she includes the sourced signal instead of the standard cosmological model. In fact, the value $\xi_{*,\mathrm{limit}}$ obtained in this way is conservative, as we do not vary any of the cosmological parameters $\mathcal{C}_0$. Varying them, we can only improve the fit of the WMAP data for that given value of ξ_*, and so likely obtain larger values for $\xi_{*,\mathrm{limit}}$. However, changing values in $\mathcal{C}_0$ may give a disagreement with data at smaller angular scales than the WMAP ones, and for this reason we do not vary such parameters. As we show below, in most cases the values of $\xi_{*,\mathrm{limit}}$ obtained with this procedure already provide a visible GW signal, which is the goal of this present analysis (in summary, we are not interested in providing precise Bayesian limits on ξ_* within this model - for which we should provide priors, marginalize over all the other parameters and include smaller scales data - but only in the goal specified at the beginning of this subsection).

[19] We use the WMAP power spectrum likelihood code: `http://lambda.gsfc.nasa.gov/`.

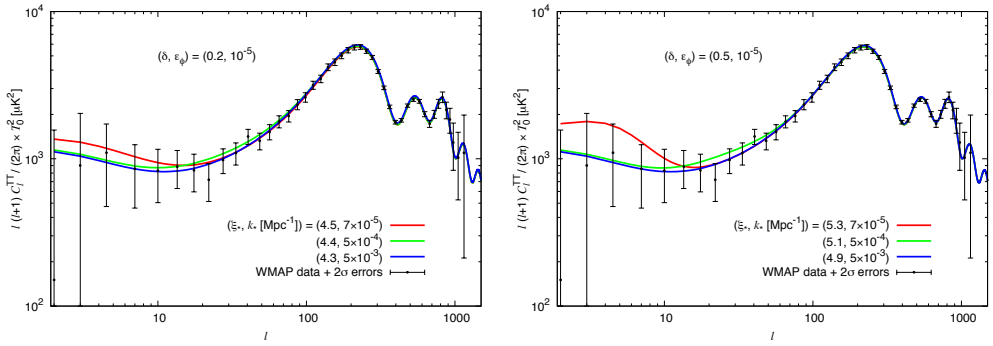

Figure 4.5: Temperature-temperature correlation of WMAP data [65, 66] is compared against the three theoretical curves for three different values of k_* and with limiting value $\xi_* = \xi_{*,\rm limit}$, evaluated for $\epsilon_\phi = 10^{-5}$ and for $\delta = 0.2$ (left) and $\delta = 0.5$ (right).

In Figure 4.4 we present the value of $\xi_{*,\rm limit}$ obtained with this procedure as a function of the slow roll parameter ϵ_ϕ. In the left (right) panel of the figure we set $\delta = 0.2$ (0.5), corresponding to a significant $\dot\sigma$ for about 5 (2) e-folds. In each panel we fix $k_* = 7 \times 10^{-5}\,{\rm Mpc}^{-1}$, $k_* = 5 \times 10^{-4}\,{\rm Mpc}^{-1}$, and $k_* = 5 \times 10^{-3}\,{\rm Mpc}^{-1}$, producing a bump, respectively at the very largest angular scales ($\ell \lesssim 5$), on the rise of the first peak, and in the region around the first two peaks. [20] In the same figure we also show with black dashed lines the ratio $\mathcal{P}_\zeta^{(1)}/\mathcal{P}_\zeta^{(0)}$ at the peak of the GW bump. We see that the allowed amount of scalar signal strongly depends on the scale. In the examples with the bump at the largest scales, the sourced signal can be as large as the vacuum one at the peak, due to the large cosmic variance present at those scales. A significantly smaller fraction, $\mathrm{O}\,(1\% - 10\%)$, is allowed in the examples in which the signal affects the acoustic peaks. By comparing the left and right panel of Figure 4.4 we again see that, for any fixed value of ξ_*, the sourced signal is stronger at small values of δ.

In Figure 4.5 we show the TT power spectrum obtained for the same choices of δ and k_* as in Figure 4.4, for $\epsilon_\phi = 10^{-5}$, and for the corresponding value of $\xi_* = \xi_{*,\rm limit}$. The theoretical curves present a bump due to the sourced scalar modes. As we already mentioned, the bump ranges from the lowest ℓ multipoles (for the smallest k_* chosen) to around the first two acoustic peaks (for the largest k_* chosen).

[20] We verified that, apart from the $\left\{\delta = 0.5,\ k_* = 7 \times 10^{-5}\,{\rm Mpc}^{-1}\right\}$ case, the sourced GW give a negligible contribution to the TT signal, and in all the other cases the limits shown in the figure are due to $\zeta_{\rm sourced}$.

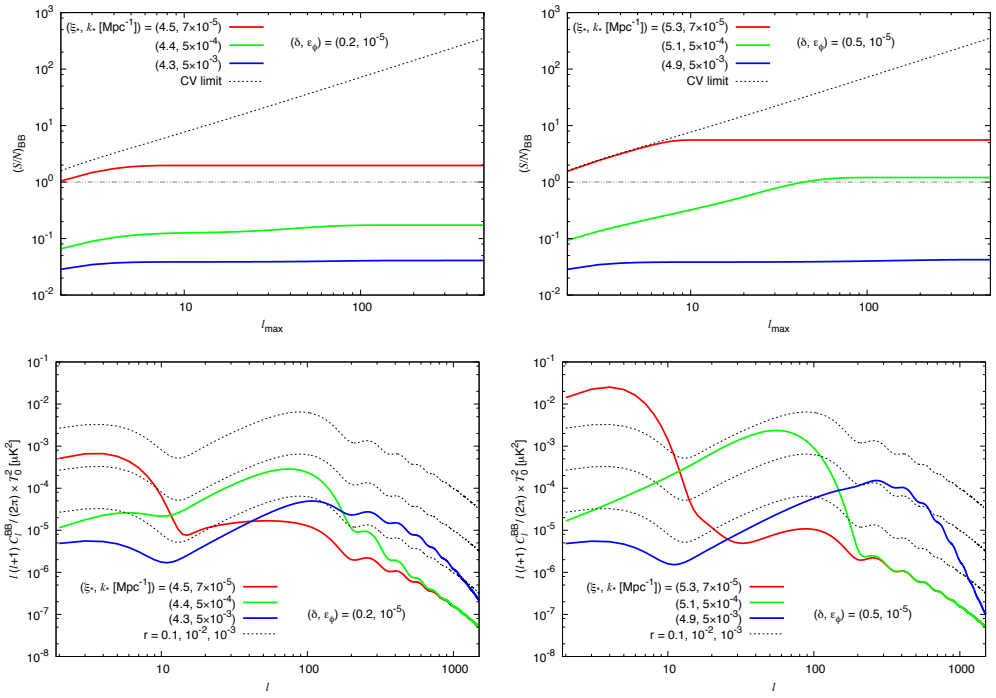

Figure 4.6: First row: Forecasted signal-to-noise ratio for B-mode auto-correlations in a CMB experiment with *Planck*-like sensitivity (Colored solid lines), and in a cosmic variance limited (ideal noise-free) CMB experiment (Black dotted line). Second row: C_l^{BB} coefficients are shown for chosen parameters with solid color lines. The C_l^{BB} coefficients for scale invariant tensor-to-scalar-ratio (r) for 10^{-1}, 10^{-2} and 10^{-3} are shown with dots from top to bottom respectively.

In Figure 4.6 we show the auto-correlations between the B modes of the CMB polarizations, (BB), sourced by the tensor modes when $\xi_* = \xi_{*,\rm limit}$. The parameters ϵ_ϕ, δ, and k_* are chosen as in the two previous figures. For comparison, we also show the BB correlation obtained for a scale invariant r of 0.1, 10^{-2}, and 10^{-3} (from top to bottom, respectively) with black dashed lines. As we already mentioned in the Introduction, the proposed stage 4 CMB experiments claim an expected statistical uncertainty $\sigma(r) = 10^{-3}$ or below [9] in the scale invariant case. If this is achieved, the theoretical curves chosen in Figure 4.6 appear to be within observational reach. We recall that $\epsilon_\phi = 10^{-5}$ corresponds to a vacuum tensor-to-scalar ratio $r_{\rm vac} \simeq 1.6 \cdot 10^{-4}$. Therefore, the enhancement of the BB signal visible in the figure is entirely due to the sourced tensor modes. The enhancement is present at progressively larger ℓ for increasing values of k_* shown, namely for bumps of gauge field production at progressively smaller scales. By comparing the left and the right panel of Figure 4.6 we observe that BB can reach greater values at increasing δ. This is consistent with what we have already mentioned: at fixed ξ_*, both the sourced scalar and tensor modes decrease with increasing δ. However, the scalar mode decreases more. Therefore, at larger values of δ, larger values of ξ_* can be compatible with the WMAP TT bounds (cf. Figure 4.4). Such values lead to a larger amount of sourced tensor modes. The signal-to-noise (S/N) ratio shown in the figure is evaluated through

$$\left(\frac{S}{N}\right)^2_{BB} = \sum_{\ell=2}^{\ell_{\rm max}} \frac{2\ell+1}{2} \left(\frac{C_\ell^{BB}}{C_{\ell,\rm dat}^{BB}}\right)^2 . \tag{4.44}$$

Here, $(C_\ell^{BB})^2$ corresponds to the signal given by our theory, while the other terms in this relation account for the uncertainty of the BB power spectrum in a given experiment. For simplicity, we here (and also in the other S/N estimations) assume a full-sky isotropic CMB measurement, thus, the summations in terms of m disappear in the S/N formula. The data spectrum in a given experiment is regarded as the sum of the signal and instrumental noise, reading $C_{\ell,\rm dat}^{BB} = C_\ell^{BB} + N_\ell^{BB}$. In this study, we analyze two different types of measurements: a realistic measurement including a *Planck*-level noise spectrum [69] (as described in Appendix A of [70]) and an ideal noise-free cosmic variance dominated measurement (i.e., $N_\ell^{BB} = 0$).

The results are shown in the upper panels of Figure 4.6. In the cosmic variance limited case, because of $C_\ell^{BB}/C_{\ell,\rm dat}^{BB} = 1$, S/N becomes a simple increasing function:

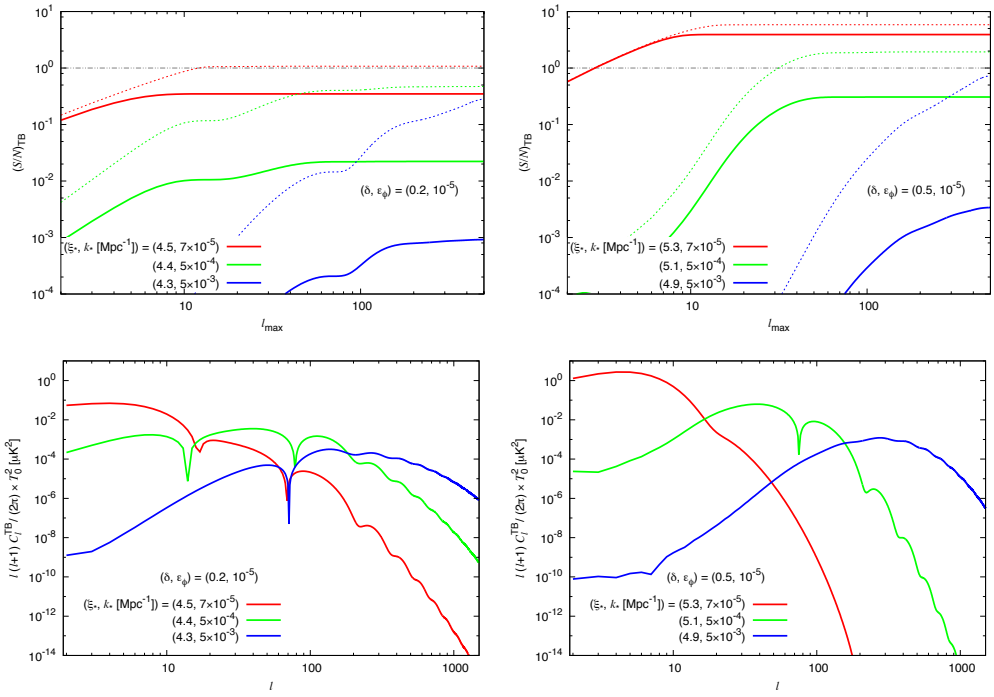

Figure 4.7: First row: Forecasted signal-to-noise ratio for the detection of the TB correlation in a realistic CMB experiment with *Planck*-like sensitivity (Colored solid lines), and in a cosmic variance limited, CMB experiment (Colored dotted lines), as a function of the maximum multipole ℓ included in the analysis. Second row: TB spectra.

$(S/N)_{BB} = \sqrt{(\ell_{\rm max}+3)(\ell_{\rm max}-1)/2}$ (black dotted lines), independently of the shape of C_ℓ^{BB} and the values of input model parameters. The S/N is lower in the *Planck*-like realistic experiment; however it can exceed one in the examples with the smallest values of k_* shown. A greater BB signal can be obtained at larger values of δ.

The sourced GW signal breaks parity, generating a nonvanishing correlation between the CMB temperature anisotropy and B-mode polarization (TB) [42, 43, 44, 71, 45]. In Figure 4.7, we compute the forecasted signal-to-noise ratio for our model with same parameters used in the previous figures. The S/N ratio has been computed via

$$\left(\frac{S}{N}\right)^2_{TB} = \sum_{\ell=2}^{\ell_{\rm max}} (2\ell+1) \frac{\left(C_\ell^{TB}\right)^2}{C_\ell^{TT} C_{\ell,{\rm dat}}^{BB}} \ , \tag{4.45}$$

in the *Planck*-like realistic experiment and the ideal cosmic variance-limited experiment. In the *Planck*-like measurement, we can neglect the noise spectrum of temperature mode

N_ℓ^{TT}, since this is negligibly small compared with the signal C_ℓ^{TT} on the scales of our interest ($\ell \leq 500$). We see that, among the examples shown, such a signature can be marginally detected only for the examples shown at $\delta = 0.5$ in the cosmic-variance-limited experiment. Not surprisingly, these are the cases that also lead to a stronger BB signal, cf. Figure 4.6. Among the examples we considered, these are the only cases for which $r_{\rm peak}$ (namely the tensor-to-scalar ratio evaluated at the top of the GW signal) is substantially greater than 10^{-2}. Based on the difference between the $\delta = 0.2$ and $\delta = 0.5$ cases, it is very likely that a large TB correlation can be produced at greater values of δ, possibly at a detectable level even in a *Planck*-like experiment. As a comparison, Ref. [44] forecasted that a one σ detection is possible for $r \gtrsim 0.002$ in the scale invariant case, and a few σ detection for the largest values of $r \sim .05$ that can be achieved in our scenario. The results of [44] are slightly more optimistic than ours because of the scale invariance of the correlator considered in that paper, that allows to use information from a larger number of multipoles.

4.3.2.2 CMB bispectra

Let us now study the possibility of detecting the non-gaussian statistics of the sourced modes. All the CMB temperature and polarization bispectra due to the scalar and tensor non-gaussianities, discussed in the following analysis, are computed by means of the techniques outlined in [72, 73].

In Figure 4.8 we show the forecasted signal-to-noise ratio for the detection of the sourced TTT bispectrum as a function of the maximum multipole ℓ included in the analysis, reading

$$\left(\frac{S}{N}\right)^2_{TTT} = \sum_{\ell_1,\ell_2,\ell_3=2}^{\ell_{\rm max}} \frac{\left|B^{TTT}_{\ell_1\ell_2\ell_3}\right|^2}{6C^{TT}_{\ell_1}C^{TT}_{\ell_2}C^{TT}_{\ell_3}} \,, \tag{4.46}$$

with

$$B_{\ell_1\ell_2\ell_3} \equiv \sum_{m_1m_2m_3} \begin{pmatrix} \ell_1 & \ell_2 & \ell_3 \\ m_1 & m_2 & m_3 \end{pmatrix} \langle a_{\ell_1 m_1} a_{\ell_2 m_2} a_{\ell_3 m_3} \rangle \tag{4.47}$$

denoting the angle-averaged bispectrum. Here we show only the results in a cosmic variance-limited CMB experiment. The same results will be obtained also in the *Planck*-like experiment, since the instrumental noise is perfectly negligible for $\ell \leq 500$. All the

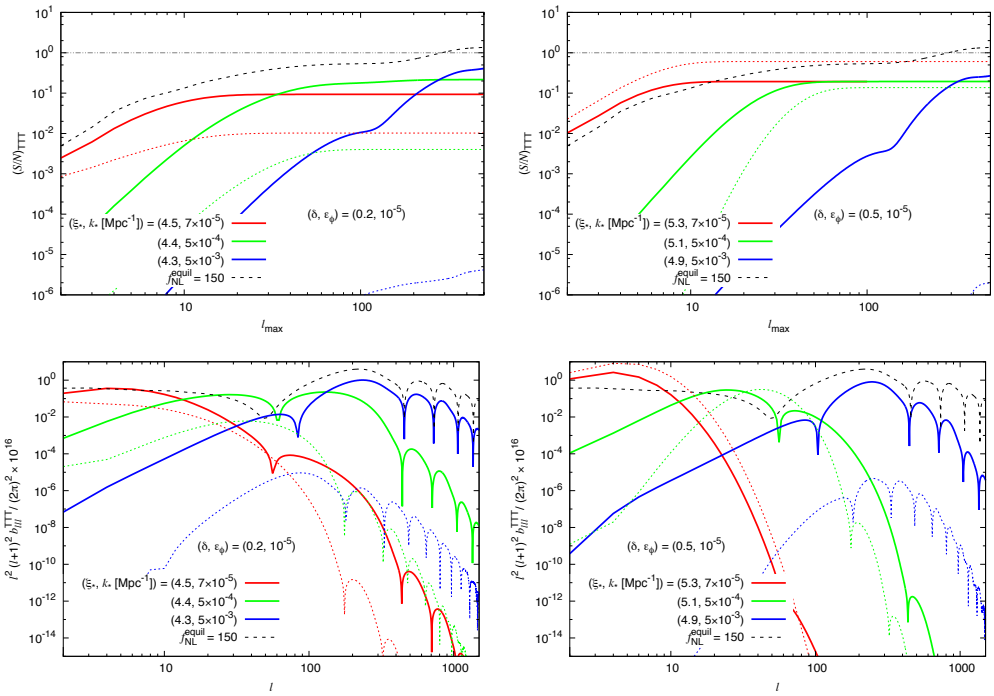

Figure 4.8: First row: Forecasted signal-to-noise ratio for the detection of the sourced TTT bispectrum in a cosmic variance-limited, CMB experiment, as a function of the maximum multipole ℓ included in the analysis. Second row: TTT reduced bispectrum for equilateral triangles of multipole ℓ. The colored lines are for the same parameters as in the previous figures. Solid (dotted) lines refer to the contribution to TTT from the sourced scalar (tensor) modes. The forecasted S/N ratio for scale-invariant equilateral non-gaussianity of magnitude $f_{\rm NL}^{\rm equil} = 150$ is added for comparison.

lines shown are for the maximum amount of particle production allowed by the WMAP TT data (namely, for $\xi_* = \xi_{*,\,\rm limit}$ shown in Figure 4.4).

Given that the sourced signal has a much greater deviation from gaussianity than the vacuum one [48], and given the stringent limit on non-gaussianity, one may have expected to find detectable non-gaussianity in the examples shown. Figure 4.8 shows that this is not the case. The main reason is that, for the values of k_* that we have chosen, the sourced signal manifests itself only at the largest CMB scales, so that only those scales are relevant for the phenomenological study of the bispectrum. This is confirmed by the colored lines shown in the Figure, where the signal-to-noise ratio saturates at values of $\ell_{\rm max}$ well below those included in the *Planck* studies (in particular, the smaller k_* is, the smaller is the value of $\ell_{\rm max}$ at which the signal-to-noise ratio saturates). This contrasts with the scale invariant case shown by the dashed line, where we can see that S/N continues to grow with increasing $\ell_{\rm max}$. The strong weakening of the non-gaussianity limits with decreasing values of $\ell_{\rm max}$ can be also seen for example in Figure 11 of [74].

In the analysis, we distinguish between the scalar $\left\langle \zeta^{(1)3} \right\rangle$ and tensor $\left\langle h_+^{(1)3} \right\rangle$ contribution to the TTT signal. In the tensor case, both even ($\ell_1+\ell_2+\ell_3 =$ even) and odd ($\ell_1+\ell_2+\ell_3 =$ odd) cases are included in the analysis [75, 71]. We can also see this from the second row of Figure 4.8, which presents the TTT reduced bispectrum, defined as

$$b_{\ell_1\ell_2\ell_3} \equiv \left[\sqrt{\frac{(2\ell_1+1)(2\ell_2+1)(2\ell_3+1)}{4\pi}} \begin{pmatrix} \ell_1 & \ell_2 & \ell_3 \\ 0 & 0 & 0 \end{pmatrix} \right]^{-1} B_{\ell_1\ell_2\ell_3} \ , \tag{4.48}$$

on equilateral triangles as a function of the multipole ℓ. We observe that, contrary to the scale invariant case, the bispectrum significantly decreases at the higher multipoles shown in the figure. Also in the second row, we distinguish between the contribution of the scalar and the tensor mode. While in the examples with $\delta = 0.2$ the scalar contribution dominates over the tensor one, the tensor mode plays a non-negligible or even dominant role in two of the examples shown at $\delta = 0.5$.

Another interesting non-gaussian signature of the sourced tensor mode is the BBB correlation. The signal-to-noise ratio is computed as

$$\left(\frac{S}{N}\right)^2_{BBB} = \sum_{\ell_1,\ell_2,\ell_3=2}^{\ell_{\rm max}} \frac{\left|B^{BBB}_{\ell_1\ell_2\ell_3}\right|^2}{6C^{BB}_{\ell_1,{\rm dat}}C^{BB}_{\ell_2,{\rm dat}}C^{BB}_{\ell_3,{\rm dat}}} \ . \tag{4.49}$$

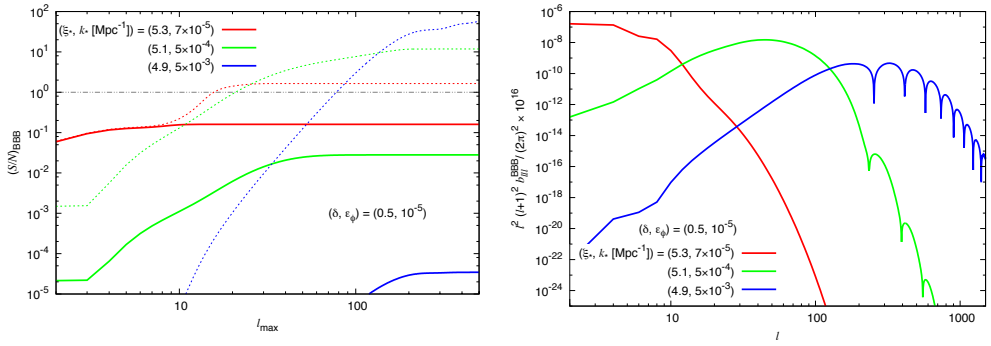

Figure 4.9: Left panel: Forecasted signal-to-noise ratio for the detection of the sourced BBB bispectrum in a realistic CMB experiment with *Planck*-like sensitivity (Colored solid lines), and in a cosmic variance limited, CMB experiment (Colored dotted lines), as a function of the maximum multipole ℓ included in the analysis. Right panel: BBB reduced bispectrum for equilateral triangles of multipole ℓ. The examples shown are for $\delta = 0.5$; the other parameters are chosen as in the previous figures.

Like the BB case, we here analyze the detectability both in a *Planck*-like experiment and in a cosmic-variance-limited experiment. In Figure 4.9 we show that this signal has a much higher prospect of being detected than the TB one in the cosmic-variance-limited measurement. Such large S/N seen in the figure is due to the fact that no instrumental error is assumed, so that all the noise is due to the small BB signal (instead, the largest TT signal due to the vacuum scalar modes constitutes a stronger noise for the TB measurement in the cosmic variance-dominated case).

We also computed the B-mode bispectrum for $\delta = 0.2$, obtaining a larger S/N ratio than in the $\delta = 0.5$ case shown in Figure 4.9. We do not show this result, as we are concerned about its reliability: the expression for the noise in (4.46) and (4.49) assumes that the signal is approximately gaussian. We investigate whether this is the case in Appendix C.5, where we estimate the departure from gaussianity of the full ζ and h_+ signals. Our estimate suggests that the departure is very small in the scalar case, and marginally small for h_+ at $\delta = 0.5$. However, this is not the case for $\delta = 0.2$. The result performed there suggests that the noise in this case may increase by a O (1) factor with respect to what we computed using (4.49). This still likely results in a potentially visible signal in a cosmic-variance-limited experiment, but, due to this uncertainty, we do not show this result here.

As in the TTT case, the S/N shown in the Figure 4.9 is computed by summing all the signals in $\ell_1 + \ell_2 + \ell_3 =$ even and $\ell_1 + \ell_2 + \ell_3 =$ odd. The sum enhances the S/N. On the other hand, the analysis in the limited domain, $\ell_1 + \ell_2 + \ell_3 =$ odd in TTT or $\ell_1 + \ell_2 + \ell_3 =$ even in BBB, is also very informative, since such signals originate from nonvanishing parity-odd non-gaussianity [76, 77], namely a distinctive signature of this model [21]. More comprehensive analysis with the other auto- and cross-bispectra including the E-mode polarization, not discussed above, may also help to improve the detectability [83, 84, 85, 70, 71, 74].

4.4 Summary

Given the expected improvements in sensitivity of the measurements aiming at the detection of primordial tensor modes, it is crucial to determine whether there are viable alternatives to the standard mechanism of creation of GWs through the amplification of vacuum fluctuations.

In this chapter we have shown that, if an axion-like field that is only gravitationally coupled to the inflaton experiences a transient epoch of relatively fast roll, then tensor perturbations can receive an additional contribution whose amplitude is not proportional to the energy scale of inflation. This implies that, for a broad range of parameters, tensors of inflationary origin might be detectable even if inflation happens at a low scale, and even for subplanckian inflaton displacements, without contradicting the existing constraints. Remarkably, the simple potential (4.3) naturally satisfies our requirements. To leave an observable GW signal, the transient epoch must occur while the large scale CMB modes leave the horizon.

The system we have considered comes with a rich set of signatures. First, the amplitude of the induced tensor modes can be strongly scale dependent. As a consequence significant B-mode CMB fluctuations might be detected only at scales related to the reionization bump, or only at the B-peak at $\ell \sim 80$, but not at both angular scales. In particular, detection at $\ell \sim 80$ without a corresponding detection at $\ell \sim 10$ would be interpreted as a locally blue tilt (similarly to the case in Ref. [55]) for the primordial

[21] See [78, 79, 77, 80, 75, 71] for the other possibilities to generate parity-violating CMB bispectra. See also [81, 82, 74] for the WMAP and *Planck* constraints.

tensor spectrum.

Moreover, the parity-violating nature of the process generates a characteristic $\langle TB \rangle$ correlator, that, in an ideal experiment, might be marginally detectable if the amplitude of the induced tensors is large enough.

Finally, the statistics of the produced gravitational waves has a departure from gaussianity that is significantly more marked than the vacuum modes. We have shown that for some choices of parameters, a cosmic variance limited experiment could detect a nonvanishing $\langle BBB \rangle$ correlator at a very high level of significance. We have studied only for a very few choices of parameters, but as we mentioned in the previous section, a larger tensor mode can be produced for increasing values of the axion mass (greater δ). In result, this can lead to larger TB and BBB correlators, which may be observable (particularly in the BBB case) already in a *Planck*-like experiment.

For the examples we have studied, the effect on the temperature correlators is statistically small. This is the case because *(i)* due to helicity conservation, the amplitude of the sourced scalar perturbations is smaller than that of the tensors, and *(ii)* all relevant effects take place at multipoles with $\ell \lesssim \mathcal{O}(10^2)$, where cosmic variance is large. We have thus explicitly verified that the model studied here is one of the very few existing examples for which a sourced GW signal is produced, while respecting the strong limits imposed from the observed T modes of the CMB.

On the other hand, different choice of parameters can be made in the same model that can result in a stronger scalar mode production than a tensor mode. This can easily be the case if the field σ rolls for a considerable amount to e-folds during inflation. This would generate a bump in the scalar modes with significant departure from gaussianity and with a greater width than in the examples considered above. By tuning the moment at which the considerable roll of σ takes place, the bump can manifest itself either at CMB or LSS scales.

Chapter 5

Small Scale Phenomenology of Axion-Gauge Interaction

"Ladies and gentleman, we have detected gravitational waves. We did it!" David Reitze

Previous chapter focused on the phenomenology resulting from the interaction of a pseudo-scalar and an Abelian gage field at the largest scales of our observable Universe. Remarkably, all the shown features originate from the single operator that is naturally expected to occur in theories with pseudo-scalar fields. In this chapter, we direct our focus towards the signatures of this interaction at scales much smaller than CMB ones. We will observe that this coupling has a small scale phenomenology that is as rich as the one at large scales.

Although CMB and LSS observations provide huge amount of vital information about the cosmological inflation [67, 87], they allow us to directly probe only a small fraction of the inflationary evolution. CMB and LSS probe the range of wave numbers $10^{-4}\,\mathrm{Mpc}^{-1} \lesssim k \lesssim 0.1\,\mathrm{Mpc}^{-1}$, corresponding to about 7 e-folds of inflation. CMB $y-$ and $\mu-$distortions may allow us to probe smaller scales, extending the above range to $\sim 10^{4}\,\mathrm{Mpc}^{-1}$. Even this extended range would cover only ~ 18 out of the $50-60$ e-folds of inflation that produce perturbations within our horizon. This leaves the remaining $\sim 30-40$ e-folds largely unexplored, apart from the bounds and the potential signatures

associated with primordial black holes (PBHs) that arise if the scalar perturbations have a sufficiently high amplitude at those scales [88, 89].

The recent gravitational wave observations at the Laser Interferometer Gravitational-Wave Observatory (LIGO) [90, 91] have opened a new observational window on general relativity, astrophysics and cosmology. Concerning cosmology, GW measurements from a network of terrestrial (such as LIGO, Advanced Virgo, KAGRA, and LIGO-India), from Pulsar Timing Array experiments, and from space interferometers (such as LISA) will provide invaluable information on galactic and stellar evolution. They will also give us the unique opportunity to probe specific models of inflation or specific mechanisms that could have been acting during inflation, at much smaller scales than those probed by CMB acoustic peaks, LSS and CMB distortions.

We explore here the possibility that an enhanced GW background is produced directly during inflation, in the frequency ranges probed by terrestrial or spatial GW interferometers. For instance, LIGO is mostly sensitive to GWs in the frequency range $(10 - 200)$ Hz [92], corresponding to wavenumbers $k \sim \left(10^{16} - 10^{17}\right) \mathrm{Mpc}^{-1}$. LISA is instead mostly sensitive to GWs in the frequency range $\left(10^{-4} - 10^{-1}\right)$ Hz [93, 94] corresponding to wavenumbers $k \sim \left(10^{11} - 10^{14}\right) \mathrm{Mpc}^{-1}$. Finally, PTA experiments are mostly sensitive to GWs in the frequency range $\left(10^{-9} - 10^{-7}\right)$ Hz [95, 96, 97] corresponding to wavenumbers $k \sim \left(10^{6} - 10^{8}\right) \mathrm{Mpc}^{-1}$ [1].

A different possibility is that density perturbations produced during inflation collapse to form PBH, which then evolve to the present universe, and ultimately give rise to BH-BH binary mergers, such as those observed by the LIGO detectors. This is a different mechanism of GW production, which is sensitive to modes of different scales. LIGO is sensitive to collisions between black hole binaries up to a few tens of solar masses, since the frequency of the innermost stable circular orbit $f_{\mathrm{ISCO}} = 4.4\,\mathrm{kHz}\, M_{\odot}/M$ has to be above the seismic noise to be detectable by LIGO [100]. As we discuss in Section 5.3.3, these black holes are expected to arise from merging and accretion from initial PBH seeds of masses between a few thousandth and a few hundredth of solar masses, corresponding to wavenumbers in the $\sim \left(10^{7} - 10^{8}\right) \mathrm{Mpc}^{-1}$ range. LISA is instead sensitive to black hole binaries from 10^5 to roughly 10^8 solar masses [101, 102, 103]. As we discuss in Section 5.3.3, these black holes are expected to arise from merging and

[1] Constrains on inflationary models from PTA experiments can be found for instance in [98, 99].

	$k \ \left[\mathrm{Mpc}^{-1}\right]$	$N_{\mathrm{estim.}}$
CMB / LSS	$10^{-4} - 10^{-1}$	$56 - 63$
$y-$ & $\mu-$distortions	$10^{-1} - 10^{4}$	$45 - 56$
$P_\zeta \rightarrow$ PBH $\rightarrow$ GW @ PTA	$10^{4} - 10^{5}$	$41 - 44$
$P_\zeta \rightarrow$ PBH $\rightarrow$ GW @ LISA	$10^{5} - 10^{7}$	$38 - 41$
$P_\zeta \rightarrow$ PBH $\rightarrow$ GW @ LIGO	$10^{7} - 10^{8}$	$35 - 37$
$P_{\delta g} \rightarrow$ GW @ PTA	$10^{6} - 10^{8}$	$36 - 40$
$P_{\delta g} \rightarrow$ GW @ LISA	$10^{11} - 10^{14}$	$22 - 28$
$P_{\delta g} \rightarrow$ GW @ LIGO	$10^{16} - 10^{17}$	$15 - 17$

Table 5.1: First column: list of observational windows on inflation. Second column: order of magnitude of the wavenumber of the primordial modes in the corresponding window. Third column: estimated number of efolds before the end of inflation at which corresponding modes exit the horizon. The 3rd, 4th and 5th rows refer to GWs produced by the mergers of BH binaries originated by PBHs due to enhanced primordial scalar perturbations. The last three rows denote primordial stochastic GW from inflation.

accretion from initial PBH seeds of masses in the $\sim 1 - 10^3\, M_\odot$ range, corresponding to wavenumbers in the $\sim \left(10^5 - 10^7\right) \mathrm{Mpc}^{-1}$ range. PTA experiments are mostly sensitive to black hole masses roughly from 10^8 to 10^{10} solar masses [104], which, assuming a comparable merging to the PBHs probed by LISA, corresponds to PBH seed massess in the $\sim 10^3 - 10^5\, M_\odot$ range, and to wavenumbers in the $\sim \left(10^4 - 10^5\right) \mathrm{Mpc}^{-1}$ range.

Table 5.1 summarizes these observational windows, together with the number of e-folds before the end of inflation at which the corresponding modes were generated [2]. It is fair to say that, while the near scale invariance and the other properites that we observe in the CMB radiation are a general prediction of inflation, the inflationary GW signals discussed in the table do not need to be present, and in fact do not arise in the minimal models characterized by an uncoupled inflaton moving in slow roll. Nonetheless, the unique opportunity offered by this new observational windows highly motivates the study of inflationary models or mechanisms that can provide such signals.

[2] The figures in the table should be understood as order of magnitude estimates, and have been obtained with some rounding errors. In these figures, we have assumed a constant Hubble rate $H = 10^{13}\,\mathrm{GeV}$ during inflation, and that the Planck pivot scale $k = 0.002\,\mathrm{Mpc}^{-1}$ exited the horizon at $N = 60$, resulting in $N \simeq 53.8 - \ln(k/\mathrm{Mpc}^{-1})$. In relating N to the PBH mass we assumed instantaneous thermalization after inflation. From eq. (D.5), this gives $N \simeq 37.9 + 1/2\, \ln(M/M_\odot)$, where $M_\odot \simeq 2 \times 10^{33}\, g$ is the mass of the sun.

One such mechanism that might leave imprints on those scales is the gauge field amplification in axion inflation. The chiral coupling between an axion (pseudo-scalar) and a gauge field enhances one of the polarizations of the gauge field, as shown in Chapter 3, and in turn amplified gauge modes source GW [3] [4] .

Obtaining an inflationary GW signal at interferometer scales requires either a bump or a blue spectrum, to increase the GW signal from the low value that it has at CMB scales. Such a blue signal is a natural expectation from the interaction $\Delta\mathcal{L}_{\rm int} \propto \phi F\tilde{F}$. This term is a total derivative in the case of constant ϕ. Therefore, the gauge field amplification is proportional to the speed of the inflaton field, which naturally increases towards the end of inflation. As with signatures on CMB scales [48], the main issue in models that generate a large GW signal is to make sure that they do not simultaneously overproduce scalar perturbations. For observables generated in the later stages of inflation, such as GWs at terretrial interferometers, the main concern is that the scalar perturbations could lead to the overproduction of PBHs [51, 116, 117, 118]. In fact, Ref. [51] showed that, if the existing analytic computations of the scalar perturbations induced from the chiral axion and gauge coupling at small scales are accurate, the PBH limits prevent the gauge field amplification to be strong enough to generate a visible GW signal at LISA and LIGO in models of chaotic inflation. However, we show in this chapter that PBH constraints preventing detectable GW are model dependent and can be evaded.

The first observation, is that there is an $\mathcal{O}(1)$ uncertainty on the amount of scalar perturbations generated by this mechanism in the regime which is necessary to produce a large enough signal. As already pointed out in Ref. [51], an $\mathcal{O}(1)$ decrease of the scalar signal would be enough for relaxing the PBH limit to allow a visible GW signal. Here we stress two additional possibilities.

[3] See Ref. [105] for a review of GW production during inflation from this and from other mechanims.

[4] The produced vector modes can then have several phenomenological consequences, including the generation of primordial magnetic fields [38], CMB non-gaussianity [48], increasing scalar power at large scales [50], primordial black holes [51, 107], chiral gravitational waves (While the original formulations via Non-Abelian fields [110, 111] are ruled out by CMB observations [17, 18, 20], chiral gravity waves can also be sourced by gauge fields in extensions of Chromo-Natural inflation and Gauge-flation [112, 113, 114, 115].) at CMB [39, 33, 171] and interferometer [31, 108, 109] scales.

Firstly, we note that, due to the typical blue spectrum of the sourced perturbations, the PBH limit is enforced by modes at much smaller scales than those probed by interferometers, particularly for the LISA and PTA cases. The PBH limit is enforced by modes generated around 50 efolds after CMB modes are generated (explicitly, assuming CMB modes are produced around $N = 60$, the PBH constraint comes from the modes around $N \simeq 10$), while LISA is mostly sensitive to modes produced at $N \sim 25$ before the end of inflation and for PTA, it is $N \sim 40$. Without committing to any specific inflationary potential (which is a necessity, if one wants to relate signatures at different scales), we ask the question whether the PBH limit at any given scale precludes an observable GW signal at that scale. The question is nontrivial, and it must be answered by an explicit computation, as the answer ultimately depends on the sensitivity of the GW measurement. Our computations provide a positive answer for the PTA-SKA projected sensitivity [119] and for the LISA sensitivity curves reported in [94], and a negative one for the current and projected AdvLIGO sensitivity curves reported in [92]. We reached this conclusion for two different implementation of the axion-gauge coupling mechanism that are studied in Chapter 3. The first one employs an axion as the inflaton and couples it to a gauge field via chiral coupling. The details of gauge amplification in this case can be seen at Subsection 3.1.1. First implemention employs a modification of the inflaton (axion) potential short after the LISA (or AdvLIGO) modes are produced. Specifically, a mild decrease of the inflaton slope is arranged for this purpose (in the concrete example we studied, we showed that a decrease of the slope of a factor of 3 is sufficient to slow down the inflaton, and to sufficiently weaken the PBH constraint). The second model we considered is a two field model, introduced in Ref. [171] and already studied in Section 4, to produce a localized bump in the GW spectrum at CMB scales. In this model, the gauge field amplification is due to the chiral coupling with a pseudoscalar σ that is not the inflaton, and it rolls only for a few e-folds of inflation. The details of gauge amplification in this case can be seen at Subsection 3.1.2. Both implementations lead to a positive (negative) conclusion for the projected PTA-SKA and LISA (AdvLIGO) sensitivity curves.

The discussion above refers to the GW signal directly sourced by the gauge fields during inflation, and that gives rise to the observational windows listed in the last three rows of Table 5.1. The mechanism of gauge field amplification may also give rise to a

different, and more complicated, mechanism of GW production. Specifically, it may be possible that the scalar perturbations give rise to a significant amount of PBHs compatible with observations, that act as seeds for structure and may be responsible for most of the observed non-stellar black holes. Their mergers lead to specific GW signals at detectors and their mergers throughout the cosmic history lead to a different type of stochastic GW background than primordial one [5]. These PBH could also be identified as the dominant component of the dark matter of the universe [89, 121, 122, 123, 124, 125]. The evolution from the seeds to the present black holes involves merging of the different PBHs and gas accretion [122], and is beyond the scope of this chapter. Nevertheless, we briefly review this possibility here, since the gauge field amplification provides a mechanism for the generation of the seeds which is alternative to another mechanism that have been proposed in the context of hybrid inflation [88, 89]. We discuss this possibility in the context of the two-field $\phi - \sigma$ model, as it produces a localized bump of scalar field modes, and therefore a narrow spectrum of black hole masses, for which estimates can be more easily made. As mentioned, this new mechanism of GW production provides a different window on inflation (third, fourth and fifth rows of Table 5.1).

This chapter has been organized as follows. In Section 5.1 we review the limits on PBH and on the scalar perturbations generated from this mechanism. In Section 5.2 we discuss the GW production for the direct coupling $\phi F\tilde{F}$ between the inflaton and the gauge field. In Section 5.3 we discuss the case of localized GW production from a field σ different from the inflation. Section 5.4 provides a summary of our results and some concluding remarks. Some details of calculations are presented at Appendix D. This Chapter is mainly based on Ref. [173].

[5] Actually there are more stochastic GW backgrounds in PBH scenario. One of them is induced GW resulting from the schematic interaction $\zeta + \zeta \to h$ at second order in perturbation theory. Another one is the stochastic GW background due to the non-spherical collapse of the fluid during PBH formation. These are beyond the scope of this chapter.

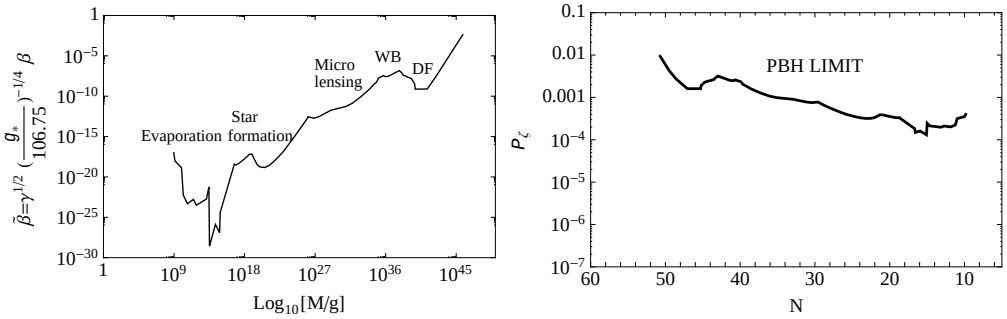

Figure 5.1: Left panel: Limits on the rescaled black hole fraction $\tilde{\beta}$ as a function of the black hole mass. Right panel: Same limits, written as a bound on the primordial curvature(density) perturbations as a function of number of e-folds before the end of inflation, assuming a constant Hubble rate $H = 10^{13}\,\mathrm{GeV}$ during inflation, and a χ^2 statistics of the density perturbations (see Appendix D.1).

5.1 Limits on scalar perturbations, and prospects for the detection of a stochastic GW background

In the left panel of Fig. 5.1, we present the limits on PBH in a wide mass spectrum. We show the limits in terms of the rescaled variable $\tilde{\beta}$ introduced in [126] (where it was denoted as β' there) as a function of the black hole mass. As we explain in Appendix D.1, the quantity $\tilde{\beta}$ is related through equation (D.13) to β, that is the fraction of regions (of a given size, corresponding to a given black hole mass) that collapse to form a black hole. We now list the origin of the limits included in this figure.

Going from smaller to greater black hole mass M,[6] the first limits shown in Fig. 5.1 are a consequence of the black hole evaporation which, depending on M, can photodissociate elements formed during Big-Bang Nucleosynthesis, modify the CMB, distort the galactic and extra-galactic $\gamma-$ray background. This set of constraints is studied in details in Ref. [126] (see also [127]). The constraints we show in the mass range $5 \times 10^{16} \lesssim M(\mathrm{g}) \lesssim 10^{26}$ are obtained from the effects of the capture of black holes by stars (the black holes would eventually destroy the neutron star or white dwarf remnants),[7] according to the updated computations of Ref. [130]. The limits in the

[6] We do not include limits at $M < 10^9 g$ shown in Fig. 9 of [126] as they are model dependent, and assume that the black hole evaporation leaves behind stable relics.

[7] These updated constrains are stronger than those arising from the lack of observation of femtolensing

$10^{26} \lesssim M(\mathrm{g}) \lesssim 10^{35}$ range are due to the lack of observations of short duration microlensing events by the MACHO and EROS Collaborations [131, 132]. These experiments lasted for approximately six years each, and thus could not constrain higher masses of Massive Compact Halo Objects, which correspond to long duration events of order a decade. The limit indicated as "WB" is obtained from the non observation of wide binary disruption [133]. Finally, the "DF" limit refers to dragging of halo objects into the Galactic nucleus by dynamical friction [134]. For the last three constraints, we took the limits as reported in Figure 3 of [135]. We did not include the CMB bounds from $y-$ and $\mu-$distortions [8] due to X-rays emitted by gas accretion onto PBHs before recombination, because there was an error in Ref. [139] and with a recent reanalysis, the bounds have shifted by a few orders of magnitude towards larger masses [140]. We also ignored the Eridanus-II bounds of Ref. [141] because the star cluster at the center of the dwarf galaxy could be stabilized by an intermediate mass BH, which would prevent the puffing up of the system. This effect shifts the bounds again below the DF bounds.

In Appendix D.1 we show how these limits translate into an upper bound on the amount of primordial scalar perturbations P_ζ as a function of the number of e-folds N before the end of inflation at which they leave the horizon (see the right panel of Figure 5.1). Our computations focus on the PBH formed by scalar perturbations caused by gauge field amplification in axion inflation. The scalar modes obey a χ^2 statistics [51], which significantly improves PBH production and tightens bounds on P_ζ with respect to Gaussian statistics, as we show in Appendix D.1. We also show there that β changes dramatically with P_ζ, which explains why the limit in the left panel of Figure 5.1 changes by ~ 25 orders of magnitude, while that in the right panel changes by only ~ 2.

---

of $\gamma-$ray bursts [128], and the lack of microlensing events at Kepler [129], which we therefore do not show here.

[8] $y-$ and $\mu-$distortions also put a bound on the scalar power spectrum (independently on whether PBH form) for modes that re-enter the horizon at $z \lesssim 10^6$, due to the fact that the energy associated with these modes does not perfectly thermalizes with the background energy density. $\mu-$distortions are mostly affected by primordial perturbations of wavenumbers $50\,\mathrm{Mpc}^{-1} \lesssim k \lesssim 10^4\,\mathrm{Mpc}^{-1}$ [136, 138], which roughly corresponds to modes that left the horizon at $45 \lesssim N \lesssim 50$ e-folds before the end of inflation (this assumes that the Planck pivot scale $k = 0.002\,\mathrm{Mpc}^{-1}$ corresponds to $N = 60$.) $y-$distortions are instead mostly sensitive to modes $1\,\mathrm{Mpc}^{-1} \lesssim k \lesssim 50\,\mathrm{Mpc}^{-1}$ [136, 138], which roughly corresponds to $50 \lesssim N \lesssim 54$. All the sourced signals that we consider in this chapter take place at scales much smaller than these, and therefore do not induce these distortions.

The field amplification enhancing the scalar perturbations also produces a primordial stochastic background of gravitational waves. We aim to understand under which conditions this background can be observed, without violating the bounds from PBH.

It is customary to express the amplitude of the GW background in terms of their present fractional energy density per logarithmic wavenumber interval $\Omega_{\rm GW}$, which is related to the GW power spectrum by (see [108] for details)

$$\Omega_{\rm GW} \equiv \frac{1}{3H_0^2 M_P^2}\frac{\partial \rho_{\rm GW,0}}{\partial \log\, k} = \frac{\Omega_{\rm R,0}}{24}\left(P_L + P_R\right)\ , \tag{5.1}$$

where $\Omega_{\rm R,0}\, h^2 \simeq 4.2 \times 10^{-5}$ refers to radiation today (including neutrinos, as if they were still relativistic). The quantity $\Omega_{\rm GW}$ is typically plotted as a function of frequency $f = k/2\pi$, which is related to the number of e-folds by

$$N = N_{\rm CMB} - 44.92 + \ln\left(\frac{k_{\rm CMB}}{0.002\,{\rm Mpc}^{-1}}\right) - \ln\left(\frac{f}{100\,{\rm Hz}}\right) + \ln\left(\frac{H_N}{H_{\rm CMB}}\right) \tag{5.2}$$

where $N_{\rm CMB}$ is the number of e-folds at which the mode $k_{\rm CMB}$ left the horizon. In (5.2) we have set this scale to the Planck pivot scale, which in this chapter we assume to correspond to $N_{\rm CMB} = 60$. We note that the last term in (5.2) accounts for the variation of the Hubble rate during inflation (H_N denotes the value at N e-folds before the end of inflation, and $H_{\rm CMB}$ at $N = N_{\rm CMB}$). This factor was neglected in Ref. [108].

In the following sections we compare the GW signal produced in models of axion inflation with the sensitivity curves of AdvLIGO (from top to bottom, O1-O3-O5 lines of Figure 1 of [92]), LISA (from bottom to top, A5M5-A5M2-A2M5-A2M2-A1M5-A1M2 lines of Figure 1 of [94]; the various lines refer to different choices for the length of the LISA arms and for the LISA duration. Specifically, the labels A1, A2, and A5 correspond, respectively, to 1, 2, and 5 million km; the labels M2 and M5, correspond, respectively, to 2 and 5 years), and of Pulsar Timing Array experiments (the curve labeled by PTA corresponds to the combination of the current limits of [95, 96, 97]; the curve labeled by SKA corresponds to the forecast sensitivity of the Square Kilometer Array PTA experiment, obtained using the GWPlotter tool [119]).

5.2 Production from a rolling inflaton ϕ

In this section we study the small scale phenomenology of the inflationary model

$$\mathcal{L} = -\frac{1}{2}\left(\partial\phi\right)^2 - V\left(\phi\right) - \frac{1}{4}F^2 - \frac{\phi}{4f}\,F\,\tilde{F}\,, \tag{5.3}$$

for a pseudo-scalar inflaton ϕ coupled to a U(1) vector field (F is the field strength associated to the vector, and $\tilde{F}$ its dual). We divide the discussion in two subsections. In the first one, we review results from the literature to compute the scalar and tensor (GW) primordial perturbations generated in this model. In the second subsection we then show that, depending on the inflaton potential and on the coupling strength to vector, this model can result in observable gravity waves at interferometer scales, without overproducing primordial black holes.

5.2.1 Production of scalar and tensor modes

We consider inflation in the model described by the lagrangian (5.3). Due to the motion of the inflaton, the coupling amplifies one circular polarization of the vector field, leading to (See [38] and Chapter 3 for details)

$$A_+ \simeq \frac{1}{\sqrt{2k}}\left(\frac{-k\tau}{2\xi}\right)^{1/4}\exp\left(\pi\xi - 2\sqrt{-2\xi k\tau}\right)\,, \qquad\qquad \xi \equiv \frac{\dot{\varphi}}{2fH}\,, \tag{5.4}$$

where k is the comoving momentum of the gauge field mode, τ is conformal time, and H the Hubble rate (we are assuming $\xi > 0$; in the opposite case, the A_- polarization is amplified). Moreover, φ denotes the zero mode of the inflaton field, $\phi = \varphi(t) + \delta\phi\,(t,\,\vec{x})$. The amplification of any gauge field mode takes place only when the size of the mode is comparable to the horizon, so that this mechanism has no UV nor IR singularities. When deep inside the horizon, the gauge field mode has a standard dispersion relation, and it is not amplified. At super-horizon scales, the growth weakens and it becomes subdominant to the expansion of the universe, so that the gauge field is diluted away by the expansion. The approximate expression (5.4) is valid in the interval $1/8\xi \ll -k\tau \ll 2\xi$. These are the times during which the mode grows, and remains at a sizable level, before being diluted away. Therefore this approximation allows to obtain a good estimate of the phenomenological signatures caused by the mode.[9]

[9] We omit several details of the computations. One can refer to Section 2.1 of [172] or Subsection 3.1.1 for a detailed summary of the gauge field amplification; to Section II.B of [108] or Chapter 6 for

The gauge modes source scalar perturbations (through the inverse decay $A_+ + A_+ \to \delta\phi$ process) and gravitational waves (through the gravitational interaction $A_+ + A_+ \to h_+$, and $A_+ + A_+ \to h_-$, where $h_\pm$ denotes the two GW polarizations). These signals add up incoherently to the usual vacuum ones, so that the scalar and tensor correlators are the decoupled sum of a vacuum (which we denote by the suffix v) and sourced (suffix s) contribution. The fact that only A_+ modes are amplified (which is due to the breaking of parity associated to the pseudo-scalar inflaton) results in a much greater production of h_+ with respect to h_-, namely the sourced GW background breaks parity nearly maximally [39]. In the following, we disregard the highly subdominant sourced h_- mode. One finds [10]

$$\begin{aligned} P_\zeta(k) &\simeq P_{\zeta,v}(k) + P^2_{\zeta,v}(k)\ \hat{f}_{2,\zeta}(\xi)\ \mathrm{e}^{4\pi\xi}\ , \\ P_{\rm GW}(k) &= P_{GW,+}(k) + P_{GW,-}(k) \simeq \frac{2H^2}{\pi^2 M_p^2}\left[1 + \frac{H^2}{M_p^2}\,\hat{f}_{2,+}(\xi)\ \mathrm{e}^{4\pi\xi}\right]\ , \end{aligned} \tag{5.5}$$

where we recall the standard vacuum result $P_{\zeta,v} \simeq\ H^4/(4\pi^2\dot{\varphi}^2)$.

Typically, the parameter ξ adiabatically grows during inflation (we note that $\xi \simeq \sqrt{\frac{\epsilon}{2}}\,M_p/f$, where ϵ is the usual slow roll parameter). Therefore, the quantity ξ in eqs. (5.4) and (5.5) should be understood as the value acquired by ξ when the mode in consideration crosses the horizon (the same is true for the quantity H appearing in (5.5)). At CMB scales, ξ is constrained by non-gaussianity [48, 67] and by the growth of the scalar spectrum with k [50, 67] (one typically obtains $\xi_{\rm CMB} \lesssim 2.2 - 2.5$, depending on the specific potential, and priors [67]). For such values of ξ, the amplified gauge quanta modify the background dynamics in a negligible manner.

As the inflaton speeds up during inflation, ξ increases. At larger values of ξ, the amplified gauge modes can significantly backreact on the background evolution. The

the study of the backreaction of the vector field on the background dynamics; to Section III of [49] and Section II of [51] for the computation of the scalar perturbations sourced by the vector modes during inflation; finally, to Section V of [49] and to Section V of [108] for the computation of the GW sourced by the vector modes during inflation.

[10] The two functions in this parametrization have the behavior $\hat{f}_{2,\zeta}(\xi) \simeq 7.5\times10^{-5}/\xi^6$ and $\hat{f}_{2,+}(\xi) \simeq 4.3\times10^{-7}/\xi^6$ in the $\xi \gg 1$ regime. The full dependence is given in [49]. We note the presence of a typo in eq. (3.40) of [49], namely the r.h.s. should contain an additional $\frac{1}{4}$ factor. This typo did not propagate to any of the other equations or figures of that work.

dominant effect is an additional friction in the equation for the inflaton field (see Subsection 6.2.1 for eqn of motion and more details). (the physical reason for this is that the gauge field amplification occurs due to the motion of φ, and therefore at the expense of the inflaton kinetic energy). This can give rise to a transition [108] between the usual slow roll evolution at early times and a new attractor solution at late times, where the gauge field amplification dominates over the Hubble friction. The increase of ξ also gives rise to a significant increase of the sourced inflaton perturbations and gravity waves.

The increase of the inflaton perturbations complicates the system of scalar perturbations. Eq. (5.4) for the vector modes has been obtained for a homogeneous inflaton (we note that $A_+ [\xi [\varphi]]$ in that expression). However, we expect that at sufficiently large ξ the inflaton perturbations will be large enough to significantly impact the gauge mode solution; hence, we need a solution solution for a more general $A_+ [\varphi + \delta\phi]$ case. This quantity acts as a source in the equation for the inflaton perturbations. Expanding this source in $\delta\phi$ introduces additional terms in the equation for the inflaton perturbations, which must be relevant at sufficiently high ξ. A complete equation for the scalar perturbations in this regime has not yet been obtained. Here we employ the approximate analytic equation first derived in [142], and later used in [108, 51] [11]

$$\delta\ddot{\phi} + 3\beta_{\rm fric} H \delta\dot{\phi} + k^2 \delta\phi + V'' \delta\phi = \frac{\vec{E}\cdot\vec{B} - \langle \vec{E}\cdot\vec{B}\rangle}{f} \,, \tag{5.6}$$

where

$$\beta_{\rm fric} \equiv 1 - \frac{2\pi\xi}{f} \frac{\langle \vec{E}\cdot\vec{B}\rangle}{3H\dot{\varphi}} \,. \tag{5.7}$$

In our expressions, $\vec{E}$ and $\vec{B}$ denote the "electric" and "magnetic" field associated with the solution (5.4).[12] Taking $\beta_{\rm fric} = 1$ in (5.6) amounts in neglecting any dependence of the vector fields on $\delta\phi$. The sourced scalar solution in (5.5) has been obtained with this assumption, and, for the reasons we just discussed we expect it to be accurate at sufficiently small ξ. Taking instead $\beta_{\rm fric}$ as in (5.7) amounts into including one of the effects arising from the dependence of the gauge field from $\delta\phi$. As the solution (5.4) depends on the time derivative of the inflaton zero mode, it is reasonable to

[11] Following standard notation, dot denotes derivative with respect to physical time, while prime on a function denotes derivative with respect to its argument.

[12] We use standard electromagnetic notation for convenience, but we are not necessarily implying that the vector field in (5.3) is the Standard Model photon.

expect that the first effect of $\delta\phi$ in the source will be through the change $\delta\xi = \frac{\delta\xi}{\delta(\delta\dot{\phi})}\delta\dot{\phi}$, which precisely leads to (5.7). This was the reasoning adopted in [142, 108, 51] and we also follow it in the present work. However, we alert the reader that eq. (5.6) is not a complete one, and that additional terms, not included in this equation, may also become important when the departure of $\beta_{\rm fric}$ from 1 becomes relevant.

As shown in [108, 51], eq. (5.6) leads to the following estimate for the sourced scalar power spectrum

$$P_{\zeta,s}\left(k\right) \simeq \left(\frac{\langle \vec{E}\cdot\vec{B}\rangle}{3\beta_{\rm fric}H\dot{\varphi}\,f}\right)^2 \mathcal{F}^2\,. \tag{5.8}$$

As seen for instance from Figure 4 of [51] the sourced scalar solutions in (5.5) and (5.8) are in remarkable agreement with each other at sufficiently small ξ. This is in particular true for the values of ξ at which the CMB bounds have been derived. However, as ξ increases, the solution (5.8) becomes significantly smaller than that in (5.5), due to the additional friction included in (5.6) for $\beta_{\rm fric} \neq 1$. We use eq. (5.8) for our results below.

The factor $\mathcal{F}$ in the expression (5.8) was not present in the computations of refs. [142, 108, 51]. This factor accounts for the impact of the energy density in the gauge field to the denominator of $\zeta \equiv -\frac{H\delta\rho}{\dot{\rho}}$. We evaluate it in Appendix D.2, following the observations recently made in [143] although it has only a marginal relevance. From both numerical and analytical computations, we find that this factor evolves from 1 in the regime of negligible backreaction of the gauge field on the background dynamics (appropriate at CMB scales) to $\frac{7}{8}$ in the regime of strong backreaction (appropriate of late times). The limiting value $\frac{7}{8}$ is independent of the inflaton potential, of the value of f, and of the number of amplified gauge fields. In the evolutions studied in this study, this limiting value is reached only at the very end of inflation. To give a reference value, $\mathcal{F} \simeq 0.98$ at $N = 10$ in the evolution shown in Figure 5.2.

The gauge fields also source metric perturbations, and the solution (5.4) has been used in obtaining the second line of (5.5). Metric perturbations would modify (5.4) in a completely negligible manner (due to gravity). Therefore we can ignore any $\frac{\delta A_+}{\delta h}\,\delta h$ correction in the source of the equation for the gravitational waves, and use the second line of (5.5) in the results presented below.

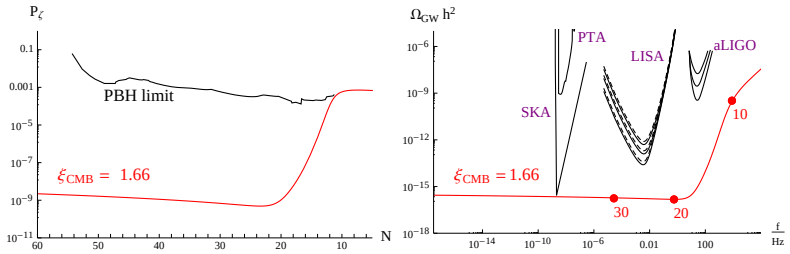

Figure 5.2: On left: Scalar power spectrum in axion inflation for a linear inflaton potential, in the approximation (5.8). The coupling to gauge field is chosen as large as allowed by the PHB bounds shown in the figure; this gives $\xi_{\rm CMB} \lesssim 1.66$ at 60 e-folds before the end of inflation. On right: Corresponding GW signal for the same model and parameters chosen in the left panel. The modes that left the horizon $30, 20$, and 10 e-folds before the end of inflation are shown with red dots.

5.2.2 Phenomenology at sub-CMB scales

We are now ready to discuss the phenomenology of this model at scales much smaller than the CMB ones. In particular, we want to review the result of Ref. [51], which appears to be a major obstacle against the possibility of observing GW at interferometer scales from the model given in (5.3). Ref. [51] computed the primordial scalar and tensor perturbations produced in this model for a quadratic inflaton potential. They found that, due to the non-Gaussian nature of the scalar perturbations, the scalar field amplification can easily overcome bounds imposed by PBH. They can be avoided only provided that $\xi_{\rm CMB} \lesssim 1.5$ at $N = 60$ e-folds before the end of inflation. Once this limit is respected, the GW production is below the PTA-SKA, LISA, and AdvLIGO sensitivities. As by now the quadratic inflaton potential is ruled out by the CMB observations [67], we perform an analogous computation for a linear inflaton potential, $V_{\rm inf} = M^3\phi$ (M is set by COBE normalization as usual), which is motivated by monodromy [144, 145].

We numerically integrate the background equation of motion for the inflaton and the Friedmann equation, keeping into account the backreaction of the produced gauge quanta in both equations (see [108] and eqns. 6.10 and 6.11 in Subsection 6.2.1). We iteratively vary the axion scale f and the mass parameter in the linear potential so to obtain the correct power spectrum normalization $P_\zeta = 2.2 \times 10^{-9}$ [67] at $N = 60$, and so to obtain the largest inflaton-vector coupling (smallest f) allowed by the PBH limit. This results in $\xi_{\rm CMB} \simeq 1.66$ at $N = 60$, close to the value found in [51] for a quadratic

inflaton potential.[13] We show the scalar spectrum, and the PBH bound, in the left panel of Fig. 5.2. The right panel of the figure shows the GW produced for the same linear potential and parameters choice. Also in this case, the limit from PBH bound on the gauge field enhancement forces the GW signal to be too small to be observed at PTA-SKA, LISA, and AdvLIGO scales.

We stress that this conclusion strongly relies on the scalar modes being accurately described by Eq. (5.6) in the $\xi \gg 1$ regime. As we discussed after Eq. (5.6), this equation should receive additional corrections in this regime, that can change the result (5.8) by an $\mathcal{O}(1)$ factor. As already remarked in Ref. [51], an $\mathcal{O}(1)$ decrease of the scalar power spectrum would be enough to make the PBH limit unimportant. Ref. [146] proposed some conditions for the validity of perturbative computations of the scalar perturbations in this model. The conditions were reanalyzed in Ref. [172], which showed that these criteria are satisfied for $\xi \lesssim 4.8$. This is parametrically close to the values necessary to generate PBH, indicating that, while Eq. (5.6) very likely provides a correct estimate for the amplitude of the scalar modes, $\mathcal{O}(1)$ corrections are a possibility.

If we assume that the result (5.8) is reliable, we can still have two simple possibilities that make the PBH limit less important from the specific case studied in [51]. We discuss these two possibilities in the two separate parts in the reminder of this subsection.

5.2.2.1 Dependence on the inflaton potential

We observe from Fig. 5.2 that the PBH limit $\xi_{\rm CMB} \lesssim 1.66$ is enforced by modes that left the horizon at $N \simeq 10$ e-folds before the end of inflation. On the other hand, the

[13] We note that the upper bound on ξ is obtained from PBH bounds at the latest times of the evolution (namely, from the smallest values of N). Since $M \propto \mathrm{e}^{2N}$, these smallest scales correspond to the smallest PBH masses. (i) We only consider limits for $M > 10^9 g$, for the physical reasons that we stated in footnote 1. Ref. [51] made the same physical assumption, but it considered masses starting from $M > 10^8 g$ (we believe that the $10^9 g$ figure is more in line with Fig. 9 of [126]). (ii) We included an efficiency factor $\gamma \simeq 0.2$ in our relation (D.5). (iii) Our relation (D.5) accounts for the variation of the Hubble rate during inflation. All these three factors contribute to increase the value of $N_{\rm min}$ at which the PBH bound is present, giving a weaker constraint on P_ζ in our case, with respect to [51]. We repeated their computation for quadratic inflaton potential, but with our limit on P_ζ, obtianing $\xi_{\rm CMB} \lesssim 1.82$, rather than their result $\xi_{\rm CMB} \lesssim 1.5$. This slightly weaker limit does not change the physical conclusion of [51] that the PBH bound prevents GWs from being observable in a quadratic inflaton potential.

PTA, LISA, and AdvLIGO bands include modes that left the horizon earlier. This is particularly true for PTA and LISA, which are mostly sensitive to modes produced, respectively, at $N \simeq 40$ and at $N \simeq 25$. Therefore, the interplay between the PBH limit and the possible GW signal strongly depends on the evolution of ξ, and, ultimately, on the inflaton potential, in the latest stages of inflation. We have very little knowledge of the inflaton potential after the CMB and LSS modes are produced, and we can easily imagine potentials for which ξ has a peak at some intermediate value of N, and then decreases, without ever violating the PBH bounds.

This is for example immediately achieved if the linear potential changes its slope at some given point during inflation, as in the Starobinsky model [147]. In that work, the potential changes its slope abruptly at some given value $\phi = \phi_*$. Here, we consider a "regularized" version of that model, that has the smooth transition

$$V = \begin{cases} -M^3\,\phi & , \quad \phi < \phi_1 \\ M^3\,\frac{(1-r)(\phi+\phi_1)^2 - 2\phi(\phi_1 - 2r\phi_1 + \phi_2)}{2(\phi_2-\phi_1)} & , \quad \phi_1 < \phi < \phi_2 \\ -M^3\,\frac{(1-r)(\phi_1+\phi_2)}{2} - r\,M^3\,\phi & , \quad \phi > \phi_2 \end{cases} . \tag{5.9}$$

We choose the potential to be linear both at $\phi < \phi_1$ and $\phi > \phi_2$, with a smaller slope (by a factor $r < 1$) in the second region. The potential in the intermediate region is a second order polynomial chosen so that V and V' are continuous at both ϕ_1 and ϕ_2.

In Figure 5.3 we compare this modified potential (solid line) with the unmodified linear potential (dashed line). we note that the potential (5.9) is unbounded from below and it needs to be further modified at greater field values to have a stable minimum with $V = 0$. The value of ϕ_1 is chosen so that the departure from the initial linear potential occurs at $N = 24$ (this gives $\phi_1 \simeq -5.22\,M_p$; we then choose $\phi_2 = -4.22\,M_p$). We then choose $r = 0.3$, so that the derivative of the potential decreases of a factor of about $\sim 1/3$ from ϕ_1 to ϕ_2.

We choose the inflaton-gauge field maximum coupling allowed by CMB in the case of a linear potential, $f = M_p/48$, see Ref. [67]. This corresponds to $\xi_{\rm CMB} \simeq 2.41$ at $N = 60$. The inflaton speed increases in the initial linear potential until ϕ reaches ϕ_1 and at this moment, $\xi \simeq 4.43$. After the transition $\phi = \phi_1$, the inflaton speed, and the parameter ξ decrease due to the decrease of the slope of the inflation potential. This significantly reduces the gauge field amplification and the sourced scalar and tensor modes. In Figures 5.3 and 5.4, we also show the unmodified linear potential, the corresponding

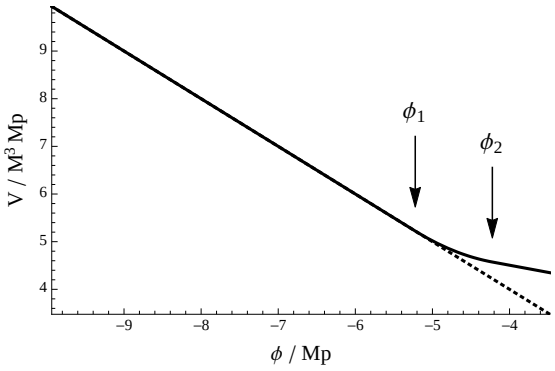

Figure 5.3: The solid line shows the inflaton potential (5.9) spanned by the inflation from $N = 60$ to $N = 5$, with parameters leading to the spectra of Figure 5.4. The two arrows indicate the position of the two transition regions (the potential is linear both at $\phi < \phi_1$ and $\phi > \phi_2$, but with a different slope). The dotted lines shows an unmodified linear inflaton potential.

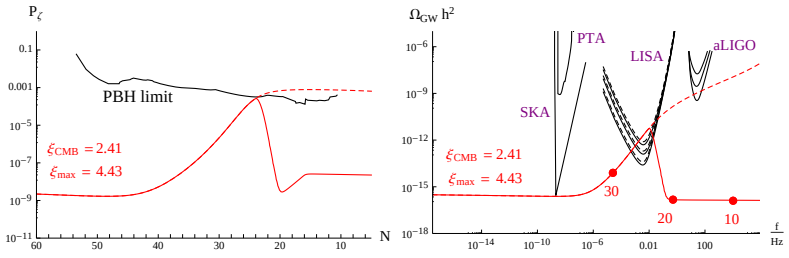

Figure 5.4: As in Figure 5.2, but with a larger coupling of the inflaton to the gauge field, and with the modified inflaton potential (5.9). The solid lines are the spectra obtained in this case (the corresponding potential is shown in the solid line of Figure 5.3). The dashed lines show how the spectra would continue at small scales if the instead the inflaton potential remained linear at all values (corresponding to the dashed line in Figure 5.3).

scalar and GW spectra with dashed lines for a clear comparison. Because the gauge field amplification is strongly dependent on the particle production parameter ξ, the mild change of the potential results in completely different signal for the modes that exit the horizon at those scales.

We see that the potential (5.9) can indeed result in a visible signal at LISA scales, without violating bounds from PBH. Many other examples can be constructed. Although we do not show here explicitly, it is also clear to see that same potential feature (this time slope change corresponding to $N \sim 40$) can lead to a detectable signal at PTA-SKA experiment without violating PBH limits.

5.2.2.2 Dependence on the number of gauge fields

Let us assume that $\mathcal{N} > 1$ vector fields are amplified by the $\mathcal{L} = -\frac{\phi}{4f} F_i \tilde{F}_i$ interaction ($i = 1, \ldots, \mathcal{N}$). For simplicity, we assume that all the fields have the same coupling to the inflaton. This is what happens if the vectors are the different components of a Non-Abelian group. This has several consequences: (i) an increased backcreaction, that will slow the motion of the inflaton more than in the $\mathcal{N} = 1$ case; (ii) an increased GW source: as the different gauge fields are statistically uncorrelated with each other, the GW power spectrum - for any given value of ξ - increases by $\mathcal{N}$ with respect to the case of a single vector field; [14] (iii) an analogous increase $\propto \mathcal{N}$ taking place for the power spectrum scalar perturbations, schematically, for $\zeta \propto \sum_{i=1}^{\mathcal{N}} \vec{E}_i \cdot \vec{B}_i$, we have

$$\langle \zeta\zeta \rangle \propto \sum_{i,j} \left\langle \left(\vec{E}_i \cdot \vec{B}_i\right) \left(\vec{E}_j \cdot \vec{B}_j\right) \right\rangle = \sum_i \left\langle \left(\vec{E}_i \cdot \vec{B}_i\right)^2 \right\rangle = \mathcal{N} \left\langle \left(\vec{E}_1 \cdot \vec{B}_1\right)^2 \right\rangle , \quad (5.10)$$

(namely, the different sources are statistically uncorrelated, resulting in an $\mathcal{N}$ enhancement with respect to the case of a single gauge field); this is contrasted by the fact that also the second term in (5.7) increases by $\mathcal{N}$. Therefore, as we can observe from (5.8), the scalar power spectrum has a $\mathcal{N}$ enhancement in the $\xi \gtrsim 1$ regime, when $\beta_{\rm fric} \simeq 1$, while a $1/\mathcal{N}$ suppression [142] in the $\xi \gg 1$ regime, when the second term dominates in $\beta_{\rm fric}$. Therefore, in the $\xi \gg 1$ regime, the ratio between the GW and the scalar power spectra scales as $\mathcal{N}^2$. It is reasonable to expect that even mild values of $\mathcal{N}$ can lead to an observable GW signal, while respecting the PBH bound.

[14] For any given model and coupling, this does not imply a growth of the GW power spectrum by $\mathcal{N}$, due to the increase backreaction on the background.

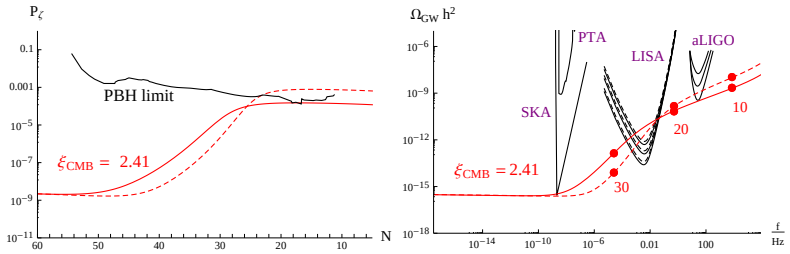

Figure 5.5: Scalar and tensor signals for a linear inflation potential. The solid lines show the signal if $\mathcal{N} = 6$ gauge fields are amplified. For comparison, the dashed lines show the signal when 1 gauge field is amplified.

This is confirmed by Fig. 5.5, where the solid (dashed) lines show the scalar and tensor power spectra generated if $\mathcal{N} = 6$ (1) gauge fields are amplified. When comparing the solid with the dashed lines, we notice an increased GW signal at LISA scales, while the scalar signal is now below the PBH bound at all scales. We note that, for $\mathcal{N} = 6$, the sourced scalar signal is enhanced more than single gauge field case for $N \gtrsim 30$ (corresponding to $\xi \gtrsim 1$ and $\beta_{\rm fric} \sim 1$), and suppressed more for $N \lesssim 20$ due to strong backreaction (corresponding to $\xi \gg 1$ and $\beta_{\rm fric} \gg 1$) [15]. We also note that in multiple field case, the GW spectrum is suppressed in the strong backreaction regime with respect to the case of single gauge field. This suppression results from the fact that enhanced backreaction in multiple vector case is stronger and it slows the inflaton more than single field case, which decreases ξ more.

5.3 Production from a rolling field σ different from the inflaton

In this Section we provide a different example on how to obtain a large GW signal at interferometer scales without conflicting with the PBH limit at $N \simeq 10$. We employ the model of [171] (or Chapter 4), which provided a localized bump in the spectrum of scalar

[15] We fixed the the coupling $f = M_p/48$ to the same value used in the previous figure, corresponding to the Planck limit for a linear potential and a single amplified gauge field [67]. It is possible that, for $\mathcal{N} > 1$ a slightly smaller coupling should be considered. This would require a dedicated analysis on the CMB limits, which is beyond our scope. A slightly smaller coupling would not change our findings, and the present discussion.

and tensor perturbations. The model was proposed to provide an explicit example that can generate a visible tensor-to-scalar ratio at the CMB scale for very small scale of inflation (and, therefore, for very small vacuum GWs), without conflicting with limits imposed by the non-gaussianity of the scalar perturbations at CMB scales. Here we show that this model can also provide a sufficiently large GW signal for detection at interferometer scales, particularly for LISA and PTA-SKA experiments. The model is (For details, see Section 4.1)

$$\mathcal{L} = -\frac{1}{2}\left(\partial\phi\right)^2 - V_\phi\left(\phi\right) - \frac{1}{2}\left(\partial\sigma\right)^2 - V_\sigma(\sigma) - \frac{1}{4}F^2 - \alpha\frac{\sigma}{4f}F\tilde{F}\,, \tag{5.11}$$

where ϕ is the inflaton field, σ is a pseudo-scalar field different from the inflaton that leads to gauge field amplification, and α a dimensionless parameter. For definiteness, we assume that σ has the simplest potential typically associated to a pseudo-scalar given in 4.3, We tune the curvature of the potential to be of the same order as the Hubble rate H during inflation. We encode this tuning into the parameter

$$\delta \equiv \frac{\Lambda^4}{6H^2f^2} \lesssim 1\,, \tag{5.12}$$

so that the mass of σ in the minimum of the potential $m_\sigma = \sqrt{3\delta}\,H$ is slightly smaller, but comparable to H (we choose $\delta = 0.2$ in our computations). The pseudoscalar then experiences the slow roll evolution

$$\sigma = 2\,f\arctan\left[\mathrm{e}^{\delta\,H(t-t_*)}\right] \quad \Rightarrow \quad \dot{\sigma} = \frac{f\,H\,\delta}{\cosh\left[\delta\,H\,(t-t_*)\right]}\,. \tag{5.13}$$

We see that the evolution is non-negligible for $1/\delta \sim$ few e-folds. In our computations below we fix $\delta = 0.2$ for definiteness. The quantity t_* is the time at which σ is in the steepest position of the potential ($\sigma = f\pi/2$), and at which it has maximum speed. This value depends on the initial conditions, and we simply treat it as a free parameter of the model. [16]

The rest of this section is divided into three parts. In the first part, we review the results on the scalar and tensor modes sourced during inflation in this model [171]. In the second part, we study the prospect of detection of the inflationary GW signal at

[16] One could imagine a more complicated model, with a different potential V_σ close to the origin, that fixes the initial condition for σ at the required position.

interferometers. In the third part, we discuss a different potential mechanism for GW production. Specifically, we study the possibility that the sourced scalar perturbations produce PBHs (in an amount consistent with the limits shown in Figure 5.1), and that the merging of two such PBHs in the recent universe gives rise to detectable GWs by PTA-SKA, LISA, or AdvLIGO. We stress that this is an independent mechanism of GW production with respect to the one discussed in the second part, and that the two mechanisms are actually sensitive to gauge field amplification taking place at different times during inflation.

We conclude this discussion by pointing out that a different way to produce a localized bump, without resorting to this second field σ, is to assume that the vector field is massive, and that its mass is modulated by the value of the inflaton field ϕ. Refs. [50, 51] also studied the possibility that the gauge field has a mass $> \xi H$, which highly suppresses the gauge field amplification, and the consequent PBH production. If the mass depends on the inflaton, in such a way that the vector is light only in a neighborhood of some given value $\phi = \phi_*$ assumed during inflation, then only the gauge modes produced while ϕ spans this interval are produced, generating an enhanced scalar and tensor signal at these scales, similarly to the one that we consider in this section.

5.3.1 Production of scalar and tensor modes

For sufficiently large coupling strength α/f, the motion of σ can lead to a strong amplification of the vector modes that leave the horizon during the $\sim 1/\delta$ e-folds of inflation in which σ has a non-negligible roll (Section 4.1). In turn, the amplified gauge modes source perturbations of σ and gravity waves, through the $2 \to 1$ processes that we have already discussed in the previous section. During this time, the simultaneous roll of ϕ and σ gives rise to a $\delta\sigma - \delta\phi$ coupling between the perturbations of the two fields. As long as this coupling is active, the perturbations $\delta\sigma$ produced by the vector field source inflaton perturbations (see Sections 4.2 and 4.3),[17] which give rise to a bump in the primordial scalar curvature.[18]

[17] This channel of production of inflaton perturbations is more efficient [57] than the gravitational production of inflaton perturbations from the gauge modes [33].

[18] The primordial scalar curvature ζ is a linear combination $\zeta(t) = A(t)\,\delta\phi(t) + B(t)\,\delta\sigma(t)$, where the two coefficients A and B depend on the background. In this model, the field σ becomes massive

The bumps in the primordial scalar and tensor perturbations due to this mechanism add up incoherently to the standard modes from the vacuum, and the total power spectra are given by

$$\begin{aligned} P_\zeta(k) &\simeq P_{\zeta,v}(k) + \left[\frac{H^2(k)}{8\pi^2 M_p^2}\right]^2 f_{2,\zeta}\left(\frac{k}{k_*},\, \xi_*,\, \delta\right) \quad , \\ P_{\rm GW}(k) &\simeq 16\,\epsilon_\phi P_{\zeta,v}(k) + \left[\frac{H^2(k)}{8\pi^2 M_p^2}\right]^2 f_{2,+}\left(\frac{k}{k_*},\, \xi_*,\, \delta\right) \quad , \end{aligned} \tag{5.14}$$

where again we disregard the sourced but unenhanced "-" GW polarization, which is much smaller than the sourced "+" polarization. Above we denote the inflaton slow-roll parameter with ϵ_ϕ, to distinguish it from the slow roll parameter $\epsilon_\sigma \equiv \dot\sigma^2/2H^2M_p^2$ associated with the field σ. The quantity k_* denotes the comoving momentum of the mode that leaves the horizon at t_*, while $\xi_* \equiv \alpha\,\dot\sigma_*/2fH = \alpha\cdot\delta/2$ with $\dot\sigma_* \equiv \sigma(t_*)$.

Ref. [171] evaluated the sourced power spectra numerically for the two specific values of $\delta = 0.2, 0.5$ and for several values of ξ_*, and showed that they are well fitted by

$$f_{2,j}\left(\frac{k}{k_*},\, \xi_*,\, \delta\right) \simeq f^c_{2,j}\left[\xi_*,\, \delta\right] \exp\left[-\frac{1}{2\sigma^2_{2,j}\left[\xi_*,\, \delta\right]} \ln^2\left(\frac{k}{k_*\, x^c_{2,j}\left[\xi_*,\, \delta\right]}\right)\right] \quad , \quad j = \zeta,\, +\ , \tag{5.15}$$

which is a Gaussian bump (in terms of $\ln k$) centered at $k = x^c_{2,j}\, k_*$. The quantity $x^c_{2,j}$ is of $\mathcal{O}(1)$ so that, as expected, the sourced signals are peaked at the scales that leave the horizon close to the time at which the roll of σ is fastest. The function $f^c_{2,j}$ controls the amplitude of the bump, and, analogously to (5.5), it grows exponentially with ξ_*. The function $\sigma^2_{2,j}$ controls the width of the bump, and it decreases with increasing δ. This is also to be expected, since greater δ corresponds to a shorter duration of the roll of σ. The precise dependence of these three functions on ξ_* is given in Section 4.3, for the two cases $\delta = 0.2,\, 0.5$.

---

shortly after t_*. As σ becomes a massive field in an inflationary universe, its energy density and pressure rapidly drops to zero, and so does the coefficient B. The only potentially observable effect of $\delta\sigma$ is through its linear coupling to the inflaton perturbations that we are considering, and that is in act only as long as $\dot\sigma \neq 0$.

5.3.2 Direct Detection of Inflationary Signatures at Interferometer Scales

To obtain the precise scalar and tensor perturbations generated in the model (5.11) we need to specify the inflaton potential. From the potential we derive the slow roll parameters $\epsilon_\phi \equiv \frac{M_p^2}{2}\left(\frac{\partial_\phi V_\phi}{V}\right)^2$ and $\eta_\phi \equiv M_p^2 \frac{\partial_{\phi\phi} V_\phi}{V}$. As long as the background and the perturbation contributions from σ and the vector fields can be neglected, we recover the standard results $\dot{H} \simeq -\epsilon_\phi H^2$ for the evolution of the Hubble rate, $n_s \simeq 1 + 2\eta_\phi - 6\epsilon_\phi$ for the tilt of the scalar spectrum, and $r \simeq 16\epsilon_\phi$ for the tensor-to-scalar ratio. For definiteness, we assume that $r = 0.01$ (parametrically close to the current bound 0.064 at 95% confidence [149]), giving $\epsilon_\phi \simeq 6.25 \cdot 10^{-4}$. From the observed value $n_s - 1 \simeq -0.035$ [67] we then obtain $\eta_\phi \simeq -0.015$. Having $|\eta_\phi| \gg \epsilon_\phi$ is for example typical of top-hill inflationary potentials [150].

In the examples that we show in this subsection we avoid specifying an inflationary potential, and we assume that ϵ_ϕ and η_ϕ remain constant all throughout inflation. It is immediate to modify this, once a specific V_ϕ is given. However, since the slow roll parameters vary at second order in slow roll, this approximation is sufficiently adequate for our purposes, and it does not affect our general conclusions for the mechanism that we are studying in this section. Therefore, we take

$$H(N) = H_{\rm CMB}\, \mathrm{e}^{-\epsilon_\phi (N_{\rm CMB} - N)} \quad , \quad P_{\zeta,v}(k_N) = P_{\zeta,v}(k_{N_{\rm CMB}})\, \mathrm{e}^{-\left(1-\epsilon_\phi\right)(1-n_s)(N_{\rm CMB}-N)} \quad . \tag{5.16}$$

(where, clearly, ϵ_ϕ can be disregarded in the second relation), with ϵ_ϕ, n_s, fixed at the CMB scales. We then assume $N_{\rm CMB} = 60$, and take $P_\zeta(k_{N_{\rm CMB}}) \simeq 2.2 \cdot 10^{-9}$ [67].

With these assumptions, the mechanism only depends on the three parameters ξ_*, N_* and δ discussed in the previous subsection, that control the dynamics of σ and the field amplification. More precisely, N_* is the number of e-folds corresponding to t_*, at which the motion of σ is fastest. For definiteness, we take $\delta = 0.2$, corresponding to a roll of sigma for $\Delta N \simeq 1/\delta = 5$ e-folds, and to a comparable width of the sourced signal. We then choose N_* so that the peak of the sourced GW signal is either at PTA, LISA or AdvLIGO scales, and we choose ξ_* so that the sourced scalar modes saturate the PBH bounds. We then study whether this value of ξ_* is enough to provide a visible GW signal.

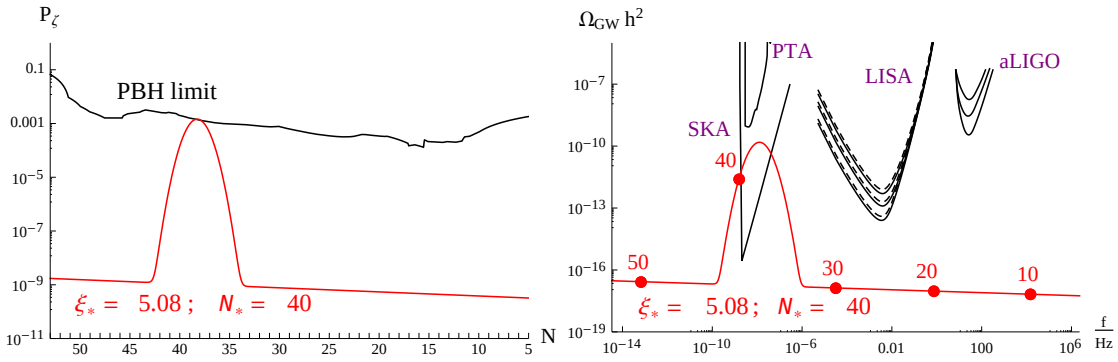

Figure 5.6: Scalar power spectrum and GW power spectrum produced during inflation in the two field mode (5.11), assuming a bump at PTA scales. We see that, it is possible to produce a visible GW signal without violating the PBH bounds.

The results of Figures 5.6 and 5.7 show that it is indeed possible to obtain a visible signature at, respectively, PTA and LISA scales. The same does not appear to be true for a signal at the AdvLIGO scale, and with the AdvLIGO sensitivity, as can be seen from Figure 5.8. Analogous conclusions can be reached from the single field model (5.3) of Section 5.2, as seen in Figure 5.4. From the comparison of the two models, we believe that this is a generic feature associated to this mechanism. We stress that the negative concliusion reached on the AdvLIGO case depend on the computed scalar spectrum, which is more uncertain than the GW one.

The computations performed in this section have been obtained from the two-field model (5.11), under the assumptions that (i) the gauge field amplification backreacts in a negligible way on the background solution and (ii) the perturbations remain in the perturbative regime. In Chapter 6, we showed that this is the case provided the axion scale f is within a certain interval, given by the expression 6.37. Using eqs. (5.1) and (5.14) with $f^c_{+,2}\,[\xi_*,\,\delta=0.2] \simeq 3.6\cdot 10^{-5}\,\mathrm{e}^{3.48\pi\xi_*}$ given in eq. (6.7), we have

$$\left(\Omega_{\rm GW}\,h^2\right)^{1/4}_{\rm peak} \simeq 1.32\cdot 10^{-7}\,\sqrt{\epsilon_\phi}\,\mathrm{e}^{2.74\,\xi_*}\ , \tag{5.17}$$

at the peak of the sourced GW signal (we are disregarding the variation of H during inflation, which provides a negligible correction to this relation for the values $r_{\rm vacuum} = 0.01$ considered here). Using this relation, the condition (6.37) rewrites as

$$\left(\frac{\Omega_{\rm GW}\,h^2}{2\cdot 10^{-9}}\right)^{1/4}_{\rm peak} \lesssim \frac{f}{M_p} \lesssim 1\ . \tag{5.18}$$

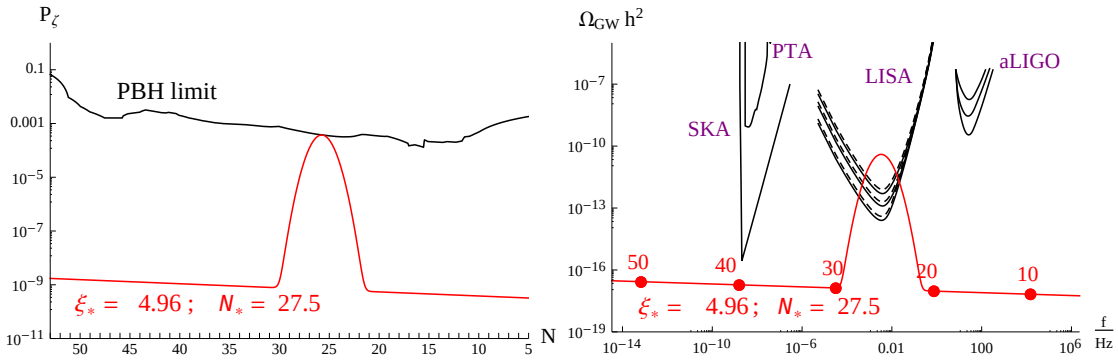

Figure 5.7: Scalar power spectrum and GW power spectrum produced during inflation in the two field mode (5.11), assuming a bump at LISA scales. We see that, similarly to the example shown in Figure 5.4, it is possible to produce a visible GW signal without violating the PBH bounds.

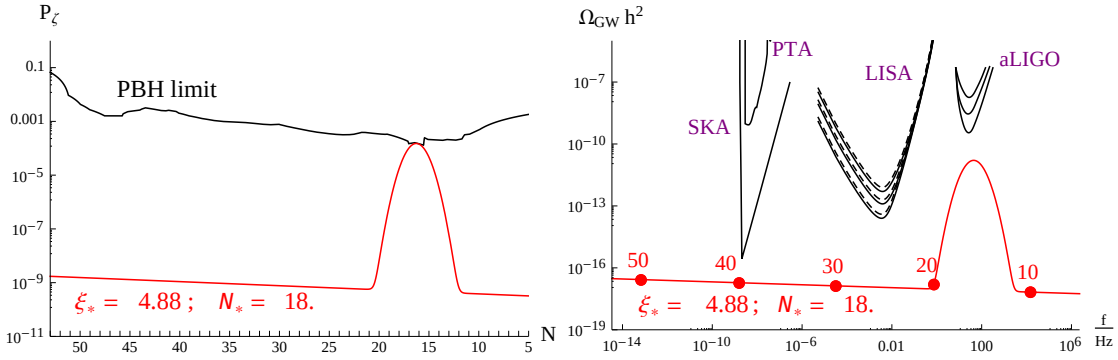

Figure 5.8: Scalar power spectrum and GW power spectrum produced during inflation in the two field model (5.11), assuming a bump at AdvLIGO scales.

The peak values of the GW signals shown in Figures 5.6, 5.7, and 5.8 is always below $2 \cdot 10^{-9}$. Therefore, the condition (5.18) is satisfied in a nonvanishing interval for f. The interval grows at decreasing values of the peaked GW signal.

5.3.3 GWs from merging PBHs

In this subsection we discuss the GW emission of inspiraling primordial BHs formed when the enhanced curvature fluctuations re-enter the horizon during the radiation epoch. Such PBHs present a broad mass distribution and satisfy the bounds in Figure 5.1 while still comprising all of the Dark Matter [89]. When they form, their contribution

to the energy density of the universe is negligible and do not affect BBN, but by the time of matter-radiation equality they begin to dominate the total energy density. After recombination, these PBHs start to merge through hierarchical structure formation and acquire today a mass distribution peaked around a hundred solar masses. These PBHs would act as seeds for structure formation [89]. Fewer heavier PBHs may have acquired significantly more mass today due to gas accretion, as well as merging, and constitute the supermassive BHs at the centers of galaxies and quasars.[19]

The exact numbers and mass distributions are still uncertain and require detailed N-body simulations to compute the transfer function from the primordial mass distribution to the present PBH distribution. In particular, merging between different PBHs will create PBHs of larger masses, shifting the mass distribution. We will roughly estimate a factor of 10^3 shift for the mass corresponding to the peak of PBH seeds, and at least a factor 10^5 for the extra increase due to gravitational collapse of gas onto the high end (more massive) part of the distribution.[20] The first population will be responsible for the emission of GWs in the AdvLIGO band and the enhanced tail of the distribution will correspond to the IMBH and SMBH population, responsible for the GW emission in the PTA and LISA bands. Note that the broad peak in the spectrum of fluctuations is responsible also for a clustering of PBHs upon reentry, which explains the rapid growth in mass and the enhanced rate of events [122] with respect to the stellar black holes of similar mass. Keeping this growth of mass into account, we find that, as discussed in the Introduction, AdvLIGO, LISA and PTA are sensitive, respectively, to modes that left the horizon about $N \sim 35 - 37$, $N \sim 38 - 41$, and $N \sim 41 - 44$ e-folds before the end of inflation.

We assume that an episode of localized field amplification, as the one obtained from the model (5.11) generates a bump in the scalar perturbations (as the one given by Eqs. (5.14) and (5.15)) in one of these three intervals. We then assume that this initial bump produced PBH that acts as a seeds of a population of current black holes that can be identified with the dark matter of the universe. Sizable PBHs in the model (5.11) can be generated for $\xi_* \sim 4.5 - 5$, which is compatible with limits from perturbativity.

[19] For a recent analysis of the growth of an initial black hole seed up to supermassive BHs, see Ref. [152].

[20] There will also be a decrease in the amplitude of the whole mass distribution due to the energy loss in gravitational waves from the merging of PBHs, but we will ignore it here.

We are interested in the collision rate of the PBHs in these distributions. For a generic PBH mass spectrum, the number of collisions per volume and time is given by

$$\bar{\Gamma}^{\rm tot} \equiv \frac{1}{2}\sum_{A,B} \langle n_{\rm BH}\,(M_A,\,t_0)\; n_{\rm BH}\,(M_B,\,t_0)\; \sigma(M_A,\,M_B,\,v)\,v\rangle \;, \tag{5.19}$$

where $n_{\rm BH}\,(M,\,t_0)$ is the number density of black holes with mass M at the present time t_0, and where $\sigma(M_A,\,M_B,\,v)$ is the cross section (merger rate) for the merging (inspiraling) of one black hole of mass M_A on one black hole of mass M_B, colliding at the relative velocity v. Finally, $\langle \ldots \rangle$ denotes average over volume and velocity.

To perform our estimate, we assume a very narrow distribution of black hole masses corresponding to a relatively large value of δ in the model (5.11); in this case, we can assume a single value for the mass in the cross section (5.19), see [151, 122],

$$\sigma\,(M_{\rm BH},\,M_{\rm BH},\,v) = 2\pi\left(\frac{85\,\pi\,2^5}{6\sqrt{2}}\right)^{2/7}\frac{G^2\,M_{\rm BH}^2}{c^4}\left(\frac{c}{v}\right)^{18/7} \simeq 10^{-37}\,{\rm Mpc}^2\left(\frac{M_{\rm BH}}{M_\odot}\right)^2\left(\frac{c}{v}\right)^{18/7} \;, \tag{5.20}$$

(where G is Newton's constant, and c the speed of light). As we are assuming that the black holes are the cold dark matter of the universe, the local black hole number density at any place in the universe is just the local dark matter number density:

$$n_{\rm BH}\,(t_0) = \frac{\delta_{\rm local}}{M_{\rm BH}}\,\Omega_{\rm CDM}\,\rho_c\,(t_0) \simeq 3.3\cdot 10^{10}\,{\rm Mpc}^{-3}\,\frac{\delta_{\rm local}}{M_{\rm BH}/M_\odot} \;, \tag{5.21}$$

where $\Omega_{\rm CDM}h^2 = 0.12$ has been used [68], and where $\delta_{\rm local} \equiv \rho_{\rm CDM}^{\rm local}/\rho_{\rm CDM}^{\rm mean}$ is the local enhancement of PBH dark matter in compact halos. Inserting all this in (5.19), gives

$$\bar{\Gamma}^{\rm tot} \simeq 2\cdot 10^{-7}\,{\rm Gpc}^{-3}\,{\rm yr}^{-1}\,\delta_{\rm local}\left(\frac{10\,{\rm km/s}}{v}\right)^{11/7} \;, \tag{5.22}$$

where we have normalized the velocity to typical velocities of compact masses in dwarf spheroidal galaxies, which are indeed in the few km/s range, up to 15 km/s [153]. We see that a reasonable local enhancement in the number density could make the signal observable. For example, this is the case of GWs from inspiralling of clustered PBHs in dense compact halos building up and orbiting around galaxies [121, 122]. Some of these have been recently discovered by DES around the Milky Way and show huge mass-to-light ratios of 500-1000 [153].

The possibility that PBHs comprise all of the Dark Matter is a very attractive scenario [88, 89] that has received special attention lately [121, 122, 123], since the detection

by AdvLIGO of GW from the merging of very massive black hole binaries [90, 91]. The systematic detection, by terrestrial laser interferometers, of merging BH binaries within a broad range of masses, will open a new window into the early universe. The characterization of the mass spectrum will tell us about the time and duration during inflation of new phenomena like particle production or new couplings of the inflaton to other fields.

5.4 Summary

In this chapter, we studied the possibility of detecting inflationary GW in terrestrial (such as AdvLIGO) and spacial (such as LISA) gravitational interferometers and Pulsar Timing Arrays. We specifically studied GWs produced by gauge fields, amplified due to their coupling $\phi F\tilde{F}$ to a pseudo-scalar inflaton ϕ, or to their coupling $\sigma F\tilde{F}$ to a different field σ that is rolling for a few e-folds during inflation. The sourced GWs are exponentially sensitive to the speed of the inflaton, so this mechanism is naturally enhanced at late times / small scales [31, 108], possibly opening new windows of exploration for inflation model building. Like in the case of the detection of sourced GWs at CMB scales [48, 33, 57, 58, 171], the main difficulty in producing a large sourced GW signal at interferometer scales is the unavoidable simultaneous production of scalar perturbations. In this case the problem is the possible overproduction of PBH from the enhanced scalar signal [51].

In this chapter, we studied whether and under which conditions the limit associated with the scalar production can be circumvented. An important consideration is that there is an intrinsic uncertainty associated to the computation if the scalar perturbations for the couplings that are necessary to produce a visible GW signal. If the correct result is $\mathcal{O}(1)$-suppressed with respect to the current estimates, then the PBH limit may not be a problem [51]. Ultimately, we believe that only a numerical computation of the scalar perturbations, along the lines of Refs. [154, 155, 156, 143], will resolve this issue. Unless proven incorrect, let us assume that the present estimates are sufficiently accurate. In this case, we note that, given the typical blue nature of the sourced signal, the PBH limit is typically enforced by the smallest scales at which it exists, namely for modes that left the horizon around 10 e-folds before the end of inflation. We therefore studied the constraints imposed by the PBH limits at a given interferometer scale, without

making assumptions on the later evolution of the inflaton (in essence, on the inflaton potential at different field values from those experimentally probed). We found that the projected LISA and PTA-SKA sensitivities are good enough to allow for the detection of a GW signal, in a regime that evades the PBH bounds. We instead obtained a negative conclusion for the expected AdvLIGO sensitivity [92]. [21]

A different possibility to circumvent the PBH limit is to assume that $\mathcal{N}$ gauge fields are amplified by the same mechanism. In this case, the ratio between the tensor and the scalar power spectra is enhanced by $\mathcal{N}^2$ in the regime of strong coupling required to produce an observable GW signal. We confirmed the finding of [109], that studied this possibility in the context of Starobinsky inflation [120], showing that in the case of chaotic inflation even the moderate value $\mathcal{N} = 6$ allows for a visible signal at LISA and PTA-SKA, while respecting the PBH bounds.

While in most of this chapter we have studied the possible detection of the stochastic GW signal directly produced during inflation, in Section 5.3.3 we have discussed the alternative possibility that density perturbations are produced during inflation collapse to form PBHs, which then evolve to the present universe, and ultimately give rise to BH-BH binary mergers, such as those observed by the AdvLIGO detectors. The possibility that these BH can be identified with the dominant component of the dark matter of the universe has been at the center of interesting recent works [89, 121, 122, 123, 124, 125]. The generation of these PBH requires enhanced density perturbations with respect to the amplitude at the CMB scale. In the literature, a broad peak in the density power spectrum, and the consequent PBH production has typically been obtained in the context of hybrid inflation. Here, we have discussed an alternative mechanism for the generation of this broad peak, in the context of sourced perturbations in axion inflation [51]. The main difference between the two cases, is that the sourced perturbations are highly non-gaussian, which, at any fixed amplitude of the two-point function, results in an increased PBH fraction (see Figure D.1).

[21] We do not have a no-go theorem in support of this statement, but only the evidence given by the two examples that we have studied. In particular, the two field $\phi-\sigma$ model is "designed" to maximize the ratio between tensor and scalar perturbations, since it avoids a direct coupling between the inflation and the gauge fields, therefore constituting an optimized situation. The example we studied, and that we showed in Figure 5.8, led to a GW signal that is about 20 times smaller than the best projected AdvLIGO sensitivity.

In Table 5.1 we have listed the (approximate) interval of modes that can potentially give observable GW signatures in various experiments. We note the presence of an interesting correspondence between the modes listed in the 6th row, with the modes listed in the 4th row of the table (and, marginally, with also those in the 5th row). This opens the interesting possibility that the same event of localized particle production during inflation can give rise to both a stochastic GW signal at PTA scales, and to scalar perturbations that eventually result in BH collisions in the present universe that are observed possibly at LISA and AdvLIGO. The PTA signal would be proportional to the amount of particle production (namely, the sourced gauge fields in our model) generated during inflation. The LISA one instead would be sensitive to both the inflationary particle production, and the merging and accretion processes that occur between the PBH formation, and the present universe. The measurement of both signals could therefore allow us to probe the evolution between the PBH seeds and the present BH.

If a stochastic GW background will be detected, the main challenge for claiming a cosmological origin will be to discriminate it against a possible astrophysics background. The GW signal sourced by this mechanism has two distinctive properties. One is its chirality, due to the preferential growth of one polarization w.r.t. the other one. The prospect of detection of a chiral GW signal from a network of interferometers was studied in Refs. [157, 158, 159]. The second is its nearly $\mathcal{O}(1)$ non-gaussianity [75, 71] (the bispectrum being about its power spectrum to the 3/2 power), which can also be probed by interferometers [160].

To summarize, the GW signal from the pseudo-scalar interaction studied in this chapter is a very natural candidate for the searches of a stochastic GW background on earth and space interferometers, due to the strong motivation of models of axion inflation, and the natural growth of the sourced signal at small scales. This potentially offers a window on scales of inflation on which we currently have little or no direct experimental knowledge. This signal has very characteristic properties (chirality, and order one non-gaussianity), which can help us discriminate it from an astrophysical background. The detectability of this signal requires that the PBH limit on scalar perturbations, that are unavoidably sourced together with the GW, are respected, possibly along the lines considered above.

Chapter 6

Constraints on the Axion-Gauge Coupling

There is more than meets the eye.

In the previous three chapters we have worked on the signatures of axion gauge coupling from very large to very small length scales. We have studied the distinct electromagnetic and GW signatures that this coupling might generate. Because this coupling produces large amount of vector particles in a non-adiabatic fashion via tachyonic instability, it is natural to verify that found results are robust under various constraints such as quantum corrections and backreaction considerations. The purpose of this chapter is to determine the validity regime of the results obtained in the previous chapters.

In the previous chapters we studied an effective and well studied particle production mechanism in which the rolling axion (inflaton or a rolling pseudo-scalar spectator) X, via a chiral coupling, sources vector modes which, in their turn, source tensor (GW) and scalar perturbations. Two particular situations have been considered in the literature and in this thesis: either the field X rolls at an approximately constant velocity [39, 33], or it experiences a transient of relatively fast [1] roll [171, 173, 174].

[1] More specifically, we assume that $\dot{X}$ is significantly different from zero only for a limited time. Also during this time we assume that X is in a regime of slow-roll, namely that $|\dot{X}| \ll HM_p$.

As we see in the previous chapters, it is not easy to introduce particle production mechanisms during inflation without spoiling the successful predictions of inflation. This task is even harder especially if the aim is to produce large amount primordial gravitational waves because any interaction responsible for GW production will also source scalar curvature perturbations, ζ, with a coupling that is at least of gravitational strength (or stronger, if the source is directly coupled to the field responsible for the observed density perturbations). Therefore, the same mechanism that generates a large GW signal can also generate too large amount of non-Gaussianity at CMB scales, or too many PBHs at smaller scales. In the previous chapters we showed that the scalar production can be kept under control in various applications of the axion-gauge coupling. The signatures that can arise form this mechanism can be listed as inflationary magnetogenesis [38, 47, 164], CMB non-Gaussianity [48, 49], growth of the scalar power spectrum at CMB scales [50], gravitational waves [2] that might be detectable by gravitational interferometers [31, 108, 109], parity violation in the CMB [39] and in interferometers [158], primordial black holes [51, 126, 116, 117, 155, 118], blue tensor spectra [55] and large and parity violating tensor bispectra [165].

Since this interaction requires that the sourced gravitational waves have a relatively large amplitude, in general the excited sector that sources the tensors must contain a sizable energy density. As a consequence, one can wonder whether such large energy densities can bring us out of the perturbative regime in which such effects are analyzed, and put into question the validity of such calculations. Some of the perturbativity requirements are rather straightforward. For instance, one should obviously demand that all the energy in produced modes is smaller than the kinetic energy of the field X, that is the source of the vector modes. If this condition is not met, a more complete analysis that includes backreaction on the inflating background is needed, and it has been taken into account in several applications of this mechanism. A less straightforward requirement is that the three point correlators be subdominant to the two point correlators. This question was tackled in Appendix C.5. More recently, Ref. [146] has considered two additional requirements from perturbativity for the models of [39, 33], where $\dot{X}$ is approximately constant:

i) The higher order effects do not spoil the leading order estimate for the amplitude of

[2] Further discussion of these, or similar mechanisms can be found in [166].

the gauge field amplified by the rolling of X field
ii) The fluctuations of X do not induce a variance $\sqrt{\langle X^2 \rangle}$ that is greater than the periodicity of the potential for X, and hence of the classical zero mode of X.

This chapter shows that the application of the mechanisms of [39, 33] (ie. we consider both cases: 1) $\dot{X}$ is approximately constant, 2) X experiences a transient roll.) that produce signatures at CMB scales are well consistent with the limits from perturbativity. On the contrary, one of these limits is marginally violated by applications that produce signals at much smaller scales, as for instance GW at interferometers and primordial black-holes. The violation we find is much smaller than that obtained in [146]: the gauge field production is controlled by a parameter ξ, that needs to be $\simeq 5$ for those signatures to be relevant, while the perturbativity criteria give $\xi \lesssim 4.8$. We therefore expect that these results remain valid, with possibly $\mathrm{O}(1)$ corrections. [3]

This chapter has the following structure. In section 6.1 we review some of the signatures from these mechanisms, and the phenomenologically interesting regions of parameter space of the model (these are the regions where the perturbative analysis is required to be consistent). In Section 6.2 we compute the limits that ensure small backreaction of the produced gauge fields on the background dynamics. Our main results on perturbativity are presented in Section 6.3. The limits from backreaction and perturbativity are then studied in Section 6.4. Section 6.5 contains our conclusions. The details of the calculations are presented in Appendix E. This Chapter is mainly based on Ref. [172].

6.1 Phenomenological signatures of the gauge field amplification

In this Section we briefly summarize which values of field amplification (controlled by the particle production parameter ξ) are needed to produce various phenomenological signatures. In the following sections, we then study whether the required amount of

[3] The criteria we formulate cannot be applied in the regime of very large ξ, as the one of [142], where the backreaction of the produced gauge field is strongly affecting the background dynamics, and the sourced scalar perturbations are much greater than the vacuum one. Ref. [142] discussed how to deal with the scalar perturbations in that case.

field amplification is compatible with limits from backreaction and perturbativity.

6.1.1 Signatures for $X = \phi$

We start with the model considered in Subsection 3.1.1, in which $X = \phi$ is the inflaton, whose speed is adiabatically evolving. The lagrangian is given as

$$\mathcal{L} = -\frac{1}{2}\left(\partial\phi\right)^2 - V\left(\phi\right) - \frac{1}{4}F^2 - \frac{\alpha}{4f}\phi\, F\,\tilde{F}\,, \tag{6.1}$$

The phenomenological signatures of this model studied in the literature are primordial non-gaussianity [48, 49, 67], growth of power-spectrum [50, 67], primordial chiral gravity waves [39] at interferometer scales [31, 108, 158, 109, 173] and primordial black holes [51, 173]. From these analyses, the value of ξ required to obtain a visible signal is approximately

$$\begin{aligned} \xi\left(N \simeq 60\right) &\simeq 2.5 \quad \text{from CMB measurement}\,, \\ \xi\left(N \simeq 15\right) &\simeq 5 \quad \text{from GW at interferometers}\,, \\ \xi\left(N \simeq 8\right) &\simeq 5 \quad \text{from primordial black holes}\,. \end{aligned} \tag{6.2}$$

The value of N in these expression is the number of e-folds before the end of inflation at which those limits apply. Specifically, these are the values assumed by ξ when the mode leading to that specific signature left the horizon. The last two limits are obtained from refs. [158] and [51], respectively. Those works cast the limit in terms of the value assumed by ξ at $N = 60$. We obtain the values written in (6.2) by computing the evolution of $\xi\left(t\right)$ in the monomial inflaton potentials used in those works.

6.1.2 Signatures for $X = \sigma$

Now, consider the model with $X = \sigma$ experiencing a momentary fast evolution studied in Subsection 3.1.2, Section 4.1, 4.2 and 4.3. The Lagrangian is given as [4]

$$\mathcal{L} = -\frac{1}{2}\left(\partial\phi\right)^2 - V_\phi\left(\phi\right) - \frac{1}{2}\left(\partial\sigma\right)^2 - V_\sigma(\sigma) - \frac{1}{4}F^2 - \frac{\alpha}{4f}\sigma\, F\tilde{F}\,. \tag{6.3}$$

This model was introduced in [171] (or Chapter 4) [5] to source an observable GW bump at CMB scales, without producing much scalar perturbations, $P_{\zeta,\text{sourced}} \ll P_{\zeta,\text{vacuum}}$.

[4] We have $V_\sigma(\sigma) = \frac{\Lambda^4}{2}\left(1 + \cos\frac{\sigma}{f}\right)$ and $\delta \equiv \frac{\Lambda^4}{6\,H^2\,f^2}$ as defined in Section 4.1.

[5] Also used in interferometer scales to produce GW without producing too many PBHs in Section 5.3

However, for smaller scales, because the main constraint comes from the PBH limit, $P_{\zeta,\text{sourced}} \gg P_{\zeta,\text{vacuum}}$ is allowed.

As seen from eq. (3.21), the spectrum of amplified gauge modes in this mechanism exhibits a peak at the scales that exited the horizon when σ reaches its maximum speed. Correspondingly, the scalar perturbations ζ, and the GW sourced by these gauge fields also present an analogous peak at these scales. The total power spectrum of scalar and tensor perturbations is a sum of the vacuum and the sourced contribution, where the latter acquires the form

$$\begin{aligned} P_{j,\text{sourced}}\left(k\right) &= \left[\epsilon_\phi \, \mathcal{P}_\zeta^{(0)}\left(k\right)\right]^2 f_{2,j}\left(\frac{k}{k_*},\, \xi_*,\, \delta\right) = \left[\frac{H^2_{\text{infla}}(k)}{8\pi^2 M_p^2}\right]^2 f_{2,j}\left(\frac{k}{k_*},\, \xi_*,\, \delta\right) \,, \\ f_{2,j}\left(\frac{k}{k_*},\, \xi_*,\, \delta\right) &\simeq f^c_{2,j}\left[\xi_*,\, \delta\right] \exp\left[-\frac{1}{2\,\sigma^2_{2,j}\left[\xi_*,\, \delta\right]} \ln^2\left(\frac{k}{k_*\, x^c_{2,j}\left[\xi_*,\, \delta\right]}\right)\right] \,, \end{aligned} \tag{6.4}$$

where $j = \{\zeta,\, +,\, -\}$, with $\pm$ referring to the two GW helicities. In this expression, ϵ_ϕ is the slow roll inflaton parameter and $P_\zeta^{(0)}$ is vacuum curvature power spectrum. The three parameters $f^c_{2,+}$, $\sigma_{2,+}$, and $x^c_{2,+}$ control, respectively, the amplitude, the width, and the position of the peak of the sourced signal, and their functional dependence on ξ_* is studied in Chapter 4. Analogous expressions apply for the sourced bispectra.

The generic expression for tensor-to-scalar-ratio is given by

$$r\left(k\right) \simeq \frac{2\frac{H^2}{\pi^2\, M_p^2} + \left(\frac{H^2}{8\pi^2 M_p^2}\right)^2 f_{2,+}}{\frac{H^2}{8\pi^2 \epsilon_\phi\, M_p^2} + \left(\frac{H^2}{8\pi^2 M_p^2}\right)^2 f_{2,\zeta}} = 16\epsilon_\phi \cdot \frac{1 + \frac{1}{16}\left(\frac{H^2}{8\pi^2 M_p^2}\right) f_{2,+}}{1 + \epsilon_\phi \left(\frac{H^2}{8\pi^2 M_p^2}\right) f_{2,\zeta}} \tag{6.5}$$

As seen from the eqn above,

- When both sourced scalar and tensor modes are subdominant wrt vacuum ones, we have standard relation : $r \simeq r_{\text{vacuum}} = 16\,\epsilon_\phi$.
- When sourced tensor modes dominate over vacuum tensor modes ($P_{\lambda,\text{sourced}} \gg P_{\lambda,\text{vacuum}}$, and sourced scalar modes are subdominant with respect to vacuum scalar modes ($P_{\zeta,\text{sourced}} \ll P_{\zeta,\text{vacuum}}$), we have : $r \simeq \epsilon_\phi \left(\frac{H^2}{8\pi^2 M_p^2}\right) f_{2,+}$.
- When both sourced tensor and scalar modes dominate over vacuum ones, ($P_{\lambda,\text{sourced}} \gg P_{\lambda,\text{vacuum}}$ and $P_{\zeta,\text{sourced}} \gg P_{\zeta,\text{vacuum}}$), we have: $r \simeq \frac{f_{2,+}}{f_{2,\zeta}}$

At CMB scales, the vacuum scalar modes dominate over the sourced ones, leading to the tensor-to-scalar ratio

$$r\left(k\right) \simeq r_{\rm vacuum} + \epsilon_\phi^2 \, P_\zeta^{(0)} \, f_{2,+}\left(k\right) \ , \tag{6.6}$$

Chapter 4 studied the model for $\delta = 0.2$ and $\delta = 0.5$. We also focus our discussion on these two cases. By fitting $f_{2,+}$ [6] in relevant ξ_* regime, we obtain the following result

$$\begin{aligned} \delta = 0.2 \ \ &\Rightarrow \ \ f_{2,+} \simeq 3.6 \cdot 10^{-5} \, {\rm e}^{3.48\,\pi\,\xi_*} \ , \\ \delta = 0.5 \ \ &\Rightarrow \ \ f_{2,+} \simeq 2.7 \cdot 10^{-4} \, {\rm e}^{3.08\,\pi\,\xi_*} \ . \end{aligned} \tag{6.7}$$

For CMB scales, sourced scalar modes are subdominant with respect to vacuum scalar modes, so we have

$$P_{\zeta,\,\rm CMB} \simeq \frac{H^2}{8\pi^2\,\epsilon_\phi\,M_p^2} \simeq 2.2 \cdot 10^{-9} \Rightarrow 16\epsilon_\phi \simeq \left(\frac{H^2}{10^{-4} M_p^2}\right)^2 \tag{6.8}$$

Using eq. (6.8) in eq. (6.6), we obtain

$$r_{\rm peak} \simeq \begin{cases} 0.006 \left(\frac{H_{\rm inflation}}{10^{-6}\,M_p}\right)^4 {\rm e}^{3.48\,\pi\,(\xi_* - 4.5)} \ \ , \ \ \delta = 0.2 \ , \\ 0.020 \left(\frac{H_{\rm inflation}}{10^{-6}\,M_p}\right)^4 {\rm e}^{3.08\,\pi\,(\xi_* - 5)} \ \ , \ \ \delta = 0.5 \ . \end{cases} \tag{6.9}$$

The result (6.9) shows that, provided ξ_* is sufficiently large, a visible sourced GWs at CMB scale can be obtained at very small energy scale of inflation. We stress again that this conclusion is only valid as sourced scalar modes are subdominant to vacuum scalar modes, which is the case for CMB scale production.

For small scale bump in which the model produces a visible signal at interferometers or produce significant amount of PBH, both the sourced scalar and tensor modes dominate over vacuum modes.

6.2 Backreaction

In this section we discuss the effects of particle production on the background motion of X. We divide the discussion into two subsections, where we separately discuss the $X = \phi$ (with adiabatic $\dot{\phi}$ evolution), and $X = \sigma$ (with a momentary speed up of this field) cases.

[6] Specifically, we linearized the expression for $f_{2,+}$ given in Tables 1 and 2 of Section 4.3 in the $3 < \xi_* < 6$ region.

6.2.1 Backreaction for $X = \phi$

The gauge field enters in the equation of motion for the inflaton field ϕ and in the Friedman equation as

$$\ddot{\phi} + 3H\dot{\phi} + \partial_\phi V = \frac{\alpha}{f}\left\langle \vec{E}\cdot\vec{B}\right\rangle \ ,$$
$$3H^2 = \frac{1}{M_p^2}\left[\frac{1}{2}\dot{\phi}^2 + V + \frac{1}{2}\left\langle \vec{E}^2 + \vec{B}^2\right\rangle\right] \ , \tag{6.10}$$

Using (3.10) one finds [142], in the $\xi \gtrsim \mathcal{O}(1)$ regime (namely, in the regime in which the gauge field amplification takes place),

$$\left\langle \vec{E}\cdot\vec{B}\right\rangle \simeq -2.4\cdot 10^{-4}\,\frac{H^4}{\xi^4}\,\mathrm{e}^{2\pi\xi} \ , \ \left\langle \frac{\vec{E}^2+\vec{B}^2}{2}\right\rangle \simeq 1.4\cdot 10^{-4}\,\frac{H^4}{\xi^3}\,\mathrm{e}^{2\pi\xi} \ . \tag{6.11}$$

Therefore [48, 49]

$$\xi^{-3/2}\,\mathrm{e}^{\pi\xi} \ll 79\frac{|\dot{\phi}|}{H^2} \ \Rightarrow \ \text{negligible backreaction on } \phi \text{ eq. ,}$$
$$\xi^{-3/2}\,\mathrm{e}^{\pi\xi} \ll 146\frac{M_p}{H} \ \Rightarrow \ \text{negligible backreaction on Friedmann eq. .} \tag{6.12}$$

The first condition is more stringent (it is easier to modify the evolution of the inflaton field, that is moving slowly, than that of the scale factor), and using the normalization $P_\zeta \simeq \frac{H_{\rm inf}^4}{4\pi^2\dot{\phi}^2} \sim 2.2\cdot 10^{-9}$, it leads to the bound

$$\text{Negligible backreaction on } \phi \ : \ \ \xi \ \ll 4.7 \ . \tag{6.13}$$

We discuss this condition in Section 6.4.1. We note that it is not inconsistent to use the relations (6.11) in which we assume $\xi \gtrsim \mathcal{O}(1)$, to obtain a limit $\xi \ll 4.7$, because the gauge field amplification depends exponentially on ξ.

6.2.2 Backreaction for $X = \sigma$

In eq. (6.9) we showed that, provided ξ_* is sufficiently large, a visible sourced GW at CMB scale can be obtained at very small energy scale of inflation. Here we study how large this field amplification can be, without violating bounds from backreaction on the dynamics of σ and ϕ.

We first impose that σ provides a negligible contribution to the energy density of the universe. To quantify this condition, in agreement with the slow roll relation $\dot{\phi} \simeq \sqrt{2\,\epsilon_\phi} H\, M_p$, we define

$$\epsilon_\sigma \equiv \frac{\dot{\sigma}^2}{2\,H^2\,M_p^2}\,. \tag{6.14}$$

(as σ is slowly rolling, we have $\epsilon_\sigma \simeq \frac{M_p^2}{2}\left(\frac{\partial_\sigma V}{V}\right)^2$). We denote by $\epsilon_{\sigma,*} = \frac{\delta^2}{2}\frac{f^2}{M_p^2}$ the maximum value acquired by this quantity, when σ reaches its maximum speed $\dot{\sigma}_*$. Using eqs. (5.12) and (5.13), we see that

$$V_{\rm max}\,(\sigma) = \Lambda^4 = 3H^2M_p^2 \times \frac{4\epsilon_{\sigma,*}}{\delta}\ \ ,\ \ \left(\frac{\dot{\sigma}^2}{2}\right)_{\rm max} = \frac{\dot{\sigma}_*^2}{2} = 3H^2M_p^2 \times \frac{\epsilon_{\sigma,*}}{3}\,. \tag{6.15}$$

We are interested in $\delta \lesssim 1$, so the potential energy dominates over the kinetic one, and we can write the condition

$$\rho_\sigma \ll 3H^2M_p^2 \quad \Rightarrow \quad \epsilon_{\sigma,*} \ll \frac{\delta}{4}\,. \tag{6.16}$$

Secondly, we impose that the gauge field amplification does not significantly alter the motion of σ. The sourced gravity waves are proportional to the energy density ρ_A of the sourcing gauge fields. The physical energy density in the gauge fields reaches its maximum when $\xi \lesssim \xi_*$. As we show in eq. (B.24), the maximum value of ρ_A is

$$\frac{\rho_{A,\rm max}}{\epsilon_\phi\,\rho_\phi} \sim \begin{cases} 2.75\cdot 10^{-12}\,{\rm e}^{1.74\,\pi\,\xi_*} & ,\quad \delta = 0.2\,, \\ 8.86\cdot 10^{-12}\,{\rm e}^{1.52\,\pi\,\xi_*} & ,\quad \delta = 0.5\,. \end{cases} \tag{6.17}$$

We find that the maximum of $\rho_{A,\rm max}$ is achieved for $\tau \simeq \tau_*/20$ in the $\delta = 0.2$ case, and for $\tau \simeq \tau_*/10$ in the $\delta = 0.5$ case.

Note that both (6.7) and (6.17) are resultant from numerical fits. The two expressions show nearly the same ξ_* dependence. This was expected since ρ_A is the dominant GW source.

The gauge field is amplified at the expense of the kinetic energy of σ, so we need to impose that $\rho_{A,\rm max}$ (which is reached short after t_*, see Figure B.1) is smaller than the kinetic energy of σ at this moment, [7]

$$\rho_{A,\rm max} \ll \frac{\dot{\sigma}_*^2}{2} = \epsilon_{\sigma,*}\,H^2\,M_p^2 \simeq \epsilon_{\sigma,*}\,\frac{\rho_\phi}{3}\,. \tag{6.18}$$

[7] We verified that, once this condition is verified, the right hand side of (B.21) can indeed be neglected.

Finally, employing the expression (6.17) in (6.18) gives

$$\begin{aligned} \delta = 0.2 \quad &: \quad \epsilon_{\sigma,*} \gg \epsilon_\phi \, \mathrm{e}^{1.74\pi \, (\xi_* - 4.67)} \, , \\ \delta = 0.5 \quad &: \quad \epsilon_{\sigma,*} \gg \epsilon_\phi \, \mathrm{e}^{1.54\pi \, (\xi_* - 5.03)} \, . \end{aligned} \tag{6.19}$$

We discuss these conditions in Section 6.4.2.

6.3 Perturbativity

We now discuss the two criteria for perturbativity considered in [146], which we want to evaluate for the two cases $X = \phi$ (with adiabatic $\dot{\phi}$ evolution), and $X = \sigma$ (with a momentary speed up of this field).

The first criterion is from the renormalization of the gauge field wave function:

$$\mathcal{R}_A \equiv \left| \frac{\delta^{(1)} \langle \hat{A} \, \hat{A} \rangle'}{\langle \hat{A} \, \hat{A} \rangle'} \right| \ll 1 \, , \tag{6.20}$$

where the numerator is the lowest order one loop contribution to the propagator and the denominator is the tree-level propagator. The expectation values are taken in momentum space, and prime denotes the expectation value without the corresponding $\delta-$function. The one (and higher) loop contributions are defined with respect to the interaction hamiltonian obtained from

$$\begin{aligned} \mathcal{L} &= \left[-\frac{1}{2} \, (\partial X)^2 - V \, (X) - \frac{1}{4} F^2 - \frac{\alpha}{4 \, f} \, X_{\mathrm{background}} \, \hat{F} \tilde{\hat{F}} \right] + \left[-\frac{\alpha}{4 \, f} \, \delta \hat{X} \, \hat{F} \tilde{\hat{F}} \right] \\ &\equiv \mathcal{L}_{\mathrm{unperturbed}} + \mathcal{L}_{\mathrm{interaction}} \, . \end{aligned} \tag{6.21}$$

We decompose $\hat{X} = X_{\mathrm{background}} \, (t) + \hat{X}^{(0)} \, (t, \, \vec{x}) + \hat{X}^{(1)} \, (t, \, \vec{x}) + \ldots$ and $\hat{A} = \hat{A}_+^{(0)} \, (t, \, \vec{x}) + \hat{A}_+^{(1)} \, (t, \, \vec{x}) + \ldots$, where the suffix indicates the order of the perturbations in the interaction defined in (6.21).

The last term in $\mathcal{L}_{\mathrm{unperturbed}}$ encodes the backreaction of the produced gauge fields on the background dynamics. By definition, in the regime of small backreaction we can disregard the effects of this term on the background geometry, and so this term has the only effect of modifying the "unperturbed" gauge mode $\hat{A}_+^{(0)}$ from the vacuum

one to the one studied in Section 3.1.1 [8]. With this understanding, and only in this limit, the expansion in (6.21) becomes an expansion in $\frac{\alpha}{f}$, or better, in the parameter $\xi = \frac{\alpha}{f}\frac{\dot{X}_{\rm background}}{2H}$ that controls the field amplification. In the case of strong backreaction, we can "no longer" assume that the perturbations $\hat{X}^{(0)}(t,\,\vec{x})$ and $\hat{A}_+^{(0)}$ are a good approximation of the full perturbations of the model, simply because in strong backreaction regime, the $X_{\rm background}$ follows a "*different attractor*" described with $V'(X) \simeq \alpha\, E\cdot B/f$ (ie. the main friction term results from the gauge field production, not Hubble friction). Since the trajectory of X is determined from the backreaction and vacuum of the gauge field is determined from this strongly backreacted pseudo-scalar background, this becomes a completely nonlinear and nonperturbative system different than what is described above. Therefore, our perturbativity set-up is guaranteed to fail in the strong backreaction regime, and this is one of the reasons why backreaction has been studied in the previous Section. We only consider our analysis meaningful as long as backreaction is negligible, or only marginally relevant (we expect that our estimate for the range of ξ under which perturbativity is under control will remain approximately valid) [9].

The one loop correction diagram can be computed via the in-in formalism as

$$\delta^{(1)}\langle AA\rangle \simeq -\int^{\tau} d\tau_1 \int^{\tau_1} d\tau_2 \left\langle \left[\left[\hat{A}_+^{(0)}\left(\vec{k}_1,\,\tau\right)\hat{A}_+^{(0)}\left(\vec{k}_2,\,\tau\right),\,\hat{H}_{\rm int}^{(0)}(\tau_1)\right],\,\hat{H}_{\rm int}^{(0)}(\tau_2)\right]\right\rangle \quad (6.22)$$

To simplify the notation, in the following we omit the suffix 0 from the zeroth-order vector mode functions.

The second criterion is that the interaction (6.21) does not lead to quantum fluctuations that more important than the evolution of X through its potential,

$$\mathcal{R}_X \equiv \frac{\sqrt{\langle \delta\hat{X}^{(1)}(\vec{x},\,\tau)\;\delta\hat{X}^{(1)}(\vec{x},\,\tau)\rangle}}{f_{\rm period}} \ll 1\,. \quad (6.23)$$

Contrary to (6.20), the expectation value appearing in this expression is in real space.

[8] This motivates the choice of "unperturbed" vs. interaction term made in eq. (6.21). Had we chosen to include the full $-\frac{\alpha}{4f}XF\tilde{F}$ interaction in $\mathcal{L}_{\rm int}$, then $\hat{A}_+^{(0)}$ would be the standard vacuum mode rather than the solution discussed in Section 3.1.1), and therefore the ratio (6.20) would not corresponds to the criterion studied in (6.20). Therefore, perturbativity as discussed in [146] means perturbativity with respect to this splitting.

[9] We stress that for strong backreaction, scalar perturbations have to be treated in a nonperturbative way as done in Ref. [142]

One can express the variance in Fourier space as follows

$$\begin{aligned}\left\langle \delta\hat{X}^{(1)}\left(\vec{x},\,\tau\right)\,\delta\hat{X}^{(1)}\left(\vec{x},\,\tau\right)\right\rangle &= \int\frac{d^3k_1\,d^3k_2}{\left(2\pi\right)^3}\,\mathrm{e}^{i\vec{x}\cdot\left(\vec{k}_1+\vec{k}_2\right)}\,\left\langle \delta\hat{X}^{(1)}\left(\vec{k}_1,\,\tau\right)\,\delta\hat{X}^{(1)}\left(\vec{k}_2,\,\tau\right)\right\rangle \\ &= \int d\ln k\;P_{\delta X}^{(1)}\left(k,\,\tau\right)\;, \end{aligned} \tag{6.24}$$

where$P_{\delta X}^{(1)}\left(k\right)\equiv\frac{k^3}{2\pi^2}\left\langle \delta X^{(1)}\left(\vec{k}\right)\delta X^{(1)}\left(-\vec{k}\right)\right\rangle'$ and prime denotes correlator without corresponding Dirac-Delta function.

For the inflaton case $X=\phi$ we employ the results already given in the literature [48, 49, 51]. For $X=\sigma$, we instead make use of the in-in formalism

$$\left\langle \delta\hat{X}^{(1)}\left(\vec{k}_1,\,\tau\right)\delta\hat{X}^{(1)}\left(\vec{k}_2,\,\tau\right)\right\rangle \simeq-\int^{\tau}d\tau_1\int^{\tau_1}d\tau_2\,\left\langle \left[\left[\delta\hat{X}^{(0)}\left(\vec{k}_1,\,\tau\right)\delta\hat{X}^{(0)}\left(\vec{k}_2,\,\tau\right),\,\hat{H}_{\mathrm{int}}\left(\tau_1\right)\right],\,\hat{H}_{\mathrm{int}}\left(\tau_2\right)\right]\right\rangle\;. \tag{6.25}$$

The scale f_{period} in eq. (6.23) is the periodicity of the potential of X. This has an immediate identification in the case $X=\sigma$, where the potential is (4.3), and therefore $f_{\mathrm{period}}=f$. As pointed out in [146], if the interaction (6.21) leads to typical field displacements comparable to (or even greater than) f, then all operators obtained by Taylor expanding (4.3) become strong, driving the system out of the perturbative regime. For the case $X=\phi$, the identification of f_{period} depends on the specific model under consideration. For instance, the potential of aligned natural inflation [167] has four axions scales $f_i\ll M_p$ $(i=1,\ldots,4)$, but two different terms for two axions are arranged so to produce a large periodicity for one linear combination of the two axions. Therefore, $f_{\mathrm{period}}\gg f_i$. The coupling between the axions and gauge field is controlled by the original axion scales in the model, leading to an interaction lagrangian (6.21) in terms of the original scales, $f=\mathrm{O}\left(f_i\right)$ (see section V of [170] for a detailed computation). However, an $\mathrm{O}\left(f_i\right)$ field displacement would have a very suppressed effect in the potential along the ϕ direction, which has the periodicity $f_{\mathrm{period}}\gg f_i$. Therefore, if $X=\phi$ is the inflaton field, the best indicator for the periodicity of the inflation potential is the classical value assumed by the inflaton $\phi_{\mathrm{cl}}\lesssim\mathrm{O}\left(f_{\mathrm{period}}\right)$ (under the assumption that the minimum of the inflaton potential is at $\phi=0$). Therefore, we write the two different conditions

$$\mathcal{R}_\phi\equiv\frac{\sqrt{\left\langle \delta\hat{\phi}^{(1)}\,\delta\hat{\phi}^{(1)}\right\rangle}}{\phi_{\mathrm{cl}}}\ll1\quad,\quad\mathcal{R}_\sigma\equiv\frac{\sqrt{\left\langle \delta\hat{\sigma}^{(1)}\,\delta\hat{\sigma}^{(1)}\right\rangle}}{f}\ll1\;. \tag{6.26}$$

Figure 6.1 provides the diagrammatic expression of the one loop terms (6.22) and (6.25).

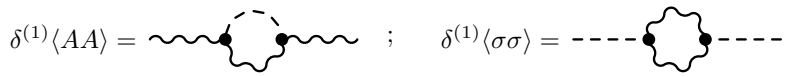

Figure 6.1: Diagrammatic representation of the one loop terms (6.22) and (6.25). Dashed lines denote δX modes, while wiggly lines denote vector field A_+ modes. The small bullets denote the interaction (6.21).

Before concluding this section, we should emphasize that all the perturbativity constraints we have considered so far concern the amplitude of the classical modes that have been generated by amplification of vacuum fluctuations. However, we should also require perturbativity in the more usual sense of sensitivity of the theory to UV quantum modes in a time-independent background. The presence of the coupling in the Lagrangian (3.1) tell us that this should be treated as an effective field theory below an energy scale $\sim 4\pi f/\alpha$, and we generally expect new states to exist at or below such energy scale. Since, as we have extensively discussed above, the typical (physical) energies of the system we are considering are of the order of $H\,\xi_*$, consistency of our analysis should require

$$\xi_*\, H \ll \frac{4\pi f}{\alpha}\,, \tag{6.27}$$

which is satisfied.

6.3.1 Perturbativity for $X = \phi$

Let us discuss the conditions $\mathcal{R}_A \ll 1$ and $\mathcal{R}_\phi \ll 1$ in the case in which X is the inflaton field ϕ. We start from the second condition, and we show that it is satisfied in all cases of interest. Using eq. (6.24), the invariant curvature (in spatially flat gauge) $\zeta = -\frac{H}{\dot\phi}\,\delta\phi$, and the slow roll relation $\dot\phi \simeq -\sqrt{2\epsilon}\,H\,M_p$, the condition (6.26) rewrites

$$\mathcal{R}_\phi \simeq \sqrt{2\epsilon}\,\times\left(\frac{M_p}{\phi_{\rm cl}}\right)\times\sqrt{\int d\ln k\, P_\zeta^{(1)}} \ll 1\,, \tag{6.28}$$

where we recall that $P_\zeta^{(1)}$ is the power spectrum of the sourced scalar mode ζ. This condition is satisfied since all the factors on the right hand side of eq. (6.28) are smaller than one. Let us discuss these factors one by one.

The first factor is $\ll 1$ due to slow roll. At CMB scales, the existing limit $\xi \lesssim 2.5$ (see eq. (6.2)), implies negligible backreaction of the gauge fields on the inflaton background dynamics. For the GW signatures at interferometers, and for production of primordial black holes, we are in a regime in which the gauge field production slows down the motion of the inflaton (see for instance Figure 2 of [108]). However, $\dot{\phi} = \mathrm{O}\left(\sqrt{2\epsilon}\, H\, M_p\right)$ is still valid, and the fact that the particle production slows down the inflaton effectively decreases the value of ϵ in eq. (6.28), further decreasing this factor.

The second factor is model dependent, but we recall that models of axion inflation realize a super-Planckian inflaton excursion. We already discussed this after eq. (6.25). Therefore $\phi_{\rm cl} \gtrsim M_p$.

Finally, the third factor is $\ll 1$ because $P_\zeta^{(1)} \ll 1$. This is for sure true at CMB scales, where $\xi \lesssim 2.5$ forces $P_\zeta^{(1)} \ll \mathcal{P}_\zeta^{(0)} = \mathrm{O}\left(10^{-9}\right)$. The sourced power is significantly greater at progressively smaller scales. However, also when the primordial black hole limit is saturated, one finds $P_\zeta^{(1)} = \mathrm{O}\left(10^{-3}\right)$, see Figure 5 of [51].

Let us now discuss the condition $\mathcal{R}_A \ll 1$. We evaluated this ratio using eqs. (E.10) and (E.11). The ratio is a function of both comoving momentum k of the mode in the propagator, and of time. Due to approximate scale invariance of the vacuum signal, the dependence on k is extremely weak, so let us first focus our discussion on CMB scales ($k_1 = k_{\rm p}$ in eq. (E.11)). For any fixed mode, the ratio $\mathcal{R}_A$ assumes a different value at different times.

As discussed in Subsection 3.1.1, the level of amplification of any given mode due to the $\phi F\tilde{F}$ interaction is a function of time. In particular, the fractional energy density $\frac{d\rho_{\rm gauge}}{d\ln k}$ of any given mode reaches a maximum value when the mode has a size comparable to the horizon, and it is then diluted away by the expansion of the universe. Most of the contribution of any given mode to a cosmological observable takes place when $\frac{d\rho_{\rm gauge}}{d\ln k}$ is close to its peak value. This defines the time interval for which we need to make sure that $\mathcal{R}_A \ll 1$ for that given mode. Also, in our computation, we use the UV cut-off $-k\tau|_{\rm max} = \xi$ for all modes [10].

In Figure 6.2 we show the value of $\mathcal{R}_A$ for one given mode with wave number equal the Planck pivot scale ($k = k_{\rm p}$) as a function of ξ. The value of ξ should be understood as the value assumed by this quantity when the mode of our interest left the horizon. In

[10] Modifying the UV cut-off only slightly changes the final results and keeps the final conclusions same.

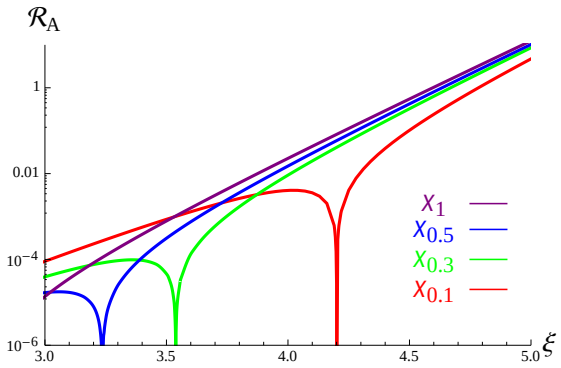

Figure 6.2: Ratio $\mathcal{R}_A$ for the $X = \phi$ case, as a function of ξ. The ratio is evaluated for a fixed mode of the size of the Planck pivot scale (due to approximate scale invariance, nearly the same bound is obtained at smaller scales). The different curves shown correspond to different values of the rescaled time $x \equiv -k\tau$ at which $\mathcal{R}_A$ is evaluated. For instance $x_{0.1}$ indicates that $\mathcal{R}_A$ is evaluated when the energy density in that mode is 10% of the peaked value that it had previously assumed (as shown in Figure 3.1, the energy density in one given mode reaches a peak value, and it then decreases).

general, a greater value of ξ results in a greater gauge field amplification, and therefore in a greater value of $\mathcal{R}_A$ [11]. Different color curves in the figure show the value of $\mathcal{R}_A$ for $k = k_{\rm p}$ as a function of ξ, at different times. The values of time shown are chosen by evaluating the value of $\frac{d\rho_{\rm gauge}}{d\ln k}$. For instance $x_{0.1}$ denotes the value of time ($x \equiv -k\,\tau$) when the energy density in that mode has been diluted to 10% of the value it had at its peak (and analogously for the other values shown in the Figure 6.2 such as 0.5, 0.3 and 0.1. Since the energy density decreases/gets diluted with the expansion, the smaller fractions are for the later moments. Because the time ($x \equiv -k\tau$) flows from ∞ to 0 during inflation, we have $x_1 > x_{0.5} > x_{0.3} > x_{0.1}$).

The strongest limit is obtained for x_1, when the energy density in that mode is maximum. In this case, a numerical fit of the curve shown in the figure gives

$$\mathcal{R}_A \simeq {\rm e}^{2.01\,\pi(\xi-4.60)}\ . \tag{6.29}$$

The fit well reproduces the $\propto {\rm e}^{2\pi\xi}$ scaling expected from analytic considerations (the numerator of eq. (E.10) has two extra powers of A_R than the denominator).

We recall that the limit in Figure 6.2 assumes a mode with wave number equal the

[11] We disregard the narrow spikes seen in the Figure, which take place when $\frac{\delta^{(1)}\langle\hat{A}\,\hat{A}\rangle'}{\langle\hat{A}\,\hat{A}\rangle'}$ changes sign.

Planck pivot scale. For signatures at smaller scales ($k > k_{\rm p}$), eq. (E.11) presents the extra factor $\left(\frac{k_1}{k_{\rm p}}\right)^{n_s-1} \simeq {\rm e}^{-(1-n_s)(60-N_k)}$, where N_k is the number of e-folds before the end of inflation when the mode of wavenumber k exited the horizon. Above we have assumed that $k_{\rm p}$ exited the horizon 60 e-folds before the end of inflation, so taking this effect into account for smaller scales, the perturbativity limit can be cast in the form

$$ {\rm e}^{2.01\,\pi(\xi_k-4.60)}\,{\rm e}^{-(1-n_s)(60-N_k)} \ll 1\ . \tag{6.30} $$

This condition is a function of wavenumber, since both ξ_k and N_k refer to the value assumed by ξ and by N when the mode of wave number k exited the horizon during inflation. We discuss this condition in Section 6.4.1.

6.3.2 Perturbativity for $X = \sigma$

In the case, $X = \sigma$ is a pseudo-scalar different from the inflaton and has a nonvanishing speed only for a few e-folds during inflation, we find the two perturbativity conditions

$$ \mathcal{R}_A \equiv {\rm R}_A\left[x_*,\,\xi_*,\,\delta,\,\frac{\tau}{\tau_*}\right]\,\frac{\epsilon_\phi}{\epsilon_{\sigma_*}} \ll 1 \qquad , \qquad \mathcal{R}_\sigma \equiv {\rm R}_\sigma\left[\xi_*,\,\delta,\,\frac{\tau}{\tau_*}\right]\,\frac{\epsilon_\phi}{\epsilon_{\sigma_*}} \ll 1\ , \tag{6.31} $$

where R_A and R_σ are given in eqs. (E.25) and (E.32), respectively.

The ratio $\mathcal{R}_A$ is evaluated mode by mode, and it therefore depends on the comoving momentum k of the mode through $x_* = -k\tau_*$. We recall that τ_* is the conformal time at which $\dot\sigma$ is maximum, and $-\frac{1}{\tau_*}$ is the comoving momentum of the mode that left the horizon at this time. For each mode, the quantity ${\rm R}_A$ then depends on the time at which it is evaluated; we express this dependence as a dependence on the ratio $\frac{\tau}{\tau_*}$. The ratio $\mathcal{R}_\sigma$ is instead obtained after an integral over momentum (performed at any given fixed time) and so it depends on the time variable $\frac{\tau}{\tau_*}$. Finally, both ratios depend on the amplification parameter ξ_* (the maximum value acquired by ξ), and on δ, which controls the duration of the phase for which the evolution of σ is significant; specifically, the field σ has a non-negligible evolution for $N \simeq \frac{1}{\delta}$ e-folds of inflation.

In Figure 6.3 we show the two quantities $R_A = \frac{\mathcal{R}_A\,\epsilon_{\sigma,*}}{\epsilon_\phi}$ (left panel) and $R_\sigma = \frac{\mathcal{R}_\sigma\,\epsilon_{\sigma,*}}{\epsilon_\phi}$ (right panel), for $\delta = 0.2$ and varying ξ_*. In the left panel, we fixed $k = 5\,k_*$. The quantity shown in the right panel is instead $k-$independent. The different color curves in the figure correspond to different times. The times are chosen when the total energy

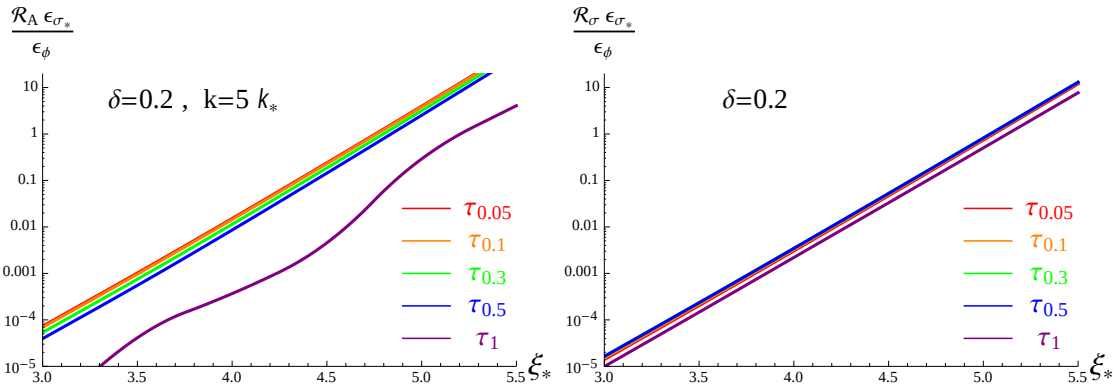

Figure 6.3: Ratio R_A (left panel) and R_A (right panel) for $\delta = 0.2$ and for varying ξ_*. The different lines correspond to different times at which the ratios are evaluated.

density in the gauge field decreases (due to the expansion of the universe) by a given amount with respect to the value it had at its peak. For example $\tau_{0.5}$, is the time at which the energy density has decreased to 50% of the peak value. We only studied the limits in the time interval between τ_1 and $\tau_{0.05}$ since the gauge field decreases significantly after these times, and it resultantly has no significant impact on observables. The ξ_* dependence of the largest value for R_A and R_σ obtained among the lines shown can be well fitted by the exponential dependence

$$\delta = 0.2 \quad : \qquad \mathrm{R}_A \simeq \mathrm{e}^{5.50\,(\xi_* - 4.75)} \qquad , \qquad \mathrm{R}_\sigma \simeq \mathrm{e}^{5.44(\xi_* - 5.03)} \tag{6.32}$$

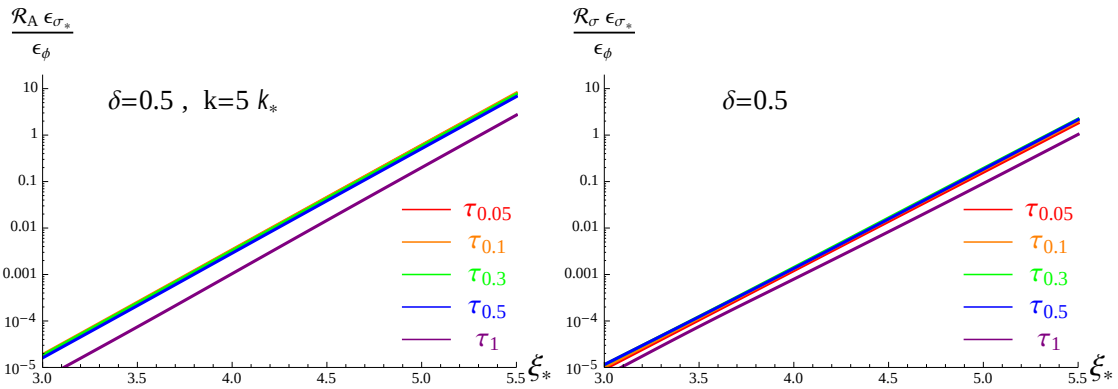

Figure 6.4: Ratio R_A (left panel) and R_A (right panel) for $\delta = 0.5$ and for varying ξ_*. The different lines correspond to different times at which the ratios are evaluated.

In Figure 6.4 we repeat the same study for $\delta = 0.5$. In this case, we obtain

$$\delta = 0.5 \quad : \quad \mathrm{R}_A \simeq \mathrm{e}^{5.19\,(\xi_* - 5.10)} \qquad , \qquad \mathrm{R}_\sigma \simeq \mathrm{e}^{4.88(\xi_* - 5.34)} \tag{6.33}$$

We find that $R_A > R_\sigma$ both for $\delta = 0.2$ and for $\delta = 0.5$. Therefore our final bounds from perturbativity, $\mathcal{R}_A \ll 1$, can be cast in the form

$$\begin{aligned} \delta = 0.2 \quad &: \quad \epsilon_{\sigma,*} \gg \epsilon_\phi \, \mathrm{e}^{5.50\,(\xi_* - 4.75)} \, , \\ \delta = 0.5 \quad &: \quad \epsilon_{\sigma,*} \gg \epsilon_\phi \, \mathrm{e}^{5.19\,(\xi_* - 5.10)} \, . \end{aligned} \tag{6.34}$$

We discuss this condition in Section 6.4.2.

6.4 Discussion of the constraints

In this section we discuss the significance of the constraints on gauge field amplification imposed by backreaction on the background evolution (obtained in Section 6.2) and by perturbativity (obtained in Section 6.3). We then compare these constraints with the amplification required to obtain visible signatures (discussed in Section 6.1). We divide the discussion in two subsections, where we separately discuss the $X = \phi$ (with adiabatic $\dot{\phi}$ evolution), and $X = \sigma$ (with a momentary speed up of this field) cases.

6.4.1 Discussion for $X = \phi$

The values in (6.2) indicate that $\xi \simeq 2.5$ is required to obtain phenomenological signatures at CMB scales, while $\xi \simeq 5$ is required for both significant GWs at interferometer scales and primordial black holes.

The condition (6.13) indicates that the vector field amplification has a negligible backreaction on the inflaton dynamics for $\xi \ll 4.7$. Since the field amplification is exponentially sensitive to ξ, we interpret this condition (and the ones discussed below) as $\xi \lesssim 4.7$. This condition is well satisfied when the phenomenological limits at CMB scales are respected, but it is violated in the realizations that produce visible GWs at interferometer scales and primordial black holes. In these two cases, the backreaction of the produced gauge fields slows down the motion of the inflaton and this effect has been taken into account in the relevant studies such as Ref. Ref. [142]. However, this problem can also be evaded as shown in Chapter 5. A slight change in the inflaton

potential, which slows the it down after interferometer scales, protects the scenario from both PBH overproduction and perturbativity constraints. See for example subsection 5.2.2.1 and Figure 5.4 for an explicit realization of this, in which $\xi_{\max} = 4.43$.

Finally, the relation (6.30) provides a condition under which the computations of the gauge field and inflaton modes are under perturbative control. This condition evaluates to $\xi \lesssim 4.6$ for the value of ξ assumed when the CMB modes left the horizon ($N = 60$). This condition becomes slightly relaxed for smaller wavelength modes. Using $n_s \simeq 0.965$ [67], we find $\xi \lesssim 4.8$ for the LIGO scale relevant for the GW signature (corresponding to $N \simeq 15$), and $\xi \lesssim 4.9$ for the scale relevant for the black hole limit. Since in both cases a visible signature is obtained for $\xi \simeq 5$, we see that this value is only marginally out of the perturbative and of the backreaction bounds. As a consequence, we do not think that this affects the conclusion that significant GW and primordial black holes will be generated for $\xi = \mathrm{O}(5)$, although order one corrections to the result present in the literature (as already mentioned in some of those works) can be expected.

6.4.2 Discussion for $X = \sigma$

Eq. (6.9) shows that, for sufficiently high field amplification (sufficiently high ξ_*), it is possible to have a sourced GW signal at very low energy scale of inflation. For a large range of parameters, this GW amplification can take place without a corresponding increase of scalar perturbations beyond the bounds of cosmic variance, and it is therefore not ruled out by the TT and TTT observations [171]. In addition, gauge field amplification can produce visible GW signals at interferometer scales and result in considerable amount of PBH by sourced curvature perturbations.

The condition from eq. (6.16) guarantees that σ affects in a negligible way the expansion of the universe, and (therefore) the motion of the inflaton. Eq. (6.19) ensures that the gauge field amplification has a negligible impact on the evolution of σ. The perturbativity considerations discussed in the previous section give instead the bound (6.34). We note that both bounds (6.19) and (6.34) can be satisfied for arbitrary values of ξ_*, provided that $\epsilon_{\sigma,*}/\epsilon_\phi$ is sufficiently large.

We note that $\epsilon_\sigma > \epsilon_\phi$ does not impact the Friedmann equation (given that with the condition (6.16) we impose that $\rho_\sigma \ll V(\phi)$), nor the background equation for the inflaton field. In principle, it may affect the relation for the spectral tilt n_s of the scalar

perturbations and scalar tilt is only constrained for CMB scales; for interferometer scales we do not have this constraint. The spectral tilt receives a contribution $\propto \frac{\dot{H}}{H^2} \simeq -\epsilon_\phi - \epsilon_\sigma$, resulting in

$$n_s - 1 \simeq 2\eta_\phi - 6\epsilon_\phi - 4\epsilon_\sigma \ . \tag{6.35}$$

(Where $\eta_\phi \equiv M_p^2\, \partial_\phi^2 V/V$ is the other standard slow roll parameter.) Given the measured value of $n_s - 1 \sim -0.03$ [67] at CMB scales, we require (for only CMB scales) $\epsilon_{\sigma,*} \lesssim 10^{-2}$ to avoid fine tunings in (6.35), but we do not need to impose $\epsilon_{\sigma,*} < \epsilon_\phi$. If the vacuum GW signal is too small to be observed, it follows that $\epsilon_\phi \ll |n_s - 1|$, so that eq. (6.35) should read $n_s - 1 \simeq 2\eta_\phi - 4\epsilon_\sigma$. Having $\epsilon_{\sigma,*} > \epsilon_\phi$ simply implies that, for the few e-folds in which the motion of σ is non negligible, $\dot{H}$ is controlled be the motion of σ. However, this has no phenomenological consequence as long as $\epsilon_{\sigma,*} \lesssim 10^{-2}$, since in this case the scalar spectral tilt will simply be controlled by η_ϕ [12].

Therefore all backreaction and perturbativity constraints can be summarized as

$$\begin{aligned}
\delta = 0.2 \quad &: \quad \mathrm{Max}\left[\epsilon_\phi\, \mathrm{e}^{5.47\,(\xi_* - 4.67)},\, \epsilon_\phi\, \mathrm{e}^{5.50\,(\xi_* - 4.75)}\right] \lesssim \epsilon_{\sigma,*} \lesssim 10^{-2} \ , \\
\delta = 0.5 \quad &: \quad \mathrm{Max}\left[\epsilon_\phi\, \mathrm{e}^{4.84\,(\xi_* - 5.03)},\, \epsilon_\phi\, \mathrm{e}^{5.19\,(\xi_* - 5.10)}\right] \lesssim \epsilon_{\sigma,*} \lesssim 10^{-2} \ .
\end{aligned} \tag{6.36}$$

For $\delta = 0.2$, the first condition in the square parenthesis (the one obtained from backreaction) dominates over the second one for $\xi_* \lesssim 19$, so we disregard the second condition. For $\delta = 0.5$, instead, the first condition (from backreaction) dominates for $\xi_* \lesssim 6$. Therefore, we will keep both conditions. Using (6.14), we can rewrite the conditions as

$$\begin{aligned}
\delta = 0.2 \quad &: \quad 2 \cdot 10^{-5}\, \mathrm{e}^{2.74\,\xi_*}\, \sqrt{\epsilon_\phi} \lesssim \frac{f}{M_p} \lesssim 0.71 \ , \\
\delta = 0.5 \quad &: \quad \mathrm{Max}\left[1.4 \cdot 10^{-5}\, \mathrm{e}^{2.42\,\xi_*}\, \sqrt{\epsilon_\phi},\, 5.1 \cdot 10^{-6}\, \mathrm{e}^{2.60\,\xi_*}\, \sqrt{\epsilon_\phi}\right] \lesssim \frac{f}{M_p} \lesssim 0.28 \ .
\end{aligned} \tag{6.37}$$

6.5 Summary

Axion fields are very natural candidates for the inflaton or for light extra degrees of freedom during inflation, since their potential is protected by a shift symmetry, that can be broken in a controllable way [106]. The main decay of a pseudoscalar X is

[12] Although, spectral tilt is not a constraint for small scale perturbations. This choice also immediately satisfies the condition given in eq (6.16) for any δ choice between 0.2 and 0.5.

through the least irrelevant operator $XF\tilde{F}$. This operator can lead to interesting gauge field amplification already during inflation: in its presence, one polarization of the gauge field becomes unstable at horizon crossing; the energy density of any given gauge mode can be highly amplified by this effect, and it is eventually diluted away by the expansion of the universe. In the few e-folds between the amplification and the dilution, the mode can give rise to a number of signatures that we have outlined in the beginning of this Chapter.

In our discussion we have distinguished between the case in which X rolls at an approximately constant velocity [39, 33], or it experiences a transient of relatively fast roll [171] (we assume that, even at its fastest roll, the field continues to satisfy $|\dot{X}| \ll HM_p$). We have reviewed both cases briefly and direct the reader for relevant sections for the details as it is one of the very few mechanisms that can produce sourced GWs at CMB scales and small interferometer scales, and at the same time avoids overproducing scalar perturbations, so that it is not ruled out by the limits on the latter.

The gauge field amplification needs to be sufficiently strong to lead to observable effects. One should therefore include its backreaction on the background dynamics, as consistently done in many applications, and also make sure that the computations remain in the perturbative regime. A strong motivation for this chapter has been the study of two criteria pointed out in [146] for the validity of the perturbative regime. Following their definitions, we have checked their computation in the case in which $\dot{X}$ is adiabatically rolling, and we have extended it to the case in which $\dot{X}$ has a momentary roll. In this second case, we have found that there exists a large region of parameters in which the two criteria are satisfied (we find that the perturbativity criteria are satisfied in most of the region in which the produced gauge field does not backreact on the background evolution). In the first case, we have found that the criteria are satisfied in most of the parameter space.

From our results, it emerges that the criteria are well satisfied in the applications that produce signatures at CMB scales. One of the two criteria is instead marginally violated when GWs and primordial black holes are produced at smaller scales. In this case, $\xi \simeq 5$ is needed to produce a visible effect (where ξ is the parameter that controls the gauge field amplification), while the perturbativity criterion fails at $\xi \simeq 4.8$. This result is not surprising, given that several of the original works already pointed out that

the scalar perturbations are in a strong coupling regime for those values of ξ, and order one corrections can be expected (we are comforted in the statement by the fact that the $\xi \lesssim 4.8$ region is not very far from $\xi = 5$) [13]. We do not believe that the conclusion that significant GWs and primordial black holes will be generated for $\xi \sim 5$ is in question. An exact computation (performed perhaps through lattice simulation) would certainly allow to refine the precise bound on ξ, but not the presence of these physical effects.

[13] It is also important to note that by adding a slight feature in potential, as done in Subsection 5.2.2.1 (also see Figure 5.4), one can satisfy all the criteria smoothly for the inflaton axion case at small scales (ie. for interferometer GWs and primordial black holes).

Chapter 7

Conclusion and Discussions

"Hancı dedi bir çiçeği yaratmak asırların, nasırların işidir.
Ben her bahar arar, arar, arar dururum.
Şu yeryüzünde kimin kimsesi yok kendinden başka.
Bir de koca evren başının üstünde.
Doğmuş ve ölmüş apansız binlercesi.
Yok henüz farkına varan, ne olacak bundan sonrası." Siya Siyabend

The inflationary era is now a cornerstone of modern cosmology, not only because it resolves the standard Big Bang model shortcomings such as horizon, flatness and unwanted relics problems, but also, because it predicts the "seed quantum perturbations" that result in the current structure of our universe with amplitude, scale dependence and statistical properties in agreement with the Cosmic Microwave Background and Large Scale Structure experiments. The merits of inflationary expansion are far more reached. For example, inflation can make us reach the physics at energy scales that are not possible to reach on any terrestrial experiments. Since Einstein's General Relativity, it has been known that geometry and the ingredients of the energy are coupled to each other. Therefore, as universe emerges as the largest particle laboratory, early universe could reveal precious information about the high energy theories. Now, inflation is accepted as the primordial era to set the stage for the dense, high energy Big Bang plasma.

Although inflation has passed the tests remarkably well up to this point, several details about this unusual era are waiting to be understood. Some of these, with the caution that this list is far away from being complete, can be listed as follows:

- The symmetries, the energy scale, the shape of the potential and the couplings of inflaton(s)
- The excursion of the inflaton(s) in the field space
- The details of reheating, the era that links the inflationary and Big Bang phases
- GW background from inflation
- The primordial signals that might have been produced during inflation at much smaller scales than the CMB

A successful inflationary era requires the inflaton potential to be considerably flat so that the expansion can continue long enough to solve the problems of standard Big Bang model. However, at very high energies and large excursions in field space, it is very hard to realize this due to quantum corrections. This task is particularly harder for large field models, ie. the ones for which the inflaton field spans a range larger than Plank Mass during inflation. The basic shift symmetry that is approximately respected by pseudo-scalar particles, called axions, become a strong motivation and hope for keeping the inflaton potential flat against quantum corrections. Although, this motivation has been raised for the inflaton field, in the particle inventory of UV complete models, these types of particles are abundant. Hence, it is important to study the axion particles in the early universe not only as a candidate for the inflaton field which dominates the energy content of our universe and drives the inflationary expansion, but also as a spectator field which is subdominant in energy content with respect to inflaton and evolves in the nearly de Sitter background as a test field. In this thesis, we focus on on the effects of parity-violating interaction between axion and gauge fields. In this mechanism, the rolling axion amplifies one helicity of the gauge field quanta, which in turn source the scalar (curvature) and tensor (GW) perturbations. Because the gauge field source the perturbations via two-to-one fashion, explicitly $A + A \to \zeta$ and $A + A \to \delta g^{\rm TT}$, the

sourced perturbations obey non-Gaussian statistics. As a result, this single operator leads to a number of unique signatures.

After summarizing the inflationary cosmology and providing relevant concepts, observables and parameters in Chapter 2, we study the effects of this coupling on vacuum mode function of gauge field in Chapter 3. We focus on two potential scenarios : One case is that the axion is the slowly rolling inflaton. The other case is axion is a spectator field which slowly rolls down in its potential and has a non-negligible speed for only a period of inflation. We devote Chapter 4 for the phenomenology of this interaction at the largest scales of our observable universe in the spectator axion case. We show that it is possible that sourced GW modes can dominate over vacuum GW modes without violating tight bounds from non-Gaussianity at CMB scales. In addition, this interaction results in non-zero (and potentially detectable) TB and EB correlators due to parity brreaking, and large tensor non-Gaussianity due to non-Gaussian sourcing. Chapter 5 is devoted for the small scale phenomenology, specifically potentially detectable GWs at gravitational interferometers such as Pulsar Timing Arrays (PTA), LISA and LIGO, which scan different frequencies of GW spectrum from nHz to tens of Hz. We show that without producing too many primordial black holes (PBHs), this mechanism can leave observable imprints on electromagnetic and gravitational detectors. In Chapter 6, we study a broad range of constraints, including various backreaction limits and quantum corrections, for the verification of calculations conducted in the previous chapters. We show that the results produced in the previous chapters are under perturbative control.

In conclusion, we show that interaction of different fields during inflation suggests a rich phenomenology without demanding fine-tuning or unreasonable assumptions. Basically, a very natural operator that is expected to arise in any pseudo-scalar theory leads to remarkable signatures from very large scales to very small scales helping us probing larger portion of the inflationary period. The modern cosmology that started in 1960s with the coincidental detection of Cosmic Microwave Background is now in the precision era with unprecedented quality and quantity of data from three orthogonal sources: Photons, Neutrinos [1] and Gravitational Waves; and there is no doubt that new breakthroughs and discoveries are on the way. Therefore, now is the very correct time to study the heavens in a careful manner.

[1] IceCube very recently detected a neutrino from a Blazar direction [168].

References

[1] A. A. Penzias and R. W. Wilson, Astrophys. J. **142**, 419 (1965). doi:10.1086/148307

[2] A. H. Guth, Phys. Rev. D **23**, 347 (1981). doi:10.1103/PhysRevD.23.347

[3] K. Freese, J. A. Frieman and A. V. Olinto, Phys. Rev. Lett. **65**, 3233 (1990).

[4] F. C. Adams, J. R. Bond, K. Freese, J. A. Frieman and A. V. Olinto, Phys. Rev. D **47**, 426 (1993) doi:10.1103/PhysRevD.47.426 [hep-ph/9207245].

[5] J. Preskill, M. B. Wise and F. Wilczek, Phys. Lett. B **120**, 127 (1983) [Phys. Lett. **120B**, 127 (1983)]. doi:10.1016/0370-2693(83)90637-8

[6] R. D. Peccei and H. R. Quinn, Phys. Rev. D **16**, 1791 (1977). doi:10.1103/PhysRevD.16.1791

R. D. Peccei and H. R. Quinn, Phys. Rev. Lett. **38**, 1440 (1977). doi:10.1103/PhysRevLett.38.1440

[7] T. Banks, M. Dine, P. J. Fox and E. Gorbatov, JCAP **0306**, 001 (2003) doi:10.1088/1475-7516/2003/06/001 [hep-th/0303252].

[8] P. A. R. Ade *et al.* [BICEP2 and Planck Collaborations], Phys. Rev. Lett. **114**, 101301 (2015) [arXiv:1502.00612 [astro-ph.CO]].

[9] K. N. Abazajian *et al.*, Astropart. Phys. **63**, 55 (2015) [arXiv:1309.5381 [astro-ph.CO]].

[10] D. H. Lyth, Phys. Rev. Lett. **78**, 1861 (1997) [hep-ph/9606387].

[11] M. Biagetti, M. Fasiello and A. Riotto, Phys. Rev. D **88**, 103518 (2013) [arXiv:1305.7241 [astro-ph.CO]].

[12] M. Biagetti, E. Dimastrogiovanni, M. Fasiello and M. Peloso, JCAP **1504**, 011 (2015) [arXiv:1411.3029 [astro-ph.CO]].

[13] T. Fujita, J. Yokoyama and S. Yokoyama, PTEP **2015**, 043E01 (2015) [arXiv:1411.3658 [astro-ph.CO]].

[14] D. Cannone, G. Tasinato and D. Wands, JCAP **1501**, no. 01, 029 (2015) [arXiv:1409.6568 [astro-ph.CO]].

[15] D. Cannone, J. O. Gong and G. Tasinato, arXiv:1505.05773 [hep-th].

[16] Y. Cai, Y. T. Wang and Y. S. Piao, Phys. Rev. D **91**, 103001 (2015) [arXiv:1501.06345 [astro-ph.CO]].

[17] E. Dimastrogiovanni and M. Peloso, Phys. Rev. D **87**, no. 10, 103501 (2013) [arXiv:1212.5184 [astro-ph.CO]].

[18] P. Adshead, E. Martinec and M. Wyman, JHEP **1309**, 087 (2013) [arXiv:1305.2930 [hep-th]].

[19] I. Obata, T. Miura and J. Soda, Phys. Rev. D **92**, no. 6, 063516 (2015) doi:10.1103/PhysRevD.92.063516 [arXiv:1412.7620 [hep-ph]];

[20] R. Namba, E. Dimastrogiovanni and M. Peloso, JCAP **1311**, 045 (2013) [arXiv:1308.1366 [astro-ph.CO]].

[21] S. Y. Khlebnikov and I. I. Tkachev, Phys. Rev. D **56**, 653 (1997) [hep-ph/9701423].

[22] R. Easther and E. A. Lim, JCAP **0604**, 010 (2006) [astro-ph/0601617].

[23] J. Garcia-Bellido and D. G. Figueroa, Phys. Rev. Lett. **98**, 061302 (2007) [astro-ph/0701014].

[24] J. F. Dufaux, A. Bergman, G. N. Felder, L. Kofman and J. P. Uzan, Phys. Rev. D **76**, 123517 (2007) [arXiv:0707.0875 [astro-ph]].

[25] J. F. Dufaux, G. Felder, L. Kofman and O. Navros, JCAP **0903**, 001 (2009) [arXiv:0812.2917 [astro-ph]].

[26] J. F. Dufaux, Phys. Rev. Lett. **103**, 041301 (2009) [arXiv:0902.2574 [astro-ph.CO]].

[27] J. F. Dufaux, D. G. Figueroa and J. Garcia-Bellido, Phys. Rev. D **82**, 083518 (2010) [arXiv:1006.0217 [astro-ph.CO]].

[28] D. G. Figueroa and T. Meriniemi, JHEP **1310**, 101 (2013) [arXiv:1306.6911 [astro-ph.CO]].

[29] I. Antoniadis and S. P. Patil, Eur. Phys. J. C **75**, 182 (2015) [arXiv:1410.8845 [hep-th]].

[30] M. Kleban, M. Mirbabayi and M. Porrati, arXiv:1508.01527 [hep-th].

[31] J. L. Cook and L. Sorbo, Phys. Rev. D **85**, 023534 (2012) [Phys. Rev. D **86**, 069901 (2012)] [arXiv:1109.0022 [astro-ph.CO]].

[32] L. Senatore, E. Silverstein and M. Zaldarriaga, JCAP **1408**, 016 (2014) [arXiv:1109.0542 [hep-th]].

[33] N. Barnaby, J. Moxon, R. Namba, M. Peloso, G. Shiu and P. Zhou, Phys. Rev. D **86**, 103508 (2012) [arXiv:1206.6117 [astro-ph.CO]].

[34] D. Carney, W. Fischler, E. D. Kovetz, D. Lorshbough and S. Paban, JHEP **1211**, 042 (2012) [arXiv:1209.3848 [hep-th]].

[35] D. J. H. Chung, E. W. Kolb, A. Riotto and I. I. Tkachev, Phys. Rev. D **62**, 043508 (2000) [hep-ph/9910437].

[36] A. Berera, Phys. Rev. Lett. **75**, 3218 (1995) [astro-ph/9509049].

[37] M. Bastero-Gil and A. Berera, Int. J. Mod. Phys. A **24**, 2207 (2009) [arXiv:0902.0521 [hep-ph]].

[38] M. M. Anber and L. Sorbo, JCAP **0610**, 018 (2006) [astro-ph/0606534].

[39] L. Sorbo, JCAP **1106**, 003 (2011) [arXiv:1101.1525 [astro-ph.CO]].

[40] D. H. Lyth, C. Quimbay and Y. Rodriguez, JHEP **0503**, 016 (2005) [hep-th/0501153].

[41] M. Satoh, JCAP **1011**, 024 (2010) [arXiv:1008.2724 [astro-ph.CO]].

[42] A. Lue, L. M. Wang and M. Kamionkowski, Phys. Rev. Lett. **83**, 1506 (1999) [astro-ph/9812088].

[43] S. Saito, K. Ichiki and A. Taruya, JCAP **0709**, 002 (2007) [arXiv:0705.3701 [astro-ph]].

[44] V. Gluscevic and M. Kamionkowski, Phys. Rev. D **81**, 123529 (2010) [arXiv:1002.1308 [astro-ph.CO]].

[45] A. Ferté and J. Grain, Phys. Rev. D **89**, no. 10, 103516 (2014) [arXiv:1404.6660 [astro-ph.CO]].

[46] C. Caprini, R. Durrer and T. Kahniashvili, Phys. Rev. D **69**, 063006 (2004) [astro-ph/0304556].

[47] C. Caprini and L. Sorbo, JCAP **1410**, no. 10, 056 (2014) [arXiv:1407.2809 [astro-ph.CO]].

[48] N. Barnaby and M. Peloso, Phys. Rev. Lett. **106**, 181301 (2011) [arXiv:1011.1500 [hep-ph]].

[49] N. Barnaby, R. Namba and M. Peloso, JCAP **1104**, 009 (2011) [arXiv:1102.4333 [astro-ph.CO]].

[50] P. D. Meerburg and E. Pajer, JCAP **1302**, 017 (2013) [arXiv:1203.6076 [astro-ph.CO]].

[51] A. Linde, S. Mooij and E. Pajer, Phys. Rev. D **87**, no. 10, 103506 (2013) [arXiv:1212.1693 [hep-th]].

[52] K. Choi, K. Y. Choi, H. Kim and C. S. Shin, JCAP **1510**, no. 10, 046 (2015) doi:10.1088/1475-7516/2015/10/046 [arXiv:1507.04977 [astro-ph.CO]].

[53] B. Ratra, Astrophys. J. **391**, L1 (1992).

[54] O. Özsoy, K. Sinha and S. Watson, Phys. Rev. D **91**, no. 10, 103509 (2015) [arXiv:1410.0016 [hep-th]].

[55] S. Mukohyama, R. Namba, M. Peloso and G. Shiu, JCAP **1408**, 036 (2014) [arXiv:1405.0346 [astro-ph.CO]].

[56] P. A. R. Ade *et al.* [BICEP2 Collaboration], Phys. Rev. Lett. **112**, no. 24, 241101 (2014) [arXiv:1403.3985 [astro-ph.CO]].

[57] R. Z. Ferreira and M. S. Sloth, JHEP **1412**, 139 (2014) [arXiv:1409.5799 [hep-ph]].

[58] M. Mirbabayi, L. Senatore, E. Silverstein and M. Zaldarriaga, Phys. Rev. D **91**, 063518 (2015) [arXiv:1412.0665 [hep-th]].

[59] S. Eccles, W. Fischler, D. Lorshbough and B. A. Stephens, arXiv:1505.04686 [astro-ph.CO].

[60] A. Riotto, "Inflation and the theory of cosmological perturbations," hep-ph/0210162.

[61] V. Mukhanov, "Physical Foundations of Cosmology ".

[62] D. Baumann, "Inflation," arXiv:0907.5424 [hep-th].

[63] A. D. Linde, Phys. Lett. B **175**, 395 (1986). doi:10.1016/0370-2693(86)90611-8

[64] C. Pattison, V. Vennin, H. Assadullahi and D. Wands, arXiv:1707.00537 [hep-th].

[65] C. L. Bennett *et al.* [WMAP Collaboration], Astrophys. J. Suppl. **208**, 20 (2013) [arXiv:1212.5225 [astro-ph.CO]].

[66] G. Hinshaw *et al.* [WMAP Collaboration], Astrophys. J. Suppl. **208**, 19 (2013) [arXiv:1212.5226 [astro-ph.CO]].

[67] P. A. R. Ade *et al.* [Planck Collaboration], Astron. Astrophys. **594**, A20 (2016) doi:10.1051/0004-6361/201525898 [arXiv:1502.02114 [astro-ph.CO]].

[68] P. A. R. Ade *et al.* [Planck Collaboration], arXiv:1502.01589 [astro-ph.CO].

[69] J. Tauber *et al.* [Planck Collaboration], astro-ph/0604069.

[70] M. Shiraishi, JCAP **1311**, 006 (2013) [arXiv:1308.2531 [astro-ph.CO]].

[71] M. Shiraishi, A. Ricciardone and S. Saga, JCAP **1311**, 051 (2013) [arXiv:1308.6769 [astro-ph.CO]].

[72] M. Shiraishi, S. Yokoyama, D. Nitta, K. Ichiki and K. Takahashi, Phys. Rev. D **82**, 103505 (2010) [arXiv:1003.2096 [astro-ph.CO]].

[73] M. Shiraishi, D. Nitta, S. Yokoyama, K. Ichiki and K. Takahashi, Prog. Theor. Phys. **125**, 795 (2011) [arXiv:1012.1079 [astro-ph.CO]].

[74] P. A. R. Ade *et al.* [Planck Collaboration], arXiv:1502.01592 [astro-ph.CO].

[75] J. L. Cook and L. Sorbo, JCAP **1311**, 047 (2013) [arXiv:1307.7077 [astro-ph.CO]].

[76] M. Kamionkowski and T. Souradeep, Phys. Rev. D **83**, 027301 (2011) [arXiv:1010.4304 [astro-ph.CO]].

[77] M. Shiraishi, D. Nitta and S. Yokoyama, Prog. Theor. Phys. **126**, 937 (2011) [arXiv:1108.0175 [astro-ph.CO]].

[78] J. M. Maldacena and G. L. Pimentel, JHEP **1109**, 045 (2011) [arXiv:1104.2846 [hep-th]].

[79] J. Soda, H. Kodama and M. Nozawa, JHEP **1108**, 067 (2011) [arXiv:1106.3228 [hep-th]].

[80] M. Shiraishi, JCAP **1206**, 015 (2012) [arXiv:1202.2847 [astro-ph.CO]].

[81] M. Shiraishi, M. Liguori and J. R. Fergusson, JCAP **1405**, 008 (2014) [arXiv:1403.4222 [astro-ph.CO]].

[82] M. Shiraishi, M. Liguori and J. R. Fergusson, JCAP **1501**, no. 01, 007 (2015) [arXiv:1409.0265 [astro-ph.CO]].

[83] D. Babich and M. Zaldarriaga, Phys. Rev. D **70**, 083005 (2004) [astro-ph/0408455].

[84] A. P. S. Yadav, E. Komatsu, B. D. Wandelt, M. Liguori, F. K. Hansen and S. Matarrese, Astrophys. J. **678**, 578 (2008) [arXiv:0711.4933 [astro-ph]].

[85] A. P. S. Yadav, E. Komatsu and B. D. Wandelt, Astrophys. J. **664**, 680 (2007) [astro-ph/0701921].

[86] E. Merzbacher, "Quantum mechanics," Wiley, 3rd edition (1997), 672 p

[87] A. J. Cuesta *et al.*, Mon. Not. Roy. Astron. Soc. **457**, no. 2, 1770 (2016) [arXiv:1509.06371 [astro-ph.CO]].

[88] J. Garcia-Bellido, A. D. Linde and D. Wands, Phys. Rev. D **54**, 6040 (1996) [astro-ph/9605094].

[89] S. Clesse and J. Garcia-Bellido, Phys. Rev. D **92**, no. 2, 023524 (2015) [arXiv:1501.07565 [astro-ph.CO]].

[90] B. P. Abbott *et al.* [LIGO Scientific and Virgo Collaborations], Phys. Rev. Lett. **116**, no. 6, 061102 (2016) [arXiv:1602.03837 [gr-qc]].

[91] B. P. Abbott *et al.* [LIGO Scientific and Virgo Collaborations], Phys. Rev. Lett. **116**, no. 24, 241103 (2016) [arXiv:1606.04855 [gr-qc]].

[92] B. P. Abbott *et al.* [LIGO Scientific and Virgo Collaborations], Phys. Rev. Lett. **116**, no. 13, 131102 (2016) [arXiv:1602.03847 [gr-qc]].

[93] C. Caprini *et al.*, JCAP **1604**, no. 04, 001 (2016) [arXiv:1512.06239 [astro-ph.CO]].

[94] N. Bartolo *et al.*, JCAP **1612**, no. 12, 026 (2016) doi:10.1088/1475-7516/2016/12/026 [arXiv:1610.06481 [astro-ph.CO]].

[95] Z. Arzoumanian *et al.* [NANOGrav Collaboration], Astrophys. J. **821**, no. 1, 13 (2016) doi:10.3847/0004-637X/821/1/13 [arXiv:1508.03024 [astro-ph.GA]].

[96] L. Lentati *et al.*, Mon. Not. Roy. Astron. Soc. **453**, no. 3, 2576 (2015) doi:10.1093/mnras/stv1538 [arXiv:1504.03692 [astro-ph.CO]].

[97] R. M. Shannon *et al.*, Science **349**, no. 6255, 1522 (2015) doi:10.1126/science.aab1910 [arXiv:1509.07320 [astro-ph.CO]].

[98] W. Zhao, Y. Zhang, X. P. You and Z. H. Zhu, Phys. Rev. D **87**, no. 12, 124012 (2013) doi:10.1103/PhysRevD.87.124012 [arXiv:1303.6718 [astro-ph.CO]].

[99] X. J. Liu, W. Zhao, Y. Zhang and Z. H. Zhu, Phys. Rev. D **93**, no. 2, 024031 (2016) doi:10.1103/PhysRevD.93.024031 [arXiv:1509.03524 [astro-ph.CO]].

[100] B. P. Abbott *et al.* [LIGO Scientific and Virgo Collaborations], arXiv:1608.01940 [gr-qc].

[101] E. Berti, V. Cardoso and C. M. Will, Phys. Rev. D **73**, 064030 (2006) [gr-qc/0512160].

[102] E. Berti, V. Cardoso and A. O. Starinets, Class. Quant. Grav. **26**, 163001 (2009) [arXiv:0905.2975 [gr-qc]].

[103] A. Klein *et al.*, Phys. Rev. D **93**, no. 2, 024003 (2016) [arXiv:1511.05581 [gr-qc]].

[104] C. J. Moore, S. R. Taylor and J. R. Gair, Class. Quant. Grav. **32**, no. 5, 055004 (2015) doi:10.1088/0264-9381/32/5/055004 [arXiv:1406.5199 [astro-ph.IM]].

[105] M. C. Guzzetti, N. Bartolo, M. Liguori and S. Matarrese, arXiv:1605.01615 [astro-ph.CO].

[106] E. Pajer and M. Peloso, Class. Quant. Grav. **30**, 214002 (2013) [arXiv:1305.3557 [hep-th]].

[107] S. L. Cheng, W. Lee and K. W. Ng, arXiv:1606.00206 [astro-ph.CO].

[108] N. Barnaby, E. Pajer and M. Peloso, Phys. Rev. D **85**, 023525 (2012) [arXiv:1110.3327 [astro-ph.CO]].

[109] V. Domcke, M. Pieroni and P. Bintruy, JCAP **1606**, 031 (2016) doi:10.1088/1475-7516/2016/06/031 [arXiv:1603.01287 [astro-ph.CO]].

[110] P. Adshead and M. Wyman, Phys. Rev. Lett. **108**, 261302 (2012) [arXiv:1202.2366 [hep-th]].

[111] A. Maleknejad and M. M. Sheikh-Jabbari, Phys. Lett. B **723**, 224 (2013) [arXiv:1102.1513 [hep-ph]].

[112] A. Maleknejad, JHEP **1607**, 104 (2016) [arXiv:1604.03327 [hep-ph]].

[113] I. Obata and J. Soda, Phys. Rev. D **94**, no. 4, 044062 (2016) [arXiv:1607.01847 [astro-ph.CO]].

[114] E. Dimastrogiovanni, M. Fasiello and T. Fujita, arXiv:1608.04216 [astro-ph.CO].

[115] P. Adshead, E. Martinec, E. I. Sfakianakis and M. Wyman, arXiv:1609.04025 [hep-th].

[116] E. Bugaev and P. Klimai, Phys. Rev. D **90**, no. 10, 103501 (2014) [arXiv:1312.7435 [astro-ph.CO]].

[117] E. Erfani, JCAP **1604**, no. 04, 020 (2016) [arXiv:1511.08470 [astro-ph.CO]].

[118] E. McDonough, H. B. Moghaddam and R. H. Brandenberger, JCAP **1605**, no. 05, 012 (2016) [arXiv:1601.07749 [hep-th]].

[119] C. J. Moore, R. H. Cole and C. P. L. Berry, Class. Quant. Grav. **32**, no. 1, 015014 (2015) doi:10.1088/0264-9381/32/1/015014 [arXiv:1408.0740 [gr-qc]].

[120] A. A. Starobinsky, Phys. Lett. B **91**, 99 (1980).

[121] S. Bird, I. Cholis, J. B. Muoz, Y. Ali-Hamoud, M. Kamionkowski, E. D. Kovetz, A. Raccanelli and A. G. Riess, Phys. Rev. Lett. **116**, no. 20, 201301 (2016) [arXiv:1603.00464 [astro-ph.CO]].

[122] S. Clesse and J. Garcia-Bellido, arXiv:1603.05234 [astro-ph.CO].

[123] M. Sasaki, T. Suyama, T. Tanaka and S. Yokoyama, Phys. Rev. Lett. **117**, no. 6, 061101 (2016) [arXiv:1603.08338 [astro-ph.CO]].

[124] A. Kashlinsky, Astrophys. J. **823**, no. 2, L25 (2016) [arXiv:1605.04023 [astro-ph.CO]].

[125] M. Kawasaki, A. Kusenko, Y. Tada and T. T. Yanagida, arXiv:1606.07631 [astro-ph.CO].

[126] B. J. Carr, K. Kohri, Y. Sendouda and J. Yokoyama, Phys. Rev. D **81**, 104019 (2010) [arXiv:0912.5297 [astro-ph.CO]].

[127] M. Y. Khlopov, Res. Astron. Astrophys. **10**, 495 (2010) doi:10.1088/1674-4527/10/6/001 [arXiv:0801.0116 [astro-ph]].

[128] A. Barnacka, J. F. Glicenstein and R. Moderski, Phys. Rev. D **86**, 043001 (2012) [arXiv:1204.2056 [astro-ph.CO]].

[129] K. Griest, A. M. Cieplak and M. J. Lehner, Astrophys. J. **786**, no. 2, 158 (2014) [arXiv:1307.5798 [astro-ph.CO]].

[130] F. Capela, M. Pshirkov and P. Tinyakov, Phys. Rev. D **90**, no. 8, 083507 (2014) [arXiv:1403.7098 [astro-ph.CO]].

[131] P. Tisserand *et al.* [EROS-2 Collaboration], Astron. Astrophys. **469**, 387 (2007) [astro-ph/0607207].

[132] C. Alcock *et al.* [MACHO and EROS Collaborations], Astrophys. J. **499**, L9 (1998) [astro-ph/9803082].

[133] D. P. Quinn, M. I. Wilkinson, M. J. Irwin, J. Marshall, A. Koch and V. Belokurov, Mon. Not. Roy. Astron. Soc. **396**, 11 (2009) [arXiv:0903.1644 [astro-ph.GA]].

[134] B. J. Carr and M. Sakellariadou, Astrophys. J. **516**, 195 (1999).

[135] B. Carr, F. Kuhnel and M. Sandstad, arXiv:1607.06077 [astro-ph.CO].

[136] J. Chluba and R. A. Sunyaev, Mon. Not. Roy. Astron. Soc. **419**, 1294 (2012) [arXiv:1109.6552 [astro-ph.CO]].

[137] D. J. Fixsen, E. S. Cheng, J. M. Gales, J. C. Mather, R. A. Shafer and E. L. Wright, Astrophys. J. **473**, 576 (1996) [astro-ph/9605054].

[138] J. Chluba, A. L. Erickcek and I. Ben-Dayan, Astrophys. J. **758**, 76 (2012) [arXiv:1203.2681 [astro-ph.CO]].

[139] M. Ricotti, J. P. Ostriker and K. J. Mack, Astrophys. J. **680**, 829 (2008) [arXiv:0709.0524 [astro-ph]].

[140] Y. Ali-Hamoud and M. Kamionkowski, Phys. Rev. D **95**, no. 4, 043534 (2017) doi:10.1103/PhysRevD.95.043534 [arXiv:1612.05644 [astro-ph.CO]].

[141] T. D. Brandt, Astrophys. J. **824**, no. 2, L31 (2016) [arXiv:1605.03665 [astro-ph.GA]].

[142] M. M. Anber and L. Sorbo, Phys. Rev. D **81**, 043534 (2010) [arXiv:0908.4089 [hep-th]].

[143] A. Notari and K. Tywoniuk, arXiv:1608.06223 [hep-th].

[144] E. Silverstein and A. Westphal, Phys. Rev. D **78**, 106003 (2008) [arXiv:0803.3085 [hep-th]].

[145] L. McAllister, E. Silverstein and A. Westphal, Phys. Rev. D **82** (2010) 046003 [arXiv:0808.0706 [hep-th]].

[146] R. Z. Ferreira, J. Ganc, J. Norea and M. S. Sloth, arXiv:1512.06116 [astro-ph.CO].

[147] A. A. Starobinsky, JETP Lett. **55**, 489 (1992) [Pisma Zh. Eksp. Teor. Fiz. **55**, 477 (1992)].

[148] P. A. R. Ade *et al.* [BICEP2 and Keck Array Collaborations], Phys. Rev. Lett. **116**, 031302 (2016) [arXiv:1510.09217 [astro-ph.CO]].

[149] Y. Akrami *et al.* [Planck Collaboration], arXiv:1807.06211 [astro-ph.CO].

[150] J. Garcia-Bellido and D. Roest, Phys. Rev. D **89**, no. 10, 103527 (2014) [arXiv:1402.2059 [astro-ph.CO]].

[151] H. Mouri and Y. Taniguchi, Astrophys. J. **566**, L17 (2002) [astro-ph/0201102].

[152] K. Sugimura, T. Hosokawa, H. Yajima and K. Omukai, arXiv:1610.03482 [astro-ph.GA].

[153] A. Drlica-Wagner *et al.* [DES Collaboration], Astrophys. J. **813**, no. 2, 109 (2015) [arXiv:1508.03622 [astro-ph.GA]].

[154] P. Adshead, J. T. Giblin, T. R. Scully and E. I. Sfakianakis, JCAP **1512**, no. 12, 034 (2015) [arXiv:1502.06506 [astro-ph.CO]].

[155] S. L. Cheng, W. Lee and K. W. Ng, Phys. Rev. D **93**, no. 6, 063510 (2016) [arXiv:1508.00251 [astro-ph.CO]].

[156] P. Adshead, J. T. Giblin, T. R. Scully and E. I. Sfakianakis, arXiv:1606.08474 [astro-ph.CO].

[157] N. Seto and A. Taruya, Phys. Rev. Lett. **99**, 121101 (2007) [arXiv:0707.0535 [astro-ph]].

[158] S. G. Crowder, R. Namba, V. Mandic, S. Mukohyama and M. Peloso, Phys. Lett. B **726**, 66 (2013) [arXiv:1212.4165 [astro-ph.CO]].

[159] T. L. Smith and R. Caldwell, arXiv:1609.05901 [gr-qc].

[160] E. Thrane, Phys. Rev. D **87**, no. 4, 043009 (2013) [arXiv:1301.0263 [astro-ph.IM]].

[161] B. J. Carr, Astrophys. J. **201**, 1 (1975).

[162] D. H. Lyth, JCAP **1205**, 022 (2012) [arXiv:1201.4312 [astro-ph.CO]].

[163] C. T. Byrnes, E. J. Copeland and A. M. Green, Phys. Rev. D **86**, 043512 (2012) [arXiv:1206.4188 [astro-ph.CO]].

[164] K. Bamba, Phys. Rev. D **91**, 043509 (2015) doi:10.1103/PhysRevD.91.043509 [arXiv:1411.4335 [astro-ph.CO]].

[165] J. L. Cook and L. Sorbo, JCAP **1311**, 047 (2013) [arXiv:1307.7077 [astro-ph.CO]]; M. Shiraishi, A. Ricciardone and S. Saga, JCAP **1311**, 051 (2013) [arXiv:1308.6769 [astro-ph.CO]]; M. Shiraishi, M. Liguori and J. R. Fergusson, JCAP **1405**, 008 (2014) doi:10.1088/1475-7516/2014/05/008 [arXiv:1403.4222 [astro-ph.CO]]; M. Shiraishi, M. Liguori and J. R. Fergusson, JCAP **1501**, no. 01, 007 (2015) doi:10.1088/1475-7516/2015/01/007 [arXiv:1409.0265 [astro-ph.CO]]; N. Bartolo *et al.*, arXiv:1806.02819 [astro-ph.CO].

[166] S. Eccles, W. Fischler, D. Lorshbough and B. A. Stephens, arXiv:1505.04686 [astro-ph.CO]; K. Choi, K. Y. Choi, H. Kim and C. S. Shin, arXiv:1507.04977 [astro-ph.CO]; I. Ben-Dayan, arXiv:1604.07899 [astro-ph.CO];

[167] J. E. Kim, H. P. Nilles and M. Peloso, JCAP **0501**, 005 (2005) doi:10.1088/1475-7516/2005/01/005 [hep-ph/0409138].

[168] M. G. Aartsen *et al.* [IceCube Collaboration], Science **361**, no. 6398, 147 (2018). doi:10.1126/science.aat2890

[169] N. Bartolo, M. Peloso, A. Ricciardone and C. Unal, JCAP **1411**, no. 11, 009 (2014) doi:10.1088/1475-7516/2014/11/009 [arXiv:1407.8053 [astro-ph.CO]].

[170] M. Peloso and C. Unal, JCAP **1506**, no. 06, 040 (2015) doi:10.1088/1475-7516/2015/06/040 [arXiv:1504.02784 [astro-ph.CO]].

[171] R. Namba, M. Peloso, M. Shiraishi, L. Sorbo and C. Unal, JCAP **1601**, no. 01, 041 (2016) doi:10.1088/1475-7516/2016/01/041 [arXiv:1509.07521 [astro-ph.CO]].

[172] M. Peloso, L. Sorbo and C. Unal, JCAP **1609**, no. 09, 001 (2016) doi:10.1088/1475-7516/2016/09/001 [arXiv:1606.00459 [astro-ph.CO]].

[173] J. Garcia-Bellido, M. Peloso and C. Unal, JCAP **1612**, no. 12, 031 (2016) doi:10.1088/1475-7516/2016/12/031 [arXiv:1610.03763 [astro-ph.CO]].

[174] J. Garcia-Bellido, M. Peloso and C. Unal, JCAP **1709**, no. 09, 013 (2017) doi:10.1088/1475-7516/2017/09/013 [arXiv:1707.02441 [astro-ph.CO]].

[175] A. Papageorgiou, M. Peloso and C. Unal, arXiv:1806.08313 [astro-ph.CO].

Appendix A

Axion Inflation and its Coupling to Gauge Fields

In order for inflation to solve the problems of the Big Bang cosmology such as the flatness, horizon and unwanted relics problems, the inflaton should have a flat enough potential to sustain a sufficiently long accelerated expansion. However, unless protected by a symmetry, the inflaton potential gets corrections of the type $\Delta V = \sum_n c_n \phi^{4+n}/\Lambda^n$, where ϕ is the inflaton, c_n a dimensionless number and Λ is the scale of the new physics. For quantum gravity, Λ is expected to be $\sim M_p$. Although this UV-sensitivity exists for all types of inflationary models, these corrections play more dramatic role for large field models, namely the models in which inflaton field makes an excursion in field space larger than Planck scale, M_p. These corrections can spoil easily the flatness of the potential by modifying slow-roll parameter $\eta \sim \mathcal{O}(1)$, defined in eq. (2.25), which results in shortening of inflationary expansion to $\mathcal{O}$(a few) e-folds.

A well known and simple symmetry that can forbid such operators is the shift symmetry, namely the invariance of the action under the transformation $\phi \to \phi +$ constant. A field enjoying this symmetry, at least at an approximate level, is denoted as an "axion". The first work that recognized the merits of employing a shift symmetry in inflation is [3], where the resulting class of models was named *Natural (or Axion) Inflation*. However, it is clear that if this symmetry is exact, the potential becomes trivial and inflation never ends. Therefore this approximate symmetry has to be broken

for a graceful exit from the inflationary era. A relevant scale in axion inflation is the axion scale (axion decay constant) f. This scale determines the least irrelevant shift-symmetric coupling, often the dimension five coupling $\frac{\phi}{f}F\tilde{F}$ to gauge fields [1]. If the gauge field is non-Abelian, gauge instantons break the shift symmetry nonperturbatively to the discrete symmetry as $\phi \to \phi + 2\pi f$. Therefore, f controls the periodicity of the axion potential, in absence of any explicit breaking of the shift-symmetry. Refs. [3, 4] studied the simplest potential with such property

$$V = \frac{\Lambda^4}{2}\left[1 + \cos\left(\frac{\phi}{f}\right)\right] . \tag{A.1}$$

This attractive idea has been studied extensively in various contexts. Since the theory of axion is obtained by integrating out the heavier degrees of freedom than the axion scale [6], it is required that m_ϕ and H (mass and Hubble scale respectively) are smaller than the axion scale. The arguments from the quantum gravity and string theory prompt to require the axion decay constant is sub-Planckian, ie. $f < M_P$ [7]. There are two problems for the simplest potential of axion inflation given in eq (A.1):

- Natural inflation can be consistent with the observations only if axion scale is super-Planckian ($f \gtrsim 4M_p$) [67].
- The predictions are out of $1-\sigma$ contours in the $n_s - r$ plane with respect to the most recent CMB data [67].

These problems have been tried to get evaded by various models and mechanisms (see [106] for a partial list of relevant literature on this topic) that use sub-Planckian axions to obtain an effective super-Planckian scale. This is the reason why the particle production mechanisms during inflation, specifically chiral coupling between axion and gauge field, which is proportional to $\frac{1}{f}$, might lead to rich and detectable phenomenology.

In order to see that clearly, assume we are in a nearly de Sitter stage and we have an axion field X, coupled to gauge field via $\frac{\alpha}{4f}XF\tilde{F}$. Resultantly, the dimensionless parameter that controls the particle production amount becomes

$$\xi = \frac{\alpha\,\dot{X}}{2Hf} = \sqrt{\frac{\epsilon_X}{2}}\,\frac{\alpha\,M_p}{f} \tag{A.2}$$

[1] or to fermions via $\frac{1}{f}\bar{\psi}\,\gamma^\mu\,\gamma_5\,\psi\,\partial_\mu\phi$

Here we define the slow-roll parameter for the field X as usual $\epsilon_X \equiv \frac{\dot{X}^2}{2H^2M_p^2}$ and as long as the field X is slowly-rolling through its potential we expect ϵ_X to be very small. In effective field theory, the coupling constant α is expected to be at most $\mathcal{O}(1)$. Hence, for a super-Planckian axion decay constant, $f \gtrsim M_p$, we have $\xi \ll 1$ which results in that this coupling has no visible effect on cosmological observables. However, according to the discussion above, we need that the axions have to have sub-Planckian decay constants and the super-Planckian scale for inflation needs to be emergent from sub-Planckian physics. Therefore, in axion inflation, it is very natural to have $\alpha\, M_p/f \gtrsim \mathcal{O}(10^2)$.

For a concrete example, we will briefly study a model, dubbed as Aligned Natural Inflation [167]. The model was suggested to solve the super-Planckian axion scale problem by aligning two sub-Planckian axions such that there emerges a flat enough direction that allows super-Planckian excursions and resultantly can sustain long enough inflation.

The general 2−field (θ, ρ) model of Natural Aligned Inflation is characterized by four sub-Planckian axion constants ($f_i, g_i \ll M_p$) and two potential scales [167]

$$V = \Lambda_1^4 \left[1 - \cos\left(\frac{\theta}{f_1} + \frac{\rho}{g_1}\right)\right] + \Lambda_2^4 \left[1 - \cos\left(\frac{\theta}{f_2} + \frac{\rho}{g_2}\right)\right] \ . \tag{A.3}$$

If the relation $f_1/g_1 = f_2/g_2$ holds, then this potential has one exactly flat direction. We denote this direction by ϕ. If this relation is only approximately valid, that direction becomes flatter than the naive expectation, namely $m_\phi \ll \frac{\Lambda_i^2}{f_i}$, $\frac{\Lambda_i^2}{g_i}$. This can be seen as having an axion ϕ with an effective scale $f_\phi \gg f_i$, g_i. This is the alignment mechanism.

The two potential scales can be described as

$$\Lambda_1^4 \equiv \frac{1}{1+r_\Lambda}\,\Lambda^4 \ \ , \ \ \Lambda_2^4 \equiv \frac{r_\Lambda}{1+r_\Lambda}\,\Lambda^4 \ \ , \tag{A.4}$$

so that Λ is an overall potential scale, and r_Λ is the ratio between the two scales in (A.3). The ratio between the axion scales can be described as

$$\frac{g_1}{f_1} \equiv \frac{r_g}{1+\kappa} \ \ , \ \ \frac{g_2}{f_2} \equiv \frac{r_g}{1-\kappa} \ , \tag{A.5}$$

Here above, κ is the degree of the alignment. As $\kappa \to 0$, the alignment gets stronger and the inflationary direction becomes more flat. Finally, we redefine axion scales as

$$f_1 \equiv r_f\, f \ \ , \ \ f_2 \equiv \frac{f}{r_f} \, . \tag{A.6}$$

In this way, we reformulate the model (A.3) in terms of two parameters of mass dimension one (f and Λ) and four dimensionless parameters:

$$\begin{aligned}\frac{V}{\Lambda^4} &= 1-\frac{1}{1+r_\Lambda}\cos\left[\frac{1}{r_f}\left(\frac{\theta}{f}+\frac{1+\kappa}{r_g}\frac{\rho}{f}\right)\right] \\ &\quad -\frac{r_\Lambda}{1+r_\Lambda}\cos\left[r_f\left(\frac{\theta}{f}+\frac{1-\kappa}{r_g}\frac{\rho}{f}\right)\right]. \end{aligned} \tag{A.7}$$

In this parametrization, $\kappa \to 0$ gives exact alignment and we are particularly interested in $|\kappa| \ll 1$. As a result of this alignment one light direction, denoted as ϕ (inflationary trajectory) and one heavy direction, denoted as ψ, emerge as eigenstates of the potential [2].

Under the rotation (given in the footnote 2), the potential becomes

$$\frac{V}{\Lambda^4} = 1-\frac{1}{1+r_\Lambda}\cos\left(-\frac{r_f^3\, r_\Lambda}{1+r_f^4\, r_\Lambda}\frac{\phi}{f_\phi}+\frac{1}{r_f}\frac{\psi}{f_\psi}\right)-\frac{r_\Lambda}{1+r_\Lambda}\cos\left(\frac{r_f}{1+r_f^4\, r_\Lambda}\frac{\phi}{f_\phi}+r_f\,\frac{\psi}{f_\psi}\right). \tag{A.9}$$

where

$$f_\phi \equiv f\,\frac{\sqrt{1+r_g^2}}{2\kappa} \tag{A.10}$$

is the emergent inflationary direction that is much flatter than the heavy direction,

$$f_\psi \equiv f\,\frac{r_g}{\sqrt{1+r_g^2}} \tag{A.11}$$

The coupling of these sub-Planckian axion fields with gauge field is expressed as

$$\mathcal{L}_{\rm int} = \left(c_\theta\,\frac{\theta}{f}+c_\rho\,\frac{\rho}{f}\right)F\,\tilde{F} \tag{A.12}$$

with f, axion scale defined in eq. A.6 and c_θ, c_ρ are model-dependent dimensionless coefficients expected to be of order one.

---

[2] The rotation matrix can be expressed as follows $\begin{pmatrix}\theta\\ \rho\end{pmatrix} = R\begin{pmatrix}\phi\\ \psi\end{pmatrix}$

$$R_{11}=R_{22}=\frac{1}{\sqrt{1+r_g^2}}+\kappa\,\frac{r_g^2}{\left(1+r_g^2\right)^{3/2}}\frac{1-r_f^4\, r_\Lambda}{1+r_f^4\, r_\Lambda}\,, \qquad R_{12}=-R_{21}=\frac{r_g}{\sqrt{1+r_g^2}}-\kappa\,\frac{r_g}{\left(1+r_g^2\right)^{3/2}}\frac{1-r_f^4\, r_\Lambda}{1+r_f^4\, r_\Lambda}\,. \tag{A.8}$$

When we rotate the fields to obtain light and heavy directions, we end up with

$$\mathcal{L}_{\rm int} = -\frac{1}{4}\left(\frac{C_\phi\,\phi}{\kappa f_\phi} + \frac{C_\psi\,\psi}{f_\psi}\right) F\tilde{F} \tag{A.13}$$

where the scales f_ϕ and f_ψ have been defined above, again, the parameters C_ϕ and C_ψ are model-dependent dimensionless coefficients which may naturally be expected to be of order one. [3]

In result we end up with the following particle production parameter

$$\xi = |C_\phi|\,\frac{\dot{\phi}}{2\,\kappa\,f_\phi\,H} \;=\; |C_\phi|\,\frac{M_p}{\kappa\,f_\phi}\,\sqrt{\frac{\epsilon_\phi}{2}} \tag{A.14}$$

which allows $\xi \gtrsim \mathcal{O}(1)$ and interesting signatures at different scales depending on model parameters.

[3] $C_\phi = \frac{c_\theta - c_\rho\, r_g}{2}$ and $C_\psi = \frac{(c_\rho + r_g\, c_\theta) r_g}{1+r_g^2}$, up to $\mathrm{O}\,(\kappa)$ corrections.

Appendix B

Details of the Abelian Gauge Field Amplification for Non-Adiabatic Evolution

B.1 Details of the derivation of $A_+(\tau, k)$

In this appendix we derive the expression (3.20) for the mode function of the photon. We start from the equation of motion (3.17) for the positive helicity photon, that, after defining $x = -k\tau$, $x_* = -k\tau_*$, reads

$$\frac{d^2 A_+}{dx^2} + \left(1 - \frac{2}{x}\,\frac{2\,\xi_*}{(x/x_*)^\delta + (x/x_*)^{-\delta}}\right) A_+ = 0\,. \tag{B.1}$$

We solve it using the WKB approximation. To do so, we write it in the general form

$$A_+''(x) + Q(x)\,A_+(x) = 0\,, \tag{B.2}$$

where $Q(x)$ vanishes for $x = \bar{x}$ and is positive for $x > \bar{x}$, so that we can define

$$Q(x) \equiv \begin{cases} p(x)^2 & , x > \bar{x} \\ -\kappa(x)^2 & , x < \bar{x}\,, \end{cases} \tag{B.3}$$

Then, for $x > \bar{x}$, in the adiabatic regime $|p'(x)| \ll p(x)^2$, the general solution reads

$$A_+(x > \bar{x}) \simeq \frac{\alpha}{\sqrt{p(x)}}\,\cos\left(\int_{\bar{x}}^{x} p(x)dx - \frac{\pi}{4}\right) - \frac{\beta}{\sqrt{p(x)}}\,\sin\left(\int_{\bar{x}}^{x} p(x)dx - \frac{\pi}{4}\right)\,, \tag{B.4}$$

with α and β constants, and where the symbol $\simeq$ denotes approximate equality in the WKB approximation. Similarly, for $x < \bar{x}$, the solution in the WKB regime $|\kappa'(x)| \ll \kappa(x)^2$ will be a linear combination of $\exp\left(-\int_x^{\bar{x}} \kappa(x)dx\right)/\sqrt{\kappa(x)}$ and $\exp\left(\int_x^{\bar{x}} \kappa(x)dx\right)/\sqrt{\kappa(x)}$. To determine the coefficients of such a combination in terms of α and β we expand eq. (B.2) near $x = \bar{x}$ as

$$A_+''(x) + Q'(\bar{x})\,(x-\bar{x})\,A_+(x) \simeq 0\,, \tag{B.5}$$

that can be solved in terms of Airy functions, and that we join to the adiabatic solutions in the regimes $x - \bar{x} \to \pm\infty$, as discussed for instance in chapter 7 of [86]. The final result is

$$A_+(x<\bar{x}) \cong \frac{\alpha/2}{\sqrt{\kappa(x)}}\,\exp\left(-\int_x^{\bar{x}} \kappa(x)\,dx\right) + \frac{\beta}{\sqrt{\kappa(x)}}\,\exp\left(\int_x^{\bar{x}} \kappa(x)\,dx\right)\,. \tag{B.6}$$

The requirement that the photons are in their adiabatic vacuum in the ultraviolet translates into the boundary condition $\alpha = \frac{1}{\sqrt{2\,k}}$, $\beta = -\frac{i}{\sqrt{2\,k}}$. In the regime $x \ll \bar{x}$ we keep only the term that corresponds to the growing mode, so that

$$A_+(x<\bar{x}) \simeq -\frac{i}{\sqrt{2\,k\,\kappa(x)}}\,\exp\left\{\int_x^{\bar{x}} \kappa(x)dx\right\}\,. \tag{B.7}$$

As a check of the validity of our procedure we can consider the limit $\delta \to 0$, so that $\frac{2\,\xi_*}{x^\delta + x^{-\delta}} \to \xi$, which brings us back to the case of a constant velocity for the rolling axion first studied in [38]. Indeed, in this regime

$$\int_x^{\bar{x}} \kappa(x)\,dx\Big|_{\delta\to 0} = \int_x^{2\,\xi} \sqrt{\frac{2\,\xi}{x} - 1}\,dx = 2\,\xi\,\arccos\left(\sqrt{\frac{x}{2\xi}}\right) - \sqrt{x\,(2\,\xi - x)} \simeq \pi\xi - 2\sqrt{2\xi\,x}\,, \tag{B.8}$$

(where in the last step we have expanded to first order in $\sqrt{x}$), that, once inserted into eq. (B.7), gives a result that coincides with the approximate expression given in [38].

In the general case $\delta \neq 0$ it is impossible to compute the integral of $\kappa(x)$ in closed form. Nevertheless, we can write

$$\int_x^{\bar{x}} \kappa(x)\,dx = \int_0^{\bar{x}} \kappa(x)\,dx - \int_0^{x} \kappa(x)\,dx\,, \tag{B.9}$$

so that only the second term depends on x. Since we care only about the regime of moderately small x, we consider only the leading part of the integrand as $x \to 0$:

$$\int_0^x \kappa(x)\,dx \simeq \int_0^x \sqrt{\frac{4\,\xi_*}{x\,(x/x_*)^{-\delta}}}\,dx = \frac{4\,\sqrt{\xi_*}}{1+\delta}\,x^{\frac{1+\delta}{2}}\,x_*^{-\frac{\delta}{2}}\,. \tag{B.10}$$

This equation, once inserted into eq. (B.7), gives the full dependence of the function $A_+(\tau,\, k)$ on the conformal time τ as it appears in eq. (3.19) in the main text. The overall normalization of $A_+(\tau,\, k)$, on the other hand, has to be computed numerically, and we determine it by matching the WKB approximate solution with the numerical solution of eq. (3.17), yielding the constant $N(\xi_*, x_*, \delta)$ defined in eq. (3.19). We have checked that, in the part of parameter space we are interested in, the expression found this way approximates the exact solution at the 30% level or better.

Performing a WKB approximation of the evolution equation, we obtained the following accurate expression for the real part of the gauge field amplitude:

$$\begin{aligned} A_R\,(\tau,\, k) &\simeq N\,[\xi_*,\, x_*,\, \delta]\,\left(\frac{-\tau}{8\,k\,\xi\,(\tau)}\right)^{1/4}\,\exp\left[-\frac{4\xi_*^{1/2}}{1+\delta}\,\left(\frac{-\tau}{-\tau_*}\right)^{\delta/2}\,(-k\tau)^{1/2}\right]\,, \\ \frac{dA_R\,(\tau,\, k)}{d\tau} &\simeq \sqrt{\frac{2\,k\,\xi\,(\tau)}{-\tau}}\,A_R\,(\tau,\, k)\,, \qquad\qquad \tau > \tau_*\,, \end{aligned} \tag{B.11}$$

The expression (B.11) is valid only for $\tau > \tau_*$. We verified numerically that the amplitude of the gauge field is much smaller at earlier times, therefore we can disregard these earlier times in our computations.

We provide the imaginary part of A_+ using the Wronskian condition $A_+\,A_+^{'*} - \text{c.c.} = i$

$$\begin{aligned} A_I\,(\tau,\, k) &\simeq \frac{1}{N\,[\xi_*,\, x_*,\, \delta]}\,\left(\frac{-\tau}{2^7\,\xi\,k}\right)^{1/4}\,\exp\left[\frac{4\xi_*^{1/2}}{1+\delta}\,\left(\frac{-\tau}{-\tau_*}\right)^{\delta/2}\,(-k\tau)^{1/2}\right]\,, \\ \frac{dA_I\,(\tau,\, k)}{d\tau} &\simeq -\sqrt{\frac{2\,k\,\xi\,(\tau)}{-\tau}}\,A_I\,(\tau,\, k)\,. \end{aligned} \tag{B.12}$$

We note that $A_+ = A_R + i\,A_I$ and its derivative also satisfy the relation (3.12).

We find that the normalization factor $N\,[\xi_*,\, x_*,\, \delta]$ is well approximated by the shape

$$N\,[\xi_*,\, q,\, \delta] \approx N^c\,[\xi_*,\, \delta]\,\exp\left(-\frac{1}{2\,\sigma^2\,[\xi_*,\, \delta]}\,\ln^2\left(\frac{q}{q^c\,[\xi_*,\, \delta]}\right)\right)\,. \tag{B.13}$$

The three parameters N^c, q^c, and σ depend on ξ_* and δ. We evaluate this dependence for the two specific cases $\delta = 0.2,\, 0.5$, and we then fit the ξ_* dependence numerically in the $3 \leq \xi_* \leq 7$ interval. We obtain

$$\begin{aligned} N^c &= \exp\left[0.437 + 2.97\,\xi_* + 0.00105\,\xi_*^2\right] \quad,\quad \delta = 0.2 \quad,\quad 3 \leq \xi_* \leq 7\,, \\ q^c &= -0.150 + 0.594\,\xi_* - 0.00105\,\xi_*^2\,, \\ \sigma &= 2.78 - 0.387\,\xi_* + 0.0229\,\xi_*^2\,, \end{aligned} \tag{B.14}$$

and

$$\begin{aligned} N^c &= \exp\left[0.117 + 2.54\,\xi_* + 0.000525\,\xi_*^2\right] \quad , \quad \delta = 0.5 \quad , \quad 3 \leq \xi_* \leq 7\,, \\ q^c &= -0.0500 + 0.683\,\xi_* - 0.000716\,\xi_*^2\,, \\ \sigma &= 1.51 - 0.220\,\xi_* + 0.0137\,\xi_*^2\,. \end{aligned} \tag{B.15}$$

B.2 Energy Density in the Abelian Gauge Field

For brevity, we use electromagnetic notation, although we are not assuming that the vector field is the Standard Model electromagnetic field. In this notation, the energy density of the gauge field acquires the form

$$\rho_A = \left\langle \frac{E^2 + B^2}{2} \right\rangle\,, \tag{B.16}$$

where E and B fields are

$$\begin{aligned} \vec{E} &= -\frac{1}{a^2}\int \frac{d^3k}{(2\pi)^{3/2}}\,\mathrm{e}^{i\vec{k}\cdot\vec{x}}\,\vec{\epsilon}_+\left(\vec{k}\right)\,\hat{A}'_+\left(\vec{k}\right)\,, \\ \vec{B} &= \frac{1}{a^2}\int \frac{d^3k}{(2\pi)^{3/2}}\,\mathrm{e}^{i\vec{k}\cdot\vec{x}}\,\vec{\epsilon}_+\left(\vec{k}\right)\,k\,\hat{A}_+\left(\vec{k}\right)\,. \end{aligned} \tag{B.17}$$

From these expressions, we see that the energy density per mode reduces to the following simple form:

$$\frac{d\rho_k}{dk} = \frac{1}{4\pi^2 a^4}\left\{k^2\,|A'_+(k)\,|^2 + k^4\,|A_+(k)\,|^2\right\} = \frac{k^3}{8\pi^2 a^4}\left\{\left|\frac{d\tilde{A}}{dx}\right|^2 + |\tilde{A}|^2\right\}\,, \tag{B.18}$$

where we have defined

$$A_+(\tau,\,k) \equiv \frac{1}{\sqrt{2k}}\,\tilde{A}\,(x \equiv -\,k\,\tau)\,. \tag{B.19}$$

A dimensionless expression is obtained by dividing the energy density by the 4^{th} power of the Hubble parameter, leading to

$$\frac{1}{H_k^4}\frac{d\,(\rho_k)}{d\ln k} = \frac{x^4}{8\pi^2}\left\{\left|\frac{d\tilde{A}}{dx}\right|^2 + |\tilde{A}|^2\right\}\,, \tag{B.20}$$

where H_k is the value of the Hubble rate when the mode k left the horizon. This is the expression plotted in Figure 3.1, for the three approximations for the gauge field mode function in eqns (3.8), (3.9) and (3.10), and in Figure 3.2 for bump model.

We also need to evaluate $\langle E \cdot B \rangle$, as it affects the evolution equation for the field X

$$\ddot{X} + 3H\dot{X} + \partial_\sigma V = \frac{\alpha}{f} \langle \vec{E} \cdot \vec{B} \rangle \, . \tag{B.21}$$

(we want to ensure that this terms can be neglected). Using (B.17), we find

$$\frac{1}{H_k^4} \frac{d \langle \vec{E} \cdot \vec{B} \rangle}{d \ln k} = \frac{x^4}{8\pi^2} \frac{d}{dx} |\tilde{A}|^2 \, . \tag{B.22}$$

For spectator axion case, by inserting the expression for the vector field amplitude into (B.20), using $\rho_\phi \simeq 3\, H^2\, M_p^2$, and eliminating H through $\mathcal{P}_{\zeta,\mathrm{cmb}} \simeq \frac{H^2}{8\pi^2 \epsilon_\phi M_p^2} \simeq 2.2 \cdot 10^{-9}$, we obtain the following expression for the energy in the vector field

$$\frac{\rho_A}{\epsilon_\phi\, \rho_\phi} = \frac{N_c^2 P_\zeta^{(0)}\, y^{7/2}}{6\sqrt{\xi_*}\sqrt{y^\delta + y^{-\delta}}} \int_0^\infty \frac{dx_*}{x_*}\, x_*^{7/2}\, \mathrm{e}^{-\frac{8\sqrt{\xi_*}\sqrt{x_* y}\, \frac{1}{2}+\frac{\delta}{2}}{1+\delta} - \frac{\ln^2\left(\frac{x_*}{q_c}\right)}{\sigma^2}} \left[4\xi_* + x_* y \left(y^\delta + y^{-\delta} \right) \right] \, , \tag{B.23}$$

where we have defined $y \equiv \tau/\tau_*$ (therefore, our expression are valid for $0 \leq y \leq 1$). We show the result for different values of ξ_* and for different times in Figure B.1.

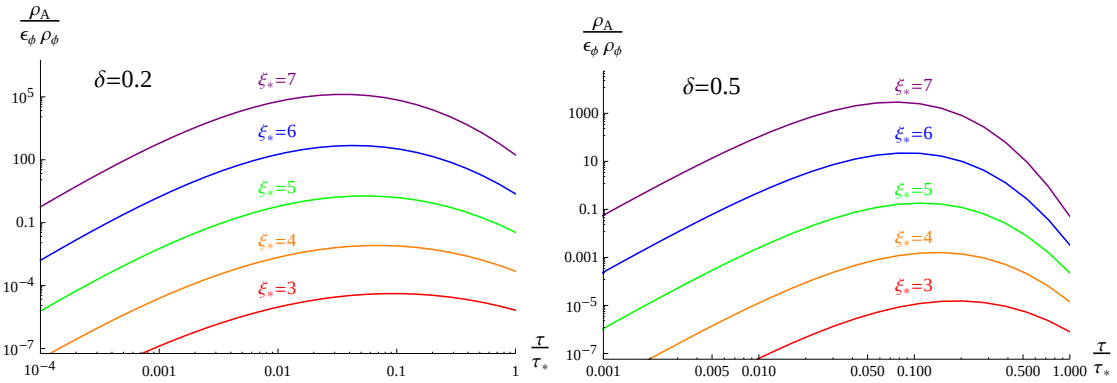

Figure B.1: Total Energy density in the gauge field, rescaled by $\epsilon_\phi\, \rho_\phi$, as a function of time, for fixed values of ξ_*

We observe that the energy density in the vector field reaches a maximum value at $y = \mathrm{O}\,(0.1)$, and it is then diluted away by the expansion of the universe. We fitted numerically the dependence on ξ_* of the maximum value assumed by ρ_A, obtaining the very accurate expression

$$\frac{\rho_{A,\mathrm{max}}}{\epsilon_\phi\, \rho_\phi} \sim \begin{cases} 2.75 \cdot 10^{-12}\, \mathrm{e}^{1.74\, \pi\, \xi_*} & , \quad \delta = 0.2 \, , \\ 7.48 \cdot 10^{-12}\, \mathrm{e}^{1.52\, \pi\, \xi_*} & , \quad \delta = 0.5 \, . \end{cases} \tag{B.24}$$

Appendix C

CMB Phenomenology For Rolling Axion Bump

C.1 Sourced scalar modes at constant ξ

In this Appendix we show how, for constant values of ξ, the isocurvature perturbation associated to σ is partially converted into curvature perturbation during superhorizon evolution [57, 58]. As a consequence, large fluctuations in the gauge mode can introduce a significant sourced component in the curvature perturbations. We start from the equations (4.17) already given in the main text, and we redefine

$$M_{ij}^2 \equiv -\tau^2 \tilde{M}_{ij}^2 \simeq \begin{pmatrix} 2 + 9\,\epsilon_\phi + 3\,\epsilon_\sigma - 3\,\eta_\phi & 6\sqrt{\epsilon_\phi \epsilon_\sigma} \\ 6\sqrt{\epsilon_\phi \epsilon_\sigma} & 2 + 9\,\epsilon_\sigma + 3\,\epsilon_\phi - 3\,\eta_\sigma \end{pmatrix} , \tag{C.1}$$

If M_{ij}^2 is approximately constant we can diagonalize the mass matrix as

$$M = C^T\,\Lambda\,C\,, \qquad C = \begin{pmatrix} \cos\theta & \sin\theta \\ -\sin\theta & \cos\theta \end{pmatrix} , \qquad \Lambda = \begin{pmatrix} \lambda_\phi & 0 \\ 0 & \lambda_\sigma \end{pmatrix} , \tag{C.2}$$

so that we can solve the system (4.17), obtaining

$$Q_\phi = \sin\theta\,\cos\theta \int d\tau' \left[G_k^{\lambda_\phi}(\tau,\,\tau') - G_k^{\lambda_\sigma}(\tau,\,\tau') \right] \hat{\mathcal{S}}_\sigma \left(\tau', \vec{k} \right) , \tag{C.3}$$

$G_k^{\lambda_{\phi,\sigma}}(\tau,\,\tau')$ is the retarded Green function associated to the operator $\frac{\partial^2}{\partial\tau^2}+\left(k^2-\frac{\lambda_{\phi,\sigma}}{\tau^2}\right)$:

$$G_k^{\lambda}(\tau,\,\tau')=\Theta(\tau-\tau')\,\frac{\pi}{2}\sqrt{\tau\,\tau'}\left(J_\mu(-k\tau)\,Y_\mu(-k\tau')-J_\mu(-k\tau')\,Y_\mu(-k\tau)\right)\,,\qquad \mu=\sqrt{\lambda+\frac{1}{4}}\,. \tag{C.4}$$

Inspection of the equations given in subsection 3.1.2 (or Appendix B.1) shows that, for $\xi\gtrsim O(1)$, the source term $\mathcal{S}_\sigma\left(\tau',\vec{k}\right)$ is exponentially suppressed for $|k\,\tau'|\gtrsim 1$. As a consequence, we can set $|k\,\tau'|\ll 1$ in the propagator. Also, since we are looking at modes far outside of the horizon, we have $|k\,\tau|\ll 1$, and we can use the approximate expression for the propagator

$$G_k^{\lambda}(\tau,\,\tau')\simeq\frac{\sqrt{\tau\,\tau'}}{2\,\mu}\left(\frac{\tau'}{\tau}\right)^{\mu}\,. \tag{C.5}$$

To first order in the slow roll parameters, denoting $\lambda_\sigma=2+\delta\lambda_\sigma$ and $\lambda_\phi=2+\delta\lambda_\phi$ we can expand

$$G_k^{\lambda}(\tau,\,\tau')\simeq\frac{\sqrt{\tau\,\tau'}}{3}\left(\frac{\tau'}{\tau}\right)^{3/2}\left(1-\frac{\delta\lambda}{3}+\frac{\delta\lambda}{3}\,\log\frac{\tau'}{\tau}\right) \tag{C.6}$$

so that, neglecting term $-\delta\lambda/3$ which is subdominant with respect to $\frac{\delta\lambda}{3}\,\log\frac{\tau'}{\tau}$,

$$Q_\phi\simeq\sin\theta\,\cos\theta\,\frac{\delta\lambda_\phi-\delta\lambda_\sigma}{3}\int d\tau'\,\left(\log\frac{\tau'}{\tau}\right)\,G_k^2(\tau,\,\tau')\,\mathcal{S}_\sigma\left(\tau',\vec{k}\right)\,. \tag{C.7}$$

Since most of the integral in $d\tau'$ gets contribution from $\tau'\simeq -1/k$, we can approximate $\log\frac{\tau'}{\tau}\simeq-\log(-k\,\tau)\simeq N_k$, the number of efoldings of inflation from the time the mode k has left the horizon.

As a consequence, the perturbation in $\delta\phi$ is the perturbation that would be obtained if axion was the inflaton times the factor $\sin\theta\,\cos\theta\,\frac{\delta\lambda_\phi-\delta\lambda_\sigma}{3}\,N_k\,=\,2\sqrt{\epsilon_\sigma\,\epsilon_\phi}\,N_k$, that accounts for the fact that in this model $\sigma\neq\phi$. The multiplicative factor arises for the conversion of quanta of σ to ϕ.

C.2 Scalar Modes

In this appendix section, we show the explicit derivation of the scalar power spectrum and bispectrum in the model (4.2), whose fitting functions used for the phenomenological studies are given in expression (4.41) in Subsection 4.3.1.

Starting from (4.22), we split $\hat{\zeta}$ into the vacuum mode and sourced contribution in the same way as $\hat{Q}_\phi$ in (4.23). Using the solution (4.26) for $\hat{Q}_\phi^{(1)}$, we find the sourced mode of $\hat{\zeta}$ as

$$\hat{\zeta}^{(1)}\left(\tau,\vec{k}\right) \simeq \frac{3\sqrt{2}\,H\tau}{M_p}\int d\tau'\,G_k(\tau,\tau')\,\frac{\sqrt{\epsilon_\sigma(\tau')}}{\tau'^2}\int d\tau''\,G_k(\tau',\tau'')\,\hat{\mathcal{S}}_\sigma(\tau'',\vec{k})\,. \tag{C.8}$$

where $\hat{\mathcal{S}}_\sigma$ and $G_k(\tau,\tau')$ are defined in (4.21) and (4.27), respectively. The explicit expression for $\hat{\mathcal{S}}_\sigma$ is obtained by using (4.11) as

$$\begin{aligned}\hat{\mathcal{S}}_\sigma(\tau,\vec{k}) &= \alpha\frac{a^3}{f}\int\frac{d^3x}{(2\pi)^{3/2}}\,\mathrm{e}^{-i\vec{k}\cdot\vec{x}}\,\hat{\vec{E}}\cdot\hat{\vec{B}}\\ &\simeq \frac{\alpha H\tau}{4f}\int\frac{d^3p}{(2\pi)^{3/2}}\,\epsilon_i^{(+)}(\vec{p})\,\epsilon_i^{(+)}(\vec{k}-\vec{p})\,p^{1/4}|\vec{k}-\vec{p}|^{1/4}\left(p^{1/2}+|\vec{k}-\vec{p}|^{1/2}\right)\\ &\quad\times\tilde{A}\,(\tau,p)\,\tilde{A}\left(\tau,|\vec{k}-\vec{p}|\right)\left[\hat{a}_+\,(\vec{p})+\hat{a}_+^\dagger\,(-\vec{p})\right]\left[\hat{a}_+\left(\vec{k}-\vec{p}\right)+\hat{a}_+^\dagger\left(-\vec{k}+\vec{p}\right)\right]\,,\end{aligned} \tag{C.9}$$

after symmetrizing p and $|\vec{k}-\vec{p}|$, where

$$\begin{aligned}\tilde{A}\,(\tau,p)\,\tilde{A}\left(\tau,|\vec{k}-\vec{p}|\right) &= N\left[\xi_*,-p\tau_*,\delta\right]N\left[\xi_*,-|\vec{k}-\vec{p}|\tau_*,\delta\right]\\ &\quad\times\exp\left[-\frac{4\,\xi_*^{1/2}}{1+\delta}\left(\frac{\tau}{\tau_*}\right)^{\delta/2}\left(\sqrt{-p\tau}+\sqrt{-|\vec{k}-\vec{p}|\tau}\right)\right]\end{aligned} \tag{C.10}$$

Since we are interested in large-scale modes, we can safely assume $-k\tau\ll 1$, leading to

$$G_k\left(\tau,\tau'\right)\simeq\Theta\left(\tau-\tau'\right)\sqrt{\frac{\pi}{2}}\,\frac{\sqrt{-\tau'}}{-k^{3/2}\tau}\,J_{3/2}\left(-k\tau'\right)\,,\quad -k\tau\ll 1\,, \tag{C.11}$$

while this approximation is not valid for $G_k\left(\tau',\tau''\right)$. plugging this and (4.27) into (C.8), we have

$$\begin{aligned}\hat{\zeta}^{(1)}\left(\tau,\vec{k}\right) &\simeq \frac{3\pi^{3/2}\,H}{2M_p\,k^{3/2}}\int_{-\infty}^{\tau}\frac{d\tau'}{\tau'}\,J_{3/2}\left(-k\tau'\right)\,\sqrt{\epsilon_\sigma(\tau')}\int_{-\infty}^{\tau'}d\tau''\sqrt{-\tau''}\,\hat{\mathcal{S}}_\sigma(\tau'',\vec{k})\\ &\quad\times\left[J_{3/2}\left(-k\tau'\right)\,Y_{3/2}\left(-k\tau''\right)-Y_{3/2}\left(-k\tau'\right)\,J_{3/2}\left(-k\tau''\right)\right]\end{aligned} \tag{C.12}$$

We then plug (C.9) into the above expression and rescale

$$\vec{\tilde{p}}\equiv\frac{\vec{p}}{k}\,,\quad x'\equiv-k\tau'\,,\quad x''\equiv-k\tau''\,, \tag{C.13}$$

to obtain

$$\hat{\zeta}^{(1)}\left(\tau,\vec{k}\right) \simeq \frac{3\pi^{3/2}H^2\alpha\sqrt{\epsilon_{\sigma,*}}}{8M_p f}\int\frac{d^3\tilde{p}}{(2\pi)^{3/2}}\,\tilde{p}^{1/4}|\hat{k}-\vec{\tilde{p}}|^{1/4}\left(\tilde{p}^{1/2}+|\hat{k}-\vec{\tilde{p}}|^{1/2}\right) \times N\left[\xi_*,\,\tilde{p}\,x_*,\,\delta\right]N\left[\xi_*,\,|\hat{k}-\vec{\tilde{p}}|\,x_*,\,\delta\right]\hat{\mathcal{P}}\left[\vec{p},\,\vec{k}\right]\mathcal{T}_\zeta\left[\xi_*,\,x_*,\,\delta,\,\sqrt{\tilde{p}}+\sqrt{|\hat{k}-\vec{\tilde{p}}|}\right], \tag{C.14}$$

where we have defined

$$\hat{\mathcal{P}}\left[\vec{p},\vec{k}\right]\equiv\epsilon_i^{(+)}\left(\vec{\tilde{p}}\right)\,\epsilon_i^{(+)}\left(\hat{k}-\vec{\tilde{p}}\right)\left[\hat{a}_+\left(\vec{p}\right)+\hat{a}_+^\dagger\left(-\vec{p}\right)\right]\left[\hat{a}_+\left(\vec{k}-\vec{p}\right)+\hat{a}_+^\dagger\left(-\vec{k}+\vec{p}\right)\right]$$

$$\mathcal{T}_\zeta\left[\xi_*,\,x_*,\,\delta,\,Q\right]\equiv\int_0^\infty\frac{dx'}{x'}J_{3/2}\left(x'\right)\sqrt{\frac{\epsilon_\sigma(x')}{\epsilon_{\sigma,*}}}\int_{x'}^\infty dx''\,x''^{3/2}\exp\left[-\frac{4\,\xi_*^{1/2}}{1+\delta}\frac{x''^{(1+\delta)/2}}{x_*^{\delta/2}}\,Q\right] \times\left[J_{3/2}\left(x'\right)\,Y_{3/2}\left(x''\right)-Y_{3/2}\left(x'\right)\,J_{3/2}\left(x''\right)\right], \tag{C.15}$$

where we have sent $-k\tau\to 0$ for the lower bound of the integral. The functional forms of ξ and ϵ_σ are shown in (4.7). Using this, and the fact that $\sqrt{\epsilon_\sigma}=\frac{\dot{\sigma}}{\sqrt{2}M_pH}=\text{const.}\times\xi$, we have

$$\xi(x)=\frac{2\xi_*}{(x/x_*)^\delta+(x_*/x)^\delta}\,,\quad\sqrt{\frac{\epsilon_\sigma(x)}{\epsilon_{\sigma,*}}}=\frac{2}{(x/x_*)^\delta+(x_*/x)^\delta}\,, \tag{C.16}$$

where $x_*=-k\tau_*=\left[k/a(\tau_*)\right]/H$ is the ratio between the physical momentum of the mode and the horizon at the moment in which ξ is at its maximum. We emphasize that apart from the creation and annihilation operators, the dependence on k arises only through $x_*=k/k_*$ in the expression (C.14). Using (C.14), we proceed to the calculations of the scalar power spectrum and bispectrum in the following subsections.

C.2.1 Scalar Power Spectrum

The power spectrum of curvature perturbations $\hat{\zeta}$ can be defined as

$$\mathcal{P}_\zeta\left(k\right)\,\delta^{(3)}\left(\vec{k}+\vec{k}'\right)\equiv\frac{k^3}{2\pi^2}\left\langle\hat{\zeta}\left(\vec{k}\right)\hat{\zeta}\left(\vec{k}'\right)\right\rangle, \tag{C.17}$$

and it consists of vacuum mode and sourced contribution, namely,

$$\mathcal{P}_\zeta(k)=\mathcal{P}_\zeta^{(0)}(k)+\mathcal{P}_\zeta^{(1)}(k)\,. \tag{C.18}$$

Notice that these two modes are uncorrelated, and thus there is no cross term. Here $\mathcal{P}_\zeta^{(0)}(k)$ is the standard vacuum mode, for which, using eq. (4.25), we find

$$\mathcal{P}_\zeta^{(0)}(k) = \frac{H^2}{8\pi^2\epsilon_\phi M_p^2} \,, \tag{C.19}$$

neglecting the slow-roll corrections. For the sourced mode, we compute, using (C.14),

$$\begin{aligned}\left\langle \hat{\zeta}^{(1)}\left(\vec{k}\right)\hat{\zeta}^{(1)}\left(\vec{k}'\right)\right\rangle \simeq \frac{9\pi^3 H^4\alpha^2\epsilon_{\sigma,*}}{64M_p^2 f^2}\int\frac{d^3\tilde{p}\,d^3\tilde{p}'}{(2\pi)^3}\left\langle\hat{\mathcal{P}}\left[\vec{p},\vec{k}\right]\hat{\mathcal{P}}\left[\vec{p}',\vec{k}'\right]\right\rangle \\ \times\left(\tilde{p}\,\tilde{p}'|\hat{k}-\vec{\tilde{p}}||\hat{k}'-\vec{\tilde{p}}'|\right)^{1/4}\left(\tilde{p}^{1/2}+|\hat{k}-\vec{\tilde{p}}|^{1/2}\right)\left(\tilde{p}'^{1/2}+|\hat{k}'-\vec{\tilde{p}}'|^{1/2}\right) \\ \times N\left[\xi_*,\,\tilde{p}\,x_*,\,\delta\right]N\left[\xi_*,\,|\hat{k}-\vec{\tilde{p}}|\,x_*,\,\delta\right]N\left[\xi_*,\,\tilde{p}'\,x_*,\,\delta\right]N\left[\xi_*,\,|\hat{k}'-\vec{\tilde{p}}'|\,x_*,\,\delta\right] \\ \times\mathcal{T}_\zeta\left[\xi_*,\,\frac{k}{k_*},\,\delta,\,\sqrt{\tilde{p}}+\sqrt{|\hat{k}-\vec{\tilde{p}}|}\right]\mathcal{T}_\zeta\left[\xi_*,\,\frac{k'}{k_*},\,\delta,\,\xi_*,\sqrt{\tilde{p}'}+\sqrt{|\hat{k}'-\vec{\tilde{p}}'|}\right] \,,\end{aligned} \tag{C.20}$$

where k_* is the mode that exits the horizon at the moment when ξ takes its maximum value ξ_*, namely $k_* = a(\tau_*)H$. Evaluating

$$\begin{aligned}\left\langle\hat{\mathcal{P}}\left[\vec{p},\vec{k}\right]\hat{\mathcal{P}}\left[\vec{p}',\vec{k}'\right]\right\rangle &= \delta^{(3)}\left(\vec{k}+\vec{k}'\right)\left[\delta^{(3)}\left(\vec{p}+\vec{p}'\right)+\delta^{(3)}\left(\vec{k}-\vec{p}+\vec{p}'\right)\right] \\ &\quad\times\epsilon_i^{(+)}\left(\vec{\tilde{p}}\right)\epsilon_i^{(+)}\left(\hat{k}-\vec{\tilde{p}}\right)\epsilon_j^{(+)}\left(\vec{\tilde{p}}\,'\right)\epsilon_j^{(+)}\left(\hat{k}'-\vec{\tilde{p}}\,'\right) \,,\end{aligned} \tag{C.21}$$

and using the definition (C.17), we obtain

$$\begin{aligned}\mathcal{P}_\zeta^{(1)}(k) &\simeq \frac{9\pi\,H^4\alpha^2\epsilon_{\sigma,*}}{64M_p^2 f^2}\int\frac{d^3\tilde{p}}{(2\pi)^3}\left|\epsilon_i^{(+)}\left(\vec{\tilde{p}}\right)\epsilon_i^{(+)}\left(\hat{k}-\vec{\tilde{p}}\right)\right|^2\tilde{p}^{1/2}|\hat{k}-\vec{\tilde{p}}|^{1/2}\left(\tilde{p}^{1/2}+|\hat{k}-\vec{\tilde{p}}|^{1/2}\right)^2 \\ &\quad\times N^2\left[\xi_*,\,\tilde{p}\,x_*,\,\delta\right]N^2\left[\xi_*,\,|\hat{k}-\vec{\tilde{p}}|\,x_*,\,\delta\right]\mathcal{T}_\zeta^2\left[\xi_*,\,x_*,\,\delta,\,\sqrt{\tilde{p}}+\sqrt{|\hat{k}-\vec{\tilde{p}}|}\right] \,.\end{aligned} \tag{C.22}$$

Expressing H^2/M_p^2 and $\alpha^2\epsilon_{\sigma,*}/f^2$ in terms of $\mathcal{P}_\zeta^{(0)}$ and ξ_*, respectively, by (C.19) and $\alpha^2\epsilon_{\sigma,*}/f^2 = \dot{\sigma}^2(\tau_*)/(2M_p^2H^2f^2) = 2\xi_*^2/M_p^2$, we find

$$\mathcal{P}_\zeta^{(1)}(k) \simeq \left[\epsilon_\phi\mathcal{P}_\zeta^{(0)}\right]^2 f_{2,\zeta}\left(\xi_*,\,x_*,\,\delta\right) \,, \tag{C.23}$$

where

$$\begin{aligned}f_{2,\zeta}\left(\xi_*,\,x_*,\,\delta\right) &\equiv \frac{9\pi^5}{2}\,\xi_*^2\int\frac{d^3\tilde{p}}{(2\pi)^3}\left(1-\frac{\vec{\tilde{p}}}{\tilde{p}}\cdot\frac{\hat{k}-\vec{\tilde{p}}}{|\hat{k}-\vec{\tilde{p}}|}\right)^2\tilde{p}^{1/2}|\hat{k}-\vec{\tilde{p}}|^{1/2}\left(\tilde{p}^{1/2}+|\hat{k}-\vec{\tilde{p}}|^{1/2}\right)^2 \\ &\quad\times N^2\left[\xi_*,\,\tilde{p}\,x_*,\,\delta\right]N^2\left[\xi_*,\,|\hat{k}-\vec{\tilde{p}}|\,x_*,\,\delta\right]\mathcal{T}_\zeta^2\left[\xi_*,\,x_*,\,\delta,\,\sqrt{\tilde{p}}+\sqrt{|\hat{k}-\vec{\tilde{p}}|}\right] \,,\end{aligned} \tag{C.24}$$

using the property of the polarization vector, $|\epsilon_i^{(\lambda)}(\vec{p})\,\epsilon_i^{(\lambda')}(\vec{q})|^2 = (1-\lambda\lambda'\hat{p}\cdot\hat{q})^2/4$. For the concrete evaluation of the $\tilde{p}$ integral, we denote the cosine of the angle between $\vec{\tilde{p}}$ and $\hat{k}$ by η. After taking the trivial angular integral, we have

$$\begin{aligned} f_{2,\zeta}(\xi_*,\, x_*,\, \delta) \quad &= \frac{9\pi^3}{8}\,\xi_*^2 \int_0^\infty d\tilde{p} \int_{-1}^1 d\eta\, \tilde{p}^{5/2} \left(1-2\tilde{p}\eta+\tilde{p}^2\right)^{1/4} \left[\tilde{p}^{1/2}+\left(1-2\tilde{p}\eta+\tilde{p}^2\right)^{1/4}\right]^2 \\ &\times \left[1+\frac{\tilde{p}-\eta}{(1-2\tilde{p}\eta+\tilde{p}^2)^{1/2}}\right]^2 N^2\left[\xi_*,\, \tilde{p}\,x_*,\, \delta\right] N^2\left[\xi_*,\, \left(1-2\tilde{p}\eta+\tilde{p}^2\right)^{1/2} x_*,\, \delta\right] \\ &\times \mathcal{T}_\zeta^2\left[\xi_*,\, x_*,\, \delta,\, \tilde{p}^{1/2}+\left(1-2\tilde{p}\eta+\tilde{p}^2\right)^{1/4}\right] . \end{aligned} \tag{C.25}$$

Alternatively, we can change the variables of integration from $\tilde{p}$ and η to x and y such that $x = \tilde{p} + |\hat{k}-\vec{\tilde{p}}|$ and $y = \tilde{p} - |\hat{k}-\vec{\tilde{p}}|$. Then the integral reduces to

$$\begin{aligned} f_{2,\zeta}(\xi_*,\, x_*,\, \delta) \quad &= \quad \frac{9\pi^3}{32}\,\xi_*^2 \int_1^\infty dx \int_0^1 dy\, \frac{\left(1-x^2\right)^2\left(\sqrt{x+y}+\sqrt{x-y}\right)^2}{\sqrt{x+y}\sqrt{x-y}} \\ &\times \quad N^2\left[\xi_*,\, \frac{x+y}{2}\,x_*,\, \delta\right] N^2\left[\xi_*,\, \frac{x-y}{2}\,x_*,\, \delta\right] \mathcal{T}_\zeta^2\left[\xi_*,\, x_*,\, \delta,\, \frac{\sqrt{x+y}+\sqrt{x-y}}{\sqrt{2}}\right] . \end{aligned} \tag{C.26}$$

We evaluate f_2 numerically using either (C.25) or (C.26). The total power spectrum of the curvature perturbations is, from (C.18) and (C.23),

$$\mathcal{P}_\zeta = \mathcal{P}_\zeta^{(0)}\left[1+\epsilon_\phi^2 \mathcal{P}_\zeta^{(0)}\, f_{2,\zeta}(\xi_*,\, x_*,\, \delta)\right] , \tag{C.27}$$

where $\mathcal{P}_\zeta^{(0)}$ is given in (C.19).

C.2.2 Scalar Bispectrum

We define the bispectrum of the curvature perturbations as

$$\mathcal{B}_\zeta(k_1,k_2,k_3)\;\delta^{(3)}\left(\vec{k}_1+\vec{k}_2+\vec{k}_3\right) \equiv \left\langle \hat{\zeta}\left(\vec{k}_1\right)\hat{\zeta}\left(\vec{k}_2\right)\hat{\zeta}\left(\vec{k}_3\right)\right\rangle , \tag{C.28}$$

where $\mathcal{B}_\zeta$ depends only on the magnitudes of the three momenta, under the restriction that they form a triangle. The bispectrum in principle consists of the vacuum and sourced modes, similarly to the power spectrum. However the vacuum mode bispectrum $\mathcal{B}_\zeta^{(0)}$ is small, and we focus on the contribution from the source, i.e.

$$\mathcal{B}_\zeta \cong \mathcal{B}_\zeta^{(1)} . \tag{C.29}$$

Taking the 3-point function of $\hat{\zeta}^{(1)}$ in (C.14), we have

$$\left\langle \hat{\zeta}^{(1)}\left(\vec{k}_1\right)\hat{\zeta}^{(1)}\left(\vec{k}_2\right)\hat{\zeta}^{(1)}\left(\vec{k}_3\right)\right\rangle \simeq \frac{3^3\pi^{9/2}H^6\alpha^3\epsilon_{\sigma,*}^{3/2}}{2^9M_p^3f^3}\int\frac{d^3\tilde{p}_1\,d^3\tilde{p}_2\,d^3\tilde{p}_3}{(2\pi)^{9/2}}\left\langle\hat{\mathcal{P}}\left[\vec{p}_1,\vec{k}_1\right]\hat{\mathcal{P}}\left[\vec{p}_2,\vec{k}_2\right]\hat{\mathcal{P}}\left[\vec{p}_3,\vec{k}_3\right]\right\rangle$$
$$\times\prod_{i=1}^{3}\left(\tilde{p}_i|\hat{k}_i-\vec{\tilde{p}}_i|\right)^{1/4}\left(\tilde{p}_i^{1/2}+|\hat{k}_i-\vec{\tilde{p}}_i|^{1/2}\right)N\left[\xi_*,\,\tilde{p}_i\,x_*,\,\delta\right]N\left[\xi_*,\,|\hat{k}_i-\vec{\tilde{p}}_i|\,x_*,\,\delta\right]$$
$$\times\mathcal{T}_\zeta\left[\xi_*,\,\frac{k_i}{k_*},\,\delta,\,\sqrt{\tilde{p}}_i+\sqrt{|\hat{k}_i-\vec{\tilde{p}}_i|}\right]\,. \tag{C.30}$$

Evaluating the vacuum expectation value, we find

$$\begin{aligned}\mathcal{B}_\zeta^{(1)}\left(\vec{k}_1,\,\vec{k}_2,\,\vec{k}_3\right) \;\simeq\; & \frac{3^3\pi^{9/2}H^6\alpha^3\epsilon_{\sigma,*}^{3/2}}{2^6M_p^3f^3}\,\frac{1}{k_1^4k_2^4k_3^4}\int\frac{d^3p}{(2\pi)^{9/2}}\,\tilde{P}\left[\vec{p},\vec{p}+\vec{k}_1,\vec{p}-\vec{k}_3\right]\sqrt{p|\vec{p}+\vec{k}_1||\vec{p}-\vec{k}_3|}\\
&\times\left(\sqrt{p}+\sqrt{|\vec{p}+\vec{k}_1|}\right)\left(\sqrt{|\vec{p}+\vec{k}_1|}+\sqrt{|\vec{p}-\vec{k}_3|}\right)\left(\sqrt{|\vec{p}-\vec{k}_3|}+\sqrt{p}\right)\\
&\times N^2\left[\xi_*,\,\frac{p}{k_*},\,\delta\right]N^2\left[\xi_*,\,\frac{|\vec{p}+\vec{k}_1|}{k_*},\,\delta\right]N^2\left[\xi_*,\,\frac{|\vec{p}-\vec{k}_3|}{k_*},\,\delta\right]\\
&\times\mathcal{T}_\zeta\left[\xi_*,\,\frac{k_1}{k_*},\,\delta,\,\frac{\sqrt{p}+\sqrt{|\vec{p}+\vec{k}_1|}}{\sqrt{k_1}}\right]\mathcal{T}_\zeta\left[\xi_*,\,\frac{k_2}{k_*},\,\delta,\,\frac{\sqrt{|\vec{p}+\vec{k}_1|}+\sqrt{|\vec{p}-\vec{k}_3|}}{\sqrt{k_2}}\right]\\
&\times\mathcal{T}_\zeta\left[\xi_*,\,\frac{k_3}{k_*},\,\delta,\,\frac{\sqrt{|\vec{p}-\vec{k}_3|}+\sqrt{p}}{\sqrt{k_3}}\right]\,,\end{aligned} \tag{C.31}$$

where

$$\begin{aligned}\tilde{P}\left[\vec{v}_1,\vec{v}_2,\vec{v}_3\right] &\equiv \epsilon_i^{(+)*}\left(\vec{v}_1\right)\epsilon_i^{(+)}\left(\vec{v}_2\right)\epsilon_j^{(+)*}\left(\vec{v}_2\right)\epsilon_j^{(+)}\left(\vec{v}_3\right)\epsilon_k^{(+)*}\left(\vec{v}_3\right)\epsilon_k^{(+)}\left(\vec{v}_1\right)\\
&=\frac{1}{8}\Big[\hat{v}_1\cdot\hat{v}_2+\hat{v}_2\cdot\hat{v}_3+\hat{v}_3\cdot\hat{v}_1+\left(\hat{v}_1\cdot\hat{v}_2\right)^2+\left(\hat{v}_2\cdot\hat{v}_3\right)^2+\left(\hat{v}_3\cdot\hat{v}_1\right)^2\\
&\quad+\left(\hat{v}_1\cdot\hat{v}_2\right)\left(\hat{v}_2\cdot\hat{v}_3\right)+\left(\hat{v}_2\cdot\hat{v}_3\right)\left(\hat{v}_3\cdot\hat{v}_1\right)+\left(\hat{v}_3\cdot\hat{v}_1\right)\left(\hat{v}_1\cdot\hat{v}_2\right)-\left(\hat{v}_1\cdot\hat{v}_2\right)\left(\hat{v}_2\cdot\hat{v}_3\right)\left(\hat{v}_3\cdot\hat{v}_1\right)\Big]\\
&\quad+\frac{i}{8}\,\hat{v}_1\cdot\left(\hat{v}_2\times\hat{v}_3\right)\left(1+\hat{v}_1\cdot\hat{v}_2+\hat{v}_2\cdot\hat{v}_3+\hat{v}_3\cdot\hat{v}_1\right)\,.\end{aligned} \tag{C.32}$$

We can disregard the imaginary part as the bispectrum is real (see Appendix C.4). Rescaling

$$k\equiv k_1\,,\quad x_2\equiv\frac{k_2}{k}\,,\quad x_3\equiv\frac{k_3}{k}\,,\quad x_*\equiv\frac{k}{k_*}\,,\quad \vec{\tilde{p}}\equiv\frac{\vec{p}}{k}\,, \tag{C.33}$$

and using the relations

$$\frac{H^2}{M_p^2}=8\pi^2\epsilon_\phi\mathcal{P}_\zeta^{(0)}\,,\quad \frac{\alpha\sqrt{\epsilon_{\sigma,*}}}{f}=\frac{\sqrt{2}\,\xi_*}{M_p}\,, \tag{C.34}$$

we obtain

$$\mathcal{B}_\zeta^{(1)} \simeq \frac{\left[\epsilon_\phi \mathcal{P}_\zeta^{(0)}\right]^3}{k_1^2 k_2^2 k_3^2} f_{3,\zeta}\left(\xi_*, x_*, \delta, x_2, x_3\right) \ , \tag{C.35}$$

where

$$\begin{aligned} f_{3,\zeta}\left(\xi_*, x_*, \delta, x_2, x_3\right) &= 2^{9/2} 3^3 \pi^{21/2} \frac{\xi_*^3}{x_2^2 x_3^2} \int \frac{d^3\tilde{p}}{(2\pi)^{9/2}} \Re\left(\tilde{P}\left[\vec{\tilde{p}}, \vec{\tilde{p}} + \hat{k}_1, \vec{\tilde{p}} - x_3 \hat{k}_3\right]\right) \\ &\times \sqrt{\tilde{p}|\vec{\tilde{p}} + \hat{k}_1||\vec{\tilde{p}} - x_3\hat{k}_3|}\left(\sqrt{\tilde{p}} + \sqrt{|\vec{\tilde{p}} + \hat{k}_1|}\right)\left(\sqrt{|\vec{\tilde{p}} + \hat{k}_1|} + \sqrt{|\vec{\tilde{p}} - x_3\hat{k}_3|}\right)\left(\sqrt{|\vec{\tilde{p}} - x_3\hat{k}_3|} + \sqrt{\tilde{p}}\right) \\ &\times N^2\left[\xi_*, \tilde{p}\, x_*, \delta\right] N^2\left[\xi_*, |\vec{\tilde{p}} + \hat{k}_1|\, x_*, \delta\right] N^2\left[\xi_*, |\vec{\tilde{p}} - x_3\hat{k}_3|\, x_*, \delta\right] \mathcal{T}_\zeta\left[\xi_*, x_*, \delta, \sqrt{\tilde{p}} + \sqrt{|\vec{\tilde{p}} + \hat{k}_1|}\right] \\ &\times \mathcal{T}_\zeta\left[\xi_*, x_2 x_*, \delta, \frac{\sqrt{|\vec{\tilde{p}} + \hat{k}_1|} + \sqrt{|\vec{\tilde{p}} - x_3\hat{k}_3|}}{\sqrt{x_2}}\right] \mathcal{T}_\zeta\left[\xi_*, x_3 x_*, \delta, \frac{\sqrt{|\vec{\tilde{p}} - x_3\hat{k}_3|} + \sqrt{\tilde{p}}}{\sqrt{x_3}}\right] \ , \end{aligned} \tag{C.36}$$

where $\Re$ denotes the real part.

In order to evaluate the integrals, we can orient $\vec{k}_1$ along the x axis and express $\vec{k}_2$ and $\vec{k}_3$ in terms of x_2 and x_3, namely,

$$\begin{aligned} \vec{k}_1 &= k\,(1,\,0,\,0) \ , \\ \vec{k}_2 &= \frac{k}{2}\left(-1 - x_2^2 + x_3^2,\, \sqrt{-\left(1 - x_2 + x_3\right)\left(1 + x_2 - x_3\right)\left(1 - x_2 - x_3\right)\left(1 + x_2 + x_3\right)},\, 0\right) \ , \\ \vec{k}_3 &= \frac{k}{2}\left(-1 + x_2^2 - x_3^2,\, -\sqrt{-\left(1 - x_2 + x_3\right)\left(1 + x_2 - x_3\right)\left(1 - x_2 - x_3\right)\left(1 + x_2 + x_3\right)},\, 0\right) \ , \end{aligned} \tag{C.37}$$

and then perform numerical integration. The phenomenology of this result is extensively studied in Section 4.3.

C.3 Tensor Modes

In this appendix, we present the detailed derivation of the tensor power spectrum and bispectrum from the source, parallel to the scalar counterparts derived in Appendix C.2. The phenomenological study in Section 4.3 is done with the use of fitting functions (4.41) for the results derived in this appendix.

We define the tensor mode operators in the basis of circular polarization,

$$\hat{h}_\lambda\left(\tau,\vec{k}\right) \equiv \Pi_{ij,\lambda}\left(\hat{h}\right)\,\hat{h}_{ij}\left(\tau,\vec{k}\right) = \frac{2}{M_p\,a(\tau)}\,\hat{Q}_\lambda\left(\tau,\vec{k}\right)\ , \tag{C.38}$$

where the tensor canonical mode $\hat{Q}_\lambda$ and the polarization tensor $\Pi_{ij,\lambda}$ are defined in (4.30) and (4.31), respectively. The equation of motion for the canonical operator $\hat{Q}_\lambda$ is shown in (4.32). We can decompose the solution into the homogeneous and particular ones, corresponding to the vacuum and sourced modes, respectively, in the same way as for the case of the scalar perturbations (4.23). The solution for the vacuum mode is given in (4.33), and the sourced contribution $\hat{Q}^{(1)}_\lambda$ can be solved formally by (4.34). This, together with (C.38), provides the solution for the sourced mode $\hat{h}^{(1)}_\lambda$ as

$$\hat{h}^{(1)}_\lambda\left(\tau,\vec{k}\right) \simeq -\frac{2H\tau}{M_p}\int_{-\infty}^{\infty} d\tau'\,G_k(\tau,\tau')\,\hat{\mathcal{S}}_\lambda\left(\tau',\vec{k}\right)\ , \tag{C.39}$$

where we have used $a(\tau)\simeq -1/(H\tau)$, the Green function is given in (4.27), and the source $\hat{\mathcal{S}}_\lambda$ is defined in (4.32). The explicit expression for $\hat{\mathcal{S}}_\lambda$ can be found by using (4.10) as

$$\begin{aligned}
\hat{\mathcal{S}}_\lambda\left(\tau,\vec{k}\right) &= -\frac{a^3}{M_p}\,\Pi_{ij,\lambda}\left(\hat{k}\right)\int\frac{d^3x}{(2\pi)^{3/2}}\,\mathrm{e}^{-i\vec{k}\cdot\vec{x}}\left[\hat{E}_i\,\hat{E}_j+\hat{B}_i\,\hat{B}_j\right]\\
&\simeq -\frac{H\sqrt{-\tau\,\xi(\tau)}}{\sqrt{2}M_p}\int\frac{d^3p}{(2\pi)^{3/2}}\,\mathcal{P}_\lambda\left[\vec{k},\vec{p},\vec{k}-\vec{p}\right]p^{1/4}|\vec{k}-\vec{p}|^{1/4}\left(1+\frac{-\tau}{2\,\xi(\tau)}\sqrt{p|\vec{k}-\vec{p}|}\right)\\
&\quad\times\tilde{A}\,(\tau,p)\ \tilde{A}\left(\tau,|\vec{k}-\vec{p}|\right)\left[\hat{a}_\lambda\,(\vec{p})+\hat{a}^\dagger_\lambda\,(-\vec{p})\right]\left[\hat{a}_\lambda\left(\vec{k}-\vec{p}\right)+\hat{a}^\dagger_\lambda\left(-\vec{k}+\vec{p}\right)\right]\ ,
\end{aligned} \tag{C.40}$$

where $\hat{a}^\dagger_\lambda$ and $\hat{a}_\lambda$ are the creation and annihilation operators, respectively, of the helicity 2λ graviton modes. Recalling the relation (4.31), we have defined

$$\mathcal{P}_\lambda\left[\vec{k},\vec{p},\vec{k}-\vec{p}\right] \equiv \epsilon^{(\lambda)*}_i\left(\vec{k}\right)\,\epsilon^{(+)}_i\,(\vec{p})\,\epsilon^{(\lambda)*}_j\left(\vec{k}\right)\,\epsilon^{(+)}_j\left(\vec{k}-\vec{p}\right)\ . \tag{C.41}$$

Since we are interested in large-scale modes $-k\tau\ll 1$, we can approximate

$$G_k\left(\tau,\tau'\right)\simeq\frac{\Theta\left(\tau-\tau'\right)}{k^3\tau\tau'}\left[k\tau'\cos\left(k\tau'\right)-\sin\left(k\tau'\right)\right]\ ,\quad -k\tau\ll 1\ , \tag{C.42}$$

which is identical to (C.11). Combining (C.39) with (C.40) and (C.42), we obtain

$$\hat{h}^{(1)}_\lambda\left(\tau,\vec{k}\right) \simeq \frac{\sqrt{2}\,H^2}{M_p^2\,k^{7/2}}\int\frac{d^3p}{(2\pi)^{3/2}}\,\mathcal{P}_\lambda\left[\vec{k},\vec{p},\vec{k}-\vec{p}\right]p^{1/4}|\vec{k}-\vec{p}|^{1/4}$$

$$\times N\left[\xi_*,\,\frac{p}{k_*},\,\delta\right] N\left[\xi_*,\,\frac{|\vec{k}-\vec{p}|}{k_*},\,\delta\right] \mathcal{T}_h\left[\xi_*,\,x_*,\,\delta,\,\frac{p}{k},\,\frac{|\vec{k}-\vec{p}|}{k}\right]$$
$$\times\left[\hat{a}_\lambda\left(\vec{p}\right)+\hat{a}^\dagger_\lambda\left(-\vec{p}\right)\right]\left[\hat{a}_\lambda\left(\vec{k}-\vec{p}\right)+\hat{a}^\dagger_\lambda\left(-\vec{k}+\vec{p}\right)\right]\,, \tag{C.43}$$

where

$$\mathcal{T}_h\left[\xi_*,\,x_*,\,\delta,\,,\tilde{p},\,\tilde{q}\right]\equiv\mathcal{T}_{h1}\left[\xi_*,\,x_*,\,\delta,\,\sqrt{\tilde{p}}+\sqrt{\tilde{q}}\right]+\frac{\sqrt{\tilde{p}\,\tilde{q}}}{2}\,\mathcal{T}_{h2}\left[\xi_*,\,x_*,\,\delta,\,\sqrt{\tilde{p}}+\sqrt{\tilde{q}}\right]\,,$$
$$\mathcal{T}_{h1}\left[\xi_*,\,x_*,\,\delta,\,Q\right]\equiv\int_0^\infty dx'\left(x'\cos x'-\sin x'\right)\sqrt{\frac{\xi(x')}{x'}}\,\exp\left[-\frac{4\,\xi_*^{1/2}}{1+\delta}\frac{x'^{(1+\delta)/2}}{x_*^{\delta/2}}\,Q\right],$$
$$\mathcal{T}_{h2}\left[\xi_*,\,x_*,\,\delta,\,Q\right]\equiv\int_0^\infty dx'\left(x'\cos x'-\sin x'\right)\sqrt{\frac{x'}{\xi(x')}}\,\exp\left[-\frac{4\,\xi_*^{1/2}}{1+\delta}\frac{x'^{(1+\delta)/2}}{x_*^{\delta/2}}\,Q\right]. \tag{C.44}$$

Here we have rescaled the variables $x'\equiv-k\tau'$, and $x_*=-k\tau_*=\left[k/a(\tau_*)\right]/H$ is the ratio between the physical momentum of the mode and the horizon at the moment in which ξ is at its maximum. For the evaluation of the integral, recall

$$\xi(x)=\frac{2\xi_*}{\left(x/x_*\right)^\delta+\left(x_*/x\right)^\delta}\,. \tag{C.45}$$

Using the expression (C.43), we compute the tensor power spectrum and bispectrum in the following subsections.

C.3.1 Tensor Power Spectrum

We define the power spectrum of the tensor mode as

$$\mathcal{P}_\lambda(k)\,\delta_{\lambda\lambda'}\delta^{(3)}\left(\vec{k}+\vec{k}'\right)\equiv\frac{k^3}{2\pi^2}\left\langle\hat{h}_\lambda\left(\vec{k}\right)\hat{h}_{\lambda'}\left(\vec{k}'\right)\right\rangle\,, \tag{C.46}$$

and separate it into the vacuum mode and the component sourced by the gauge field, as in (4.36). The vacuum mode is the standard one, and we focus on the computation of the sourced contribution in this appendix. Using (C.43) and taking the two-point correlator of $\hat{h}^{(1)}_\lambda$, we find

$$\left\langle\hat{h}^{(1)}_\lambda\left(\vec{k}\right)\hat{h}^{(1)}_{\lambda'}\left(\vec{k}'\right)\right\rangle\;\simeq\;\delta^{(3)}\left(\vec{k}+\vec{k}'\right)\frac{4\,H^4}{M_p^4\,k^7}\int\frac{d^3p}{(2\pi)^3}\,\mathcal{P}_\lambda\left[\vec{k},\vec{p},\vec{k}-\vec{p}\right]\mathcal{P}^*_{\lambda'}\left[\vec{k},\vec{p},\vec{k}-\vec{p}\right]\sqrt{p|\vec{k}-\vec{p}|}$$
$$\times N^2\left[\xi_*,\,\frac{p}{k_*},\,\delta\right]N^2\left[\xi_*,\,\frac{|\vec{k}-\vec{p}|}{k_*},\,\delta\right]\mathcal{T}_h^2\left[\xi_*,\,x_*,\,\delta,\,\frac{p}{k},\,\frac{|\vec{k}-\vec{p}|}{k}\right]\,. \tag{C.47}$$

One can show that

$$\int d\phi\, \mathcal{P}_\lambda\left[\vec{k},\vec{p},\vec{q}\right]\mathcal{P}^*_{\lambda'}\left[\vec{k},\vec{p},\vec{q}\right] = \frac{\delta_{\lambda\lambda'}}{16}\int d\phi\left(1+\lambda\,\hat{k}\cdot\hat{p}\right)^2\left(1+\lambda\,\hat{k}\cdot\hat{q}\right)^2\,, \qquad \text{(C.48)}$$

and therefore we find the sourced part of the tensor power spectrum

$$\begin{aligned}\mathcal{P}^{(1)}_\lambda(k) &\simeq \frac{H^4}{8\pi^2 M_p^4\,k^4}\int\frac{d^3p}{(2\pi)^3}\left(1+\lambda\,\hat{k}\cdot\hat{p}\right)^2\left(1+\lambda\,\hat{k}\cdot\frac{\vec{k}-\vec{p}}{|\vec{k}-\vec{p}|}\right)^2\sqrt{p|\vec{k}-\vec{p}|}\\ &\quad\times N^2\left[\xi_*,\,\frac{p}{k_*},\,\delta\right]N^2\left[\xi_*,\,\frac{|\vec{k}-\vec{p}|}{k_*},\,\delta\right]\mathcal{T}_h^2\left[\xi_*,\,x_*,\,\delta,\,\frac{p}{k},\,\frac{|\vec{k}-\vec{p}|}{k}\right]. \qquad \text{(C.49)}\end{aligned}$$

After rescaling $\vec{\tilde{p}}\equiv\vec{p}/k$, we arrive at the expression

$$\mathcal{P}^{(1)}_\lambda(k)\simeq\left[\epsilon_\phi\mathcal{P}^{(0)}_\zeta\right]^2 f_{2,\lambda}(\xi_*,\,x_*,\,\delta)\,, \qquad \text{(C.50)}$$

where $\mathcal{P}^{(0)}_\zeta$ is given in (C.19) and

$$\begin{aligned}f_{2,\lambda}(\xi_*,\,x_*,\,\delta) &= 8\pi^2\int\frac{d^3\tilde{p}}{(2\pi)^3}\left(1+\lambda\,\hat{k}\cdot\hat{\tilde{p}}\right)^2\left(1+\lambda\,\hat{k}\cdot\frac{\hat{k}-\vec{\tilde{p}}}{|\hat{k}-\vec{\tilde{p}}|}\right)^2\sqrt{\tilde{p}|\hat{k}-\vec{\tilde{p}}|}\\ &\quad\times N^2\left[\xi_*,\,\tilde{p}\,x_*,\,\delta\right]N^2\left[\xi_*,\,|\hat{k}-\vec{\tilde{p}}|\,x_*,\,\delta\right]\mathcal{T}_h^2\left[\xi_*,\,x_*,\,\delta,\,\tilde{p},\,|\hat{k}-\vec{\tilde{p}}|\right]. \qquad \text{(C.51)}\end{aligned}$$

For the concrete evaluation of the integrals, we denote by η the cosine of the angle between $\vec{\tilde{p}}$ and $\hat{k}$. After taking the trivial angular integral, we have

$$\begin{aligned}f_{2,\lambda}(\xi_*,\,x_*,\,\delta) &= 2\int_0^\infty d\tilde{p}\int_{-1}^1 d\eta\,\frac{\tilde{p}^{5/2}(1+\lambda\eta)^2\left(1-\tilde{p}\eta+\lambda\sqrt{1-2\tilde{p}\eta+\tilde{p}^2}\right)^2}{(1-2\tilde{p}\eta+\tilde{p}^2)^{3/4}}\\ &\quad\times N^2\left[\xi_*,\,\tilde{p}\,x_*,\,\delta\right]N^2\left[\xi_*,\,\sqrt{1-2\tilde{p}\eta+\tilde{p}^2}\,x_*,\,\delta\right]\mathcal{T}_h^2\left[\xi_*,\,x_*,\,\delta,\,\tilde{p},\,\sqrt{1-2\tilde{p}\eta+\tilde{p}^2}\right]. \qquad \text{(C.52)}\end{aligned}$$

Alternatively, as is done for (C.26), we can change the variables of integration from $\tilde{p}$ and η to x and y such that $x=\tilde{p}+|\hat{k}-\vec{\tilde{p}}|$ and $y=\tilde{p}-|\hat{k}-\vec{\tilde{p}}|$. Then $f_{2,\lambda}$ takes the form

$$\begin{aligned}f_{2,\lambda}(\xi_*,\,x_*,\,\delta) &= \frac{1}{4}\int_1^\infty dx\int_0^1 dy\,\frac{\left(1-y^2\right)^2(1+\lambda x)^4}{\sqrt{x+y}\sqrt{x-y}}\,N^2\left[\xi_*,\,\frac{x+y}{2}\,x_*,\,\delta\right]\\ &\quad\times N^2\left[\xi_*,\,\frac{x-y}{2}\,x_*,\,\delta\right]\mathcal{T}_h^2\left[\xi_*,\,x_*,\,\delta,\,\frac{x+y}{2},\,\frac{x-y}{2}\right]. \qquad \text{(C.53)}\end{aligned}$$

We can now readily evaluate $f_{2,\lambda}$ numerically. All the phenomenological features of the tensor power spectrum in this model are captured in $f_{2,\lambda}$. Since we are choosing $\xi > 0$ (i.e. $\dot{\sigma} > 0$) so that the A_+ modes are produced through the tachyonic instability (see discussion around (3.18)), only the + helicity state of the tensor modes is efficiently sourced by the gauge field, leading to the hierarchy $f_{2,+} \gg f_{2,-}$.

The total tensor power spectrum for each helicity state is

$$\mathcal{P}_\lambda = \frac{H^2}{\pi^2 M_p^2}\left[1+\frac{H^2}{64\pi^2 M_p^2}\, f_{2,\lambda}\left(\xi_*,\, x_*,\, \delta\right)\right] = 8\epsilon_\phi \mathcal{P}_\zeta^{(0)}\left[1+\frac{\epsilon_\phi}{8}\,\mathcal{P}_\zeta^{(0)}\, f_{2,\lambda}\left(\xi_*,\, x_*,\, \delta\right)\right] , \tag{C.54}$$

and the tensor-to-scalar ratio is, using (C.27),

$$r \equiv \frac{\sum_\lambda \mathcal{P}_\lambda}{\mathcal{P}_\zeta} = 16\epsilon_\phi\, \frac{1+\frac{\epsilon_\phi}{16}\mathcal{P}_\zeta^{(0)}\left(f_{2,+}+f_{2,-}\right)}{1+\epsilon_\phi^2 \mathcal{P}_\zeta^{(0)} f_{2,\zeta}} . \tag{C.55}$$

Interesting phenomenological features arise when the sourced contribution dominates the tensor spectrum while it is subdominant for the scalar spectrum.

C.3.2 Tensor Bispectrum

We define the tensor bispectrum as

$$\mathcal{B}_{\lambda_1\lambda_2\lambda_3}\left(k_1,k_2,k_3\right)\,\delta^{(3)}\left(\vec{k}_1+\vec{k}_2+\vec{k}_3\right) \equiv \left\langle \hat{h}_{\lambda_1}\left(\vec{k}_1\right)\hat{h}_{\lambda_2}\left(\vec{k}_2\right)\hat{h}_{\lambda_3}\left(\vec{k}_3\right)\right\rangle , \tag{C.56}$$

where in general $\mathcal{B}_{\lambda_1\lambda_2\lambda_3}$ is real and depends only on the magnitude of the three momenta, forming a triangle. While it consists of the two contributions from the vacuum fluctuations and the source effects, the former is unobservable, and we focus on the latter. Moreover, since only one polarization state of the gauge field is enhanced, the produced gauge quanta efficiently source only one of the tensor helicity states. We thus define and have

$$\mathcal{B}_\lambda^{(1)} \equiv \mathcal{B}_{\lambda\lambda\lambda}^{(1)} \cong \mathcal{B}_{\lambda\lambda\lambda} , \tag{C.57}$$

where the superscript (1) denotes the sourced mode. We compute the 3-point correlation function of $\hat{h}_\lambda^{(1)}$ with the same λ using (C.43),

$$\left\langle \hat{h}_\lambda^{(1)}\left(\vec{k}_1\right)\hat{h}_\lambda^{(1)}\left(\vec{k}_2\right)\hat{h}_\lambda^{(1)}\left(\vec{k}_3\right)\right\rangle \simeq \delta^{(3)}\left(\vec{k}_1+\vec{k}_2+\vec{k}_3\right)\,\frac{2^{9/2}\,H^6}{M_p^6\left(k_1k_2k_3\right)^{7/2}}\int\frac{d^3p}{(2\pi)^{9/2}}$$

$$\times\mathcal{P}_\lambda\left[\vec{k}_1,\,-\vec{p},\,\vec{p}+\vec{k}_1\right]\mathcal{P}_\lambda\left[\vec{k}_2,\,-\vec{p}-\vec{k}_1,\,\vec{p}-\vec{k}_3\right]\mathcal{P}_\lambda\left[\vec{k}_3,\,-\vec{p}+\vec{k}_3,\,\vec{p}\right]\sqrt{p|\vec{p}+\vec{k}_1||\vec{p}-\vec{k}_3|}$$
$$\times N^2\left[\xi_*,\,\frac{p}{k_*},\,\delta\right]N^2\left[\xi_*,\,\frac{|\vec{p}+\vec{k}_1|}{k_*},\,\delta\right]N^2\left[\xi_*,\,\frac{|\vec{p}-\vec{k}_3|}{k_*},\,\delta\right]$$
$$\times\mathcal{T}_h\left[\xi_*,\,\frac{k_1}{k_*},\,\delta,\,\frac{p}{k_1},\frac{|\vec{p}+\vec{k}_1|}{k_1}\right]\mathcal{T}_h\left[\xi_*,\,\frac{k_2}{k_*},\,\delta,\,\frac{|\vec{p}+\vec{k}_1|}{k_2},\frac{|\vec{p}-\vec{k}_3|}{k_2}\right]\mathcal{T}_h\left[\xi_*,\,\frac{k_3}{k_*},\,\delta,\,\frac{|\vec{p}-\vec{k}_3|}{k_3},\frac{p}{k_3}\right]. \tag{C.58}$$

After rescaling

$$k\equiv k_1\,,\quad x_2\equiv\frac{k_2}{k}\,,\quad x_3\equiv\frac{k_3}{k}\,,\quad x_*\equiv\frac{k}{k_*}\,,\quad \vec{\tilde{p}}\equiv\frac{\vec{p}}{k}\,, \tag{C.59}$$

and recalling (C.19), we obtain

$$\mathcal{B}_\lambda^{(1)}\simeq\frac{\left[\epsilon_\phi\mathcal{P}_\zeta^{(0)}\right]^3}{k_1^2k_2^2k_3^2}\,f_{3,\lambda}\left(\xi_*,\,x_*,\,\delta,\,x_2,\,x_3\right)\,, \tag{C.60}$$

where

$$\begin{aligned}f_{3,\lambda}\left(\xi_*,\,x_*,\,\delta,\,x_2,\,x_3\right)=\frac{2^{27/2}\pi^6}{x_2^{3/2}x_3^{3/2}}\int\frac{d^3\tilde{p}}{(2\pi)^{9/2}}\sqrt{\tilde{p}|\vec{\tilde{p}}+\hat{k}_1||\vec{\tilde{p}}-x_3\hat{k}_3|}\,\mathcal{P}_{\lambda\lambda\lambda}\left[\vec{k}_i,\,\vec{\tilde{p}}\right]\\ \times N^2\left[\xi_*,\,\tilde{p}\,x_*,\,\delta\right]N^2\left[\xi_*,\,|\vec{\tilde{p}}+\hat{k}_1|\,x_*,\,\delta\right]N^2\left[\xi_*,\,|\vec{\tilde{p}}-x_3\hat{k}_3|\,x_*,\,\delta\right]\\ \times\mathcal{T}_h\left[\xi_*,\,x_1x_*,\,\delta,\,\tilde{p},|\vec{\tilde{p}}+\hat{k}_1|\right]\mathcal{T}_h\left[\xi_*,\,x_2x_*,\,\delta,\,\frac{|\vec{\tilde{p}}+\hat{k}_1|}{x_2},\frac{|\vec{\tilde{p}}-x_3\hat{k}_3|}{x_2}\right]\\ \times\mathcal{T}_h\left[\xi_*,\,x_3x_*,\,\delta,\,\frac{|\vec{\tilde{p}}-x_3\hat{k}_3|}{x_3},\frac{\tilde{p}}{x_3}\right]\,,\end{aligned} \tag{C.61}$$

and

$$\begin{aligned}\mathcal{P}_{\lambda\lambda\lambda}\left[\vec{k}_i,\,\vec{\tilde{p}}\right]&\equiv\mathcal{P}_\lambda\left[\vec{k}_1,\,-\vec{p},\,\vec{p}+\vec{k}_1\right]\mathcal{P}_\lambda\left[\vec{k}_2,\,-\vec{p}-\vec{k}_1,\,\vec{p}-\vec{k}_3\right]\mathcal{P}_\lambda\left[\vec{k}_3,\,-\vec{p}+\vec{k}_3,\,\vec{p}\right]\\ &=\epsilon_i^{(\lambda)*}\left(\hat{k}_1\right)\epsilon_j^{(\lambda)*}\left(\hat{k}_1\right)\epsilon_j^{(+)}\left(\vec{\tilde{p}}+\hat{k}_1\right)\epsilon_k^{(+)*}\left(\vec{\tilde{p}}+\hat{k}_1\right)\epsilon_k^{(\lambda)*}\left(\hat{k}_2\right)\epsilon_l^{(\lambda)*}\left(\hat{k}_2\right)\\ &\quad\times\epsilon_l^{(+)}\left(\vec{\tilde{p}}-x_3\hat{k}_3\right)\epsilon_m^{(+)*}\left(\vec{\tilde{p}}-x_3\hat{k}_3\right)\epsilon_m^{(\lambda)*}\left(\hat{k}_3\right)\epsilon_n^{(\lambda)*}\left(\hat{k}_3\right)\epsilon_n^{(+)}\left(\vec{\tilde{p}}\right)\epsilon_i^{(+)*}\left(\vec{\tilde{p}}\right)\,.\end{aligned} \tag{C.62}$$

In order to perform explicit evaluations of the integrals in (C.61), we fix $\vec{k}_1$ along the x axis and write $\vec{k}_2$ and $\vec{k}_3$ in terms of x_2 and x_3, namely,

$$\begin{aligned}
\vec{k}_1 &= k\,(1,\,0,\,0)\ , \\
\vec{k}_2 &= \frac{k}{2}\left(-1-x_2^2+x_3^2,\,\sqrt{-\left(1-x_2+x_3\right)\left(1+x_2-x_3\right)\left(1-x_2-x_3\right)\left(1+x_2+x_3\right)},\,0\right)\ , \\
\vec{k}_3 &= \frac{k}{2}\left(-1+x_2^2-x_3^2,\,-\sqrt{-\left(1-x_2+x_3\right)\left(1+x_2-x_3\right)\left(1-x_2-x_3\right)\left(1+x_2+x_3\right)},\,0\right)\ ,
\end{aligned} \tag{C.63}$$

and the polarization vector for a given momentum $\vec{q}$ can be written in terms of its components as

$$\epsilon^{(\pm)}\left(\vec{q}\right) = \frac{1}{\sqrt{2}}\left(\frac{q_x q_z \mp i\,q_y\sqrt{q_x^2+q_y^2+q_z^2}}{\sqrt{q_x^2+q_y^2}\sqrt{q_x^2+q_y^2+q_z^2}},\,\frac{q_y q_z \pm i\,q_x\sqrt{q_x^2+q_y^2+q_z^2}}{\sqrt{q_x^2+q_y^2}\sqrt{q_x^2+q_y^2+q_z^2}},\,-\frac{\sqrt{q_x^2+q_y^2}}{\sqrt{q_x^2+q_y^2+q_z^2}}\right)\ . \tag{C.64}$$

Using these explicit forms, we can evaluate (C.61) numerically for any given set of parameters. In the present case with $\xi > 0$ (i.e. $\dot{\sigma} > 0$), the positive helicity state of the gauge field is produced, and consequently only the positive tensor mode $\hat{h}_+^{(1)}$ is efficiently sourced, resulting in $f_{3,+} \gg f_{3,-}$. The phenomenology of the tensor bispectrum is featured by $f_{3,\lambda}$ and is discussed in detail in Section 4.3.

C.4 Shape and properties of the bispectrum

Let us first verify that our expressions for the scalar and tensor bispectrum given above are symmetric under the exchange of the external momenta $\vec{k}_i$, and real. In this discussion, we refer to the scalar bispectrum for definiteness. However, all our statements also apply to the tensor bispectrum. To show that the bispectrum is invariant under the exchange of any two momenta it is enough to show that $\mathcal{B}_\zeta^{(1)}\left(k_3,\,k_1,\,k_2\right) = \mathcal{B}_\zeta^{(1)}\left(k_1,\,k_2,\,k_3\right)$ and that $\mathcal{B}_\zeta^{(1)}\left(k_1,\,k_3,\,k_2\right) = \mathcal{B}_\zeta^{(1)}\left(k_1,\,k_2,\,k_3\right)$. To verify the first equality, we express $\mathcal{B}_\zeta^{(1)}\left(\vec{k}_3,\,\vec{k}_1,\,\vec{k}_2\right)$ through expression (C.31) (namely, we replace $\vec{k}_1 \to \vec{k}_3$, $\vec{k}_2 \to \vec{k}_1$ and $\vec{k}_3 \to \vec{k}_2$ both at the left and right hand sides of eq. (C.31)), and we relabel the integration variable as $\vec{p} \to \vec{p} - \vec{k}_3$. Using the fact that the three external momenta add up to zero, it is immediate to verify that the resulting expression coincides with the expression (C.31) for $\mathcal{B}_\zeta^{(1)}\left(k_1,\,k_2,\,k_3\right)$. To verify the second equality, we again start from the

expression (C.31) to express $\mathcal{B}_\zeta^{(1)}\left(\vec{k}_1,\,\vec{k}_3,\,\vec{k}_2\right)$ and we relabel $\vec{p}\to-\vec{p}-\vec{k}_1$. Also in this case, we recover the expression (C.31) for $\mathcal{B}_\zeta^{(1)}\left(k_1,\,k_2,\,k_3\right)$.

To verify that $\mathcal{B}_\zeta$ is real we instead use the reality of $\hat{\zeta}\left(\vec{x}\right)$, and the consequent identity $\hat{\zeta}\left(\vec{k}\right)=\hat{\zeta}^*\left(-\vec{k}\right)$, to write $\mathcal{B}_\zeta\left(\vec{k}_1,\,\vec{k}_2,\,\vec{k}_3\right)=\mathcal{B}_\zeta^*\left(-\vec{k}_1,\,-\vec{k}_2,\,-\vec{k}_3\right)$. We then perform a 180^0 rotation around the axis perpendicular to the plane defined by the three vectors $\vec{k}_i$ (recall that they define a plane since they add up to zero). Under this rotation, the three vectors change sign. Due to statistical isotropy, the rotation does not change the bispectrum, and so $\mathcal{B}_\zeta^*\left(-\vec{k}_1,\,-\vec{k}_2,\,-\vec{k}_3\right)=\mathcal{B}_\zeta^*\left(\vec{k}_1,\,\vec{k}_2,\,\vec{k}_3\right)$. From the two identities that we have just written we see that the bispectrum is real.

As mentioned, identical properties apply also for $\mathcal{B}_\lambda$, due to statistical isotropy, and to the fact that $h_\lambda\left(\vec{x}\right)$ is scalar and real.

We just proved exact identities, that apply to our explicit final results for $f_{3,\zeta}$ and $f_{3,\lambda}$. We now provide an approximate expression for the bispectra, written as a sum of factorized terms. Namely, each of these terms appears as a product of three functions, each of which depends on one and only one of the external momenta. As well known, a factorized approximate expression for the bispectrum considerably speeds up its use in the data analysis. We conjecture this expression by noting that we expect the bispectrum to have a bump at the value of momenta $k_1\simeq k_2\simeq k_3\simeq k_*$ at which the particle production is maximum, namely at which also the two point function is maximum. This leads us to expect a shape dependence of the type

$$f_{3,j}\left(k_1,\,k_2,\,k_3\right)\simeq\text{Normalization}\times\left[f_{2,j}\left(k_1\right)\,f_{2,j}\left(k_2\right)\,f_{2,j}\left(k_3\right)\right]^{1/2}\,, \tag{C.65}$$

both in the scalar ($j=\zeta$) and tensor ($j=\lambda$) case. The normalization factor can be obtained by evaluating the bispectrum in the exact equilateral limit. A form that is factorized, and symmetric in the three momenta is

$$\begin{aligned} f_{3,j}\left(k_1,\,k_2,\,k_3\right) \;\simeq\; & \left[\frac{f_{3,j}\left(k_1,\,k_1,\,k_1\right)}{3f_{2,j}^{3/2}\left(k_1\right)}+\frac{f_{3,j}\left(k_2,\,k_2,\,k_2\right)}{3f_{2,j}^{3/2}\left(k_2\right)}+\frac{f_{3,j}\left(k_3,\,k_3,\,k_3\right)}{3f_{2,j}^{3/2}\left(k_3\right)}\right] \\ & \times\left[f_{2,j}\left(k_1\right)\,f_{2,j}\left(k_2\right)\,f_{2,j}\left(k_3\right)\right]^{1/2}\,, \end{aligned} \tag{C.66}$$

The approximate expression (C.66) has the additional computational advantage that we simply need to evaluate f_3 in the equilateral limit.

To verify the accuracy of (C.66), in Figure C.1 we show the comparison between the exact and the approximate bispectrum on isosceles triangles, $k_2=k_3$. The black/solid

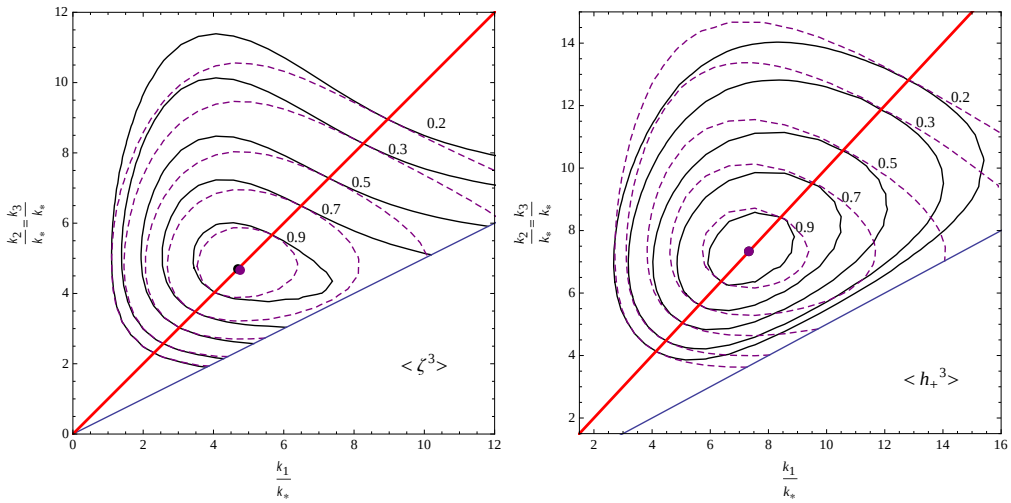

Figure C.1: Exact (black solid lines) vs. approximate (purple dashed lines; eq. (C.66)) expression for the scalar (left panel) and tensor (right panel) bispectrum, for isosceles triangles, $k_2 = k_3$, and for $\xi_* = 5$ and $\delta = 0.5$. The black (purple) dot indicates the triangle for which the exact (approximate) bispectrum is maximum. The contour lines indicate the triangles for which the bispectrum evaluates to (from inner to outer, respectively) a fraction of $0.9, 0.7, 0.5, 0.3, 0.2$ than the maximum value of the exact bispectrum. The red line at $x_2/x_1 = 1$, indicates the equilateral triangles, while the lower slope $x_2 = x_1/2$ line indicates folded triangles (smaller ratios are not possible for isosceles triangles).

contours refer to the left hand side of (C.66), while the purple/dashed contours refer to the left hand side. The contour lines shown in the the figures are obtained by evaluating the bispectra on a grid of values in the region shown, and by interpolation (for the functions $f_{2,\zeta}$ and $f_{2,\lambda}$ used to produce the dashed lines we instead employ the fitting functions given in Subsection 4.3.2). In each panel, a black (purple) dot indicates the triangle for which the exact (approximate) bispectrum is maximum. In both cases, the two dots actually appear as nearly superimposed or as superimposed to each other, as the locations of the two maxima are nearly coincident. We see that indeed the bispectrum is maximum on an equilateral triangle of scale $k_1 = k_2 = k_3 \simeq \text{few} \times k_*$ approximately equal to the scale at which the sourced power spectrum is also maximum. Most importantly, as shown by the figure, the approximate bispectrum provides a very accurate description of the exact one (particularly, close to the maximum).

C.5 Deviation from gaussianity

In this Appendix we estimate the departure from gaussianity of the statistics of the sourced $\hat{\zeta}^{(1)}$ and $h_+^{(1)}$ modes. For brevity we denote either of the two fields as $\hat{f}$, and we distinguish between the two fields only at the end of the appendix, when we make explicit evaluations. We assume that $\hat{f}$ is approximately gaussian (to be verified by this computation) and, to estimate the departure from gaussianity we start from the conventional definition of the local $f_{\rm NL}^{\rm local}$ parameter

$$\hat{f}\left(\vec{x}\right) = \hat{f}_g\left(\vec{x}\right) + f_{\rm NL}^{\rm local}\left[\hat{f}_g^2\left(\vec{x}\right) - \left\langle \hat{f}_g^2\left(\vec{x}\right)\right\rangle\right] , \tag{C.67}$$

where $\hat{f}_g$ is gaussian. The statistics of $\hat{f}$ is nearly gaussian if the first term in this decomposition dominates, namely if

$$f_{\rm NL}^{\rm local}\,\hat{f}_g\left(\vec{x}\right) < 1 \quad \leftrightarrow \quad \mathcal{R} \equiv \left(f_{\rm NL}^{\rm local}\right)^2 \left\langle \hat{f}\left(\vec{x}\right)\,\hat{f}\left(\vec{x}\right)\right\rangle < 1 \, . \tag{C.68}$$

When this condition is satisfied, we are also estimating that the presence of a nonvanishing three-point function does not change the two-point function significantly (namely, we are in this way estimating the loop diagram where the nonvanishing three-point function enters as a vertex).

In Fourier space, the decomposition (C.67) reads

$$\hat{f}\left(\vec{k}\right) = \hat{f}_g\left(\vec{k}\right) + f_{\rm NL}^{\rm local} \int \frac{d^3p}{(2\pi)^{3/2}}\, \hat{f}_g\left(\vec{p}\right)\, \hat{f}_g\left(\vec{k}-\vec{p}\right) . \tag{C.69}$$

Under the assumption of small departure from gaussianity, namely that the first term dominates in (C.69), we obtain the three point correlation function

$$\mathcal{B}\left(k_1,\, k_2,\, k_3\right) = 2\sqrt{2}\pi^{5/2} f_{\rm NL}^{\rm local} \left[\frac{\mathcal{P}\left(k_1\right)}{k_1^3}\,\frac{\mathcal{P}\left(k_2\right)}{k_2^3} + \frac{\mathcal{P}\left(k_1\right)}{k_1^3}\,\frac{\mathcal{P}\left(k_3\right)}{k_3^3} + \frac{\mathcal{P}\left(k_2\right)}{k_2^3}\,\frac{\mathcal{P}\left(k_3\right)}{k_3^3}\right] , \tag{C.70}$$

where the two- and three-point correlation functions are expressed, respectively, in terms of $\mathcal{P}$ and $\mathcal{B}$ as in eq. (4.35). The constant $f_{\rm NL}^{\rm local}$ corresponds to a specific shape of the bispectrum, denoted as local non-gaussianity (the standard local non-gaussianity parameter is obtained from using $\hat{\zeta}$ in (C.69), and from rescaling $f_{\rm NL}^{\rm local} \to \frac{3}{5} f_{\rm NL}^{\rm local}$). In the present case, we promote $f_{\rm NL}^{\rm local}$ to an effective momentum-dependence nonlinear parameter $f_{\rm NL}\left(k_i\right)$, by inserting in (C.70) the power spectra and bispectra of the sourced functions $\hat{\zeta}^{(1)}$ and $\hat{h}_+^{(1)}$. We evaluate this expression in the equilateral limit, where the bispectrum of our sourced signals is maximum (this likely overestimates the departure of gaussianity of the sourced signals). In this way we obtain

$$f_{{\rm NL},i}\left(k\right) \equiv \frac{k^6\, \mathcal{B}_i\left(k,\, k,\, k\right)}{6\sqrt{2}\pi^{5/2}\mathcal{P}_i^2\left(k\right)} \quad , \quad i = \zeta,\, \lambda\, . \tag{C.71}$$

To estimate the departure from gaussianity we write the analogous of (C.68) in momentum space, accounting for the momentum dependence of $f_{{\rm NL},i}$. We thus obtain the condition

$$R_i = \int_0^\infty \frac{dk}{k} f_{{\rm NL},i}^2\left(k\right)\, \mathcal{P}_i\left(k\right) = \int_0^\infty \frac{dk}{k}\, \frac{k^{12}\, \mathcal{B}_i^2\left(k,\, k\, k\right)}{72\, \pi^5\, \mathcal{P}_i^3\left(k\right)} \equiv \int_0^\infty \frac{dk}{k}\, r_i\left(k\right) < 1\, . \tag{C.72}$$

Using the parametrization (4.40), we obtain

$$r_i\left(k\right) \equiv \frac{k^{12}\, \mathcal{B}_i^2\left(k,\, k\, k\right)}{72\, \pi^5\, \mathcal{P}_i^3\left(k\right)} = \begin{cases} \frac{\epsilon_\phi^6\, \mathcal{P}_\zeta^{(0)3}\, f_{3,\zeta}^2}{72\, \pi^5 \left(1+\epsilon_\phi^2 \mathcal{P}_\zeta^{(0)}\, f_{2,\zeta}\right)^3} \quad , \quad i = \zeta\, , \\ \frac{\epsilon_\phi^3\, \mathcal{P}_\zeta^{(0)3}\, f_{3,\lambda}^2}{36{,}864\pi^5 \left(1+\frac{1}{8}\, \epsilon_\phi \mathcal{P}_\zeta^{(0)}\, f_{2,\lambda}\right)^3} \quad , \quad i = \lambda\, . \end{cases} \tag{C.73}$$

In Figure C.2 we show the quantity $r_\zeta\left(k\right)$ (left panel) and $r_+\left(k\right)$ (right panel) for the greatest values of ξ_* considered in the previous figures, and for which the departure

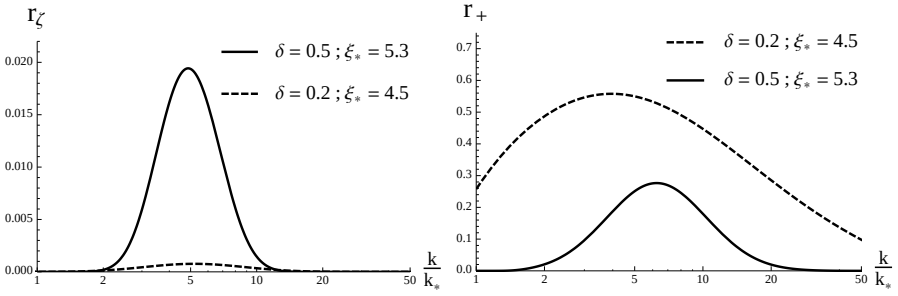

Figure C.2: Left (right) panel: parameter $r_\zeta(k)$ ($r_+(k)$) for the greatest value of ξ_* used in the previous figures, for $\delta = 0.2$, 0.5 and for $\epsilon_\phi = 10^{-5}$.

from gaussianity is therefore greatest. The quantity $r_i(k)$ is maximized at the bump of the sourced signal, $k \simeq$ few $\times\ k_*$. We note that $r_\zeta(k) \ll 1$, while $r_+(k) < 1$. The integrals of the curve shown evaluate to

$$R_\zeta(\delta = 0.2,\, \xi_* = 4.5) \simeq 0.00098 \ , \quad R_\zeta(\delta = 0.5,\, \xi_* = 5.3) \simeq 0.015 \ ,$$
$$R_+(\delta = 0.2,\, \xi_* = 4.5) \simeq 1.6 \ , \quad R_+(\delta = 0.5,\, \xi_* = 5.3) \simeq 0.35 \ . \tag{C.74}$$

The ζ signal is approximately gaussian, as the two-point function is dominated by the vacuum mode (which thus dilutes the non-gaussianity of the sourced mode). The tensor signal is mildly gaussian (we recall that the expression (C.71) likely overestimates the departure from gaussianity). This explains why in the examples we have studied in the main text the S/N ratio for detecting BBB is greater than that for TTT. It is possible that the large BBB signal can impact (at one loop) the BB correlator, thus inducing a greater two-point function (and that, in general, higher order correlators may increase the lower order ones). However, the fact that $R_+ \simeq 1$ suggests that this cannot change the order of magnitude of the result we have computed (nor the conclusion that the model can produce a visible BB signal, while being compatible with the limits from TT).

Appendix D

Small Scale Phenomenology

D.1 Non-Gaussian scalar modes, and PBH formation

In this Appendix we discuss the necessary steps to obtain the upper limit in the right panel of Figure 5.1 from the curve in the left panel. Namely, we discuss how the PBH mass is related to the number of e-folds when a mode left the horizon, and how the fraction β is related to the primordial scalar power spectrum P_ζ. We do this in two separate parts.

D.1.1 $M - N$ relation

We derive here the relation between the number of e-folds N before the end of inflation when a mode leaves the horizon, and the mass of the PBH that can be formed by this mode, if it has a large enough amplitude [88, 51]. We are interested in modes that re-enter the horizon during radiation domination. We assume that the radiation dominated era started right after inflation and we denote the end of inflation by $t_{\rm end}$.

Let us consider a density mode of physical wavelength $\lambda(t)$. We assume that this mode has a large enough amplitude to lead to a PBH when it re-enters the horizon after inflation. As customarily done, we take the inverse of the comoving momentum $k^{-1} = \frac{\lambda(t)}{2\pi\, a(t)}$ of the mode as our best estimate for the comoving radius of the region associated to this mode that collapses to form the PBH. Therefore, the physical radius of this region at any given time is given by $R_k(t) = a(t)\, k^{-1}$.

The comoving momentum of a mode that exited the horizon N e-folds before the end of inflation is

$$k_N = a_N \, H_N = a_{\rm end} \, {\rm e}^{-N} \, H_N \ , \tag{D.1}$$

where a_N and H_N are, respectively, the value of the scale factor and of the Hubble rate when the mode exits the horizon during inflation. Therefore we have

$$R_{k_N} \left(t \right) = \frac{a \left(t \right)}{a_{\rm end}} \, {\rm e}^N \, H_N^{-1} \ . \tag{D.2}$$

The black hole mass is obtained from the mass contained in this region when the mode re-enters the horizon, namely the mass in a sphere of radius $R_{k_N} \left(t = t_{\rm re-enter} \right)$.

During radiation domination, $H = \frac{1}{2t}$. Assuming radiation domination immediately from the end of inflation gives $t_{\rm end} = \frac{1}{2 H_{\rm end,inf}}$, where $H_{\rm end,inf}$ is the Hubble rate at the end of inflation. The scale factor during the radiation dominated era is given by

$$a \left(t \right) = a_{\rm end} \left(\frac{t}{t_{\rm end}} \right)^{1/2} = a_{\rm end} \sqrt{2 \, H_{\rm end,inf} \, t} \ . \tag{D.3}$$

The re-enter time is obtained by equating $H^{-1} \left(t_{\rm re-enter} \right)$ with $R_{k_N} \left(t = t_{\rm re-enter} \right)$. Using the above expressions we obtain $t_{\rm re-enter} = \frac{H_{\rm end,inf}}{2 \, H_N^2} \, {\rm e}^{2N}$. Inserting this value in (D.2), we find the physical radius at re-entry. Multiplying the volume of the corresponding sphere by the physical energy density at that time, $\rho \left(t_{\rm re-enter} \right) = 3 M_p^2 H^2 \left(t_{\rm re-enter} \right)$ we obtain the mass in that region. It is expected that a fraction γ of this mass collapses into the black hole [126], giving the black hole mass

$$M \simeq \gamma \, 4 \pi M_p^2 \, \frac{H_{\rm end,inf}}{H_N^2} \, {\rm e}^{2N} \ , \tag{D.4}$$

or

$$\frac{M_{\rm BH}}{\rm g} = 13.3 \, \gamma \, \frac{10^{13} \, {\rm GeV} \times H_{\rm end,inf}}{H_N^2} \, {\rm e}^{2 \, N} \tag{D.5}$$

The derivation we have just presented closely follows the analogous one in Ref. [51], that obtained $\frac{M_{\rm BH}}{\rm g} \simeq 10 \, {\rm e}^{2N}$. Compared with [51], we have also accounted for the variation of H during inflation, and we have included the efficiency factor γ [126]. [1]

One can also relate the PBH mass with the wavenumber of the modes. We start by writing $H_N = k_N / a_N = k_N \, {\rm e}^N / a_{\rm end}$

[1] We use the numerical value $\gamma = 3^{-3/2} \simeq 0.2$ suggested by the analytic computation of [161] for a collapse in the radiation dominated era (see [126] for a discussion).

$$\frac{M_{\rm BH}}{\rm g} = 13.3\,\gamma\,\frac{10^{13}\,{\rm GeV}\times H_{\rm end,inf}}{\left(k_N\,{\rm e}^N/a_{\rm end}\right)^2}\,{\rm e}^{2\,N} \tag{D.6}$$

or equivalently

$$\frac{M_{\rm BH}}{\rm g} = 13.3\,\gamma\,\frac{10^{13}\,{\rm GeV}\times H_{\rm end,inf}\cdot a_{\rm end}^2}{k_N^2} \tag{D.7}$$

Recall that we assume instant reheating, so $t_{\rm end}$ is the moment for the beginning of radiation domination era. We denote a_0 as today's scale factor and normalize it to 1, then we have

$$\begin{aligned}\frac{\rho_{\rm end,inf}}{\rho_{\rm rad,0}} &= \left(\frac{a_0}{a_{\rm end}}\right)^4\left(1+\frac{7}{8}N_\nu\left(\frac{4}{11}\right)^{4/3}\right)\\ \frac{3\,H_{\rm end,inf}^2\,M_p^2}{3\,H_0^2\,M_p^2\cdot\Omega_{\rm rad,0}} &\simeq \left(\frac{a_0}{a_{\rm end}}\right)^4 (1.68)\Rightarrow H_{\rm end,inf}\cdot a_{\rm end}^2 = \frac{H_0}{h}\sqrt{1.68\cdot\Omega_{\rm rad,0}\,h^2}\,,\end{aligned} \tag{D.8}$$

above we used $N_\nu = 3$. Plugging this expression in eq. D.7 and employing $H_0 \simeq 2.13\,h\cdot 10^{-42}\,{\rm GeV}$ and ${\rm GeV} \simeq 1.56\cdot 10^{38}\,{\rm Mpc}^{-1}$, we end up with

$$M_{\rm BH} = 29\,\gamma\,M_\odot\left(\frac{k}{10^6\,{\rm Mpc}^{-1}}\right)^{-2} \tag{D.9}$$

D.1.2 $P_\zeta - \beta$ relation

We derive here the relation between the curvature power spectrum P_ζ, and the quantity β, which is the fraction of regions collapsing to a PBH. A PBH is formed when a mode re-enters the horizon if the amplitude of this mode is above a certain threshold. Using the scalar curvature associated to this mode, the formation occurs if $\zeta(k_N) \gtrsim \zeta_{\rm c}$, where we recall that k_N indicates the wavenumber corresponding to the mode that left the horizon N e-folds before the end of inflation. Therefore, the probability of forming a PBH is

$$\beta^{\rm form}\left(M_k\right) = \int_{\zeta_c}^{\infty}\mathcal{P}\left(\zeta_k\right)\,d\zeta_k \tag{D.10}$$

where $\mathcal{P}\left(\zeta_k\right)$ is a probability density for the scalar curvature ζ. Since the primordial perturbations are Gaussian at CMB scales, it is common to assume that this probability is Gaussian. In the cases of interest in the present study, the scalar curvature is the sum of a vacuum part plus a part sourced by the gauge modes. The vacuum term is always negligibly small for PBH formation, so we focus on the formation due to the

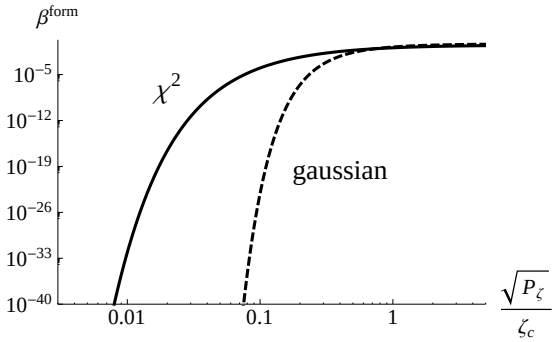

Figure D.1: Fraction of the universe that collapses to a PBH for any given mode, as a function of the ratio between the root-mean-square of scalar curvature and critical curvature value. The same power spectrum results in a much greater PBH fraction in the case of χ^2 statistics with respect to a Gaussian statistics.

source term. This term originates from the convolution of two Gaussian modes, and it therefore obeys a χ^2 statistics [51]. The PBH formation in the case of this distribution has been studied in Ref. [162], and then also in [51, 163]. In this case, the expression (D.10) gives (see for example Section IV of Ref. [51] for details)

$$\beta^{\rm form}_{\chi^2}(N) = {\rm Erfc}\left(\sqrt{\frac{1}{2}+\frac{\zeta_c}{\sqrt{2P_\zeta(N)}}}\right) \ , \tag{D.11}$$

where ${\rm Erfc}\,(x) \equiv 1 - {\rm Erf}\,(x)$ is the complementary error function. It is beneficial [162] to contrast this result with the Gaussian perturbations case:

$$\beta^{\rm form}_{\rm Gaussian}(N) = {\rm Erfc}\left(\frac{\zeta_c}{\sqrt{2P_\zeta(N)}}\right) \ . \tag{D.12}$$

In Figure D.1 we show the fraction $\beta^{\rm form}$ as a function of the power spectrum, for both χ^2 and Gaussian statistics of the primordial scalar perturbations. This result has been used to convert the PBH limits from the left to the right panel of Figure 5.1. Therefore, we are mostly interested in the values of P_ζ that result into a $\beta^{\rm form}$ in the $\left[10^{-30} - 10^{-5}\right]$ interval. We see from the figure that, in this regime, a given value of the power spectrum results in a much bigger value of $\beta^{\rm form}$ in χ^2 vs. the Gaussian case.

The result (D.11) provides the limit on the scalar perturbations from the PBH fraction β. In turn, this quantity is related to the parameter $\tilde{\beta}$ used in the left panel of

Figure 5.1 by the relation [126]

$$\tilde{\beta} = \gamma^{1/2} \left(\frac{g_*}{106.75}\right)^{-1/4} \beta \,. \tag{D.13}$$

In this expression, g_* is the number of (effective bosonic) relativistic degrees of freedom in the thermal bath at the time in which a perturbation that gives rise to a PBH of mass M re-enters the horizon, which we have normalized to the number of degrees of freedom in the Standard Model. From the relations written in Appendix D.1.1, the Hubble rate at the time of re-entry is related to the PBH mass M by $H_{\rm re-enter} \simeq 4\pi M_p^2 \gamma / M$. This corresponds to the temperature

$$T_{\rm re-enter} \simeq 97\,{\rm MeV} \left(\frac{106.75}{g_*}\right)^{1/4} \sqrt{\frac{M_\odot}{M}} \,. \tag{D.14}$$

We see from this relation that PBH masses $M \lesssim 3 \cdot 10^{-7}\, M_\odot$ correspond to modes that re-enter at temperatures above the top quark mass, where the full Standard Model field content is relativistic. Using the relation (D.5), with $H_N = H_{\rm end,inflation} = 10^{13}\,{\rm GeV}$ as a reference, this corresponds to $N \lesssim 30$. which is always the case for us, apart from the the discussion in Subsection 5.3.3. For this reason, when we convert the limits from $\tilde{\beta}$ to P_ζ, we simply fix $g_* = 106.75$ at all values of N. We note however that, strictly speaking, the value of g_* decreases for modes that re-enter the horizon at later times, corresponding to lower temperatures and larger PBH masses. When the re-enter temperature drops well below the electron mass, one has $g_* = 3.36$. This happens for PBH masses $M \gg 2 \cdot 10^5\, M_\odot$, corresponding to $N \gg 44$. In the worst case, our approximation introduces a mistake $\propto \left(\frac{106.75}{3.36}\right)^{1/4} \simeq 2.4$ in the value of β (when used in Eq. (D.13)), which propagates in a negligible way on the limit on P_ζ (we see from Figure D.1 that β strongly depend on P_ζ; therefore, inverting this dependence, P_ζ is very weakly dependent on β in the regime of interest).

D.2 Suppression factor $\mathcal{F}$

In this Appendix we discuss and evaluate the factor $\mathcal{F}$ introduced in eq. (5.8). We start from the definition of the gauge invariant scalar curvature, evaluated in spatially flat gauge, $\zeta \equiv -\frac{H\delta\rho}{\dot{\rho}}$. From the background equations of the model (5.3) one finds [143]

$\dot{\rho} = -3H\dot{\phi}^2 - 4H\rho_R$, where ρ is the total energy density in the model, and ρ_R is the energy density in the vector field [142]

$$\rho_R = \frac{\langle \vec{E}^2 + \vec{B}^2 \rangle}{2} \simeq 1.4 \cdot 10^{-4} \frac{H^4}{\xi^3} \mathrm{e}^{2\pi\xi} \,. \tag{D.15}$$

We then find

$$\zeta = -\frac{H\,\delta\phi}{\dot{\phi}} \times \mathcal{F} \quad , \quad \mathcal{F} = \frac{-\dot{\phi}\,V'}{H\left(3\dot{\phi}^2 + 4\frac{\langle E^2+B^2\rangle}{2}\right)} \,. \tag{D.16}$$

We have written the first equation as the standard relation $\zeta = -\frac{H\,\delta\phi}{\dot{\phi}}$, times a correction factor. The standard relation applies in the regime of negligible backreaction of the vector field on the background evolution of the inflaton and of the scale factor, namely when $\frac{\langle E^2+B^2\rangle}{2}$ is negligible, and $3H\dot{\phi} \simeq -V'$ (in which case, $\mathcal{F} = 1$). However, more in general, this factor needs to be included [143], and properly evaluated. Refs. [142, 108, 51] did not include this effect. So, the power spectrum expression that we have given in (5.8) is the one considered in those works, times a $\mathcal{F}^2$ correction.

The point that is raised in Ref. [143] is that $\mathcal{F}$ is important when gauge field energy is dominant over inflaton kinetic energy. We start our discussion by stressing that

$$\mathcal{F} \neq \frac{3\,\dot{\phi}^2}{3\dot{\phi}^2 + 4\frac{\langle E^2+B^2\rangle}{2}} \,. \tag{D.17}$$

This relation is correct only in the regime of negligible backreaction, ie. $\mathcal{F} \to 1$. However, one needs to evaluate $\mathcal{F}$ using the generic expression (D.16), especially in the strong backreaction regime.

We do so in Figure D.2 where, as in the main text, we have chosen a linear inflaton potential, and a coupling to the gauge field as large as allowed by the CMB data in the model that we are considering. The solid line shown in the figure is the quantity $\mathcal{F}^2$ evaluated through the proper expression (D.16). On the other hand, the dashed line is obtained from the incorrect evaluation of $\mathcal{F}$ using eq. (D.17), which makes use of the ratio between the energy in the vector field and the kinetic energy of the inflaton. We see that second case results in a great overestimate of the effect of the correction factor.

In fact, we can obtain the asymptotic value of $\mathcal{F}$ analytically in the regime of strong backreaction. In this case, one has [142]

$$\frac{\langle \vec{E}^2 + \vec{B}^2 \rangle}{2} \simeq -\frac{4}{7}\,\xi\,\langle \vec{E}\cdot\vec{B}\rangle \simeq -\frac{4}{7}\,\xi\,f\,V' \,. \tag{D.18}$$

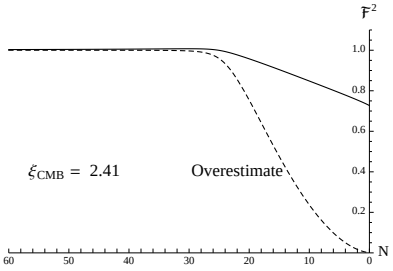

Figure D.2: Correction factor on the power spectrum, $\mathcal{F}$, as a function of the number of e-folds of inflation, for a linear potential, and for an inflaton-gauge coupling that saturates the Planck bounds. The solid line is obtained from generic eq. (D.16) which is for both negligible and strong backreaction regimes. The dashed line uses the negligible backreaction approximation in (D.17) which results in an incorrect expression due to overestimation of suppression.

Inserting this in (D.16), and disregarding the $3\dot{\phi}^2$ contribution to the denominator (which is appropriate in the regime of strong backreaction), we immediately obtain $\mathcal{F} \simeq \frac{7}{8}$, in excellent agreement with the late time behavior of the solid line of Figure D.2. This is the asymptotic value that is reached in the limit of strong backreaction, independently of the inflaton potential, of the coupling f, and of the number of gauge fields amplified by this mechanism.

Appendix E

Details of Perturbativity Constraint Calculations

E.1 Computation of the perturbativity limits for $X = \phi$

In this appendix we derive the limits discussed in Section 6.3.1 for the $X = \phi$ case.

We compute the gauge field two-point correlator at leading (zeroth) and first subleading (one loop) order in the interaction (6.21), where X is the inflaton field ϕ. We note that this interaction term involves the inflaton perturbation $\delta\phi$, and not the inflaton vev. The inflaton zeroth mode modifies the vector amplitude from the vacuum mode to (3.8). [1] The resulting wave function is used as the "unperturbed" wave function at the right hand side of (6.22) (namely, we are perturbing in $\delta\phi F\tilde{F}$, not in $\phi F\tilde{F}$; this is the same starting point as the computations of [146]).

The unperturbed two point correlator is

$$\left\langle \hat{A}_+^{(0)}\left(\vec{k}_1,\,\tau\right)\hat{A}_+^{(0)}\left(\vec{k}_2,\,\tau\right)\right\rangle = \left|A_+\left(k_1,\,\tau\right)\right|^2\delta^{(3)}\left(\vec{k}_1+\vec{k}_2\right)\ . \tag{E.1}$$

For the one loop expression, using eqs. (6.22) and (6.21), we obtain

$$\delta^{(1)}\left\langle \hat{A}_+\left(\vec{k}_1,\,\tau\right)\hat{A}_+\left(\vec{k}_2,\,\tau\right)\right\rangle = -\frac{\alpha^2}{f^2}\int\frac{d^3kd^3pd^3k'd^3p'}{\left(2\pi\right)^3}\left|\vec{k}+\vec{p}\right|\left|\vec{k}'+\vec{p}'\right|$$
$$\times\left[\vec{\epsilon}^{(+)}\left(\vec{p}\right)\cdot\vec{\epsilon}^{(+)}\left(-\vec{k}-\vec{p}\right)\right]\left[\vec{\epsilon}^{(+)}\left(\vec{p}'\right)\cdot\vec{\epsilon}^{(+)}\left(-\vec{k}'-\vec{p}'\right)\right]\int^{\tau}d\tau_1\int^{\tau_1}d\tau_2\ \mathcal{C}\ , \tag{E.2}$$

[1] More accurately, we use the approximation (3.10) in most of our explicit computations, for the reasons explained at the end of Section 3.1.1.

where the integrand is

$$\mathcal{C} = \left\langle \left[\left[\hat{A}_+^{(0)}\left(\vec{k}_1,\,\tau\right) \hat{A}_+^{(0)}\left(\vec{k}_2,\,\tau\right),\, \delta\hat{\phi}\left(\vec{k},\,\tau_1\right) \frac{d\hat{A}_+^{(0)}\left(\vec{p},\,\tau_1\right)}{d\tau_1} \hat{A}_+^{(0)}\left(-\vec{k}-\vec{p},\,\tau_1\right) \right], \right.$$
$$\left. \delta\hat{\phi}\left(\vec{k}',\,\tau_2\right) \frac{d\hat{A}_+^{(0)}\left(\vec{p}',\,\tau_2\right)}{d\tau_2} \hat{A}_+^{(0)}\left(-\vec{k}'-\vec{p}',\,\tau_2\right) \right] \right\rangle . \quad \text{(E.3)}$$

The explicit evaluation of the commutators and the expectation values gives

$$\delta^{(1)}\left\langle \hat{A}_+\left(\vec{k}_1,\,\tau\right) \hat{A}_+\left(\vec{k}_2,\,\tau\right)\right\rangle = \frac{2\alpha^2\;\delta^{(3)}\left(\vec{k}_1+\vec{k}_2\right)}{f^2} \int^{\tau} d\tau_1 \int^{\tau_1} d\tau_2 \int \frac{d^3p}{(2\pi)^3} \left[1-\frac{\vec{k}_1\cdot\vec{p}}{k_1\,p}\right]^2$$
$$\times\left\{ k_1^2\,\mathrm{Im}\left[A_+\left(k_1,\,\tau\right)\,A_+^*\left(k_1,\,\tau_1\right)\right]\,\mathcal{C}_1 + k_1\,p\,\mathrm{Im}\left[A_+\left(k_1,\,\tau\right)A_+^{'*}\left(k_1,\,\tau_1\right)\right]\,\mathcal{C}_2 \right.$$
$$\left. + k_1\,p\,\mathrm{Im}\left[A_+\left(k_1,\,\tau\right)\,A_+^*\left(k_1,\,\tau_1\right)\right]\,\mathcal{C}_3 + p^2\,\mathrm{Im}\left[A_+\left(k_1,\,\tau\right)A_+^{*'}\left(k_1,\,\tau_1\right)\right]\,\mathcal{C}_4 \right\}, \quad \text{(E.4)}$$

where

$$\begin{aligned}
\mathcal{C}_1 &= \mathrm{Im}\left[A_+\left(k_1,\,\tau\right)\,A_+^{'*}\left(p,\,\tau_2\right)\,A_+'\left(p,\,\tau_1\right)\,A_+^*\left(k_1,\,\tau_2\right)\,\delta\phi\left(|\vec{k}_1+\vec{p}|,\,\tau_1\right)\,\delta\phi^*\left(|\vec{k}_1+\vec{p}|,\,\tau_2\right)\right]\,, \\
\mathcal{C}_2 &= \mathrm{Im}\left[A_+\left(k_1,\,\tau\right)A_+^{'*}\left(p,\,\tau_2\right)A_+\left(p,\,\tau_1\right)A_+^*\left(k_1,\,\tau_2\right)\delta\phi\left(|\vec{k}_1+\vec{p}|,\,\tau_1\right)\delta\phi^*\left(|\vec{k}_1+\vec{p}|,\,\tau_2\right)\right]\,, \\
\mathcal{C}_3 &= \mathrm{Im}\left[A_+\left(k_1,\,\tau\right)\,A_+^*\left(p,\,\tau_2\right)\,A_+'\left(p,\,\tau_1\right)\,A_+^{'*}\left(k_1,\,\tau_2\right)\,\delta\phi\left(|\vec{k}_1+\vec{p}|,\,\tau_1\right)\,\delta\phi^*\left(|\vec{k}_1+\vec{p}|,\,\tau_2\right)\right]\,, \\
\mathcal{C}_4 &= \mathrm{Im}\left[A_+\left(k_1,\,\tau\right)A_+^*\left(p,\,\tau_2\right)A_+\left(p,\,\tau_1\right)A_+^{'*}\left(k_1,\,\tau_2\right)\delta\phi\left(|\vec{k}_1+\vec{p}|,\,\tau_1\right)\delta\phi^*\left(|\vec{k}_1+\vec{p}|,\,\tau_2\right)\right]\,.
\end{aligned} \quad \text{(E.5)}$$

This expression is exact. We now note that it is highly dominated by terms which have the highest possible powers of A_R. These are terms $\propto A_R^5\,A_I \propto \mathrm{e}^{4\pi\xi}$. Keeping only these terms, we have the very accurate approximation

$$\delta^{(1)}\left\langle \hat{A}_+\left(\vec{k}_1,\,\tau\right) \hat{A}_+\left(\vec{k}_2,\,\tau\right)\right\rangle \simeq \frac{2\,\alpha^2\;\delta^{(3)}\left(\vec{k}_1+\vec{k}_2\right)}{f^2} \int^{\tau} d\tau_1 \int^{\tau_1} d\tau_2 \int \frac{d^3p}{(2\pi)^3} \left[1-\frac{\vec{k}_1\cdot\vec{p}}{k_1\,p}\right]^2$$
$$\times\mathrm{Im}\left[\delta\phi\left(|\vec{k}_1+\vec{p}|,\,\tau_1\right)\delta\phi^*\left(|\vec{k}_1+\vec{p}|,\,\tau_2\right)\right]\,A_R\left(k_1,\,\tau\right)\times\left[p\,A_R\left(p,\,\tau_2\right)\,A_R'\left(k_1,\,\tau_2\right)+k_1\,A_R\left(k_1,\,\tau_2\right)\,A_R'\left(p,\,\tau_2\right)\right]$$
$$\times\left\{ p\,A_R\left(p,\,\tau_1\right)\left[A_I\left(k_1,\,\tau\right)\,A_R'\left(k_1,\,\tau_1\right)-A_R\left(k_1,\,\tau\right)\,A_I'\left(k_1,\,\tau_1\right)\right] \right.$$
$$\left. + k_1\,A_R'\left(p,\,\tau_1\right)\left[A_I\left(k_1,\,\tau\right)\,A_R\left(k_1,\,\tau_1\right)-A_R\left(k_1,\,\tau\right)\,A_I\left(k_1,\,\tau_1\right)\right] \right\}. \quad \text{(E.6)}$$

As we already remarked, the expressions for A_+ and for $\delta\phi$ entering at the right hand side are the unperturbed ones, namely those obtained without the interaction (6.21). For the inflaton field we have

$$\delta\phi\left(k,\,\tau\right)=\frac{H_k\left(1+i\,k\,\tau\right)\mathrm{e}^{-i\,k\,\tau}}{\sqrt{2}\,k^{3/2}}\;, \tag{E.7}$$

where H_k denotes the value of the Hubble rate when the $\delta\phi\left(k\right)$ left the horizon

Defining the dimensionless quantities

$$x\equiv -k_1\,\tau\;\;,\;\;x_1\equiv -k_1\,\tau_1\;\;,\;\;x_2\equiv -k_2\,\tau_2\;\;,\;\;\vec{q}\equiv\frac{\vec{p}}{k_1}\;\;,\;\;\tilde{A}\left(x\right)\equiv\sqrt{2k_1}\,A\left(k_1,\,\tau\right)\;, \tag{E.8}$$

we arrive to

$$\left\langle\hat{A}_+^{(0)}\left(\vec{k}_1,\,\tau\right)\hat{A}_+^{(0)}\left(\vec{k}_2,\,\tau\right)\right\rangle'\simeq\frac{\tilde{A}_R^2\left(x\right)}{2\,k_1}\;, \tag{E.9}$$

for the tree level correlator (we recall that the prime denotes the expectation value without the corresponding $\delta-$function), and, after some algebra, to

$$\begin{aligned}\mathcal{R}_A=\left|\frac{\delta^{(1)}\langle AA\rangle'}{\langle AA\rangle'}\right|\simeq\frac{\alpha^2\,H_{k_1}^2}{4\,f^2}\Bigg|\int\frac{d^3q}{\left(2\pi\right)^3}\,\frac{q\,\left[1-\hat{k}_1\cdot\hat{q}\right]^2}{|\hat{k}_1+\vec{q}|^3}\int_x dx_1\int_{x_1}dx_2\left[\tilde{A}_R\left(q\,x_2\right)\tilde{A}_R'\left(x_2\right)+\tilde{A}_R\left(x_2\right)\tilde{A}_R'\left(q\,x_2\right)\right]\\ \times\left\{\frac{\tilde{A}_I\left(x\right)}{\tilde{A}_R\left(x\right)}\left[\tilde{A}_R\left(q\,x_1\right)\tilde{A}_R'\left(x_1\right)+\tilde{A}_R\left(x_1\right)\tilde{A}_R'\left(q\,x_1\right)\right]-\left[\tilde{A}_R\left(q\,x_1\right)\tilde{A}_I'\left(x_1\right)+\tilde{A}_I\left(x_1\right)\tilde{A}_R'\left(q\,x_1\right)\right]\right\}\\ \times\left\{|\hat{k}_1+\vec{q}|\left(x_2-x_1\right)\cos\left[|\hat{k}_1+\vec{q}|\left(x_1-x_2\right)\right]+\left(1+|\hat{k}_1+\vec{q}|^2\,x_1\,x_2\right)\sin\left[|\hat{k}_1+\vec{q}|\left(x_1-x_2\right)\right]\right\}\Bigg|\;,\end{aligned} \tag{E.10}$$

where prime on the function denotes derivative with respect to its argument. We stress that this is the leading term for $\mathcal{R}_A$ in an expansion series in A_I/A_R. This is very accurate, since $A_I/A_R=\mathrm{O}\left(\mathrm{e}^{-2\pi\xi}\right)\ll 1$.

In eq. (E.10) we approximated $H_{k_1q}\simeq H_{k_1|\vec{q}+\hat{k}_1|}\simeq H_{k_1}$. This is a good approximation since H is slowly evolving, and since most of the support of the integral is at $q=\mathrm{O}\left(1\right)$. We can then evaluate the prefactor using

$$\frac{\alpha^2H_{k_1}^2}{4f^2}=\frac{\xi^2H_{k_1}^4}{\dot{\phi}^2}=4\pi^2\xi^2P_\zeta^{(0)}\left(k_1\right)\simeq 8.7\cdot 10^{-8}\,\xi^2\left(\frac{k_1}{k_{\mathrm{p}}}\right)^{n_s-1}\;. \tag{E.11}$$

where k_{p} indicates the pivot scale ($0.05\ \mathrm{Mpc}^{-1}$), and n_s-1 the scalar spectral tilt.

E.2 Computation of the perturbativity limits for $X = \sigma$

Here we derive the limits stated in Section 6.3.2 in the case in which $X = \sigma$. In evaluating the condition $\mathcal{R}_A \ll 1$, the formal expression (E.6) still applies, where we need to use the unperturbed gauge functions appropriate for this case. In the next subsection we provide an approximate solution (not given in [171] or Chapter 4) for the unperturbed fluctuations of σ. In Subsection E.2.2 we then provide the expression for $\mathcal{R}_A$ for this case. Finally, in Subsection E.2.3 we compute the expression for $\mathcal{R}_\sigma$.

E.2.1 $\delta\sigma$ vacuum solutions

As remarked, in the in-in expression (E.6) the unperturbed operators for the gauge and pseudo-scalar field must be used (where by unperturbed we mean the mode at zeroth order in the interaction (6.21); we remark that this is the same starting point of the computations of ref. [146]). The unperturbed pseudo-scalar modes satisfy the equation

$$\delta\ddot{\sigma} + 3H\delta\dot{\sigma} + \left(\frac{k^2}{a^2} + \partial_\sigma^2 V\right)\delta\sigma = 0 \,. \tag{E.12}$$

Using the background solution (5.13), we find that the mass term evolves with time as

$$\partial_\sigma^2 V(t) = -3\,\delta\,H^2\,\frac{1 - \mathrm{e}^{2\,\delta\,H\,(t-t_*)}}{1 + \mathrm{e}^{2\,\delta\,H\,(t-t_*)}} = -3\,\delta\,H^2\,\frac{1 - \left(\frac{\tau_*}{\tau}\right)^{2\delta}}{1 + \left(\frac{\tau_*}{\tau}\right)^{2\delta}} \,. \tag{E.13}$$

In terms of $y \equiv a\,\delta\sigma$, $x \equiv -k\tau$, and $x_* \equiv -k\tau_*$, eq. (E.12) rewrites

$$\frac{d^2y}{dx^2} + \left[1 - \frac{2}{x^2}\left(1 + \frac{3\,\delta}{2}\,\frac{1 - \left(\frac{x_*}{x}\right)^{2\delta}}{1 + \left(\frac{x_*}{x}\right)^{2\delta}}\right)\right] y = 0 \,. \tag{E.14}$$

The last fraction in the round parenthesis varies from $\simeq 1$ at $x > x_*$ to $\simeq -1$ at $x < x_*$. This transition is very fast for $\delta < 1$. We can obtain an approximate analytic solution for the unperturbed $\delta\sigma$ modes in the limit in which the transition is replaced by a step function

$$\begin{cases} \frac{d^2y}{dx^2} + \left[1 - \frac{2}{x^2}\left(1 + \frac{3\,\delta}{2}\right)\right] y = 0 \quad , \quad x > x_* \\ \\ \frac{d^2y}{dx^2} + \left[1 - \frac{2}{x^2}\left(1 - \frac{3\,\delta}{2}\right)\right] y = 0 \quad , \quad x < x_* \end{cases} \tag{E.15}$$

The early time ($x > x_*$) solution that reduces to the adiabatic vacuum mode in the deep UV is

$$y\left(x\right) = \frac{1}{2}\sqrt{\frac{\pi}{k}}\,\sqrt{x}\,H^{(1)}_{\frac{3}{2}\sqrt{1+\frac{4\delta}{3}}}\left(x\right) \quad , \quad x > x_* \tag{E.16}$$

We then solve the late time ($x < x_*$) equation, and impose continuity of y and $\frac{dy}{dx}$ at $x = x_*$, to obtain

$$\delta\sigma = \frac{H}{k^{3/2}}x^{3/2}\left\{C_1\left[\,\delta,\,x_*\right]\,J_{\Delta_-}\left(x\right) + C_2\left[\,\delta,\,x_*\right]\,Y_{\Delta_-}\left(x\right)\right\} \quad , \quad x < x_*\,, \tag{E.17}$$

where

$$\begin{aligned}
C_1\left[\delta,\,x_*\right] &= \frac{\pi^{3/2}}{4}\Bigg[x_*\left(Y_{\Delta_-}\left(x_*\right)H^{(1)}_{1+\Delta_+}\left(x_*\right) - Y_{1+\Delta_-}\left(x_*\right)H^{(1)}_{\Delta_+}\left(x_*\right)\right) \\
&\qquad + \left(\Delta_- - \Delta_+\right)Y_{\Delta_-}\left(x_*\right)H^{(1)}_{\Delta_+}\left(x_*\right)\Bigg]\,, \\
C_2\left[\delta,\,x_*\right] &= -\frac{\pi^{3/2}}{4}\Bigg[x_*\left(J_{\Delta_-}\left(x_*\right)H^{(1)}_{1+\Delta_+}\left(x_*\right) - J_{1+\Delta_-}\left(x_*\right)H^{(1)}_{\Delta_+}\left(x_*\right)\right) \\
&\qquad + \left(\Delta_- - \Delta_+\right)J_{\Delta_-}\left(x_*\right)H^{(1)}_{\Delta_+}\left(x_*\right)\Bigg]\,,
\end{aligned} \tag{E.18}$$

and where

$$\Delta_+ \equiv \frac{3}{2}\sqrt{1+\frac{4\delta}{3}} \quad , \quad \Delta_- \equiv \frac{3}{2}\sqrt{1-\frac{4\delta}{3}}\,. \tag{E.19}$$

E.2.2 Vector field renormalization

As discussed in Appendix B.1, also in this case the gauge modes satisfy the approximate relation (3.12). Using this in eq. (E.6), which, as remarked above, continues to hold also in the present case, we can write

$$\begin{aligned}
\delta^{(1)}\left\langle \hat{A}_+\left(\vec{k}_1,\,\tau\right)\hat{A}_+\left(\vec{k}_2,\,\tau\right)\right\rangle' &\simeq \frac{4\,\alpha^2}{f^2}\int_{\tau_*}^{\tau}\frac{d\tau_1\,\sqrt{\xi\left(\tau_1\right)}}{\sqrt{-\tau_1}}\int_{\tau_*}^{\tau_1}\frac{d\tau_2\,\sqrt{\xi\left(\tau_2\right)}}{\sqrt{-\tau_2}} \\
&\int\frac{d^3p}{\left(2\pi\right)^3}\,p\,k_1\left[1-\frac{\vec{k}_1\cdot\vec{p}}{k_1\,p}\right]^2 A_R\left(k_1,\,\tau\right)A_R\left(p,\,\tau_1\right)A_R\left(k_1,\,\tau_2\right)A_R\left(p,\,\tau_2\right) \\
&\times\left[\left(-k_1+p\right)A_R\left(k_1,\,\tau\right)A_I\left(k_1,\,\tau_1\right) + \left(\sqrt{k_1}+\sqrt{p}\right)^2 A_R\left(k_1,\,\tau_1\right)A_I\left(k_1,\,\tau\right)\right] \\
&\times\mathrm{Im}\left[\delta\sigma\left(|\vec{k}_1+\vec{p}|,\,\tau_1\right)\,\delta\sigma^*\left(|\vec{k}_1+\vec{p}|,\,\tau_2\right)\right]\,.
\end{aligned} \tag{E.20}$$

To evaluate this expression, we again introduce rescaled dimensionless times and momenta

$$x \equiv -k_1\,\tau \;\;,\;\; x_1 \equiv -k_1\,\tau_1 \;\;,\;\; x_2 \equiv -k_1\,\tau_2 \;\;,\;\; \vec{q} \equiv \frac{\vec{p}}{k_1} \;\;, \tag{E.21}$$

and we rescale the pseudo-scalar and vector functions according to

$$\begin{aligned}
\tilde{A}_R\,(x) &\equiv \left(\frac{8k_1\xi\,(\tau)}{-\tau}\right)^{1/4} A_R\,(\tau,\,k_1) \simeq N\,[\xi_*,\,x_*,\,\delta]\,\exp\left[-\frac{4\xi_*^{1/2}}{1+\delta}\,\left(\frac{x}{x_*}\right)^{\delta/2}\,x^{1/2}\right]\,, \\
\tilde{A}_I\,(x) &\equiv \left(\frac{8k_1\xi\,(\tau)}{-\tau}\right)^{1/4} A_I\,(\tau,\,k_1) \simeq \frac{1}{2N\,[\xi_*,\,x_*,\,\delta]}\,\exp\left[\frac{4\xi_*^{1/2}}{1+\delta}\,\left(\frac{x}{x_*}\right)^{\delta/2}\,x^{1/2}\right]\,, \\
\delta\tilde{\sigma}\,(x) &\equiv \frac{k^{3/2}}{H}\,\delta\sigma\,(\tau,\,k_1) \simeq x^{3/2}\,\left\{C_1\,[\,\delta,\,x_*]\;J_{\Delta_-}\,(x) + C_2\,[\,\delta,\,x_*]\;Y_{\Delta_-}\,(x)\right\}\;.
\end{aligned} \tag{E.22}$$

(We only specify the $x-$dependence of the rescaled quantities; their dependence on x_*, ξ_*, δ is left understood). In this notation, we can rewrite

$$\begin{aligned}
\mathcal{R}_A = \frac{\delta^{(1)}\left\langle \hat{A}_+\left(\vec{k}_1,\,\tau\right)\hat{A}_+\left(-\vec{k}_1,\,\tau\right)\right\rangle'}{\left\langle \hat{A}_+\left(\vec{k}_1,\,\tau\right)\hat{A}_+\left(-\vec{k}_1,\,\tau\right)\right\rangle'} &\simeq \frac{\alpha^2 H^2}{f^2}\,\int_x^{x_*} dx_1 \int_{x_1}^{x_*} dx_2 \\
\times \int \frac{d^3q}{(2\pi)^3}\,\frac{q^{1/2}\left[1-\hat{k}_1\cdot\hat{q}\right]^2}{2|\hat{k}_1+\vec{q}|^3}\;\tilde{A}_R\,(q\,x_1)\;\mathrm{Im}\left[\delta\tilde{\sigma}\left(|\hat{k}_1+\vec{q}|\,x_1\right)\;\delta\tilde{\sigma}^*\left(|\hat{k}_1+\vec{q}|\,x_2\right)\right] \\
\times\left[(-1+q)\,\tilde{A}_I\,(x_1) + (1+\sqrt{q})^2\,\frac{\tilde{A}_R\,(x_1)}{\tilde{A}_R\,(x)}\,\tilde{A}_I\,(x)\right]\;\tilde{A}_R\,(x_2)\,\tilde{A}_R\,(q\,x_2)\;.
\end{aligned} \tag{E.23}$$

Let us rewrite the prefactor $\frac{\alpha^2 H^2}{f^2}$. In succession, we use the definition (3.6) of ξ, evaluated at $\tau = \tau_*$, to eliminate $\frac{\alpha}{f}$; then, the relation (6.14) to eliminate $\dot{\sigma}_*$; finally, the scalar power spectrum normalization to eliminate H. We find

$$\frac{\alpha^2\,H^2}{f^2} \simeq 16\pi^2\mathcal{P}_\zeta^{(0)}\,\xi_*^2\,\frac{\epsilon_\phi}{\epsilon_{\sigma,*}} \simeq 3.5\cdot 10^{-7}\,\xi_*^2\,\frac{\epsilon_\phi}{\epsilon_{\sigma,*}}\;. \tag{E.24}$$

Combining the last two expressions, we can write

$$\begin{aligned}
\mathcal{R}_A &\equiv R_A\,[x_*,\,\xi_*,\,\delta,\,x]\;\frac{\epsilon_\phi}{\epsilon_{\sigma,*}}\;, \\
R_A &\simeq 3.5\cdot 10^{-7}\,\xi_*^2\int_x^{x_*} dx_1\int_{x_1}^{x_*} dx_2\int\frac{d^3q}{(2\pi)^3}\,\frac{q^{1/2}\left[1-\hat{k}_1\cdot\hat{q}\right]^2}{2|\hat{k}_1+\vec{q}|^3} \\
&\quad\times\tilde{A}_R\,(q\,x_1)\;\tilde{A}_R\,(x_2)\,\tilde{A}_R\,(q,\,x_2)\;\mathrm{Im}\left[\delta\tilde{\sigma}\left(|\hat{k}_1+\vec{q}|\,x_1\right)\;\delta\tilde{\sigma}^*\left(|\hat{k}_1+\vec{q}|\,x_2\right)\right]
\end{aligned}$$

$$\times \left[(-1+q)\,\tilde{A}_I\,(x_1) + (1+\sqrt{q})^2\,\frac{\tilde{A}_R\,(x_1)}{\tilde{A}_R\,(x)}\,\tilde{A}_I\,(x) \right] , \tag{E.25}$$

were we remarked the parametric dependence of R_A, and where we recall that the gauge and pseudo-scalar mode functions are given in eq. (E.22). We note that, since $x_* = -k\,\tau_*$, and $x = -k\,\tau$, we can express the functional dependence of R_A also as $R_A\left[x_*,\,\xi_*,\,\delta,\,\frac{\tau}{\tau_*}\right]$. This is the form that appears in the main text.

E.2.3 Pseudo-scalar field renormalization

We now evaluate the condition (6.26) for R_σ. From eqs. (6.21) and (6.25) we obtain

$$\begin{aligned}\langle \delta\hat{\sigma}^{(1)}(\tau,\vec{k_1})\delta\hat{\sigma}^{(1)}(\tau,\vec{k_2})\rangle \;=\; & -\frac{\alpha^2}{f^2}\int \frac{d^3k\,d^3p\,d^3k'\,d^3p'}{(2\pi)^3}\int^{\tau} d\tau_1\int^{\tau_1} d\tau_2 \\ & \times|\,\vec{k}+\vec{p}\,|\,|\,\vec{k}'+\vec{p}'\,|\,\left(\vec{\epsilon}^{\,+}(\vec{p})\cdot\vec{\epsilon}^{\,+}(-\vec{k}-\vec{p})\right)\left(\vec{\epsilon}^{\,+}(\vec{p}\,')\cdot\vec{\epsilon}^{\,+}(-\vec{k}\,'-\vec{p}\,')\right) \\ \times\Big\langle\; & \Big[\Big[\delta\hat{\sigma}(\tau,\vec{k_1})\,\delta\hat{\sigma}(\tau,\vec{k_2})\,,\,\delta\hat{\sigma}(\tau_1,\vec{k})\,\hat{A}'(\tau_1,\vec{p})\,\hat{A}(\tau_1,-\vec{k}-\vec{p})\Big]\,,\,\delta\hat{\sigma}(\tau_2,\vec{k}\,')\,\hat{A}'(\tau_2,\vec{p}\,')\,\hat{A}(\tau_2,-\vec{k}\,'-\vec{p}\,')\Big]\;\Big\rangle\,.\end{aligned} \tag{E.26}$$

We decompose this expression in several terms, each containing propagators of two different fields. Each commutator of two fields is proportional to the imaginary part of the product of the wave functions of the two fields. The real A_R and imaginary A_I parts of the gauge field amplitude are given by eqs. (B.11) and (B.12), respectively. With the phase convention that we have chosen, only the real part is amplified. For this reason the expression that we have just written is strongly dominated by the terms that contain the largest powers of A_R. These are the terms in which the vector fields are not commuted over, and are therefore proportional to $A^2\,A'^2 \simeq A_R^2\,A_R'^2$. These terms give

$$\begin{aligned}\Big\langle \delta\hat{\sigma}^{(1)}(\tau,\vec{k_1})\delta\hat{\sigma}^{(1)}(\tau,\vec{k_2})\Big\rangle \quad \simeq\; & \delta^3(\vec{k_1}+\vec{k_2})\frac{4\alpha^2}{f^2}\int\frac{d^3p}{(2\pi)^3}\;\left|\vec{\epsilon}^{\,+}(\vec{p})\cdot\vec{\epsilon}^{\,+}(\vec{k_1}-\vec{p})\right|^2 \\ & \int_{\tau_*}^{\tau} d\tau_1\int_{\tau_*}^{\tau_1} d\tau_2\;\Big\{|\,\vec{k_1}-\vec{p}\,|^2 A_R'(\tau_1,p)\,A_R'(\tau_2,p\,)\,A_R(\tau_1,|\vec{k_1}-\vec{p}|\,)\,A_R(\tau_2,|\vec{k_1}-\vec{p}\,|\,) \\ & \qquad + p\,|\,\vec{k_1}-\vec{p}\,|A_R'(\tau_1,p)\,A_R(\tau_2,p\,)\,A_R(\tau_1,|\vec{k_1}-\vec{p}|\,)\,A_R'(\tau_2,|\vec{k_1}-\vec{p}|\,)\Big\} \\ & \qquad \times\Big(\mathrm{Im}\,[\delta\sigma(\tau,k_1)\,\delta\sigma^*(\tau_1,k_1)]\;\mathrm{Im}\,[\delta\sigma(\tau,k_1)\,\delta\sigma^*(\tau_2,k_1)]\;+\vec{k_1}\leftrightarrow k_2\Big)\,.\end{aligned} \tag{E.27}$$

Working out the product of the polarization operators, and symmetrizing the time integration, we obtain, after some algebra,

$$\left\langle \delta\hat{\sigma}^{(1)}\left(\tau,\vec{k}_1\right)\,\delta\hat{\sigma}^{(1)}\left(\tau,\vec{k}_2\right)\right\rangle' \simeq \frac{\alpha^2}{2f^2}\int\frac{d^3p}{(2\pi)^3}\,\frac{\left(p^{1/2}+|\vec{k}_1-\vec{p}|^{1/2}\right)^2\left[\left(p+|\vec{k}_1-\vec{p}|\right)^2-k_1^2\right]^2}{4\,p\,|\vec{k}_1-\vec{p}|}$$
$$\times\left[\int_{\tau_*}^{\tau}d\tau_1\sqrt{\frac{2\xi\,(\tau_1)}{-\tau_1}}\mathrm{Im}\left[\,\delta\sigma\,(\tau,k_1)\;\delta\sigma^*\,(\tau_1,k_1)\,\right]A_R\,(\tau_1,\,p)\,A_R\left(\tau_1,\,|\vec{k}_1-\vec{p}|\right)\right]^2 . \quad \text{(E.28)}$$

In terms of the dimensionless quantities introduced in (E.21) and (E.22), and recalling the definition of the power spectrum given after eq. (6.24), we can then write

$$P^{(1)}_{\delta\sigma}\,(k,\,\tau) \simeq \frac{\alpha^2H^4}{64\pi^2f^2}\int\frac{d^3q}{(2\pi)^3}\,\frac{\left(q^{1/2}+|\hat{k}-\vec{q}|^{1/2}\right)^2\left[\left(q+|\hat{k}-\vec{q}|\right)^2-1\right]^2}{q^{3/2}\,|\hat{k}-\vec{q}|^{3/2}}$$
$$\times\left[\int_x^{x_*}dx_1\,\mathrm{Im}\left[\,\delta\tilde{\sigma}\,(x)\;\delta\tilde{\sigma}^*\,(x_1)\,\right]\tilde{A}_R\,(q\,x_1)\,\tilde{A}_R\left(|\hat{k}-\vec{q}|\,x_1\right)\right]^2 , \quad \text{(E.29)}$$

where we have relabeled $\vec{k}_1$ as $\vec{k}$, the momentum of the generic mode under consideration.

As can be seen from the rhs of (E.29), the power spectrum dependence on the momentum and on time can be written as a dependence on the dimensionless quantities $-k\tau_*$ and $\frac{\tau}{\tau_*}$. We therefore write the power spectrum as $P^{(1)}_{\delta\sigma}\left(x_*=-k\tau_*,\,\frac{\tau}{\tau_*}\right)$. In [171], it was shown that the power spectra of the sourced GWs and inflaton perturbations in this model are well fitted by a Gaussian peak. Not surprisingly, the same is true for the power spectrum (E.29) (the reason is that the amplitude of the sourcing gauge field is well fitted by this parametrization, cf. eq. (B.13)). Indeed, we evaluated the expression (E.29) numerically, and we found that it is well parametrized by

$$P^{(1)}_{\delta\sigma}\left(x_*,\,\frac{\tau}{\tau_*}\right) \simeq \frac{\alpha^2H^4}{f^2}\,\mathcal{M}\left[\xi_*,\,\delta,\,\frac{\tau}{\tau_*}\right]\,\exp\left[-\frac{\ln^2\left(\frac{x_*}{x_{c,\mathcal{M}}\left[\xi_*,\,\delta,\,\frac{\tau}{\tau_*}\right]}\right)}{2\sigma^2_{\mathcal{M}}\left[\xi_*,\,\delta,\,\frac{\tau}{\tau_*}\right]}\right] . \quad \text{(E.30)}$$

As an example of the goodness of this fit, in Figure E.1 we show the power spectrum for two specific values of δ and ξ_*, and for a specific time τ. Equally good fits are obtained in the other cases we have studied.

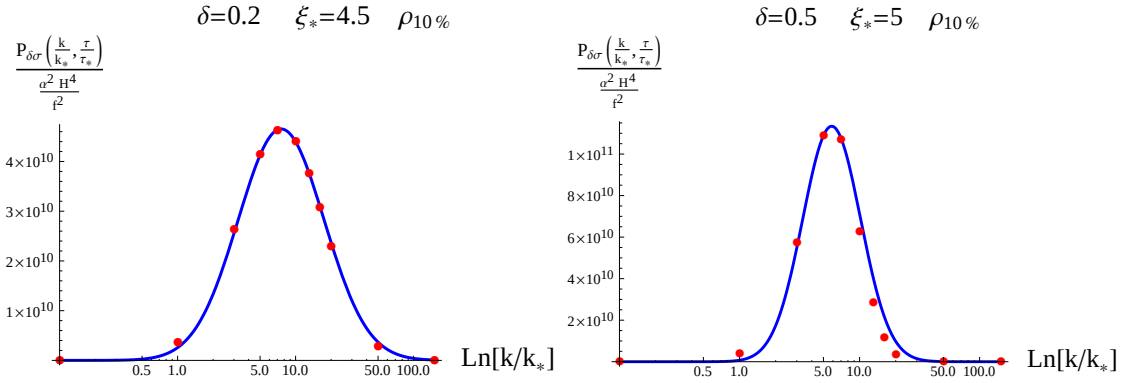

Figure E.1: Power spectrum of the pseudo-scalar $\delta\sigma$ sourced by the gauge field, for two specific values of δ and ξ_*. The time τ/τ_* is chosen to be the moment at which the total energy density in the gauge field has decreased to 10% than the value it had at its peak. The red dots are the values obtained from a numerical evolution of eq. (E.29). The blue solid line is the fitting function (E.30).

The amplitude $\mathcal{M}$, the central position x_c, and the width of the peak $\sigma_{\mathcal{M}}$, evolve with time, as they parametrize the growth of the power spectrum sourced by the gauge fields A_+ [2]. Since the amplitude of A_+ is negligible at $\tau < \tau_*$, all our results, and in particular the expression (E.30), are valid for $\frac{\tau}{\tau_*} < 1$, while we can simply set $P^{(1)}_{\delta\sigma}\left(x_*,\, \frac{\tau}{\tau_*}\right) \simeq 0$ at $\frac{\tau}{\tau_*} > 1$. The power spectrum then experiences a fast growth at $|\tau| \lesssim |\tau_*|$, and it eventually saturates to a constant value at $|\tau| \ll |\tau_*|$. The parameter $x_{c,\mathcal{M}} = \mathrm{O}\,(1)$. So, expression (E.30) has a peak at $x_* = \mathrm{O}\,(1)$, namely for the modes that left the horizon close to the $\dot\sigma$ was maximum.

Using the fit (E.30), we can perform the integral (6.24) analytically. We can then express the condition (6.26) as

$$\mathcal{R}_\sigma = \frac{\sqrt{\int d\ln x_*\, P^{(1)}_{\delta\sigma}}}{f} = \frac{\alpha\, H^2}{f^2}\, (2\pi)^{1/4} \sqrt{\mathcal{M}\left[\xi_*,\, \delta,\, \frac{\tau}{\tau_*}\right] \sigma_{\mathcal{M}}\left[\xi_*,\, \delta,\, \frac{\tau}{\tau_*}\right]} \ll 1\,. \quad \text{(E.31)}$$

Using the relation (E.24), as well as $\alpha = \frac{2\xi_*}{\delta}$ (as can be obtained from eqs. (3.6) and (5.13)), we can rewrite this as

$$\mathcal{R}_\sigma \;\equiv\; \frac{\epsilon_\phi}{\epsilon_{\sigma_*}}\, \mathrm{R}_\sigma\left[\xi_*,\, \delta,\, \frac{\tau}{\tau_*}\right] \ll 1\,,$$

[2] The three parameters $\mathcal{M}$, $x_{c,\mathcal{M}}$, $\sigma_{\mathcal{M}}$, also depend on the two parameters ξ_* and δ that control the motion of the field σ.

$$\mathrm{R}_\sigma \;\simeq\; 2.8\cdot 10^{-7}\,\delta\,\xi_*\sqrt{\mathcal{M}\left[\xi_*,\,\delta,\,\frac{\tau}{\tau_*}\right]\,\sigma_{\mathcal{M}}\left[\xi_*,\,\delta,\,\frac{\tau}{\tau_*}\right]}\,. \tag{E.32}$$

We recall that the parameters $\mathcal{M}$ and $\sigma_{\mathcal{M}}$ parametrize, respectively, the amplitude and the width of the peak in the power spectrum of sourced $\delta\sigma$ modes, see eq. (E.30).